ENZYMATIC CLEAVAGE OF CARBON-PHOSPHORUS BONDS

by

Fern R. M^{c}Sorley

A thesis submitted to the Department of Chemistry

In conformity with the requirements for

the degree of Doctor of Philosophy

Queen's University

Kingston, Ontario, Canada

(September, 2013)

Abstract

Inorganic phosphate (P_i) plays a critical role in many biological structures and processes. However, P_i typically occurs at low concentrations, particularly in marine environments. In comparison, naturally occurring organophosphonates, which are characterized by a stable carbon-phosphorus (CP) bond, are frequently present at higher concentrations. Accordingly, bacteria have evolved different mechanisms for cleaving the CP bond of organophosphonates to liberate P_i for metabolic use. Two prominent enzyme pathways for catabolic cleavage of a CP bond are examined in this thesis.

The first, called CP-lyase, is encoded by the *phn* operon that consists of 14 genes (*phnCDEFGHIJKLMNOP*). CP-lyase has long been of interest for its ability to degrade a wide array of organophosphonates through a homolytic CP bond cleaving reaction. A soluble protein complex consisting of PhnGHIJK was isolated from *E. coli*, suggesting that protein-protein interactions are important for CP bond cleavage. Intermediates of organophosphonate catabolism by *E. coli* CP-lyase were also detected and isolated, including α-D-ribosyl-1,2-cyclic phosphate and *N*-acetylated aminoalkylphosphonates, 2-*N*-acetamidoethylphosphonate and 5'-phospho-α-D-ribosyl-1'-alkylphosphonates. The former compound was shown to be converted by the phosphodiesterase PhnP to α-D-ribosyl-1-phosphate. It was also shown that PhnO is an aminoalkylphosphonate *N*-acetyl transferase and that *N*-acetylation by this enzyme is necessary for CP bond cleavage of 1-aminoalklyphosphonates. These results demonstrated that in addition to forming protein complexes, CP-lyase also comprises a catabolic pathway, with ribosylation of organophosphonates playing a key part in setting up the CP bond cleaving reaction.

The second pathway examined in this thesis is comprised of marine bacterial enzymes PhnY and PhnZ and is specific for 2-aminoethylphosphonate. PhnY was shown to be an α-ketoglutarate / Fe(II) dependent dioxygenase that hydroxylates the α-carbon of 2-

aminoethylphosphonate to form (*R*)-2-amino-1-hydroxyethylphosphonate. PhnZ was shown to be a novel Fe(II) dependent oxygenase that converts (*R*)-2-amino-1-hydroxyethylphosphonate to glycine and P_i. Site directed mutagenesis, kinetic analysis, reactions with substrate analogues, and X-ray crystallography examined the roles of active site residues and the di-iron active site. Additionally, a unique induced-fit mechanism was discovered which appears to synchronize substrate binding with activation of molecular oxygen. Overall these results show that PhnZ represents a new mechanism for catabolic cleavage of a CP bond.

Co-Authorship

A description of the contributions of each author to the experimental work for each chapter is presented here.

Chapter 2: Towards the reaction pathway of CP-lyase

2.2. Isolation, detection and characterization of CP-lyase pathway intermediates

This project was initiated by collaboration between Bjarne Hove-Jensen, David Zechel and Fern M^{c}Sorley. Work from this chapter was published in the Journal of the American Chemical Society in February of 2011 (J. Am. Chem. Soc. (2011), **133**:3617-3624) and in PLOS ONE in October of 2012 (Plos One. (2012), **7**(10):e46416. Doi:10.1371/journal.pone.0046416). The manuscripts were written by Bjarne Hove-Jensen, Fern M^{c}Sorley and David Zechel. Bjarne Hove-Jensen, Fern M^{c}Sorley and David Zechel were responsible for experimental design. Bjarne Hove-Jensen performed liquid culture growth for analysis of intermediates, cloning of the *phnO* gene, synthesis of radiolabelled material, purification and characterization of CP-lyase intermediates, the PhnP reaction, and the PhnO reaction. Fern M^{c}Sorley performed protein expression and purification, purification and characterization of CP-lyase intermediates, analysis of *E. coli* growth on solid media and all other work not published in the above articles.

2.3. Discovery of protein complexes in the CP-lyase pathway

Work from this chapter was published in Proceedings of the National Academy of Sciences of the United States of America in July of 2011 (Proc. Natl. Acad. Sci. (2011), **108**(28):11392-11398). This project was initiated by Bjarne Hove-Jensen. The manuscript was written by Bjarne Jochimsen, Fern M^{c}Sorley, Jens Stougaard, David Zechel and Bjarne Hove-Jensen. Bjarne Hove-Jensen, Bjarne Jochimsen and David Zechel were responsible for overall experimental design. Bjarne Jochimsen performed protein expression and purification of the Phn-complex as well as cross-linking experiments. Signe Lolle performed protein expression and purification. Bjarne Hove-Jensen constructed pHO571, pHO572, and pHO575. Mariah Nabi

constructed pMN1. Fern M^{c}Sorley constructed pFM31, pFM32, pFM33, pFM34 and pFM35 and performed analysis of *E. coli* growth on solid media along with all other work not published in the above article.

Chapter 3: A new oxidative pathway for CP bond cleavage

Work from this chapter was published in the Journal of the American Chemical Society in March of 2012 (J. Am. Chem. Soc. (2012), **134**:8364-8367). This project was initiated by Fern M^{c}Sorley and David Zechel. Fern M^{c}Sorley and David Zechel were responsible for experimental design. Manuscript was prepared by Fern M^{c}Sorley and David Zechel with editorial input from all other contributing authors. An additional manuscript is currently in preparation for publication as a result of collaboration between Fern M^{c}Sorley, David Zechel, Laura van Staalduinen and Zongchao Jia.

Fern M^{c}Sorley optimized protein expression and purification; designed and constructed pFM36, pFM37 and pFM39; performed all PhnY and PhnZ reactions and product analysis. Site-directed mutagenesis of active site residues was performed by Fern M^{c}Sorley and Laura van Staalduinen. Laura van Staalduinen was responsible for PhnZ protein expression and purification for crystallization, along with X-ray data collection, structural determination and analysis of PhnZ crystals. Initially crystallization of PhnZ was performed by Margaret Kim. Peter Wyatt supplied the *R*-enantiomer and racemic mixture of 2-amino-1-hydroxyethylphosphonate. Friedrich Hammerschmidt supplied 2-amino-(*S*)-1-hydroxyethylphosphonate, (*R*,*R*)- and (*R*,*S*/*S*,*R*)-2-amino-1-hydroxypropylphosphonates. Wilfred van der Donk supplied 1-hydroxyethylphosphonate. ICP-MS was performed by Alemayehu Asfaw. CD was performed by Kim Munro.

Acknowledgements

First off I want to thank my supervisor David Zechel for all of his support and guidance, without which I would not have been able to complete this thesis. I want to thank my committee members Derek and Anne as well as their lab members for welcoming me into their group meetings, for their thoughtful discussions and their support, especially during Dave's absence.

Bjarne Hove-Jensen I am indebted to you for your constant encouragement that helped me through. I am forever grateful for your continuous support, your thought provoking discussion, and the time you spent teaching me in the lab. You have made me a better scientist and a better person. Collaborating with you has been a highlight of my thesis career and one I will not forget anytime soon. To my parents for pulling through when I needed you the most. Your support has been astonishing and I am extremely appreciative for everything you have done for me. Dad you seem to understand me when I make absolutely no sense and Mum your patience is a virtue I only wish I had.

I am grateful to all of my friends that have supported me throughout my graduate studies, especially to those of you who kept me sane enough during these last months to somehow produce a final written document. There is no way I can thank all those that deserve it, as my time here has been effected by countless individuals that have walked through the dusty hallways of Chernoff Hall, and many who have never even set foot through the door. I want to thank the past and present members of the Zechel lab for sharing this experience with me at some point during my time here, a special thank you to Zechel alumni Dasha, Ryan, and Zhi. I want to also give a shout out to a few other people who made life a little easier whether it be by dragging me to the pool, gym or bar to clear my head, helping me out in the lab or for being great friends during this process (Matt, Graham, Tim, Kevin, Lynn, Alanna, Erika, Maria, Elize, Cathy, Mike, Michael, Crystal, Emily, Steph, Tine, Trisha and Tamara).

Statement of Originality

I hereby certify that all of the work described within this thesis is the original work of the author. Any published (or unpublished) ideas and/or techniques from the work of others are fully acknowledged in accordance with the standard referencing practices.

(Fern R. M^{c}Sorley)

(September, 2013)

Table of Contents

List of Figures

List of Tables

List of Abbreviations

1-HEP	1-hydroxyethylphosphonate
2-HEP	2-hydroxyethylphosphonate
acetyl-CoA	acetyl coenzyme A
ADP	adenosine diphosphate
AEP	2-aminoethylphosphonate, **1g**
aKG	α-ketoglutarate
AMPA	aminomethylphosphonate, **1f**
API	atmospheric pressure ionization
APPA	2-amino-5-phosphono-3-*cis*-pentenoic acid
ATP	adenosine triphosphate
C-terminal (terminus)	carboxy-terminal (terminus)
COSY	correlation spectroscopy
CP	carbon-phosphorus
d	doublet
DNA	deoxyribonucleic acid
DEPT	distortionless enhancement by polarization transfer
DNPH	dinitrophenylhydrazine
E. coli	*Escherichia coli*
EDTA	ethylenediaminetetraacetic acid
ESI-MS	electro spray ionization – mass spectrometry
FDA	Food and Drug Administration
FPLC	fast protein liquid chromatography
GST	glutathione S-transferase

HAD	2-haloalkanoic acid dehalogenase
HEDP	1-hydroxyethane(1,1-diylbisphosphonic acid)
HIV	human immunodeficiency virus
HMBC	heteronuclear multiple-bond correlation spectroscopy
HPLC	high-performance liquid chromatography
HSQC	heteronuclear single-quantum correlation spectroscopy
ICP-MS	inductively coupled plasma – mass spectrometry
IPTG	isopropyl-β-D-1-thiogalactoside
LB	Luria Bertani
LC	liquid chromatography
LMW	low molecular weight
m	multiplet
M. segmentis	*Mycobacterium segmentis*
MePn	methylphosphonate, **1a**
MOPS	3-(*N*-morpholino)propanesulfonic acid
MPnS	methylphosphonate synthase
mRNA	messenger ribonucleic acid
MS	mass spectrometry
N. maritimus	*Nitrosopumilus maritimus*
N-terminal (terminus)	amino-terminal (terminus)
NAD^+	nicotinamide adenine dinucleotide
NMR	nuclear magnetic resonance
NTA	nitrilotriacetic acid
OD	optical density
PAGE	polyacrylamide gel electrophoresis

PCR	polymerase chain reaction
PEP	phosphoenolpyruvate
PepM	phosphoenolpyruvate phosphomutase
Pho regulon	phosphate regulon
P_i	inorganic phosphate
PitA	phosphate inorganic transporter
PITC	phenylisothiocyanate
PLP	pyridoxal phosphate
PnAA	phosphonoacetaldehyde
PNP	purine nucleoside phosphorylase
PnPy	phosphonopyruvate
PRPP	5-phospho-α-D-ribosyl-1-pyrophosphate, **7**
psi	phosphate starvation-inducible
Pst	phosphate specific transporter
PT	phosphinothricin
PTT	bialaphos, phosphonothricin tripeptide
Q-TOF	quadrupole time-of-flight
R_f	retention factor
RNA	ribonucleic acid
s	singlet
S. enterica	*Salmonella enterica*
SAM	*S*-adenosyl methionine
SDS	sodium dodecyl sulfate
T	triplet
taurine	2-aminoethanesulfonic acid

TCA	trichloroacetic acid
Tris	tris(hydroxymethyl)aminomethane
TLC	thin layer chromatography
TPP	thiamine pyrophosphate
UDP	uridine diphosphate
USD	United States dollar
VX	*O*-ethyl-S-[2-(diisopropylamino)ethyl] methylphosphonothioate
WT	wild type

Chapter 1

Introduction

1.1 Organophosphonates

Organophosphonates and organophosphinates have a defining structural motif, a carbon-phosphorus (CP) bond. Phosphonates contain one CP bond (Figure 1-1C) whereas phosphinates contain either two CP bonds or one CP bond and one phosphorus-hydrogen bond to the same phosphorus atom as the carbon (Figure 1-1D).

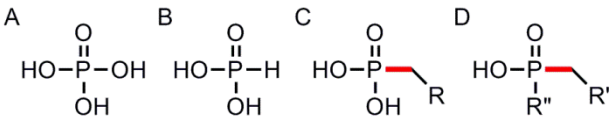

Figure 1-1. Examples of phosphorus containing compounds: (A) phosphate, (B) phosphite, (C) phosphonate, and (D) phosphinate. R, R' = any. R" = C or H.

1.1.1 Isolation and distribution of natural organophosphonates

Phosphate is of central importance in cellular metabolism and is a vital nutrient required for sustaining life. It is a key component of cellular structures, energy storage, and is involved in mediating cellular signaling pathways. For instance, phosphate is found in, but not limited to, the backbone of DNA and RNA, high energy compounds (ATP, phosphoenolpyruvate) and is involved in enzyme catalysis through such things as phosphorylation, or as part of a cofactor, such as pyridoxyl phosphate. Within biological systems phosphorus is typically found bound to four oxygen atoms in its fully oxidized state as seen in Figure 1-1A, either as inorganic phosphate (P_i) or as phosphate organic esters, amides and anhydrides. However, in 1959 the first known naturally occurring organophosphonate, 2-aminoethylphosphonic acid (AEP, **1g**, Figure 1-2), was isolated from sheep rumen protozoa[1,2], where a carbon atom replaces one of the usually bonded oxygen atoms to form a CP bond (Figure 1-1C). Originally it was hyothesized that the CP bond

of aminoalkylphosphonic acids was unstable. In the late 40s aminocarboxylic acids were known to be distributed in all organisms and taurine (2-aminoethane sulfonic acid) was also found in many organisms. However, aminoalkylphosphonic acids were not recognized in nature; Chavane and Hackspill suspected that their absence in nature was dependent on the instability of the CP bond[3,4]. Chavane and Hackspill's investigations of the properties of synthetic aminophosphonic acids illustrated that the CP bond was sufficiently stable for isolation[3,4]. Further investigation demonstrated that the CP bond is in fact highly resistant to chemical hydrolysis, thermal decomposition[5], photolysis[6] and phospholipases[7].

After the discovery of AEP from rumen protozoa, organophosphonates have since been detected in many phyla ranging from lower plants to the animal kingdom, and have even been identified in human brain, liver, heart and skeletal muscle[7]. Organophosphonates are commonly found as phosphonolipids[7-9], where the head group such as phosphocholine is replaced by an analogous organophosphonate[7-9], but have also been found as components of polysaccharides[10], glycoproteins[11], glycolipids[11] and as small bioactive molecules[12,13]. Bioactive organophosphonates have become greatly important in medicine and agriculture. The majority of these molecules are produced by actinobacteria but many other microbes can also synthesize CP bond containing compounds (see section 1.2). Some important natural bioactive organophosphonates include antibiotics, such as fosfomycin, dehydrophos, and the plumbemycins; herbicides, such as phoshinothricin tripeptide (PTT) and phosphonothrixin; antimalarial compounds, such as fosmidomycin and FR-900098 (Figure 1-2).

In some organisms, organophosphonates have been shown to account for a large percentage of the total phosphorus content. For example, in the eggs of *Helisoma*, freshwater snails, organophosphonates in the form of modified phosphonoglycans compose 95% of the overall phosphorus content[14], and in *Tealia*, a sea anemone, 30% of the total phosphorus is found as organophosphonates[15,16]. Although organophosphonates have been detected in a wide

spectrum of organisms not all of these organisms have been shown to synthesize organophosphonates. Most organisms acquire organophosphonates through their diets and then incorporate these organophosphonates into their biological material[17].

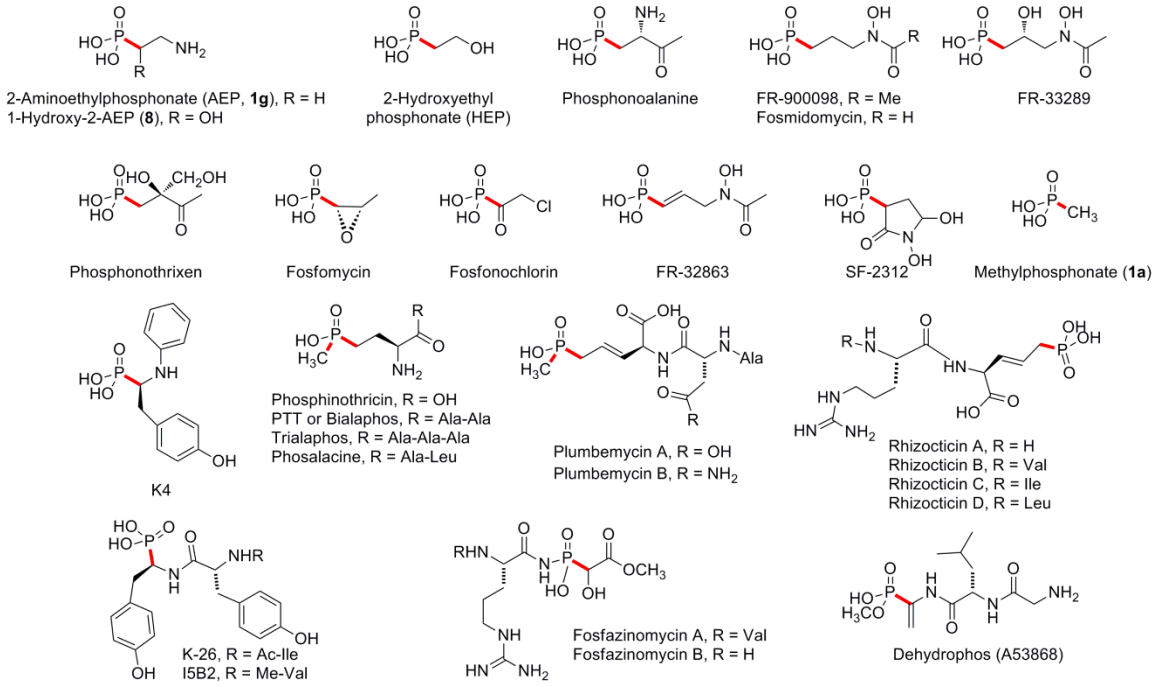

Figure 1-2. Naturally occurring organophosphonate and phosphinates. The CP bonds are shown in red. Figure adapted from reference 13.

It is important to note that phosphorus is commonly a growth limiting nutrient in some terrestrial ecosystems and its scarcity is greater in aquatic ecosystems[18,19]. The P_i concentration can be very low in some ocean gyres causing phosphorus-limited ecosystems[20]. In conjunction there has been an increase in dissolved organic phosphorus, consisting of phosphate esters, polyphosphates and organophosphonates in the marine environment relative to that of P_i, and therefore dissolved organic phosphorus is thought to be a significant source of phosphorus for marine microbes[21-25]. An example is the North Pacific subtropical gyre, which contains 80% of total soluble phosphorus as dissolved organic phosphorus[21]. Although difficult to analyze, due to the lack of appropriate analytical techniques, ^{31}P-NMR spectroscopy studies indicate that

organophosphonates encompass 20 – 30 % of the composition of dissolved organic phosphorus[26,27] and thus play an important role in the marine environment. In addition many strains of Gram positive and Gram negative bacteria, including *Escherichia coli*, are capable of using organophosphonates as their sole P_i source and are able to cleave the CP bond[7,17,28], thereby liberating P_i.

1.1.2 Bioactivity of organophosphonates

Although the biological role of organophosphonate incorporation into cellular structure is not understood, the bioactivity of organophosphonates has been fairly well studied. Organophosphonates and phosphinates can structurally mimic phosphate esters, carboxylic acids and tetrahedral intermediates formed during transformations of carbonyl groups, yet the CP bond makes them almost chemically inert. These properties allow for organophosphonates to act as potent enzyme inhibitors by competing for enzyme active sites with structurally similar substrates, and then remain unchanged due to the unreactive nature of the CP bond. The ubiquitous presence of phosphate esters, carboxylic acids and carbonyl chemistry in cellular metabolism and signaling pathways, enables organophosphonates to serve as inhibitors for an array of processes, including regulatory events. The usefulness of organophosphonates unique properties has not been overlooked, with both manmade and natural organophosphonates having found widespread use in the medicinal and agricultural industries.

Some examples of commercial natural organophosphonates are fosfomycin and bialaphos, shown in Figure 1-2. Fosfomycin is an effective antibiotic which inhibits the biosynthesis of UDP-*N*-acetylmuramic acid, an essential component for cell wall formation[12,29]. It does this by inactivating UDP-*N*-acetyl-glucosamine-3-*O*-enolpyruvyltransferase by covalent alkylation of an active site cysteine[30,31]. A derivative of fosfomycin is an FDA approved drug for the treatment of urinary tract infection and is sold under the name of Monurol®[32-35].

Phosphinothricin (PT) is a glutamate analog that mimics the tetrahedral intermediate formed during glutamine biosynthesis[36,37] and inhibits glutamine synthetase[38] causing the buildup of ammonia, killing the plant. PT and its derivatives have been widely used as herbicides[39], such as in Basta® (Hoechst AG, Germany). The resistance mechanism used by the producing organism during the biosynthesis of PT has been indentified[40,41] and developed as a selectable marker for genetically engineered plants, making Basta® a very useful herbicide. In addition recombinant plants paired with the use of PT are significantly used in agriculture[13]. Although it has found wide use as a herbicide, PT is not transported into cells, making it an ineffective antibiotic. To circumvent this problem, PT is incorporated as a component of many small peptides, such as bialaphos (PTT), trialaphos, and phosalacine (Figure 1-2). Once in the cell it undergoes proteolysis releasing the active form of the antibiotic. Antibiotics that use this method of cellular entry, followed by activation are known as Trojan horse antibiotics[42-45]. Other Trojan horse organophosphonate antibiotics include dehydrophos, and the plumbemycin and rhizocticin families that are hydrolyzed to form acetylphosphonate methyl ester and 2-amino-5-phosphono-3-*cis*-pentenoic acid (APPA), respectively. Acetylphosphonate methyl ester inhibits pyruvate oxidase and dehydrogenase[46,47] where APPA inhibits threonine synthase[48,49].

1.1.3 Synthetic organophosphonates and their environmental impact

The synthetic chemistry of organophosphonates has developed more slowly than that of organophosphate esters due to the difficulty of CP bond formation. The Michaelis-Arbuzov reaction is the most commonly used method for the synthesis of organophosphonates. This reaction was originally discovered in 1898 by August Michaelis[50] and extensively studied by Aliksandr Arbuzov in the early 20th century[51]. The reaction involves an alkyl halide treated with a trivalent trialkyl phosphite, which after substitution undergoes rearrangement to form an organophosphonate (Figure 1-3A). Several other approaches exist for the synthesis of the CP

bonds, with the Abramov, Pudovik, and Michaelis-Becker being the most well studied[52] (Figure 1-3B, C, and D). For more in depth information of the synthesis of organophosphonates please see reference 52. α-Aminophosphonic acids have recently drawn attention for their biological importance as medicinal compounds[53]. The first known method to synthesize α-aminophosphonic acids was discovered by Kabachnik and Fields in 1952[54-56], and this reaction has become important in drug discovery[57].

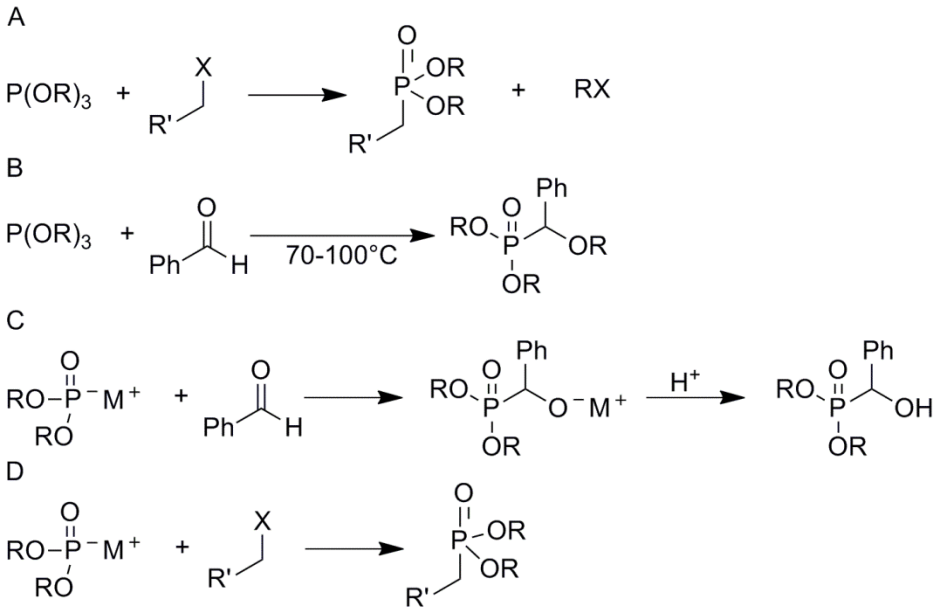

Figure 1-3. CP bond forming reactions: (A) Michaelis-Arbuzov, (B) Abramov, (C) Pudovik, and (D) Michaelis-Becker reactions.

Phosphoryl transfer reactions are prevalent in nature. Because the CP bond is not susceptible to cleavage by enzymes that catalyze phosphoryl transfer reactions (e.g. hydrolysis, phosphorylation, etc.) synthetic organophosphonates have been developed as antibacterial, antiviral, and antitumor agents, as mentioned in the above section. Many synthetic organophosphonates are also widely used in agricultural, and pharmaceutical industries. One of the most commonly used synthetic organophosphonate is the herbicide glyphosate (also known as Round-up®, Monsanto Company, Missouri, USA), which inhibits 5-enolpyruvylshikimic acid 3-

phosphate synthase[58], a critical enzyme involved in the biosynthesis of aromatic amino acids in plants. Examples of pharmaceutically important synthetic organophosphonates include alendronate (Figure 1-4), which is used to treat osteoporosis[59], adefovir, an inhibitor of hepatitis B reverse transcriptase[60,61], and tenofovir, an inhibitor of HIV reverse transcriptase [61,62]. The application of organophosphonates is not limited to biologically active compounds. They have also found important roles in an array of industries as chelating agents[63,64], corrosion inhibitors, water softeners, fire retardants[65], as well as stabilizers in the pulp, paper and textile industry[66]. In addition to this organophosphonates have been developed for more obscure uses such as adhesives for orthodontics, such as Panavia® (J. Morita, Kuraray Co., Osaka, Japan), an organophosphonated BIS-GMA resin[67]. The high aqueous solubility of organophosphonates has made them frequent additives to detergents for sequestering metals, such as 1-hydroxyethane(1,1-diylbisphosphonic acid) (Figure 1-4)[68]. They have also been developed as chemical warfare agents such as sarin and VX (Figure 1-4), which are acetylcholine esterase inhibitors[69].

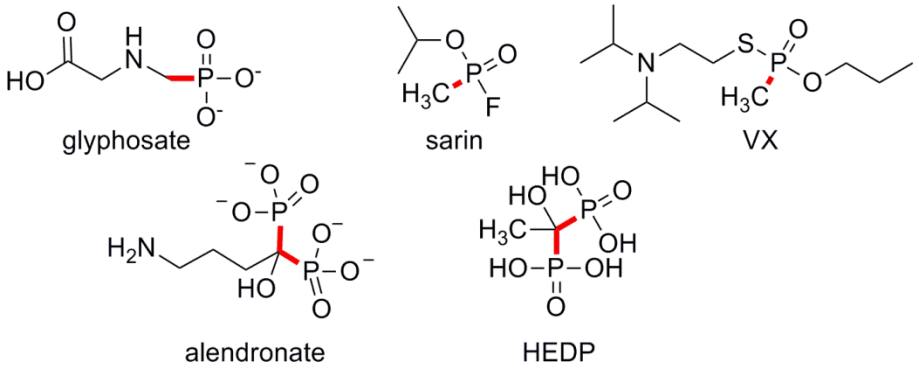

Figure 1-4. Examples of synthetic organophosphonates. The CP bonds are shown in red. Glyphosate is a herbicide, sarin and VX are chemical warfare agents, alendronate is a medicinal compound and HEDP (1-hydroxyethane(1,1-diylbisphosphonic acid)) is used in detergents, for water treatment and is found in cosmetics.

Organophosphonates are important economically, the estimated export and import of organophosphonates in the world market for 2005 was over $90 million USD[70]. Many of the economically important organophosphonates are characterized by the stability of the CP bond and

over 55,000 tonnes of organophosphonates are released into the environment annually[68,71,72]. With the large amounts of synthetic organophosphonates entering the environment, concerns over ecotoxicity and eutrophication have risen[19]. In addition, aminomethylphosphonate (AMPA, **1f**) which is a biological degradation product of the herbicide glyphosate and of detergent chelating agents aminotrimethylene phosphonic acid, ethylenediaminetetra(methylene phosphonic acid) and diethylenetriaminepenta(methylene phosphonic acid)[68], has been shown to cause teratogenic effects in vertebrates[73]. Accordingly, there has been growing interest in studying the environmental impact of organophosphonates[66,68,69,74,75]. However, analysis is still a challenge due to the difficulty in concentrating and isolating organophosphonates from complex mixtures, primarily due to their lack of chromophores and high aqueous solubility. Therefore the environmental fate of many organophosphonates is largely unknown[76-78]. Many researchers are also exploring the biodegradation of organophosphonates to understand their mechanisms and potentially harness these pathways for bioremediation strategies.

1.2 Biosynthesis of organophosphonates

After the isolation of 2-aminoethylphosphonate (AEP, **1g**) from sheep ruman, there followed the discovery of many other organophosphonates from a variety of organisms (see section 1.1.1). In many cases the organophosphonates were assimilated through dietary sources. However, the biosynthesis of some organophosphonates has been illuminated over the past 55 years.

Early labeling studies using ^{14}C labelled glucose and ^{32}P labelled phosphoenolpyruvate (PEP) revealed that AEP was derived from PEP[79-81]. It was shown that the C1 and C2 of AEP came from the C3 and C2 of PEP, respectively (Figure 1-5)[81]. On this basis it was proposed that an intramolecular rearrangement of PEP occurred to form phosphonopyruvate (PnPy), and thus creating a CP bond. However, it was another 20 years before the enzyme responsible for

catalyzing this reaction was identified[82-85]. In 1988 PEP phosphomutase (PepM) was discovered through the pioneering work of Seto and coworkers, where they studied the reverse rearrangement reaction (PnPy → PEP)[83,84]. This approach enabled them to detect PEP using a coupled enzyme assay involving pyruvate kinase and lactate dehydrogenase. It was shown that the equilibrium of the reaction carried out by PepM strongly favours the phosphorus-oxygen bond of PEP, rather than the CP bond of PnPy ($K_{eq} < 0.002$)[82]. This unfavourable equilibrium towards forming the CP bond contributed to the long struggle to isolate PepM.

The PepM reaction occurs with retention of stereochemistry at the phosphorus atom[86,87]. A proposed mechanism involving the formation of a phosphoenzyme intermediate via inversion of configuration followed by attack of the pyruvate enolate onto the phosphoenzyme intermediate again with inversion of configuration with a net retention of stereochemistry was investigated. However, intermediate trapping and enzyme variant experiments[88-90] have so far been unable to support this mechanism. A second and more recently proposed mechanism for PepM presumes that the reaction proceeds through a dissociative process forming a metaphosphate intermediate (Figure 1-5)[88]. The metaphosphate would have to be held in place by amino acids in the active site to allow for the pyruvate enolate to rotate around the C1-C2 bond. After rotation the metaphosphate would undergo nucleophilic attack from C3. This mechanism accounts for the retention in configuration and would be the first example of such a reaction.

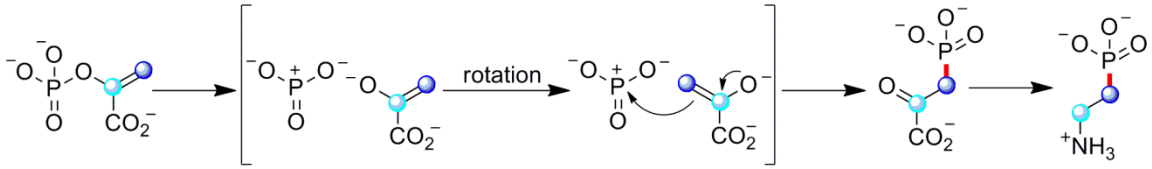

Figure 1-5. The proposed dissociative mechanism of CP bond formation by PepM. C2 and C3 of PEP are highlighted with light and dark blue circles, respectively. Adapted from reference 88.

It is only recently that some organophosphonate biosynthetic pathways have been fully characterized. In the vast majority of these pathways the CP bond of the organophosphonate arises from the PepM reaction[13,82-85]. To offset the favoured reverse reaction, these biosynthetic pathways also require an enzyme that effectively consumes PnPy as it is being produced. Thus, in the biosynthesis of fosfomycin, dehydrophos, phosphinothricin, rhizocticin, plumbemycin, MePn and AEP, PnPy is converted in an irreversible reaction to phosphonoacetaldehyde (PnAA) by phosphonopyruvate decarboxylase (Figure 1-6). However, in the biosynthesis of FR-900098 there is an enzyme that catalyzes an exergonic condensation of acetyl-CoA and PnPy to form 2-phosphonolethylmalate (Figure 1-6). There is also evidence for an alternative CP bond formation reaction. It has been shown that the biosynthesis of K-26 utilizes tyrosine to form a CP bond rather than PEP[91,92]. This suggests that another CP bond forming enzyme exists. Currently the biosynthetic pathways of fosfomycin, phosphinothricin, FR-900098, rhizocticin and MePn have been elucidated in the greatest detail. Biochemical studies have revealed the functions of many of the biosynthetic enzymes, allowing the reconstruction of partial or complete biosynthetic pathways (Figure 1-6). The biosynthesis of organophosphonates has been reviewed in references 13, 45, 93, and 94.

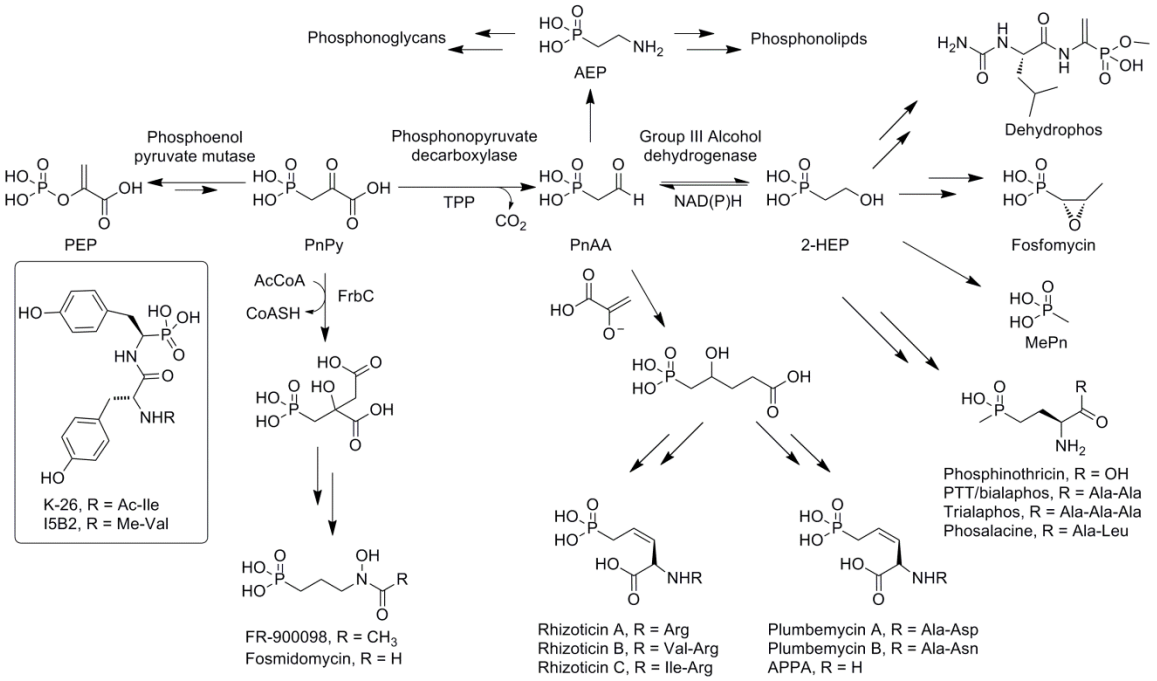

Figure 1-6. Outline of known biosynthetic pathways that form organophosphonate and phosphinate natural products. The biosynthetic routes for K-26 and I5B2 (boxed) are unknown. Abbreviations: 2-HEP, 2-hydroxyethylphosphonate; AEP, 2-aminoethylphosphonate; APPA, 2-amino-5-phosphono-3-*cis*-pentenoic acid; MePn, methylphosphonate; PEP, phosphoenolpyruvate; PnAA, phosphonoacetaldehyde; PnPy, phosphonopyruvate; PTT, phosphinothricin tripeptide; TPP, thiamine pyrophosphate. Figure adapted from reference 45.

The most recent biosynthetic pathway elucidated is that of MePn[95,96]. The catabolism of MePn by marine microbes has been linked to the release of methane[28]. However, until now MePn was not a known natural product. Metcalf and coworkers have shown that *Nitrosopumilus maritimus* contains a biosynthetic pathway that produces cell-associated MePn esters[95,96]. *N. maritimus* synthesizes MePn from PEP in a four-step process (Figure 1-6). The first three steps lead to a common organophosphonate biosynthetic intermediate, 2-hydroxyethylphosphonate (2-HEP). The fourth and final step involves the asymmetric oxidation of 2-HEP to MePn, which is catalyzed by a methylphosphonate synthase (MPnS)[95,96]. MPnS is a non-heme iron dependent oxygenase that performs the unprecedented reaction of cleaving an unactivated carbon-carbon

bond[95,96]. It is worth mentioning that biosynthetic gene clusters of CP bond containing natural products tend to possess enzymes that catalyze novel reactions.

Recent discoveries have led to a better understanding of the biosynthesis of organophosphonates as well as the discovery of unprecedented biochemical reactions, but there is still much to learn. In addition to synthesizing organophosphonates many organisms can metabolize organophosphonates and utilize them as a sole source of P_i. Much has been learned about these metabolic pathways in recent years and this is the main focus of this thesis.

1.3 Biodegradation of organophosphonates

The acquisition and assimilation of phosphorus is of fundamental importance. The preferred source of phosphorous for microorganisms is P_i. When P_i enters the cell it is captured in metabolic reactions and phosphate esters are generally formed through phosphoryl anhydride intermediates. The acquisition of P_i has been extensively studied. Initially, it was thought that in the presence of a rich P_i environment bacteria sequestered P_i by the low affinity 'phosphate inorganic transporter' PitA[97] whereas at low levels, P_i would enter the cell through the phosphate specific transporter, Pst. Pst is a member of the phosphate regulon (Pho regulon) which consists of P_i starvation-inducible (*psi*) genes that are expressed at low P_i levels[97]. However, recent studies indicate that PitA's primary role is to transport divalent metal cations (Zn^{2+}) complexed with P_i[98] and that Pst is the primary P_i transporter at both high and low concentrations of available P_i[99]. To allow for more effective uptake of P_i in limiting P_i environments ($< 10^{-6}$ M), expression of the Pst transporter is increased 100-fold[97].

When P_i is limited, some microorganisms can also use phosphate esters and organophosphonates, which are widespread in nature, as alternative sources of P_i. It took less than five years after the discovery of a naturally occurring organophosphonate to find a bacterium capable of degrading such compounds. *E. coli* was the first bacterium shown to competently

grow on methyl- and ethylphosphonic acids[100]. Later it was shown that many microorganisms, mainly bacteria, are able to degrade a variety of organophosphonates[7,28,101,102]. In these organisms, low P_i concentrations activate the Pho regulon, which in turn increases expression of *psi* genes necessary to extract P_i from organophosphate and organophosphonate sources. Phosphate esters rarely enter the cell intact but instead are degraded in the periplasm (in the case of Gram-negative bacteria), allowing the released P_i to be transported into the cell via Pst[97]. It should be noted that certain organophosphonates are proposed to use other normal transport systems. For example, *Streptococcus faecalis* is thought to use the high affinity transport system for aspartate and glutamate to transport phosphonoalanine[7]. Likewise, *E. coli* may use the glycerol-3-phosphate transport system to sequester 3,4-dihydroxybutylphosphonate, and *Streptomyces typhimurium* requires the presence of a functional aromatic amino acid permease to take up organophosphonate analogues of phenylalanine and tyrosine[7]. Additional evidence shows that 289 bacterial strains that possess genes associated with a known organophosphonate degradation pathway have no evidence of possessing the organophosphonate transporter induced by the Pho regulon[25]. This means that although the Pst transporter is the main transporter for phosphorus containing compounds, microorganisms are able to utilize other transporters for such compounds.

The first CP bond cleaving reaction related to organophosphonate degradation was identified in a metabolic pathway beginning with AEP. The pathway begins with a transamination reaction, catalyzed by the pyridoxal phosphate (PLP) dependent enzyme AEP-pyruvate aminotransferase, that converts AEP to 2-phosphonoacetaldehyde (PAA) (Figure 1-7A)[78,103-105]. Subsequently a Mg^{2+} dependent phosphonoacetaldehyde hydrolase (also known as phosphonatase) catalyzes the hydrolysis of the CP bond to form acetaldehyde and P_i (Figure 1-7A)[106-108]. In most bacterial species where this pathway is found, it is regulated by the Pho regulon with the exception of *Pseudomonas putida* NG2 where it is regulated in response to the

presence of AEP[77,109,110]. The CP bond cleaving enzyme in this pathway, phosphonoacetaldehyde hydrolase, is a member of the 2-haloalkanoic acid dehalogenase (HAD) family, and this family of enzymes is hypothesized to be metal-activated[111].

The CP bond cleavage mechanism of phosphonacetaldehyde hydrolase involves a lysine in the active site, which reacts with the aldehyde moiety of PAA to form a protonated Schiff base. This covalent intermediate acts as an electron sink that facilitates CP bond cleavage. The coordination to Mg^{2+} helps bind, orient and polarize the substrate for nucleophilic attack[111]. The hydrolytic CP bond cleaving step is promoted by nucleophilic attack by the carboxylate of an aspartate residue in the active site, to form an acyl-phosphate intermediate. Thus this enzyme employs two forms of nucleophilic catalysis to cleave a CP bond. Both covalent intermediates are subsequently hydrolyzed to give acetaldehyde and P_i. (Figure 1-7B)[108,109,112-115].

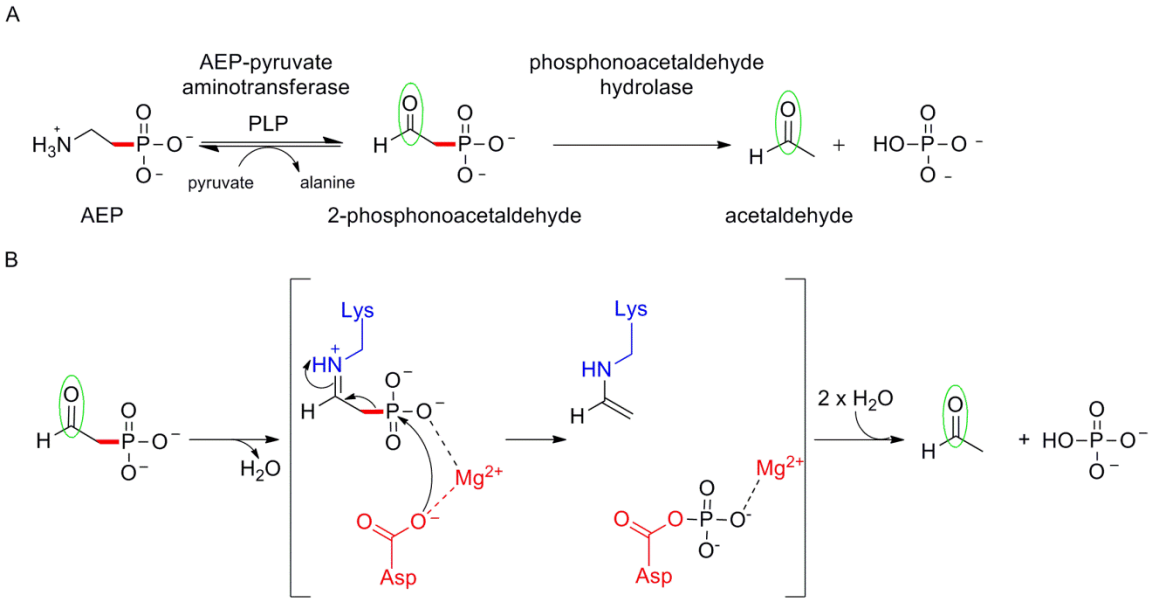

Figure 1-7. The metabolism of AEP by phosphonoacetaldehyde hydrolase. (A) Reaction scheme. (B) Mechanism. PLP-pyridoxal phosphate.

Since the discovery of phosphonoacetaldehyde hydrolase two other CP bond cleaving enzymes that employ similar electron sink mechanisms have been identified (Figure 1-10). Phosphonoacetate hydrolase degrades phosphonoacetate, an antiviral antibiotic, to acetate and P_i

allowing the utilization of phosphonoacetate as a sole carbon and phosphorus source[116,117]. This enzyme is not under the control of P_i concentration (or the Pho regulon), but instead has been demonstrated to be induced by the presence of its substrate phosphonoacetate[77], although it seems that the presence of glucose does have a regulatory role[116]. After the analysis of gene sequences phosphonoacetate hydrolase was found to be a part of a three step pathway that degrades AEP (Figure 1-10) in *Sinorrhizobium meliloti* 1021 and is likely not limited to this strain due to the detection of homologous gene clusters in other genomes[118].

Phosphonoacetate hydrolase is Zn^{2+} dependent, and performs a metal-ion assisted hydrolytic cleavage reaction. Two groups propose similar mechanisms with different leaving group stabilization strategies during the reaction[119,120]. The CP bond cleavage is hypothesized to proceed through an in-line double displacement mechanism (Figure 1-8). The first step involves a Zn^{2+} stabilized alkoxide ion of a threonine side chain that attacks the phosphorus atom, which leads to the formation of a covalent phosphoenzyme intermediate. Attack by a Zn^{2+} bound hydroxide on the phosphorus atom hydrolyses the intermediate displacing the threonine side chain. However the stabilization of the developing negative charge on the leaving group is currently under debate. In the crystal structure of phosphonoacetate hydrolase from *Sinorrhizobium meliloti* the substrate appears to be stabilized by the second Zn^{2+} ion in the active site[120] whereas the crystal structure from *Pseudomonas fluorescens* has two lysine residues close enough to aid in stabilization[119]. Site-directed mutagenesis of the conserved lysine residues of the enzyme from both strains led to loss of activity[119,120] but this does not specify direct involvement of the lysine residues in leaving group stabilization. Further investigation is required to distinguish between the two methods of leaving group stabilization.

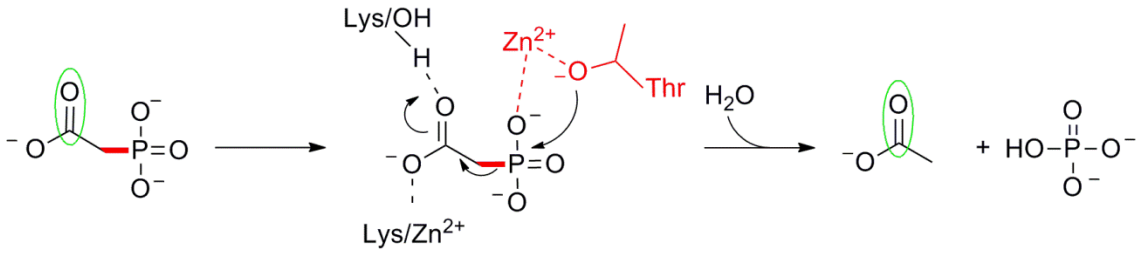

Figure 1-8. The mechanism of phosphonoacetate hydrolase.

PepM, was thought to be the only enzyme capable of cleaving the CP bond of phosphonopyruvate[85] until phosphonopyruvate hydrolase was discovered. L-Phosphonoalanine, an organophosphonate naturally synthesized by some sea anemones and protozoa, can be utilized as the sole nitrogen, carbon and/or phosphorus source in some microorganisms[121122]. L-Phosphonoalanine is not a substrate of phosphonacetaldehyde hydrolase or phosphonoacetate hydrolase and therefore another enzyme for CP bond cleavage must be required. This enzyme is phosphonopyruvate hydrolase, which hydrolyzes phosphonopyruvate to yield pyruvate and P_i[121] (Figure 1-10), which can be used directly as nutrient sources. Similar to phosphonoacetate hydrolase, phosphonopyruvate hydrolase is not under the control of the Pho regulon but rather requires induction by its substrate phosphonopyruvate or by one of phosphonopyruvate's precursors, L-phosphonoalanine[121,123]. Phosphoalanine is a component of phosphonolipids and can be found in both protein and glycoprotein complexes, formed by transamination of phosphonopyruvate[124].

Phosphonopyruvate hydrolase has a 41% sequence identity with the CP bond forming enzyme PepM. The two enzymes are theorized to follow through a similar mechanism with the divergence in substrate selectivity caused by a single amino acid substitution (asparagine versus threonine) in the active site[125]. The two enzymes require coordination to a divalent metal ion for activity; Zn^{2+} activates PepM but not phosphonopyruvate hydrolase, while Mg^{2+}, Mn^{2+} and Co^{2+} activate both enzymes[125]. A dissociative mechanism is proposed for PepM, with a pyruvate

enolate and metaphosphate intermediate that requires a rotation around the C1-C2 in the second step (Figure 1-5). The crystal structure of phosphonopyruvate points towards similar intermediates and mechanism, however it would not require rotation around the C1-C2 bond (Figure 1-9)[125]. In addition there is room in the active site of the hydrolase for retention of a water molecule, if positioned between the threonine residue and the phosphoryl group it would be activated for nucleophilic attack on the metaphosphate intermediate[125].

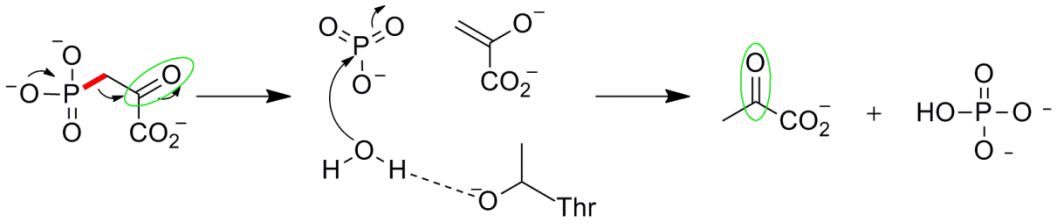

Figure 1-9. The mechanism of phosphonopyruvate hydrolase.

The three hydrolase enzymes have either been found as part of an organophosphonate catabolism pathway or can easily fit into such a pathway for the degradation of a common natural organophosphonate (Figure 1-10). Although all three phosphonohydrolases use an activating β-carbonyl to polarize the CP bond for cleavage, each enzyme has a unique substrate and they are all members of separate enzyme superfamilies. As mentioned previously, phosphonoacetaldehyde is a member of the HAD superfamily, whereas phosphonoacetate hydrolase and phosphonopyruvate hydrolase are members of the alkaline phosphatase metalloenzyme superfamily[126] and the phosphoenolpyruvate phosphomutase/isocitrate lyase superfamily[123], respectively. Each enzyme takes advantage of the β-carbonyl electron sink in different ways. Phosphonoacetaldehyde hydrolase uses it to generate a Schiff base intermediate activating the CP bond and for stabilizing a developing negative charge on the carbon via resonance. Phosphonoacetate hydrolase and phosphonopyruvate hydrolase use the carbonyl to delocalize the developing negative charge on the leaving group in either a displacement or dissociative mechanism, respectively.

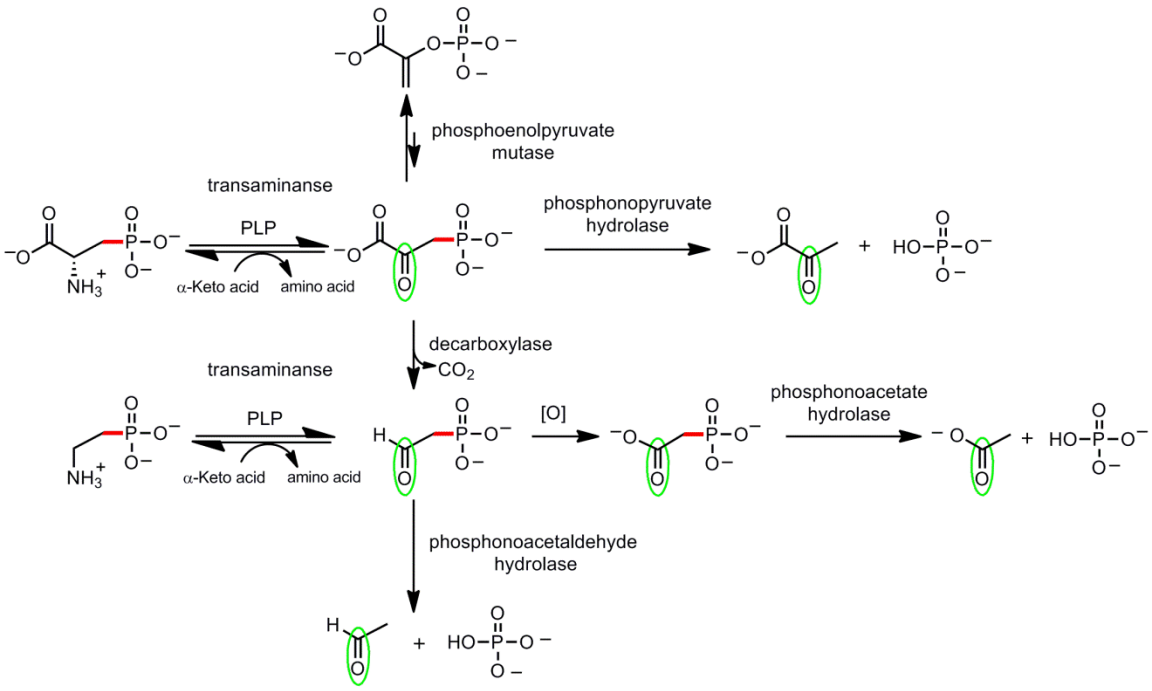

Figure 1-10. Overview of catabolic pathways that lead to enzymes that use the 'electron-sink' mechanism to cleave CP bonds.

The enzymes described above are limited to cleaving the CP bonds of substrates that have carbonyl groups beta to the phosphorus atom, and each of the enzymes has high substrate specificity. However, it was known that some bacteria, such as *E. coli*, could degrade 'unactivated' alkyl- and aryl-phosphonates (i.e. substrates lacking a β-carbonyl). Therefore another CP bond cleaving enzyme must exist. Further investigations of organophosphonate degradation led to the discovery of the multi-enzyme pathway called CP-lyase[127]. CP-lyase has been shown to cleave a broad range of substrates of alkyl- and aryl-phosphonates under limited P_i conditions (Figure 1-11). However due to the continued inability to show activity in cell free extracts, the mechanism of CP bond cleavage was only recently characterized.

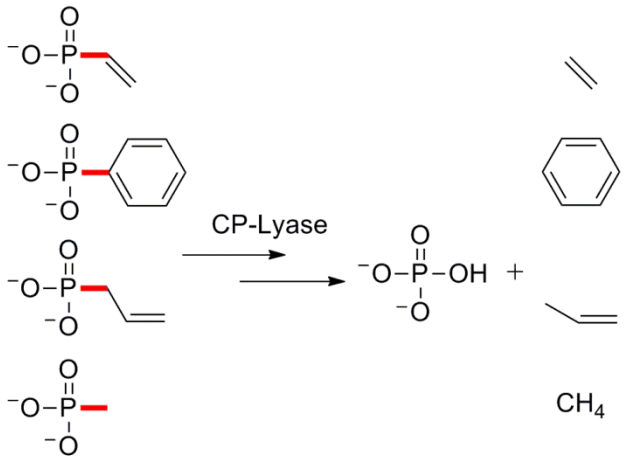

Figure 1-11. Examples of organophosphonates degraded by CP-lyase. CP bonds are shown in red.

Finally, a new organophosphonate degrading pathway was identified through a functional screen of marine metagenomic DNA. As noted above, marine environments have very low P_i concentrations, and a large fraction (ca. 30%) of the dissolved organic phosphate that is present is composed of organophosphonates[24]. The genes identified in the screen encode a pair of enzymes, PhnY and PhnZ, which allow for the production of P_i from AEP[24]. Based on amino acid sequence homology it was clear that PhnY and PhnZ used very different chemistry to cleave a CP bond to release P_i from an organophosphonate.

Degradation of organophosphonates usually requires limited P_i to induce uptake and expression of organophosphonate degrading genes, little P_i is found in the media after degradation, and organophosphonates do not accumulate in the cells[7,128,129]. For these reasons organophosphonate degradation, in most cases, is linked to P_i utilization. However, recent studies have shown that organophosphonate metabolism in both *Helicobacter pylori*[130] and *Campylobacter jejuni*[131] does not require P_i starvation, and the genomes of these organisms do not encode known organophosphonate degrading pathways. Genomic analyses reveal that 60% of strains capable of transporting organophosphonates into the cell have an apparent ability to degrade the CP bond[25]. On the other hand, 40% of the strains did not encode any known pathway

of organophosphonate degradation, suggesting that not all organophosphonate degradation pathways have yet been discovered[25].

In summary six enzymatic pathways for the cleavage of CP bonds have been established to date: i. phosphonoacetaldehyde hydrolase (phosphonatase, PhnX), ii. phosphonoacetate hydrolase (PhnA), iii. phosphonopyruvate hydrolase (PhnW); iv. PEP phosphomutase (PepM), the enzyme that catalyzes the interconversion of phosphoenolpyruvate and phosphonopyruvate; v. CP-lyase (*phn* operon), a multi-enzyme system that acts on a broad array of alkyl- and aryl-phosphonates; and vi. PhnY / PhnZ. The CP-lyase and PhnY / PhnZ reactions are of great interest from a mechanistic perspective, because these enzymes act on substrates that do not have a β-carbonyl group that facilitates direct heterolytic CP bond cleavage, and this is the topic of this thesis.

1.4 Objectives and thesis organization

Two of the six enzymatic pathways for cleavage of CP bonds, the CP-lyase pathway and the PhnY / PhnZ pathway have not been fully characterized. The objective of this thesis was to study these two pathways and contribute to the understanding of their mechanisms. Contributions to the CP-lyase pathway will be discussed further in Chapter 2. This includes the detection, isolation and characterization of pathway intermediates (Section 2.2); the characterization of PhnO and PhnY enzyme reactions (Section 2.2); and the isolation of a CP-lyase enzyme complex (Section 2.3). The elucidation of the PhnY and PhnZ pathway and studies towards the characterization of CP bond cleavage by this pair of enzymes will be covered in detail in Chapter 3.

1.5 References

1. Horiguchi, M.; Kandatsu, M. Isolation of 2-aminoethane phosphonic acid from rumen protozoa. *Nature* **1959**, *184*, 901-902.

2. Horiguchi, M.; Kandatsu, M. Ciliatine: a new aminophosphonic acid contained in rumen ciliate protozoa. *Bull. Agr. Chem. Soc. Japan* **1960**, *24*, 565-570.

3. Chavane, V.; Hackspill, L. Synthese de quelques acides phosphoniques amines de formule generale H_3N^+-$(CH_2)_n$-PO_3H^-. *C. R. Chim.* **1947**, *224*, 406-408.

4. Rumpf, P.; Chavane, V.; Hackspill, L. Etude electrochimique de quelques acides phosphoniques amines. *C. R. Chim.* **1947**, *226*, 919-920.

5. Freedman, L. D.; Doak, G. O. The preparation and properties of phosphonic acids. *Chem. Rev.* **1957**, *57*, 479-523.

6. Murai, T.; Tomizawa, C. Chemical transformation of S-benzyl O-ethyl phenylphosphonothiolate (Inezin) by ultraviolet light. *J. Environ. Sci. Health. B* **1976**, *11*, 185-197.

7. Hilderbrand, R. L. *The role of phosphonates in living systems;* CRC: 1983.

8. Kennedy, K. E.; Thompson, G. A. Phosphonolipids:Localization in surface membranes of *Tetrahymena*. *Science* **1970**, *168*, 989-991.

9. Moschidis, M. C. Phosphonolipids. *Prog. Lipid Res.* **1985**, *23*, 223-246.

10. Baumann, H.; Tzianabos, A. O.; Brisson, J.; Kasper, D. L.; Jennings, H. J. Structural elucidation of two capsular polysaccharides from one strain of *Bacteroides fragilis* using high-resolution NMR spectroscopy. *Biochemistry-US* **1992**, *31*, 4081-4089.

11. Hori, T.; Horiguchi, M.; Hayashi, A. *Biochemistry of natural CP compounds;* Kyoto Branch Publishing Service Maruzen: 1984.

12. Hendlin, D.; Stapley, E. O.; Jackson, M.; Wallick, H.; Miller, A. K.; Wolf, F. J.; Miller, T. W.; Chaiet, L.; Kahan, F. M.; Foltz, E. L.; Woodruff, H. B. Phosphonomycin, a new antibiotic produced by strains of streptomyces. *Science* **1969**, *166*, 122-123.

13. Metcalf, W. W.; van der Donk, W. A. Biosynthesis of phosphonic and phosphinic acid natural products. *Annu. Rev. Biochem.* **2009**, *78*, 65-94.

14. Miceli, M. V.; Henderson, T. O.; Myers, T. C. 2-Aminoethylphosphonic acid metabolism during embryonic development of the planorbid snail *Helisoma*. *Science* **1980**, *209*, 1245-1247.

15. Quin, L. D. The presence of the compounds with a carbon-phosphorus bond in some marine invertebrates. *Biochemistry-US* **1965**, *4*, 324-330.

16. Quin, L. D. In *The natural occurrence of compounds with the carbon–phosphorus bond;* Topics in phosphorus chemistry; John Wiley & Sons: New York, US, 1967; Vol. 4, pp 23-48.

17. White, A. K.; Metcalf, W. W. Microbial metabolism of reduced phosphorus compounds. *Annu. Rev. Microbiol.* **2007**, *61*, 379-400.

18. Sanchez, P. A. *Properties and management of soils in the tropics;* Wiley: New York, 1976; , pp 618.

19. Smil, V. Phosphorus in the environment: natural flows and human interferences. *Annu. Rev. Energy Environ.* **2000**, *25*, 53-88.

20. Karl, D. M.; Björkman, K. M.; Dore, J. E.; Fujieki, L.; Hebel, D. V.; Houlihan, T.; Letelier, R. M.; Tupas, L. M. Ecological nitrogen-to-phosphorus stoichiometry at station ALOHA. *Deep-Sea Research II* **2001**, *48*, 1529-1566.

21. Björkman, K. M.; Karl, D. M. Bioavailability of dissolved organic phosphorus in the euphotic zone at station ALOHA, North Pacific Subtropical Gyre. *Limnol. Oceanogr.* **2003**, *48*, 1049-1057.

22. Luo, H.; Benner, R.; Long, R. A.; Hu, J. Subcellular localization of marine bacterial alkaline phosphatases. *Proc. Natl. Acad. Sci. U. S. A.* **2009**, *106*, 21219-21233.

23. Luo, H.; Zhang, H. M.; Long, R. A.; Benner, R. Depth distributions of alkaline phosphatase and phosphonate utilization genes in the North Pacific Subtropical Gyre. *Aquat. Microb. Ecol.* **2011**, *62*, 61-69.

24. Martinez, A.; Tyson, G. W.; DeLong, E. F. Widespread known and novel phosphonate utilization pathways in marine bacteria revealed by functional screening and metagenomic analyses. *Environ Microbiol.* **2010**, *12*, 222-238.

25. Villarreal-Chiu, J. F.; Quinn, J. P.; McGrath, J. W. The genes and enzymes of phosphonate metabolism by bacteria, and their distribution in the marine environment. *Front. Microbiol.* **2012**, *3*, 1-13.

26. Clark, L. L.; Ingall, E. D.; Benner, R. Marine phosphorus is selectively remineralized. *Nature* **1998**, *393*, 426.

27. Clark, L. L.; Ingall, E. D.; Benner, R. Marine organic phosphorus cycling: novel insights from nuclear magnetic resonance. *Am. J. Sci.* **1999**, *2999*, 724-737.

28. Karl, D. M.; Beversdorf, L.; Björkman, K. M.; Church, M. J.; Martinez, A.; DeLong, E. F. Aerobic production of methane in the sea. *Nat. Geosci.* **2008**, *1*, 473-478.

29. Kahan, F. M.; Kahan, J. S.; Cassidy, P. J.; Kropp, H. The mechanism of action of fosfomycin (phosphonomycin). *Ann. N. Y. Acad. Sci.* **1974**, *235*, 364-386.

30. Marquardt, J. L.; Brown, E. D.; Lane, W. S.; Haley, T. M.; Ichikawa, Y.; Wong, C.; Walsh, C. T. Kinetics, stoichiometry, and identification fo the reactive thiolate in the inactivation of the UDP-GlcNAc enolpyruvoyl transferase by the antibiotic fosfomycin. *Biochemistry-US* **1994**, *33*, 10646-10651.

31. Kim, D. H.; Lees, W. J.; Kempsell, K. E.; Lane, W. S.; Duncan, K.; Walsh, C. T. Characterization of a Cys115 to Asp substitution in the *Escherichia coli* cell wall biosynthetic enzyme UDP-GlcNAc enolpyruvyl transferase (MurA) that confers resistance to inactivation by the antibiotic fosfomycin. *Biochemistry (N. Y.)* **1996**, *35*, 4923-4928.

32. Stein, G. Single-dose treatment of acute cystitis with fosfomycin tromethamine. *Ann. Pharmacother.* **1998**, *32*, 215-219.

33. Bailey, R. R. Brief overview of single-dose therapy for uncomplicated urinary-tract infections. *Chemotherapy* **1990**, *36*, 27-30.

34. Bailey, R. R. Management of lower urinary tract infections. *Drugs* **1993**, *45*, 139-144.

35. Reeves, D. S. Treatment of bacteriuria in pregnancy with single dose fosfomycin trometamol: A review. *Infection* **1992**, S313-S316.

36. Abell, L. M.; Villafranca, J. J. Investigation of the mechanism of phosphinothricin inactivation of *Escherichia coli* glutamine synthetase using rapid quench kinetic techniques. *Biochemistry-US* **1991**, *30*, 6135-6141.

37. Leason, M.; Cunliffe, D.; Parkin, D.; Lea, P. J.; Milflin, B. J. Inhibition of pea leaf glutamine synthetase by methionine sulphoximine, phosphinothricin and other glutamate analogues. *Phytochemistry* **1982**, *21*, 855-857.

38. Tebbe, C. C.; Reber, H. H. Utilization of the herbicide phosphinothricin as a nitrogen source by soil bacteria. *Appl. Microbiol. Biotechnol.* **1988**, *29*, 103-105.

39. Thompson, C. J.; Seto, H. Bialaphos. *Biotechnology* **1995**, *28*, 197-222.

40. Thompson, C. J.; Movva, N. R.; Tizard, R.; Crameri, R.; Davies, J. E.; Lauwereys, M.; Botterman, J. Characterization of theherbicide-resistance gene *bar* from *Streptomyces hygroscopicus*. *EMBO J.* **1987**, *6*, 2519-2523.

41. Wohlleben, W.; Arnold, W.; Broer, I.; Hillemann, D.; Strauch, E.; Pühler, A. Nucleotide sequence of the phosphinothricin N-acetyltransferase gene from *Streptomyces viridochromogenes* Tü494 and its expression in *Nicotiana tabacum*. *Gene* **1988**, *70*, 25-37.

42. Budzikiewicz, H. Siderophore-antibiotic conjugates used as trojan horses against *Pseudomonas aeruginosa*. *Curr. Top. Med. Chem.* **2001**, *1*, 73-82.

43. Möllmann, U.; Heinisch, L.; Bauernfeind, A.; Köhler, T.; Ankel-Fuchs, D. Siderophores as drug delivery agents: application of the "Trojan Horse" strategy. *Biometals* **2009**, *22*, 615-624.

44. Roush, R. F.; Nolan, E. M.; Löhr, F.; Walsh, C. T. Maturation of an *Escherichia coli* ribosomal peptide antibiotic by ATP-consuming N−P bond formation in microcin C7. *J. Am. Chem. Soc.* **2008**, *130*, 3603-3609.

45. Peck, S. C.; Gao, J.; van der Donk, W. A. In *Chapter Six - Discovery and biosynthesis of phosphonate and phosphinate natural products;* Methods in Enzymology; Academic Press: 2012; Vol. 516, pp 101-123.

46. Circello, B. T.; Miller, C. G.; Lee, J.; van der Donk, W. A.; Metcalf, W. W. The antibiotic dehydrophos is converted to a toxic pyruvate analog by peptide bond cleavage in *Salmonella enterica*. *Antimicrob. Agents. Ch.* **2011**, *55*, 3357-3362.

47. Kuemin, M.; van der Donk, W. A. Structure–activity relationships of the phosphonate antibiotic dehydrophos. *Chem. Commun.* **2010**, *46*, 7694-7696.

48. Laber, B.; Gerbling, K.; Harde, C.; Neff, K.; Nordhoff, E.; Pohlenz, H. Mechanism of interaction of Escherichia coli threonine synthase with substrates and inhibitors. *Biochemistry-US* **1994**, *33*, 3413-3423.

49. Kugler, M.; Loeffler, W.; Rapp, C.; Kern, A.; Jung, G. Rhizocticin A, an antifungal phosphono-oligopeptide of *Bacillus subtilis* ATCC 6633: biological properties. *Arch. Microbiol.* **1990**, *153*, 276-281.

50. Michaelis, A.; Kaehne, R. Ueber das Verhalten der Jodalkyle gegen die sogen. Phosphorigsäureester oder *O*-Phosphine. *Chem. Ber.* **1898**, *31*, 1048-1055.

51. Arbuzov, A. E. Glava IV. Izomeratsiya I perekhod soedinenii trekhatomnogo fosfora v soedineniya pyatiatomnogo. *Zh. Russ. Fiz-Khim.* **1906**, *37*, 687-721.

52. Engel, R.; Cohen, J. I. *Synthesis of carbon-phosphorus bonds;* CRC Press: Boca Raton, 2003; pp 187.

53. Naydenova, E. D.; Todorov, P. T.; Troev, K. D. Recent synthesis of aminophosphonic acids as potential biological importance. *Amino Acids* **2010**, *38*, 23-30.

54. Kabachnik, M. I.; Medved, T. Y. New method for the synthesis of 1-aminoalkylphosphonic acids Communication 1. *Russ. Chem. B+* **1952**, *2*, 769-777.

55. Medved, T. Y.; Kabachnik, M. I. New method for the synthesis of amnio phoshphonic aids. Communication 2. Reaction of ketones with dialkyl phosphites and ammonia. *Russ. Chem. B+* **1954**, *3*, 255-261.

56. Fields, E. K. The synthesis of esters of substituted amino phosphonic acids. *J. Am. Chem. Soc.* **1952**, *74*, 1528-1531.

57. Kafarski, P.; Lejczak, B. Aminophosphonic acids of potential medical importance. *Curr. Med. Chem. Anticancer Agents* **2001**, *1*, 301-312.

58. Steinrücken, H. C.; Amrhein, N. The herbicide glyphosate is a potent inhibitor of 5-enolpyruvylshikimic acid-3-phosphate synthase. *Biochem. Biophys. Res. Commun.* **1980**, *94*, 1207-1212.

59. Papapoulos, S. E. The role of bisphosphonates in the prevention and treatment of osteoporosis. *Am. J. Med.* **1993**, *95*, S48-S52.

60. De Clercq, E.; Holý, A.; Rosenberg, I.; Sakuma, T.; Balzarini, J.; Maudgal, P. C. A novel selective broad-spectrum anti-DNA virus agent. *Nature* **1986**, *323*, 464-467.

61. De Clercq, E.; Holý, A. Acyclic nucleoside phosphonates: a key class of antiviral drugs. *Nat. Rev. Drug Discov.* **2005**, *4*, 928-940.

62. Karim, Q. A.; Karim, S. S. A.; Frohlich, J. A.; Grobler, A. C.; Baxter, C.; Mansoor, L. E.; Kharsany, A. B. M.; Sibeko, S.; Mlisana, K. P.; Omar, Z.; Gengiah, T. N.; Maarschalk, S.; Arulappan, N.; Mlotshwa, M.; Morris, L.; Taylor, D. Effectiveness and safety of tenofovir gel, an antiretroviral microbicide, for the prevention of HIV infection in women. *Science* **2010**, *329*, 1168-1174.

63. Gumienna-Kontecka, E.; Jezierska, J.; Lecouvey, M.; Lerous, Y.; Kozlowski, H. Bisphosphonate chelating agents coordination ability of 1-phenyl-1hydroxymethylene bisphosphonate towards Cu^{2+} ions. *J. Inorg. Biochem.* **2002**, *89*, 13-17.

64. Bailly, T.; Burgada, R.; Prangé, T.; Lecouvey, M. Synthesis of tetradentate mixed bisphosphonates—new hydroxypyridinonate ligands for metal chelation therapy. *Tetrahedron Lett.* **2003**, *44*, 189-192.

65. Tai, Q.; Chen, L.; Song, L.; Nie, S.; Hu, Y.; Yuen, R. K. K. Preparation and thermal properties of a novel flame retardant copolymer. *Polym. Degrad. Stab.* **2010**, *95*, 830-836.

66. Nowack, B. Environmental chemistry of phosphonates. *Water Res.* **2003**, *37*, 2533-2546.

67. Lew, K. K. K.; Neo, J. C. L.; Chew, C. Shear bond strength of orthodontic brackets using panavia: an in-vitro study. *Clin. Mater.* **1993**, *12*, 89-93.

68. Jaworska, J.; Van Genderen-Takken, H.; Hanstveit, A.; van de Plassche, E.; Feijtek, T. Environmental risk assessment of phosphonates, used in domestic laundry and cleaning agents in the Netherlands. *Chemosphere* **2002**, *47*, 655-665.

69. Munro, N. B.; Talmage, S. S.; Griffin, G. D.; Waters, L. C.; Watson, A. P.; King, J. F.; Hauschild, V. The sources, fate, and toxicity of chemical warfare agent degradation products. *Environ. Health. Persp.* **1999**, *107*, 933-974.

70. Parker, P. M. The world market for phosphinates (hypophosphites) and phosphonates (phosphites): A 2005 global trade perspective. *ICON Group Ltd.* **2004**.

71. O'Loughlin, S. N.; Graham, R. L. J.; McMullan, G.; Ternan, N. G. A role for carbon catabolite repression in the metabolism of phosphonoacetate by *Agromyces fucosus* Vs2. *FEMS Microbiol. Lett.* **2006**, *261*, 133-140.

72. Jankowski, S.; Marczak, J.; Olczak, A.; Glowka, M. L. Stereochemistry of 1-hydroxyphosphonate-phosphate rearrangement. Retention of configuration at the phosphorus atom. *Tetrahedron Lett.* **2006**, *47*, 3341-3344.

73. Paganelli, A.; Gnazzo, V.; Acosta, H.; Lopez, S. L.; Carrasco, A. E. Glyphosate-based herbicides produce teratogenic effects on vertebrates by impairing retinoic acid signaling. *Chem. Res. Toxicol.* **2010**, *23*, 1586-1595.

74. Forlani, G.; Mangiagalli, A.; Nielsen, E.; Suardi, C. M. Degradation of the phosphonate herbicide glyphosate in soil: evidence for a possible involvement of unculturable microorganisms. *Soil Biol. Biochem.* **1999**, *31*, 991-997.

75. Stalikas, C. D.; Konidari, C. N. Analytical methods to determine phosphonic and amino acid group-containing pesticides. *J. Chromatogr. A* **2001**, *907*, 1-19.

76. Egli, T. (An)aerobic breakdown of chelating-agents used in household detergents. *Microbiol. Sci.* **1988**, *5*, 36-41.

77. Ternan, N. G.; Quinn, J. P. Phosphate starvation-independent 2-aminoethylphosphonic acid biodegradation in a newly isolated strain of *Pseudomonas putida*, NG2. *Syst. Appl. Microbiol.* **1998**, *21*, 346-352.

78. Ternan, N. G.; Mc Grath, J. W.; Mc Mullan, G.; Quinn, J. P. Review: Organophosphonates: occurrence, synthesis and biodegradation by microorganisms. *World J. Microb. Biot.* **1998**, *14*, 635-647.

79. Trebst, A.; Geike, F. On the biosynthesis of phosphonamino acids. The distribution of radioactivity in aminoethylphosphonic acid following incorporation of position-labelled glucose by *Tetrahymena*. *Z. Naturforsch* **1967**, *22*, 989-991.

80. Warren, W. A. Biosynthesis of phosphonic acids in T*etrahymena*. *Biochim. Biophys. Acta* **1968**, *156*, 340-346.

81. Horiguchi, M.; Kittredge, J. S.; Roberts, E. Biosynthesis of 2-aminoethylphosphonic acid in *Tetrahymena*. *Biochim. Biophys. Acta* **1968**, *165*, 164-166.

82. Bowman, E.; McQueney, M.; Barry, R. J.; Dunaway-Mariano, D. Catalysis and thermodynamics of the phosphoenolpyruvate/phosphonopyruvate rearrangement. Entry into the phosphonate class of naturally occuring organophosphorus compounds. *J. Am. Chem. Soc.* **1988**, *110*, 5575-5576.

83. Hidaka, T.; Mori, M.; Imai, S.; Hara, O.; Nagaoka, K.; Seto, H. Studies on the biosynthesis of bialaphos (SF-1293). 9. Biochemical mechanism of C-P bond formation in bialaphos: Discovery of phosphoenolpyruvate phosphomutase which catalyzes the formation of phosphonopyruvate from phosphoenolpyruvate. *J. Antibiot. (Tokyo)* **1989**, *42*, 491-494.

84. Hidaka, T.; Seto, H.; Imai, S. Biosynthetic mechanism of C-P bond formation. Isolation of carboxyphosphoenolpyruvate and its conversion to phosphinopyruvate. *J. Am. Chem. Soc.* **1989**, *111*, 8012-8013.

85. Seidel, H. M.; Freeman, S.; Seto, H.; Knowles, J. R. Phosphonate biosynthesis: isolation of the enzyme responsible for the formation of a carbon–phosphorus bond. *Nature* **1988**, *335*, 457-458.

86. Freeman, S.; Seidel, H. M.; Schwalbe, C. H.; Knowles, J. R. Phosphonate biosynthesis: The stereochemical course of phosphoenolpyruvate phosphomutase. *J. Am. Chem. Soc.* **1989**, *111*, 9233-9234.

87. McQueney, M. S.; Lee, S.; Swartz, W. H.; Ammon, H. L.; Mariano, P. S.; Dunaway-Mariano, D. Evidence for an intramolecular, stepwise reaction pathway for PEP phosphomutase catalyzed P-C bond formation. *J. Org. Chem.* **1991**, *56*, 7121-7130.

88. Liu, S.; Lu, Z.; Jia, Y.; Dunaway-Mariano, D.; Herzberg, O. Dissociative phosphoryl transfer in PEP mutase catalysis: Structure of the enzyme/sulfopyruvate complex and kinetic properties of mutants. *Biochemistry-US* **2002**, *41*, 10270-10276.

89. Kim, J.; Dunaway-Mariano, D. Phosphoenolpyruvate mutase catalysis of phosphoryl transfer in phosphoenolpyruvate: Kinetics and mechanism of phosphorus-carbon bond formation. *Biochemistry-US* **1996**, *35*, 4628-4635.

90. Jia, Y.; Lu, Z.; Huang, K.; Herzberg, O.; Dunaway-Mariano, D. Insight into the mechanism of phosphoenolpyruvate mutase catalysis derived from site-directed mutagenesis studies of active site residues. *Biochemistry-US* **1999**, *38*, 14165-14173.

91. Ntai, I.; Manier, M. L.; Hachey, D. L.; Bachmann, B. O. Biosynthetic origins of C-P bond containing tripeptide K-26. *Org. Lett.* **2005**, *7*, 2763-2765.

92. Ntai, I.; Phelan, V. V.; Bachmann, B. O. Phosphonopeptide K-26 biosynthetic intermediates in *Astrosporangium hypotensionis*. *Chem. Commun.* **2006**, *21*, 4518-4520.

93. Seto, H.; Kuzuyama, T. Bioactive natural products with carbon–phosphorus bonds and their biosynthesis. *Nat. Prod. Rep.* **1999**, *16*, 589-596.

94. Nair, S. K.; van der Donk, W. A. Structure and mechanism of enzymes involved in biosynthesis and breakdown of the phosphonates fosfomycin, dehydrophos, and phosphinothricin. *Arch. Biochem. Biophys.* **2011**, *505*, 13-21.

95. Metcalf, W. W.; Griffin, B. M.; Cicchillo, R. M.; Gao, J.; Janga, S. C.; Cooke, H. A.; Circello, B. T.; Evans, B. S.; Martens-Habbena, W.; Stahl, D. A.; van der Donk, W. A. Synthesis of methylphosphonic acid by marine microbes: a source for methane in the aerobic ocean. *Science* **2012**, *337*, 1104-1107.

96. Cooke, H. A.; Peck, S. C.; Evans, B. S.; van der Donk, W. A. Mechanistic investigation of methylphosphonate synthase, a non-heme iron dependent oxygenase. *J. Am. Chem. Soc.* **2012**, *134*, 15660-15663.

97. Metcalf, W. W.; Steed, P. M.; Wanner, B. L. Identification of phosphate starvation-inducible genes in *Escherichia coli* K-12 by DNA sequence analysis of psi::lacZ(Mu d1) transcriptional fusions. *J. Bacteriol.* **1990**, *172*, 3191-3200.

98. Beard, S. J.; Hashim, R.; Wu, G.; Binet, M. R. B.; Hughes, M. N.; Poole, R. K. Evidence for the transport of zinc(II) ions via the Pit inorganic phosphate transport system in *Escherichia coli*. *FEMS Microbiol. Lett.* **2000**, *184*, 231-235.

99. Hsieh, Y.; Wanner, B. L. Global regulation by the seven-component P_i signaling system. *Curr. Opin. Microbiol.* **2010**, *13*, 198-203.

100. Zeleznick, L. D.; Myers, T. C.; Titchener, E. B. Growth of *Escherichia Coli* on methyl- and ethylphosphonic acids. *Biochim. Biophys. Acta* **1963**, *78*, 546-547.

101. White, A. K.; Metcalf, W. W. Two C-P Lyase operons in *Pseudomonas stutzeri* and their roles in the oxidation of phosphonates, phosphite, and hypophosphite. *J. Bacteriol.* **2004**, *186*, 4730-4739.

102. Huang, J.; Su, Z.; Xu, Y. The evolution of microbial phosphonate degradative pathways. *J. Mol. Evol.* **2005**, *61*, 682-690.

103. Roseberg, H.; La Nauze, J. M. The metabolism of phosphanates by microorganisms. The transport of aminoethylphosphonic acid in *Basillus cereus*. *BBA Gen. Subjects* **1967**, *141*, 79-90.

104. La Nauze, J. M.; Rosenberg, H. The identification of 2-phosphonoacetaldehyde as an intermediate in the degradation of 2-aminoethylphosphonate by *Bacillus cereus*. *BBA Gen. Subjects* **1968**, *165*, 438-447.

105. Roberts, E.; Simonsen, D. G.; Horiguchi, M.; Kittredge, J. S. Transamination of aminoalkylphosphonic acids with alpha ketoglutarate. *Science* **1968**, *159*, 886-888.

106. La Nauze, J. M.; Rosenberg, H.; Shaw, D. C. The enzymic cleavage of the carbon-phosphorus bond: purification and properties of phosphonatase. *Biochim. Biophys. Acta* **1970**, *212*, 332-350.

107. Dumora, C.; Lacoste, A.; Cassaigne, A. Purification and properties of 2-aminoethylphosphonate: pyruvate aminotransferase from *Pseudomonas aeruginosa*. *Eur. J. Biochem.* **1983**, *133*, 119-125.

108. La Nauze, J. M.; Coggins, J. R.; Dixon, H. B. F. Aldolase-like imine formation in the mechanism of action of phosphonoacetaldehyde hydrolase. *Biochem. J.* **1977**, *165*, 409-411.

109. Baker, A. S.; Ciocci, M. J.; Metcalf, W. W.; Kim, J.; Babbitt, P. C.; Wanner, B. L.; Martin, B. M.; Dunaway-Mariano, D. Insights into the mechanism of catalysis by the P−C bond-cleaving enzyme phosphonoacetaldehyde hydrolase derived from gene sequence analysis and mutagenesis. *Biochemistry-US* **1998**, *37*, 9305-9315.

110. Lee, S.; Hepburn, T. W.; Swartz, W. H.; Ammon, H. L.; Mariano, P. S.; Dunaway-Mariano, D. Stereochemical probe for the mechanism of P-C bond cleavage catalyzed by the *Bacillus cereus* phosphonoacetaldehyde hydrolase. *J. Am. Chem. Soc.* **1992**, *114*, 7346(9)-7355.

111. Zhang, G.; Morais, M. C.; Dai, J.; Zhang, W.; Dunaway-Mariano, D.; Allen, K. N. Investigation of metal ion binding in phosphonoacetaldehyde hydrolase identifies sequence markers for metal-activated enzymes of the HAD enzyme superfamily. *Biochemistry-US* **2004**, *43*, 4990-4997.

112. Olsen, D. B.; Hepburn, T. W.; Lee, S.; Martin, B. M.; Mariano, P. S.; Dunaway-Mariano, D. Investigation of the substrate binding and catalytic groups of the P-C bond cleaving enzyme, phosphonoacetaldehyde hydrolase. *Arch. Biochem. Biophys.* **1992**, *296*, 144-151.

113. Olsen, D. B.; Hepburn, T. W.; Moos, M.; Mariano, P. S.; Dunaway-Mariano, D. Investigation of the *Bacillus cereus* phosphonoacetaldehyde hydrolase. Evidence for a Schiff base mechanism and sequence analysis of an active-site peptide containing the catalytic lysine residue. *Biochemistry-US* **1988**, *27*, 2229-2234.

114. Morais, M. C.; Zhang, W.; Baker, A. S.; Zhang, G.; Dunaway-Mariano, D.; Allen, K. N. The crystal structure of *Bacillus cereus* phosphonoacetaldehyde hydrolase: insight into catalysis of phosphorus bond cleavage and catalytic diversification within the HAD enzyme superfamily. *Biochemistry-US* **2000**, *39*, 10385-10396.

115. Morais, M. C.; Zhang, G.; Zhang, W.; Olsen, D. B.; Dunaway-Mariano, D.; Allen, K. N. X-ray crystallographic and site-directed mutagenesis analysis of the mechanism of Schiff-base formation in phosphonoacetaldehyde hydrolase catalysis. *J. Biol. Chem.* **2004**, *279*, 9353-9361.

116. McMullan, G.; Quinn, J. P. In vitro characterization of a phosphate starvation-independent carbon-phosphorus bond cleavage activity in *Pseudomonas fluorescen*s 23F. *J. Bacteriol.* **1994**, *176*, 320-324.

117. McGrath, J. W.; Wisdom, G. B.; McMullan, G.; Larkin, M. J.; Quinn, J. P. The purification and properties of phosphonoacetate hydrolase, a novel carbon-phosphorus bond-cleavage enzyme from *Pseudomonas fluorescens* 23F. *Eur. J. Biochem.* **1995**, *234*, 225-230.

118. Borisova, S. A.; Christman, H. D.; Metcalf, M. E. M.; Zulkepli, N. A.; Zhang, J. K.; van der Donk, W. A.; Metcalf, W. W. Genetic and biochemical characterization of a pathway for the degradation of 2-aminoethylphosphonate in *Sinorhizobium meliloti* 1021. *J. Biol. Chem.* **2011**, *286*, 22283-22290.

119. Kim, A.; Benning, M. M.; OkLee, S.; Quinn, J.; Martin, B. M.; Holden, H. M.; Dunaway-Mariano, D. Divergence of chemical function in the alkaline phosphatase superfamily: Structure and mechanism of the P−C bond cleaving enzyme phosphonoacetate hydrolase. *Biochemistry* **2011**, *50*, 3481-3494.

120. Agarwal, V.; Borisova, S. A.; Metcalf, W. W.; van der Donk, W. A.; Nair, S. K. Structural and mechanistic insights into C-P bond hydrolysis by phosphonoacetate hydrolase. *Chem. Biol.* **2011**, *18*, 1230-1240.

121. Ternan, N. G.; Hamilton, J. T. G.; Quinn, J. P. Initial in vitro characterisation of phosphonopyruvate hydrolase, a novel phosphate starvation-independent, carbon-phosphorus bond cleavage enzyme in *Burkholderia cepacia* Pal6. *Arch. Microbiol.* **2000**, *173*, 35-41.

122. Ternan, N. G.; Quinn, J. P. *In vitro* cleavage of the carbon-phosphorus bond of phosphonopyruvate by cell extracts of an environmental *Burkholderia cepacia* isolate. *Biochem. Biophys. Res. Commun.* **1998**, *248*, 378-381.

123. Kulakova, A. N.; Wisdom, G. B.; Kulakov, L. A.; Quinn, J. P. The purification and characterization of phosphonopyruvate hydrolase, a novel carbon-phosphorus bond cleavage enzyme from *Variovorax* sp. Pal2. *J. Biol. Chem.* **2003**, *278*, 23426-23431.

124. Horigane, A.; Horiguchi, M.; Matsumoto, T. Metabolism of 2-amino-3-phosphono[3-^{14}C]propionic acid in cell-free preparations of *Tetrahymena*. *BBA – Lipids and Lipid Metabolism* **1980**, *618*, 383-388.

125. Chen, C. H.; Han, Y.; Niu, W.; Kulakova, A. N.; Howard, A.; Quinn, J. P.; Dunaway-Mariano, D.; Herzberg, O. Structure and kinetics of phosphonopyruvate hydrolase from *Variovorax* sp. Pal2: new insight into the divergence of catalysis within the PEP mutase/isocitrate lyase superfamily. *Biochemistry-US* **2006**, *45*, 11491-11504.

126. Galperin, M. Y.; Jedrzejas, M. J. Conserved core structure and active site residues in alkaline phosphatase superfamily enzymes. *Proteins* **2001**, *45*, 318-324.

127. Wackett, L. P.; Shames, S. L.; Venditti, C. P.; Walsh, C. T. Bacterial carbon-phosphorus lyase: products, rates, and regulation of phosphonic and phosphinic acid metabolism. *J. Bacteriol.* **1987**, *169*, 710-717.

128. Harkness, D. R. Bacterial growth on aminoalkylphosphonic acids. *J. Bacteriol.* **1966**, *92*, 623-627.

129. Rosenberg, H.; La Nauze, J. M. The metabolism of phosphonates by microorganisms. The transport of aminoethylphosphonic acid in *Bacillus cereus*. *Biochim. Biophys. Acta* **1967**, *141*, 79-90.

130. Ford, J. L.; Kaakoush, N. O.; Mendz, G. L. Phosphonate metabolism in *Helicobacter pylori*. *Antonie van Leeuwenhoek* **2010**, *97*, 51-60.

131. Hartley, L. E.; Kaakoush, N. O.; Ford, J. L.; Korolik, V.; Mendz, G. L. Characterisation of *Campylobacter jejuni* genes potentially involved in phosphonate degradation. *Gut Pathog.* **2009**.

Chapter 2

Towards the reaction pathway of CP-lyase

2.1 Introduction

2.1.1 Occurrence of the CP-lyase pathway in nature

The CP-lyase pathway is the second most prevalent CP bond cleavage pathway amongst sequenced bacteria[1]. It has been identified in Gram positive and Gram negative bacteria in an array of phylum including α-, β-, γ-, δ- and ε-Proteobacteria, Actinobacteria, Archaea, Bacillales, Bacteroidetes, Chloroflexi, Clostridia, Cyanobacteria, and Firmicutes[2-4]. The importance of the CP-lyase pathway for the utilization of organophosphonates, and ultimately the global phosphorus cycle, is highlighted by the presence of the CP-lyase pathway in globally distributed organisms, such as *Trichodesmium erythraeumthe*s a dominant nitrogen-fixing phototroph in the ocean[5]. Using the Integrated Microbial Genome search engine Karl *et al.* found that a significant percentage of microorganisms in the Sargasso Sea sample contain the CP-lyase pathway, including 35 marine isolates with complete orthologue pathways[3]. CP-lyase is found in 16.1% and 23.2% of the sequenced bacterial and marine bacterial genomes, respectively[1]. Phylogenic analysis of CP-lyase genes suggests that the pathway evolved early and was shared amongst organisms via horizontal gene transfer events indicating that there is a strong selective pressure for acquisition and maintenance of this P_i assimilation and utilization pathway[2].

2.1.2 Regulation of CP-lyase as part of the Pho regulon

Regulation and environmental response of genes can provide important insights into the cellular protein function of the encoded genes. The Pho regulon members are under the control of environmental P_i levels. The corresponding genes are expressed once the concentration of P_i drops below 4 μM[6]. This includes the regulation and the expression of *psi* genes that are essential

in the acquisition, transport and assimilation of phosphorus-containing molecules. Thus far 31 genes in 9 transcriptional units have been directly shown to be under the control of the Pho regulon and most have been connected to phosphorus assimilation[6-9]. The 9 transcriptional units include: i. *eda* gene that encodes for the enter-doudoroff aldolase[8], ii. *phnCDEFGHIJKLMNOP* operon that encodes for CP-lyase enzymes involved in the transport and degradation of organophosphonates[10], iii. *phoA* operon that encodes bacterial alkaline phosphatase, a nonspecific phosphomonoesterase[11], iv. *phoBR* operon that encodes for the P_i sensor and Pho regulator proteins[12], v. *phoE* gene that encodes for an outer membrane pore, which facilitates diffusion of phosphorus-containing anions[13], vi. *phoH* gene that encodes a conserved putative ATPase[6], vii. *psiE* gene that encodes a hypothetical integral membrane protein[6], viii. *pstSCAB-phoU* operon that encodes the proteins of the P_i transport system, Pst[11]and ix. *ugpBAECQ* operon that encodes for the glycerol-3-phosphate transporter[14].

The environmental P_i levels are sensed by a membrane-associated '**p**hosphate **s**pecific **t**ransporter' (Pst) encoded by *pstSCAB* and *phoU*. The transporter is comprised of four constituents: i. the ABC transporter component, which consists of four proteins PstA, PstB, PstC and PstS that works in concert with PhoU; ii. PhoU, a protein that inhibits the functions of PhoB and PhoR; iii. PhoB a soluble transcription regulator that acts as a DNA binding protein to activate or inhibit transcription; and iv. PhoR, an ATP dependent inner membrane associated histidine kinase that controls PhoB activity via phosphorylation[6]. All four components are required for co-regulation of *psi* genes under the control of P_i. Although the Pst transporter is the primary element used for the detection of P_i, PhoR also plays an indirect role in sensing P_i levels[6]. When P_i levels are high, Pst is bound to P_i and PhoR, which prevents PhoR from phosphorylating and activating PhoB[15]. As soon as the P_i concentrations drop to 4 μM or less Pst no longer binds P_i, which allows for the autophosphorylation of PhoR that in turn activates PhoB by phosphorylation[15]. Phosphorylated PhoB binds to the promoter region found upstream of *psi*

genes, at a site called the PHO box, thus activating transcription and expression of the Pho regulon genes[15]. When PhoB is active, the protein expression of *psi* genes is induced up to 1500-fold allowing for phosphorus scavenging[16]. PhoR also has phosphorylase activity and will deactivate PhoB (via dephosphorylation) once the P_i levels increase above 4 μM[6].

The *phn* operon, encoding CP-lyase, has been shown to contain a PHO box promoter in front of the *phnC* gene, indicating that it is a member of the Pho regulon[10]. Additional studies have also established that CP-lyase is P_i and PhoB regulated[17,18]. A strain with a mutated *phoB* gene was shown to be unable to express the CP-lyase pathway and thus could not degrade methylphosphonate (**1a**, Figure 1-2)[17,18]. However strains with mutations affecting the components of the Pho repressor complex (Pst, PhoU and PhoR) result in constitutive and P_i independent expression of CP-lyase, thereby enabling the degradation of **1a** in the presence of P_i[18]. P_i independent expression of CP-lyase can also be achieved by expressing the *phn* operon under the control of a different regulator[19]. P_i independent expression of the *phn* operon has been extremely useful for studying the CP-lyase pathway.

2.1.3 The CP-lyase gene cluster

Although the name CP-lyase implies the activity of a single enzyme, there are in fact several enzymes and proteins that comprise 'CP-lyase'. The CP-lyase specifying genes are organized in a ~ 10.9 kb cluster called the *phn* operon (a mnemonic of **ph**ospho**n**ate) consisting of 14 genes, *phnCDEFGHIJKLMNOP*[20,21]. Seven of these genes, *phnGHIJKLM*, have been shown to be crucial for CP bond cleavage *in vivo*[21-23]. While *phnN* and *phnP* were shown to be required for organophosphonate utilization[21-23] (Figure 2-1).

Figure 2-1. Organization of the *phn* operon encoding CP-lyase. Overlapping genes are transcriptionally coupled, with an overlapping 3' end of one gene with a 5' end of the next gene in the operon. The line in p*hnE* represents the location of an 8-bp insertion found in *E. coli* K-12 that is not found in *E. coli* B. Genes in red are involved in transport, genes in black are not required for CP bond cleavage of alkylphosphonates, genes in blue are required for CP bond cleavage of alkylphosphonates and genes in green are accessory proteins required for organophosphonate utilization.

Although a number of bacteria contain an active CP-lyase pathway, the lab strain *E. coli* K-12 does not[10]. This strain contains an 8-bp insertion within the *phnE* gene that prevents the expression of a functional PhnE protein (this genotype is called *phn(EcoK^0)* in literature). *E. coli* K-12 will readily jettison this insertion when grown on organophosphonate as the sole source of P_i, yielding a functional *phnE* gene and *phn* operon[10]. Likewise, the *phnE* gene spontaneously corrects when *E. coli* is grown on phosphite as the sole P_i source. There is also a connection between expression of the *phn* operon and utilization of phosphate esters as a P_i source. The *phoA* gene encodes alkaline phosphatase in *E. coli*, which is used to hydrolyze phosphate esters in the periplasm of the cell wall. When the *phoA* gene is rendered non-functional through a mutation, the *phnE* gene will spontaneously correct regardless of the P_i source used for selection (e.g. organophosphonate, phosphite, phosphate esters)[10]. This indicates that the *phn* operon and specifically *phnE* gene, plays a role in the acquisition and use of organophosphonates, phosphite and phosphate esters. It is presumed that the *phnE* gene encodes part of a transport system for organophosphonates, phosphite and phosphate esters[10].

Originally it was difficult to evaluate the function of the gene products in the *phn* operon due to the inability of obtaining soluble and functional proteins in cell free extracts. To establish the purpose of the genes in the *phn* operon researchers relied on amino acid sequence homology

and mutational studies. PhnC, PhnK and PhnL have sequence similarity to the ATP-dependent permease component of a binding protein-dependent transport system[22], while PhnE and PhnM have sequence similarity to integral membrane proteins[22]. An array of *E. coli phn* mutants have been tested for growth on various P_i sources. Mutations of *phnC, phnD* and *phnE* genes each abolished the use of all three P_i sources (organophosphonates, phosphite and phosphate esters)[10,22,23] and therefore the proteins that these genes specify were proposed to play a part in the transport of these P_i sources[10,22,23]. Binding protein-dependent transporters usually contain a periplasmic binding protein (PhnD has an N-terminal periplasmic signal peptide), a membrane-associated permease with a nucleotide binding domain (PhnC is similar to nucleotide-binding proteins of binding protein dependent transporters), and two integral membrane proteins, (PhnE is an integral membrane protein candidate). Based on this it seems that a PhnCDE transporter is encoded by the *phn* operon that requires only one integral membrane protein component, which has been seen in some other transporters[10].

Protein sequence homology and mutational studies aided in the identification of the transport system of CP-lyase as well as shedding light on other proteins in the pathway. Mutations in *phnG, phnH, phnI, phnJ, phnK, phnL, phnM, phnN* and *phnP* genes abolish the ability of *E. coli* to utilize organophosphonates and phosphite as a P_i source. Thus these genes encode enzymes that are specific to the utilization of these substrates[22]. CP-lyase activity is lost upon disruption of bacterial membranes[10] and therefore PhnG, PhnH, PhnI, PhnJ, PhnK PhnL and PhnM proteins were assigned as components of a membrane associated complex. PhnF and PhnO were predicted to be regulatory proteins. However, the evidence for PhnF as a regulatory protein is more pronounced than that of PhnO. The PhnF sequence predicted it to be a member of a regulatory family that includes FadR, GntR, GenA and P30 proteins, which all share a conserved N-terminal domain that is thought to form a helix-turn-helix DNA binding motif[22]. Although PhnO was predicted to be a regulatory protein, a more recent mutational study by our

lab (see section 2.2) has demonstrated that PhnO is required for growth on certain aminoalkyphosphonates. Finally, mutational studies suggested that PhnN and PhnP are accessory proteins and PhnP is only required when PhnN is present[22]. Table 2-1 contains a summary of the Phn protein functions based on sequence similarity and mutational studies, as well as functions based on protein characterization, which is discussed below.

Table 2-1. Functions of proteins encoded by the *phn* operon.

Gene product	***Function based on sequence similarity[a]***	***Function based on mutation effects[a]***	***Function based on protein characterization***
PhnC	Transport; HisP, Mdr-like	Transport, permease	Not characterized
PhnD	Hydrophilic protein with signal sequence	Transport, periplasmic binding protein	Periplasmic binding protein[24,25]
PhnE	Hydrophobic membrane protein	Transport, integral membrane protein	Not characterized
PhnF	Regulator; GntR gene family	Gene regulation	GntR-like transcriptional regulator[9,26]
PhnG	Unknown	CP-lyase complex[b]	CP-lyase complex[27,c], required for PhnI activity[28]
PhnH	Unknown	CP-lyase complex[b]	CP-lyase complex[27,29,c], required for PhnI activity[28]
PhnI	Unknown	CP-lyase complex[b]	CP-lyase complex[27,c], nucleosidase[28]
PhnJ	Unknown	CP-lyase complex[b]	CP-lyase complex[27,c], radical SAM enzyme that cleaves the CP bond[28]
PhnK	Transport; HisP, Mdr like	CP-lyase complex[b]	CP-lyase complex[27,c]
PhnL	Transport or regulator; HisP, Mdr-like with helix-turn-helix motif	CP-lyase complex[b]	Required for PhnI activity[28]
PhnM	Membrane protein	CP-lyase complex[b]	Phosphatase[28]
PhnN	Unknown	CP-lyase accessory protein	Ribose-1,5-

			bisphosphokinase[30]
PhnO	Regulator; helix-turn-helix motif	Gene regulation[a], required for CP bond cleavage of 1-aminoalkylphosphonates[31,c]	Acetyl coenzyme A dependent *N*-acetyltransferase[31,32,c]
PhnP	Unknown	CP-lyase accessory protein	Cyclic phosphoribosyl phosphodiesterase[33-35,c]

[a] Based on original mutational and sequence similarity studies done in early 1990s[21,22].

[b] Proposed to be membrane associated due to inactivity of Phn protein in cell free extracts and the association to PhnM a 42 kDa hydrophobic protein.

[c] Discussed in this thesis.

Abbreviations: HisP, nucleotide-binding domain of histidine permease complex; Mdr, multidrug resistance protein; and GntR, a family of transcription factors named after the repressor of the *Bacillus subtilis* gluconate operon.

2.1.4 Detection of CP-lyase intermediates and product

As it was not possible until recently to study an isolated CP-lyase system, early mechanistic studies relied entirely on feeding organophosphonates to living cells. Chemical precedent suggested that the initial step in the CP-lyase pathway would be to activate the carbon α to the phosphorus atom as these products may decompose or be easily degraded[36]. For example, the reaction of trialkyl phosphites, dialkyl alkylphosphonites and alkyl dialkylphosphonites with acyl halides generates α-ketophosphonates[37,38]. Intriguingly, the CP bond of generated aryl-α-ketophosphonates is sensitive to both acid and basic conditions[37]. The α-carbon of alkylphosphonates can also be activated by addition of a hydroxyl. These activated α-keto, or α-hydroxy products could potentially be degraded by biological systems to yield P_i directly or phosphorous acid that can then be oxidized to P_i as well as their corresponding carboxylic acid or aldehyde, respectively[36]. However, *E. coli* grown with isotopically labelled organophosphonic acids, $^{13}CH_3PO_3H_2$ and $CD_3PO_3H_2$, yield $^{13}CH_4$ and CD_3H respectively. As the deuterium is not lost during degradation of $CD_3PO_3H_2$ the α-carbon cannot be oxidized before CP

bond cleavage, indicating that the CP bond is directly cleaved[36,39]. In addition it was shown that an equal molar ratio of P_i and methane were generated during methylphosphonate (**1a**) degradation[36]. Indeed, a broad range of alkylphosphonates are degraded by CP-lyase to yield their corresponding hydrocarbons (Figure 1-11)[36]. However, some alkylphosphonate degradation products include small amounts of alkene as well as the predominant alkane product (Table 2-2). Additionally, the substrate cyclopropylmethylphosphonate has been used to test for the presence of a radical intermediate. The formation of cyclopropylmethane and 1-butene strongly suggests that homolytic cleavage of the CP bond occurs, as this would yield a cyclopropylcarbinyl radical that can rearrange to form 1-butene (Table 2-2)[36,40]. A radical based dephosphorylation mechanism could account for the observed products, where the alkylphosphonate is either oxidized or reduced to form an alkylphosphonyl or alkylphosphoranyl radical, respectively (Figure 2-2). The radical species formed would subsequently undergo CP bond cleavage giving rise to either a metaphosphate or phosphite intermediate and the alkyl radical. There is precedent for the radical based dephosphorylation reaction as similar products are produced by a radical based reaction of alkylphosphonates with lead (IV) tetracetate[36].

Table 2-2. Degradation products of alkylphosphonates by CP-lyase[a]

Organophosphonate 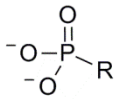	*Products*	*mole ratio, saturated:unsaturated*
R=CH_3	CH_4	-
R=CH_2CH_3	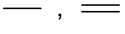	30:1
R=$CH_2CH_2CH_3$	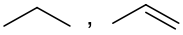	60:1
R=$CH_2CH_2CH_2CH_3$	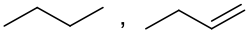	600:1
R=$CH_2CH_2CH_2CH_2CH_3$	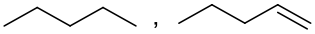	90:1
R=$CH_2CH_2CH_2CH_2CH_2CH_3$	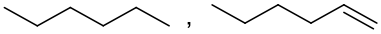	2000:1
R= 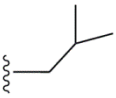	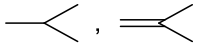	100:1
R= 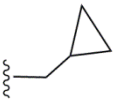	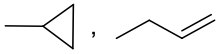	50:1
R= 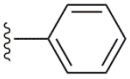		-
R= 		-
R= 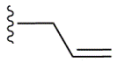		-
R=CH_2NH_3	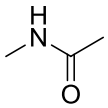	-
R=CH_2NHCH_3	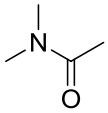	-
R=$CH_2N(CH_3)_2$	$N(CH_3)_3$	-
R= 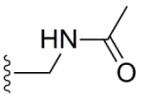	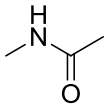	-

[a] Table constructed by compiling results from references 36, 40, and 41.

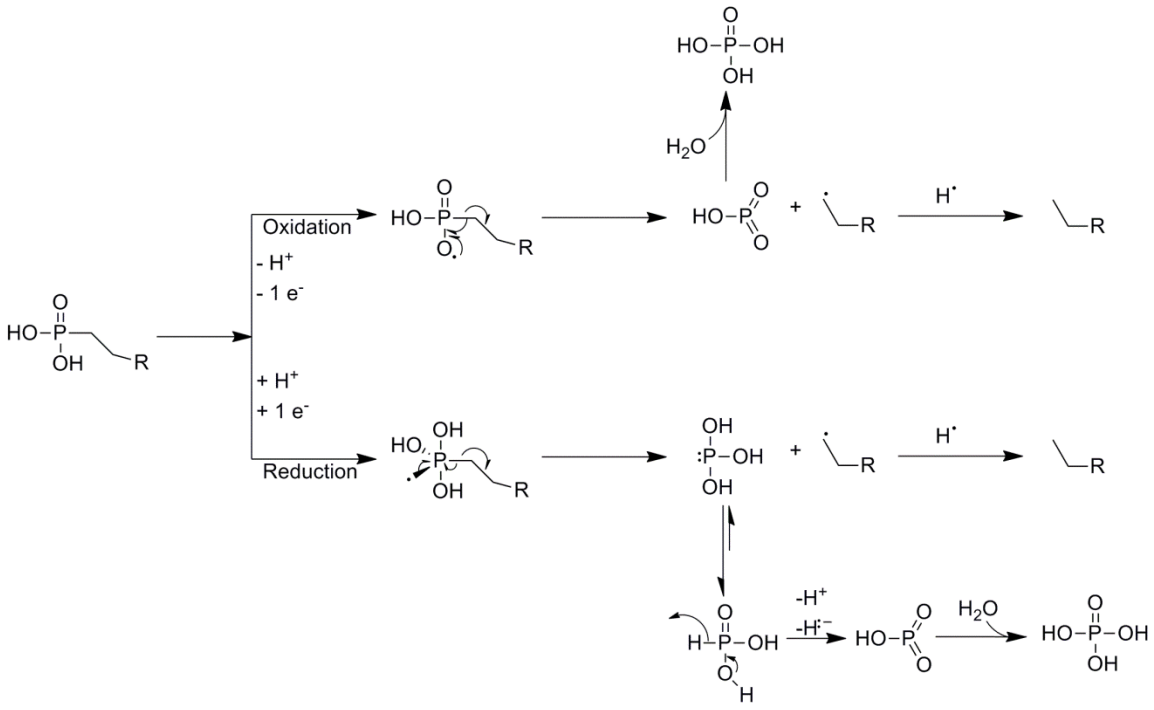

Figure 2-2. Scheme of proposed oxidative and reductive radical dephosphorylation mechanisms for CP-lyase.

Aminoalkylphosphonates were also assessed as substrates for CP-lyase by Frost *et al.* (Table 2-2). The products of *E. coli* cells fed with aminomethyl-, *N*-methylaminomethyl-, *N*,*N*-dimethylaminomethyl- and *N*-acetylaminomethylphosphonate were *N*-methylacetamide, *N*,*N*-dimethylacetamide, trimethylamine and *N*-methylacetamide, respectively[41]. The formation of the *N*-alkylacetamides as products provided further evidence for radical-based CP bond cleavage and *N*-acetylation of the amino group. However, in these early studies the timing and function of substrate *N*-acetylation was unknown. This shall be discussed further in this thesis.

To gain further mechanistic insight on the CP-lyase reactions several studies have endeavoured to isolate intermediates of organophosphonate metabolism. An unusual intermediate, α-D-ribosyl-1'-ethylphosphonate, was isolated by Frost *et al.* from *E. coli* cells that were fed ^{32}P-ethylphosphonate[42]. This result suggested that ribosylation of the substrate was a necessary step in catabolism of organophosphonates by CP-lyase, and may arise from ATP or

other nucleotides acting as glycosyl donors. This was an intriguing result because, PhnC, PhnK, PhnL and PhnN have similarity to nucleotide binding proteins[10,20].

Hove-Jensen *et al.* identified additional intermediates of organophosphonate catabolism by disrupting individual *phn* genes in *E. coli*[43]. For this to be successful is was necessary to express the *phn* operon constitutively and have expression of *phn* genes be independent of the P_i levels in the medium. This was achieved by disrupting the *pstSCAB-phoU* operon, creating an *E. coli phn*$^+$ strain that constitutively expresses the *phn* operon. This strain can be grown in the presence of P_i and still synthesizes the CP-lyase proteins encoded by the *phn* operon, which will degrade most organophosphonates supplied to the culture. However, the presence of P_i allows *E. coli* to continue to grow even if a mutation of a *phn* gene prevents conversion of organophosphonate to P_i. The accumulation of organophosphonate catabolic intermediates in various *phn* mutants was then detected via radiolabeling[43]. Mutant *phn* strains, along with the *phn*$^+$ and a negative control strain lacking everything but the organophosphonate transporter, Δ*phn*, were grown in the presence of an organophosphonate and ^{32}P labelled P_i[43]. It was hypothesized that the labelled P_i would be transferred to one or more organophosphonate intermediate via phosphorylation, yielding species that could be easily detected. The supernatants of the cultures were resolved on cellulose-polyethyleneimine thin layer chromatography (TLC) plates and analyzed[43]. The studies revealed no labelled intermediates in the *phn*$^+$ strain, the Δ*phn* mutant or in the *phnO* mutant[43]. However, intermediates accumulated in *phnG, phnH, phnI, phnJ, phnK, phnL, phnN,* and *phnP* mutants grown with various organophosphonates. No intermediates formed in the absence of organophosphonates, indicating that deletion of specific genes caused the accumulation of the detected intermediates[43] and that these intermediates are related to organophosphonate metabolism. Moreover, different intermediates accumulated when different organophosphonates were fed to the strains. Two prominent intermediates accumulated in the *phnP* mutant. The second intermediate was of great interest, as it was not found in the

other mutant strains. It was determined that this intermediate was in fact the substrate for PhnP[43]. This was shown by incubating the culture fluid containing this compound with purified PhnP enzyme, which converted this compound to a new compound with a different retention factor (R_f) on the TLC plate. The R_f value of the *in vivo* PhnP substrate did not correspond to any of the 2',3'-cyclic nucleotides previously shown to be substrates and hydrolyzed by PhnP[43]. Therefore, it is necessary to directly isolate and characterize the *in vivo* substrate to assign the physiological function of PhnP within the CP-lyase pathway. This objective is part of this thesis and will be discussed in more detail.

The application of ^{31}P-NMR spectroscopy has also enabled the detection and characterization of organophosphonate intermediates in *phn* mutant strains. Including the identification of α-D-ribose-1,2-cyclicphosphate and 5-phospho-α-D-ribose-1,2-cyclicphosphate, which turned out to be substrates for PhnP. PhnP was shown to regioselectively hydrolyze these compounds to α-D-ribose-1-phosphate and α-D-ribose-1,5-bisphosphate, respectively[35]. ^{31}P-NMR spectroscopy was also used to identify intermediates of aminoalkylphosphonate catabolism, including 5'-phospho-α-D-ribosyl-1'-(2-*N*-acetamidoethylphosphonate) and 2-*N*-acetamidoethylphosphonate[31]. Section 2.2 of this thesis will describe how the PhnP substrates and acetylated aminoalkylphosphonate degradation intermediates were isolated and characterized, as well as how these compounds played a key role in deciphering the mechanism of CP bond cleavage by the CP-lyase pathway. Gene regulation studies, mutational studies, and protein sequence homology of the *phn* operon along with detection of organophosphonate catabolic products led to a partial understanding of the CP-lyase pathway, but further studies were required to fully characterize the pathway. These studies will be discussed in this thesis.

2.1.5 CP-lyase protein structure and functions

Prior to work published from this thesis, the *E. coli* PhnD, PhnF, PhnH, PhnN and PhnP proteins, as well as a PhnO analog from *Salmonella enterica* serotype Typhimurium, were characterized *in vitro*. Publications arising from the work described in this thesis have characterized the functions of *E. coli* PhnO, and the physiological function of PhnP as well as demonstrated the isolation of a CP-lyase multienzyme complex. This work has contributed to the characterization of enzymes PhnI, PhnJ and PhnM, leading to a more in depth understanding of the CP-lyase pathway.

In an attempt to develop a biosensor of organophosphonates, the crystal structure and substrate specificity of the periplasmic binding protein PhnD was determined[24,25]. PhnD was shown to have the highest affinity for the most common naturally occurring organophosphonate, 2-aminoethylphosphonate (AEP, **1g**) (K_d = 5 nM) and micromolar affinity for other organophosphonates[24]. AEP binds to the centre of PhnD, which is commonly seen for periplasmic binding proteins[44]. Both the open (unbound) and closed (bound) forms of PhnD were crystallized[25] (Figure 2-3). There is a large conformational change between the two forms that comes from an approximately 70° pivot of the lobes around a hinge[25]. AEP is held in the active site by H-bonding of the organophosphonate oxygen atoms with Y47, Y93, S127, T128, S129 and H157 side chains along with an ordered water molecule and the backbone amide from T128 and S129[25]. The phosphonate oxygens are tightly packed and saturated with polar interactions. There are five ordered water molecules in the binding pocket along with AEP, implying that organophosphonates with longer alkylchains could be accommodated[25].

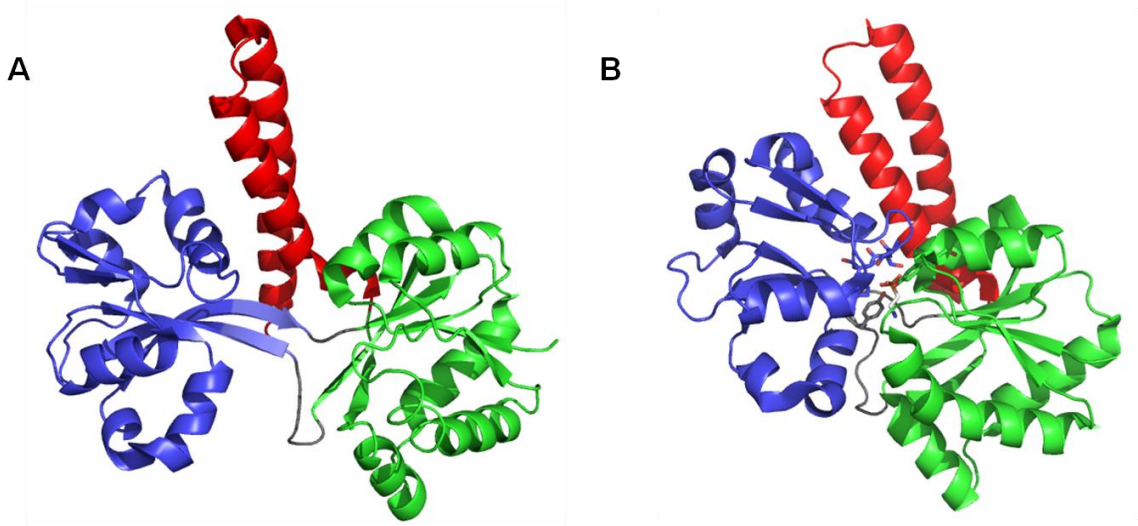

Figure 2-3. The cartoon representation of the open and closed crystal structure of PhnD. (A) The open, unbound crystal structure of PhnD. (B) The closed **1g** bound crystal structure of PhnD, **1g** and its interacting residues are shown as sticks. Lobe 1 is coloured green, lobe 2 is coloured blue, and the C-terminal coiled-coiled helices are coloured in red.

E. coli PhnF is predicted to be a transcriptional regulator based on sequence similarity to GntR transcriptional regulators. Members of the large GntR family have a conserved N-terminal winged helix-turn-helix DNA binding domain[45]. The GntR family is split into four subfamilies, FadR, HutC, MocR and YtrA, each with varying C-terminal domains[45]. The C-terminal domain is involved in the binding of ligands and protein oligomerization. The PhnF C-terminus has similarity to the HutC subfamily, which consists of 30% of the GntR-like regulators[9]. The structure of the C-terminal domain of PhnF was the first HutC type regulator to be crystallized and characterized[9]. The crystal structure (Figure 2-4) revealed a symmetrical dimeric structure with a six-stranded antiparallel β-sheet core with a two-stranded parallel β-sheet and four short α-helices that clasps the core[9]. The monomers of PhnF differ with a loop structure which contains residues 94-99 and is proposed to be important for ligand binding. The ligand-binding site of PhnF was also identified but it is unknown what ligand binds. PhnF of *Mycobacterium segmentis* shares sequence homology to the PhnF of *E. coli*, but the enzymes deviate slightly within the

ligand binding site[26]. *M. segmentis* is unusual in having only *phnCDE* genes rather than a complete *phn* operon, and the *phnCDE* transporter is unable to transport organophosphonates. The deletion of *phnF* in *M. segmentis* increased the expression of *phnCDE*, and complementation with *phnF* on a plasmid restored repression of the genes. Therefore, PhnF of *M. segmentis* was characterized as a transcriptional repressor[26]. Although the ligand binding site residues are not completely conserved, *E. coli phnF* is predicted to also be a repressor for the *phn* operon based on its similarity to that of the *phnF* of *M. segmentis*[26].

Figure 2-4. The cartoon representation of the crystal structure of PhnF. One monomer is coloured red, the other is coloured green, and the differing loop region (residues 94-99) is highlighted in blue.

The X-ray crystal structure of PhnH has also been solved. PhnH exhibits a Rossmann fold and forms a dimer in the crystal structure (Figure 2-5) and in solution[29]. A putative ligand binding pocket was also identified, but *in silico* and *in vitro* ligand screening failed to identify a ligand. It is possible that the activity of PhnH requires additional enzyme interactions or that PhnH plays a role as a structural scaffold in the CP-lyase complex[29]. The latter hypothesis was

recently strengthened by identification of PhnH as a component of a PhnGHIJK complex. Isolation of the CP-lyase complex and the postulated roles of the enzymes will be discussed further in section 2.3.

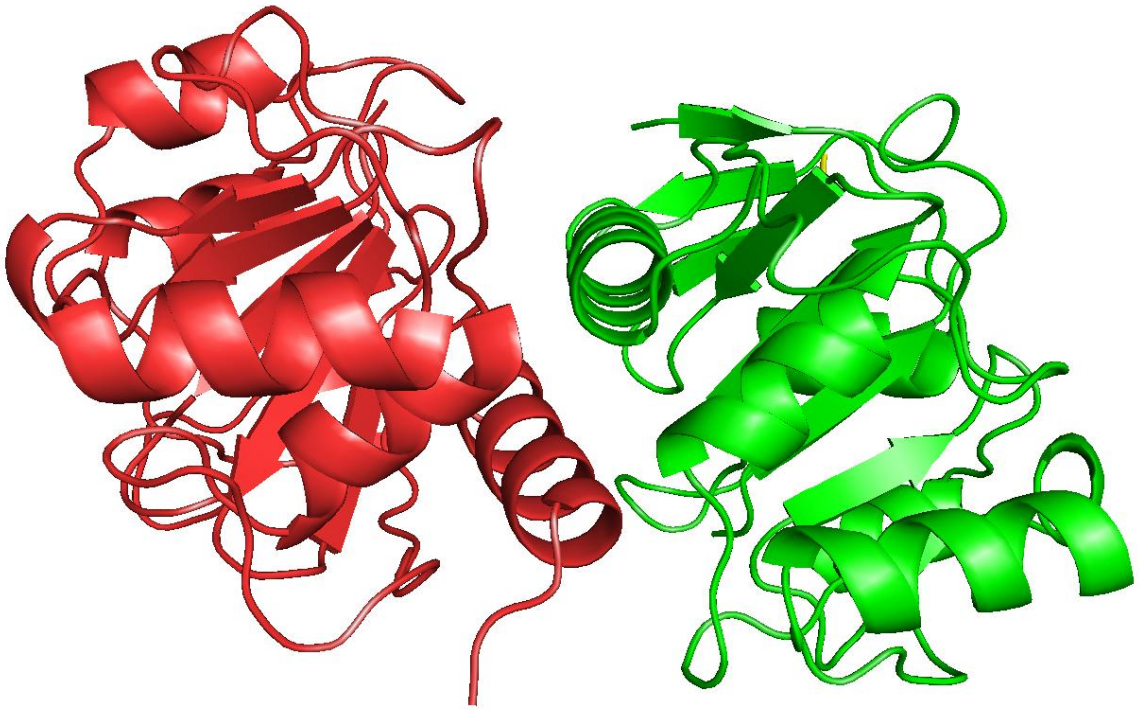

Figure 2-5. The cartoon representation of the crystal structure of PhnH. One monomer is coloured red, the other is coloured green.

PhnO from *Salmonella enterica* serotype Typhimurium has been characterized as an acetyl coenzyme A (acetyl-CoA) dependent *N*-acetyltransferase with relaxed specificity towards various aminoalkylphosphonates[32]. Like *M. segmentis,* this organism does not have a complete *phn* operon. The high sequence similarity between *phnO* of *S. enterica* and *phnO* of *E. coli* led researchers to postulate that the reaction catalyzed by *E. coli* PhnO would be similar to that of PhnO from *S. enterica*. The physiological role of PhnO in *S. enterica* is unclear, especially because *N*-acetylation would prevent transamination and subsequent CP bond cleavage by enzymes utilizing an 'electron sink' mechanism for CP bond cleavage. It was therefore proposed that the physiological role of PhnO is for P_i storage: if excess amounts of

aminoalkylphosphonates are available in the environment the organophosphonates can be stored after *N*-acetylation by PhnO[32]. When in dire need of P_i these stored compounds could then be hydrolyzed by a deacetylase and utilized as a P_i source[32]. Studies of organophosphonate utilization by *E. coli* showed that mutations of the *phnO* gene did not affect growth on alkylphosphonates, indicating that PhnO is not required for alkylphosphonate degradation. Recent studies by our lab have shown that *E. coli* PhnO *N*-acetylates a variety of aminoalkylphosphonates and *N*-acetylation is absolutely required for the catabolism of 1-aminoalkylphosphonates, but not for longer aminoalkylphosphonates such as AEP[31]. Part of this thesis includes the characterization of *E. coli* PhnO and characterization of metabolic intermediates involving aminoalkylphosphonates. The function and proposed physiological role of PhnO can be seen in Section 2.2.

The functions of PhnN and PhnP are peripheral to CP bond cleavage but are still significant for utilization of organophosphonates. Mutations in the *phnN* or *phnP* genes have the paradoxical result of preventing *E. coli* from subsisting on organophosphonates as the sole P_i source, but are not required for CP bond cleavage[21-23]. The roles of PhnN and PhnP are tied to an important molecule, 5-phospho-α-D-ribosyl-1-pyrophosphate (PRPP, **7**), which is a glycosyl donor used for the biosynthesis of purines, pyrimidines, nicotinamide adenine dinucleotide (NAD^+), histidine, and tryptophan. Hove-Jensen created an *E. coli* mutant strain with a deleted *prs* gene that encodes PRPP synthase. Without the ability to synthesize PRPP, the *E. coli Δprs* mutant was expected to require media supplemented with NAD^+, guanosine, uridine, histidine and tryptophan in order to grow. Surprisingly, an *E. coli Δprs* phenotype that did not require NAD^+ was obtained on media lacking this nutrient. It was determined that the NAD^+ suppression phenotype was arising from a derepression of the *phn* operon expression and more specifically the expression of the *phnN* gene. It was quickly discovered that *phnN* encodes a ribose 1,5-bisphosphokinase, which uses ATP as a phosphoryl donor to form PRPP[30] (Figure 2-6). If PhnN

were the final step in the CP-lyase pathway, this would provide a direct route for incorporation of P_i into essential metabolic pathways. In addition, the α-D-ribosyl-1'-ethylphosphonate intermediate, detected by Frost *et al.*[42], has surprising similarity to the substrate of PhnN suggesting that ribosylation of organophosphonates is a required step in the CP-lyase pathway.

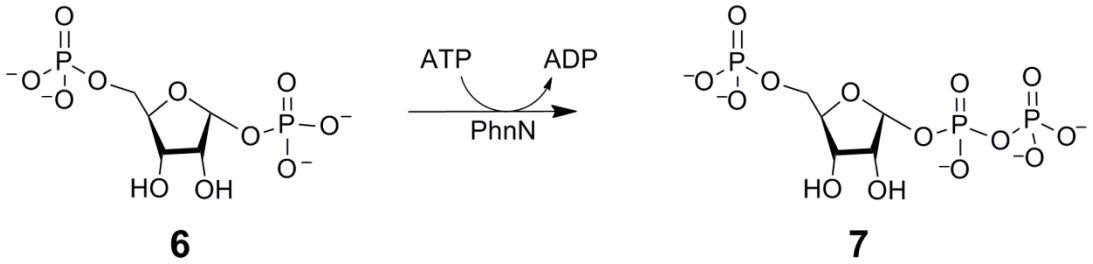

6 **7**

Figure 2-6. The reaction of PhnN, a ribose 1,5-bisphosphokinase.

PhnP belongs to the metal-ion dependent β-lactamase superfamily, which includes phosphodiesterases. Work by the Zechel and Jia labs revealed that PhnP is in fact a phosphodiesterase[33,34]. The hydrolytic activity of PhnP with bis(*p*-nitrophenyl)phosphate as a substrate was enhanced 5,000-13,000 fold in the presence of Mn^{2+} and Ni^{2+}, suggesting that one of these metal ions is the preferred ion for catalysis *in vivo*[46]. The X-ray crystal structure of PhnP revealed a dimeric enzyme with two metal ions bound in each active site (Figure 2-7). The structure also revealed a third metal ion, likely Zn^{2+}, bound outside of the active site, which is proposed to play a structure-stabilizing role[33,34]. Orthovanadate was found in the active site interacting with the Mn^{2+} ions and protein residues D80 and H200. Other active site residues (H76, H78, D80, H81, D164 and H222) were coordinating the two Mn^{2+} ions[33]. Inductively coupled plasma-mass spectrometry (ICP-MS) analysis revealed nearly stoichiometric binding of Zn^{2+} and low levels of Mn^{2+}. For the identification of an *in vivo* substrate an array of naturally occurring phosphodiester-containing molecules in the presence of various metal ions were tested for activity. The highest activity was obtained with 2',3'-cyclic nucleotides[46]. Recent studies have determined that the *in vivo* substrate of PhnP is 5-phospho-α-D-ribosyl-1,2-cyclicphosphate,

which is hydrolyzed to form α-D-ribose-1,5-bisphosphate, the substrate for PhnN[35]. With the discovery of the PhnP substrate, we proposed a CP-lyase pathway involving the α-D-ribosyl-1'-alkylphosphonate intermediate discovered by Frost *et al.*. In this scheme oxidative CP bond cleavage by CP-lyase would yield an α-D-ribosyl-metaphosphate that would rapidly react with the adjacent 2'-hydroxyl, yielding the corresponding alkyl product and the PhnP substrate, α-D-ribosyl-1,2-cyclicphosphate (Figure 2-8). This 'dead-end' intermediate would then be hydrolyzed by PhnP, yielding α-D-ribose-1,5-bisphosphate (**6**), the substrate for PhnN. Finally, phosphorylation by PhnN would yield the glycosyl donor **7**. PRPP can then distribute P_i throughout the cell and can be utilized directly for the synthesis of purines, pyrimidines, histidine, tryptophan and NAD^+. However, it was not clear how the α-D-ribosyl-1'-alkylphosphonate would be formed, although ribosylation by a nucleotide was a distinct possibility.

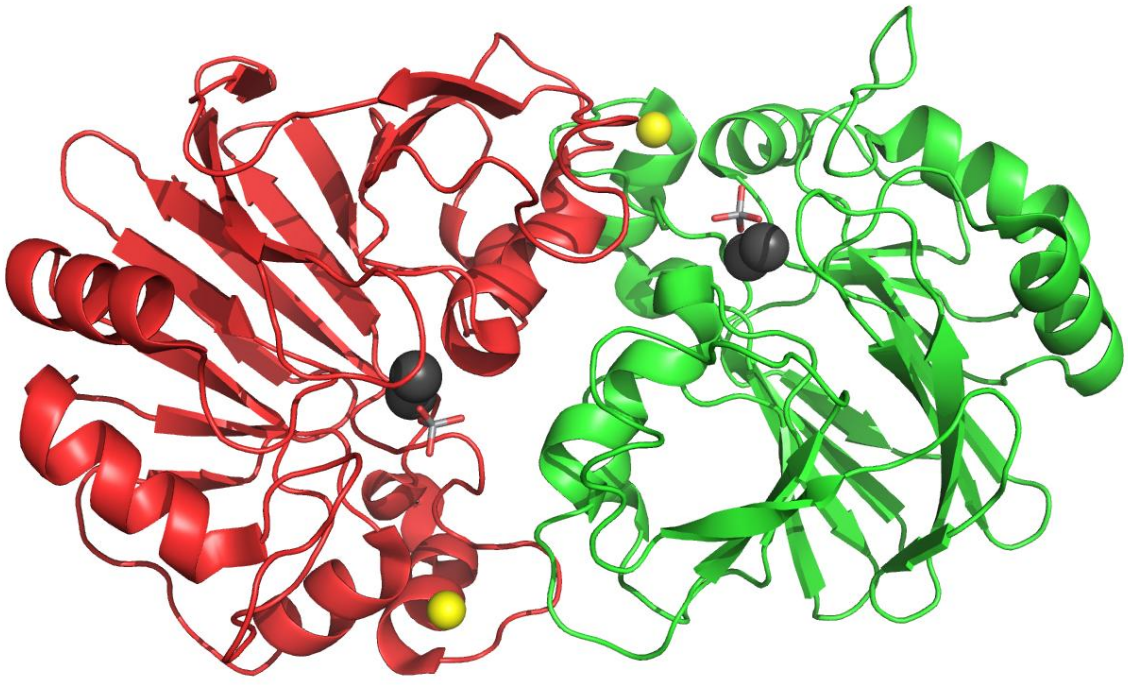

Figure 2-7. The cartoon representation of the crystal structure of PhnP bound to orthovanadate. Molecule A is coloured red and Molecule B is coloured green; the Mn^{2+} and Zn^{2+} ions are shown as grey and yellow spheres, respectively; orthovanadate is seen as grey and red sticks.

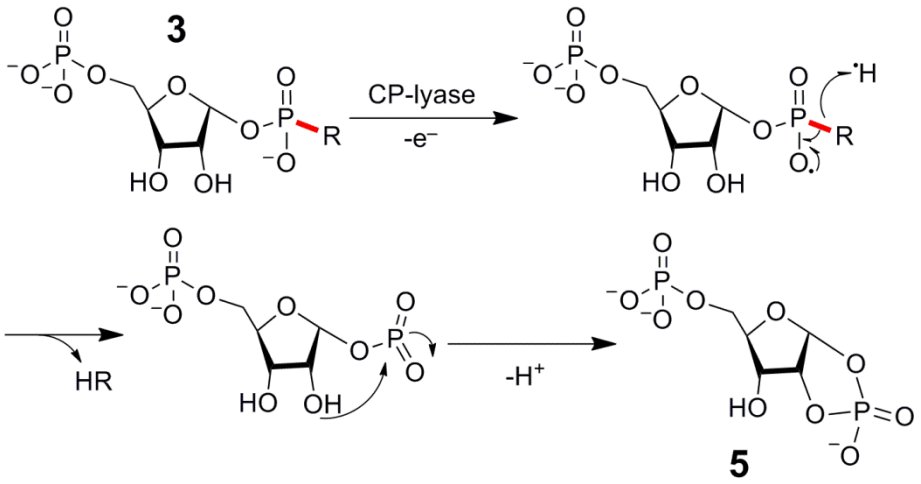

Figure 2-8. Proposed radical reaction for CP bond cleavage by CP-lyase based on detected intermediates. CP bonds are bolded and coloured red.

Adding to the mystery of the CP-lyase pathway, a multienzyme complex consisting of PhnGHIJK was generated and purified by expression of a *phnGHIJKLM* plasmid in an *E. coli Δphn* strain[27]. This work aided in the recent characterization of PhnI, PhnJ and PhnM by Raushel and co-workers[28], and will be discussed in section 2.3 of this thesis. A summary of the CP-lyase pathway based on the most recent literature, including work arising from this thesis, is shown in Figure 2-9. This thesis will return to aspects of this pathway in later pages.

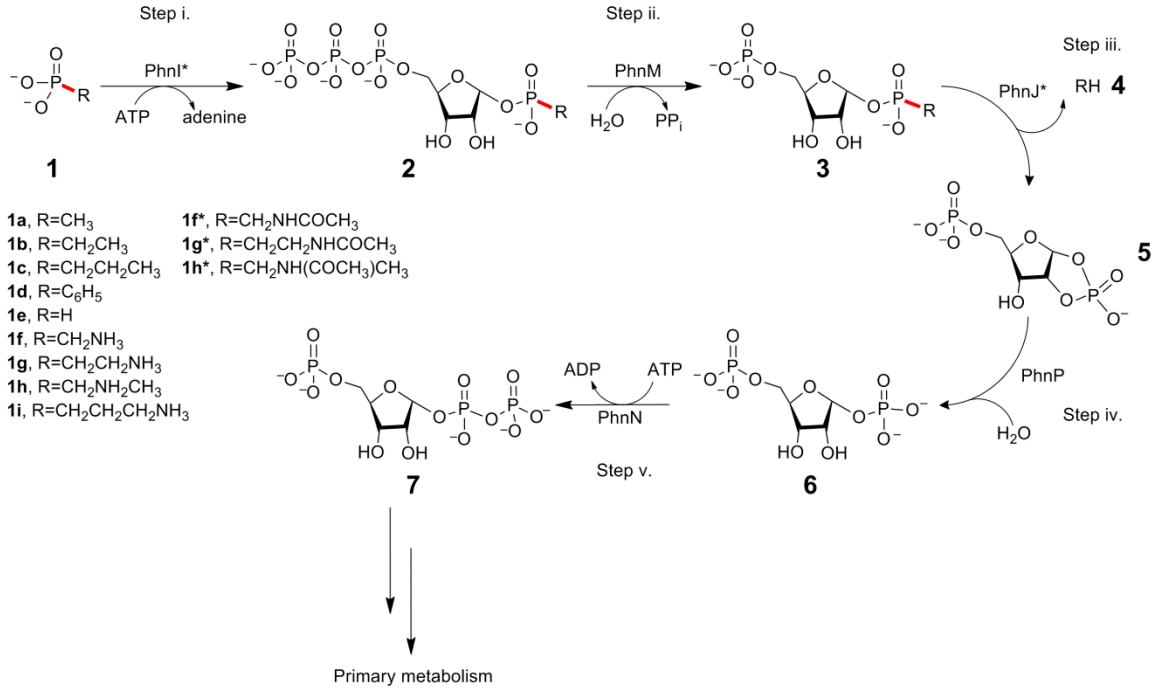

Figure 2-9. CP-lyase reaction pathway. *Denotes the potential requirement of other Phn enzymes, such as members of the CP-lyase complex (PhnGHIJK). CP bonds are bolded and coloured red.

2.1.6 Rationale and objectives

Knowledge of the CP-lyase pathway and the mechanism of CP bond cleavage has long been limited by the inability to obtain most of the enzymes in soluble form and the loss of CP bond cleavage activity in cell free extracts[16,47]. Thus a major objective was to identify catabolic intermediates and their corresponding enzyme reactions in the CP-lyase pathway.

The identification of intermediates of organophosphonate catabolism is necessary to reconstruct the CP-lyase pathway. These intermediates will provide a starting point for identification of the substrates of individual CP-lyase proteins, or CP-lyase complexes. Therefore an objective of this thesis was to isolate and characterize intermediates of organophosphonate catabolism, with a specific focus on PhnO and PhnP. At the time of my thesis studies, the roles of these two enzymes in the CP-lyase pathway were unknown.

Based on the large number of genes in the *phn* operon, we hypothesized that some of the encoded proteins would form a protein complex. This protein complex might be unstable and sensitive to cell lysis. This would explain why cell free CP bond cleavage has not been detected and why many of the individual proteins in the pathway are not soluble. Recently it was shown that proteins that could not be isolated and studied individually can be produced in a soluble form as a complex, allowing structural and mechanistic properties to be determined[48]. The isolation of a CP-lyase complex could prove to be extremely useful for future structural and mechanistic analysis. Thus the second major objective of this thesis was to attempt to isolate a CP-lyase complex.

2.2 Isolation, detection and characterization of CP-lyase pathway intermediates

The characterization of CP-lyase pathway intermediates would aid in the determination of the reaction steps in the pathway and help understand the method of CP bond cleavage. A protein complex containing PhnGHIJK has been isolated (Section 2.3) that is hypothesized to be the CP-lyase component of the pathway. The corresponding knockout strains yield a common unknown intermediate that was detected using ^{32}P radiolabelling[43]. In addition, a *phnP* knockout strain gave rise to an additional intermediate that was found to be the substrate of PhnP. The objective is to characterize these two intermediates to better understand the function of PhnP and the CP-lyase pathway as a whole.

A strategy using ^{31}P-NMR spectroscopy was chosen to further characterize and aid the isolation of these intermediates. This technique is sensitive to phosphorus-containing molecules due to the near 100% abundance of the NMR active isotope of phosphorus. Analogous to the earlier radiolabeling studies, cell extracts of *E. coli* mutant strains will be grown with various organophosphonates. The presence of phosphorus-containing molecules will be monitored in the cell culture fluids by ^{31}P-NMR spectroscopy. Growth conditions that yield large quantities of

intermediates will be determined and then used for isolating the intermediates. The intermediates of interest will be purified and structurally characterized. Another method for detecting CP-lyase catabolic intermediates using a fluorescently-labelled alkylphosphonate was performed by the author but is not described.

2.2.1 Methods

2.2.1.1 Materials and equipment

PRPP, D-alanine, D/L-alanine and acetyl-CoA, as well as methyl-, ethyl-, propyl-, phenyl-, and aminomethylphosphonate were purchased from Sigma-Aldrich. 2-Aminoethylphosphonate was purchased from Acros Organics (Geel, Belgium), and phosphite was purchased from Riedel-deHaën (Buchs, Switzerland). α-D-Ribosyl-1'-phosphate was a gift from K. F. Jensen, University of Copenhagen, where it was prepared enzymatically by phosphorolysis of uridine with uridine phosphorylase in the presence of P_i followed by ion-exchange chromatography on a Dowex-1 column. The pUHE23-2 plasmid was obtained from H. Bujard, University of Heidelberg.

NMR spectra were recorded in D_2O on Bruker Avance 300, 400, 500 or 600 MHz spectrometers at Queen's University. The ^{1}H-NMR chemical shifts (δ) are referenced to residual HDO (δ_H 4.79 ppm), whereas ^{31}P-NMR chemical shifts are referenced to external H_3PO_4 (85 %) or to with an internal 17 mM H_3PO_4 standard present in a capillary tube within the NMR tube, separate from the sample. Chemical shifts (δ) are given in ppm and coupling constants (*J*) in Hz. Electro spray ionization (ESI) – MS was performed at the Queen's University Mass Spectrometry and Proteomics Unit on an Applied Biosystems/MDS Sciex QStar XL MS instrument.

2.2.1.2 *E. coli* strains and growth conditions for analysis of intermediates

A table of the *E.* coli strains used their genotype, as well as their origin or construction is found in Appendix A. The construction of strains is only noted if done by the author. E. *coli*

Tn*phoA'-1* mutations are polar, Tn*phoA'*-9 are not[22]. A bacteriophage P1-mediated transduction method was used to construct some strains[49]. The wild type *E. coli* K-12 has a *phnE*-(EcoK^0) *phnE* allele which contains an 8-bp duplication. The duplication causes premature translation termination of the *phnE* mRNA and therefore the strains are organophosphonate growth deficient[50]. The *E. coli* K-12 strains can be made organophosphonate growth proficient by selection for growth with organophosphonate or phosphite as the sole source of P_i[50,51]. These *phnE*-(EcoK$^+$) strains are variants that have lost the 8-bp duplication that results in the entire translation of the *phnE* mRNA and therefore the strains become organophosphonate growth proficient. Strains that are noted with *phn*(EcoB) originate from the organophosphonate growth proficient *E. coli* B.

E. coli was grown at 37°C in either a low-P_i Tris buffered medium, 03P[43], containing 0.3 mM P_i, or a P_i free 3-(N-morpholino)propanesulfonic acid (MOPS) buffered medium with both using 0.2% glucose as a carbon source[43,52]. To the MOPS medium histidine and tryptophan were added to 40 mg L^{-1}, guanosine was added to 30 mg L^{-1}, uridine was added to 20 mg L^{-1}, and thiamine was added to 1 mg L^{-1}. Organophosphonates were used at concentrations of 0.3 or 2.0 mM. D/L and D-alanine were used at 100 mg L^{-1}. Antibiotics chloramphenicol and kanamycin were used as necessary at 30 and 50 mg L^{-1}, respectively. Cell growth was monitored as optical density (OD) at 600 nm by a Cary 50 spectrometer (Varian). For analysis of accumulated organophosphonate degradation intermediates, cells were grown to an OD_{600} of 0.45, at which point an organophosphonate was added to a concentration of 2 mM. At certain time intervals, or after 20 h of incubation 3 or 5 mL samples were removed and centrifuged to remove cells. The supernatant was passed through a 0.45 μm filter and either analyzed immediately or stored at -20°C. Some ^{31}P-NMR spectroscopy signals were assigned by spiking the NMR sample with the corresponding aminoalkylphosphonate *N*-acetyltransferase reaction product. Uneven acidification led to small differences in ^{31}P-NMR spectroscopy chemical shifts, due to the pH

sensitivity of the molecules. The solid medium used was P_i free MOPS with 1.8% agar. Glassware and agar were washed multiple times with deionized water (Milli-Q system) to reduce P_i contamination.

2.2.1.3 Purification and characterization of CP-lyase intermediates

A 250 mL or 2 L 03P culture of HO2542 (*phnP*) was grown at 37°C with 240 rpm shaking for aeration, to an OD_{600} of 0.5 when 0.3 or 2 mM of an organophosphonate was added. The culture was incubated for a further 20 - 24 h. The supernatant fluid was obtained by centrifugation and loaded onto either a hydroxide or formate form of AG1-8X column that was equilibrated using an ÄKTA fast protein liquid chromatography (FPLC) system (GE Healthcare, Canada). The column was washed with 300 mL of deionized water followed by a gradient of 0 - 0.4 M ammonium formate in 0.1 M formic acid for elution. A flow rate of either 2 mL min^{-1} or 0.5 mL min^{-1} was applied. Fractions were analyzed for phosphorus-containing compounds by ^{31}P-NMR spectroscopy.

The supernatant of the 2 L 03P culture of HO2542 (*phnP*) grown with 0.3 mM ethylphosphonate (**1b**) that was purified on the hydroxide form of AG1-8X, contained α-D-ribosyl-1-ethylphosphonate. α-D-Ribosyl-1-ethylphosphonate eluted at approximately 1.5 M ammonium formate and was identified by ^{31}P-NMR (δ = 30.3 ppm). The solvent was removed *in vacuo* and the product was analyzed and characterized by NMR spectroscopy.

The supernatant of the 250 mL 03P culture of HO2542 (*phnP*) grown with 2 mM **1g**, was purified on the formate form of AG1-8X. Fractions were analyzed by ^{31}P-NMR spectroscopy and quantified with the inclusion of a 17 mM phosphoric acid external standard to yield an elution profile. The fractions yielding a ^{31}P-NMR δ 19.4 ppm (elution volume 97 to 115 mL) were pooled. The solvent was removed *in vacuo*, and the material was washed with D_2O and lyophilized multiple times. The product, 2-*N*-acetamidoethylphosphonate was analyzed and

characterized by NMR spectroscopy. In addition, elution volume 125 to 130 mL (6 mL) were combined, and then washed with D_2O and lyophilized multiple times. The product, 5'-phospho-α-D-ribosyl 1'-(2-*N*-acetamidoethylphosphonate) (**3g***), was analyzed and characterized by NMR spectroscopy. The final fraction of **3g*** contained one or more compounds that did not contain a P atom as contaminants because the elution profile was monitored by ^{31}P-NMR spectroscopy.

2.2.1.4 The reaction of PhnP with 5-phospho-α-D-ribosyl-1,2-cyclic phosphate (**5**)

The PhnP enzyme was purified by summer student Matt Wong under the supervision of the author (or by the author) as described in reference 34. 5-Phospho-α-D-ribosyl-1,2-cyclic phosphate (**5**) was synthesized by Bjarne Hove-Jensen using a modified method of a previously described procedure[53]. Seventeen mg of PRPP (**7**) were dissolved in 1.0 mL of water. Barium acetate was added to a concentration of 5 mM and 0.1 M sodium hydroxide was added until a pH of 10.5 - 11.0 was reached. The mixture was incubated at room temperature for 6 days with the progress of the reaction monitored by ^{31}P-NMR spectroscopy. Upon completion the solution was clarified by centrifugation and the pH was adjusted to 7.6 with 0.5 M Tris-HCl. The product was confirmed by NMR spectroscopy in 25 mM Tris-HCl, pH 7.6 in D_2O. ^{1}H-NMR (600 MHz): δ 5.84 (H1, dd, J_{H1-H2} = 4.1 Hz, J_{H1-P} = 17 Hz, 1H), 4.81 (H2, m, 1H), 4.12 (H3, dd, J = 1.2 and 4.8 Hz, 1H), 4.09 (H4, m, 1H), 3.83 (H5a, ddd, J = 12, 4.3, and 2.3 Hz, 1H), 3.96 (H5b, ddd, J = 11, 5.8, and 4.0 Hz). ^{31}P-NMR (242.9 MHz): δ 4.1 (P5, t, J =5.0 Hz), 18.7 (P1, 2, dd, $J_{P1,2-H1}$ = 17 Hz, $J_{P1,2-H2}$ = 4.3 Hz). Radiolabelled **5** was prepared with radiolabelled **7** at the University of Copenhagen by Bjarne Hove-Jensen[35].

To a solution of 10 mM **5** in 25 mM Tris-HCl, pH 7.6 with 10 - 15% D_2O, 5 μM of purified PhnP was added. The reaction was incubated at room temperature for 1 h and then analyzed by NMR spectroscopy. ^{1}H-NMR (600 MHz): δ 5.53 (H1, dd, J_{H1-P} = 6.3 Hz, J_{H1-H2} = 4.1 Hz), 4.07 (H2, m, 1H), 4.04 (H3, dd, J_{H3-H4} = 3.6 Hz, J_{H2-H3} = 6.1 Hz, 1H), 4.21 (H4 dd, J_{H3-H4} =

3.9 Hz, $J_{H4\text{-}H5}$ = 7.6 Hz, 1H), 3.76 (H5, dq, J = 11 and 5.1 Hz, 2H). ^{31}P-NMR (242.9 MHz) δ 3.7 (P5, dd, $J_{P5\text{-}H5}$ = 4.7 Hz), 2.3 (P1, d, $J_{P1\text{-}H1}$ = 6.2 Hz).

CP-lyase intermediates of strain HO2542 (*phnP*) were labelled with ^{32}P in the presence of unlabelled methylphosphonate (**1a**) and TLC analysis was performed by Bjarne Hove-Jensen at the University of Copenhagen as described previously[43].

2.2.1.5 The reaction of PhnO with aminoalkylphosphonates

Bjarne Hove-Jensen constructed a *phnO* variant that specified a hexahistidine tag at the C-terminus of the enzyme. This construct was prepared by PCR with oligonucleotides 5'-GA*GAATTC*ATTAAAGAGGAGAAATTAACTATGCCTGCTTGTGAGCTTCGCCCGGCCA CGC- 3' and 5'-TGT*CCATGG*TTATTAatggtgatggtgatggtgCAGCGCCTTGGTGAAGCGGAA-GTGGCTCTGCTCGTAGCCTTCGCGC-3' as primers. The nucleotides that specify the hexahistidine tag are shown in lower case and restriction enzyme sites are italicised. Genomic DNA isolated from HO1429 was used as the DNA template with Vent DNA polymerase (New England Biolabs). The PCR product was digested with *Eco*RI and *Nco*I to yield a 479-bp fragment that was ligated into a similarly digested pUHE23-2 plasmid. The resulting plasmid, pHO512 (plasmid map can be seen in Appendix C) was sequenced to confirm the correct nucleotide sequence.

The pHO512 plasmid containing the *phnO* gene was transformed into HO2735. A 300 mL culture of HO2735/pHO512 was grown in LB at 37°C, 240 rpm to an OD_{600} of 0.7. The culture was then cooled on ice for 30 min and IPTG was added to induce *phnO* gene expression. The culture was grown for a further 6 h at 27°C. The culture was centrifuged and cells were resuspended in 25 mM sodium phosphate buffer, 0.3 M sodium chloride, 10 mM imidazole, 1 mM EDTA, pH 8.0. Cells were lysed by high-pressure homogenization (Emulsiflex, model C5, Avestin, Ottawa, ON). The lysate was clarified by centrifugation and supernatant fluid was

loaded onto a 2 mL Ni-NTA agarose (Qiagen) column. Column was washed with 25 mM sodium phosphate buffer, 0.3 M sodium chloride, 20 mM imidazole, pH 8.0 and then eluted with repeated additions of 0.5 mL of 25 mM sodium phosphate buffer, 0.3 M sodium chloride, 250 mM imidazole, pH 8.0. The eluted fractions were analyzed by 12% sodium dodecyl sulfate polyacrylamide gel electrophoresis (SDS-PAGE). Fractions containing pure PhnO (>95%) were pooled and dialyzed against 25 mM sodium phosphate buffer, pH 8.0.

To perform *N*-acetylation reaction, purified PhnO, 10 μl, was added to a 0.6 mL reaction mixture of 1 mM aminoalkylphosphonate, 3 mM acetyl-CoA and 3 mM $MgCl_2$ in 25 mM Tris-HCl buffer, pH 8.0. The reactions were followed by ^{31}P-NMR spectroscopy.

2.2.2 Results

2.2.2.1 Accumulation of **1a** catabolic intermediates in *phn* mutant strains of *E. coli*

If an *E. coli phn* gene is interrupted then an intermediate of the CP-lyase pathway that is processed by the encoded protein of the interrupted gene should accumulate. To analyze phosphorus-containing intermediates of **1a** catabolism an *E. coli phn*$^+$ (strain HO2568) and Δ*phn* (HO2680) strains along with mutant strains, with transposon insertions in *phnE* (strain HO2531), *phnG* (HO2533), *phnH* (HO2534), *phnI* (HO2535), *phnJ* (HO2536), *phnK* (HO2537), *phnL* (HO2538), *phnM* (HO2539), *phnN* (HO2540), *phnO* (HO2541), or *phnP* (HO2542), were used. Many of the strains are organophosphonate growth deficient[21-23] and therefore must be grown in the presence of both **1a** and P_i. To ensure that the *phn* genes are being expressed all the strains contain the Δ*pstS605* allele that renders the *phn* operon expression independent of the P_i supply[54]. The growth medium was isolated and analyzed by ^{31}P-NMR spectroscopy for phosphorus-containing compounds.

The medium was analyzed for signals other than that of **1a** and P_i. **1a** has a distinct ^{31}P-NMR signal at δ 23 - 24 ppm while P_i is observed at δ 1.2 - 1.8 ppm. Both signals are pH

dependent due to ionization of the organophosphonate, with a pk_a close to 7[45]. The *phn*$^+$, *Δphn*, *phnE*, *phnG*, *phnH*, *phnI*, *phnK*, *phnL*, *phnM*, *phnN* and *phnO* strains did not display a ^{31}P-NMR signal other than that of **1a** and P_i. This indicates that there was either an absence of phosphorus-containing compounds in these strains or not enough for detection by NMR. Both the *phnJ* and *phnP* strains contained a peak at δ 26.4 ppm, with the *phnP* strain also exhibiting a signal at δ 18.6 ppm (Figure 2-10A).

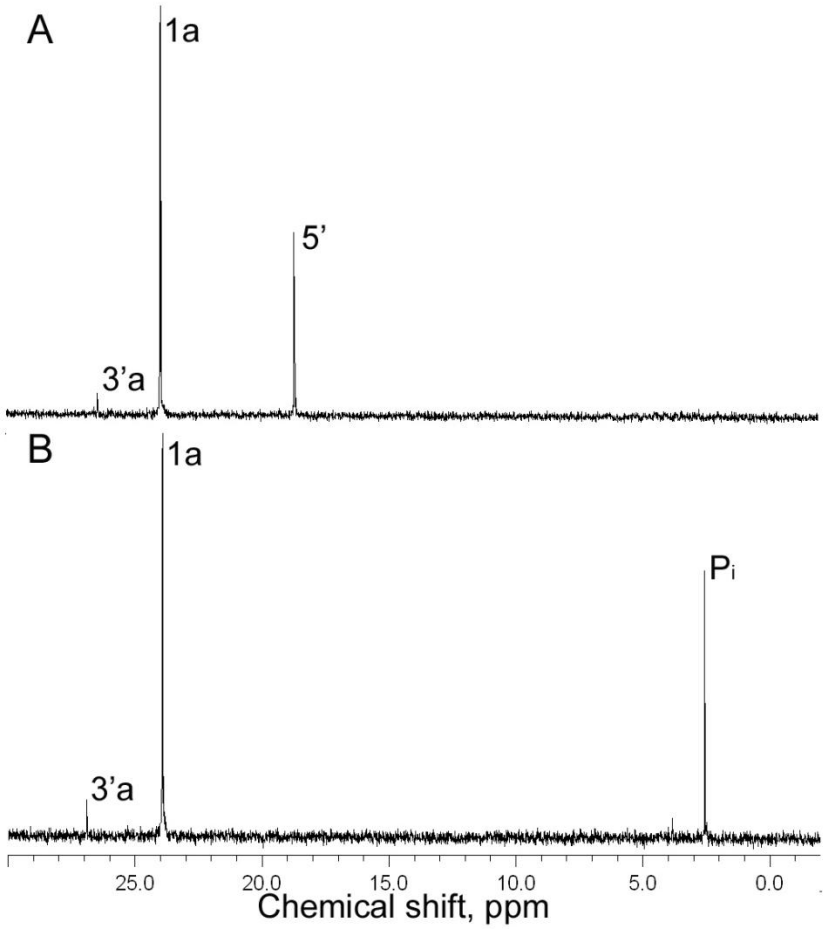

Figure 2-10. ^{31}P-NMR spectra of the growth medium of HO2542 (*phnP*) grown in the presence of methylphosphonate (1a), (A) before and (B) after reaction with purified PhnP. Figure adapted from reference 35.

2.2.2.2 Accumulation of phosphorus-containing compounds in an *E. coli phnP* mutant strain

The growth medium of the *E. coli phnP* mutant strain grown in **1a**, exhibited two additional ^{31}P-NMR signals at δ 18.6 and δ 26 ppm. To further analyze these potential CP-lyase pathway intermediates, the *phnP* strain (HO2542) was grown with a variety of organophosphonates. The growth medium of these cultures was analyzed by ^{31}P-NMR spectroscopy as described above and results are seen in Table 2-3. No matter what organophosphonate was added a signal at δ 18.6 ppm accumulated in the growth medium, as seen in Figure 2-10A when HO2542 is grown with **1a**. With the exception of phenylphosphonate, the addition of all the organophosphonates also yielded a unique signal that appeared downfield from the signal for the residual organophosphonate, as seen in Figure 2-10A (δ 26.4) when HO2542 is grown with **1a**. This unique downfield signal was also present in the *phnJ* strain (Table 2-3).

Table 2-3. Summary of ^{31}P-NMR chemical shifts observed in the growth medium of various *phn* strains grown with various organophosphonates[a]

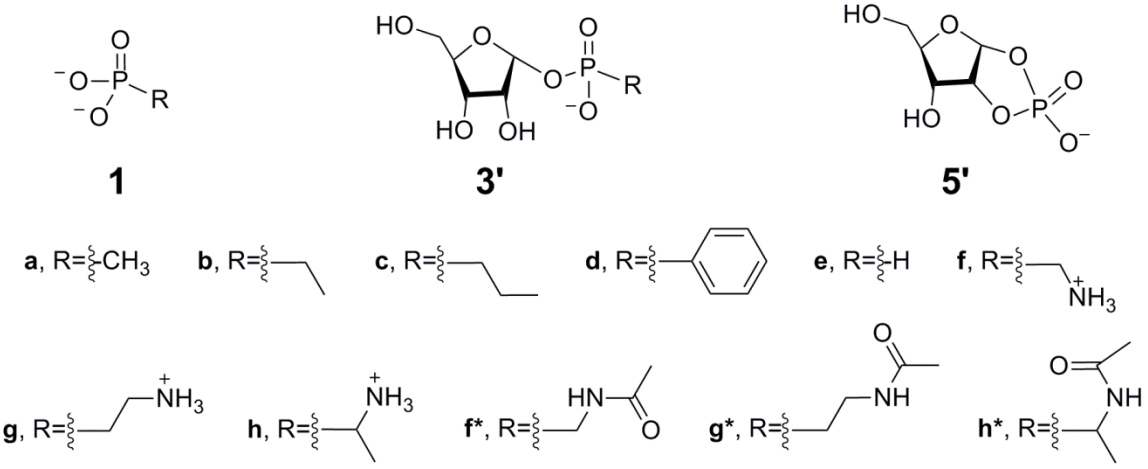

Strain	*Lesion*	*Addition*	*Chemical Shift (ppm)*	*Assignment*
HO2568	*phn*$^+$	**1f**	9.2	**1f**
			13.9[b]	**1f***
			17.4	**3'f***
		1g	16.8	**1g**

			19.4[c]	**1g***
			23.6	**3'g***
		***R*-1h**	12.6	***R*-1h**
		***S*-1h**	12.6	***S*-1h**
			18.1[d]	***S*-1h***
			20.6	***S*-3'h***
		1a	23.9	**1a**
		1b	27.5	**1b**
		1c	25.8	**1c**
HO2541	*phnO38*	**1f**	9.2	**1f**
		1g	16.8-17.0	**1g**
		***S*-1h**	12.6	***S*-1h**
		1b	27.5	**1b**
HO3412	*ΔphnO789*	**1f**	9.2	**1f**
		1g	17.0	**1g**
			18.6	**5'**
		***S*-1h**	12.6	***S*-1h**
HO2542	*phnP54*	**1f**	9.2	**1f**
			13.9-14.0	**1f***
			17.4	**3'f***
			18.6	**5'**
		1g	16.8-17.1	**1g**
			18.6	**5'**
			19.4-20.2	**1g***
			23.6	**3'g***
		***R*-1h**	12.6	***R*-1h**
		***S*-1h**	12.6	***S*-1h**
			18.0	***S*-1h***
			18.6	**5'**
			20.7	***S*-3'h***
		1a	18.6	**5'**
			23.9	**1a**
			26.4	**3'a**

		1b	18.6	**5'**
			27.6	**1b**
			30.3	**3'b**
		1c	18.6	**5'**
			25.8	**1c**
			28.7	**3'c**
		1d	18.6	**5'**
			11.9	**1d**
		1e	18.6	**5'**
			13.3	**3'e**
			3.0	**1e**
HO2536	*phnJ14*	**1f**	9.2	**1f**
			13.9	**1f***
			17.4	**3'f***
		1g	16.9-17.0	**1g**
			19.7-20.0	**1g***
			23.6	**3'g***
		1a	23.9	**1a**
			26.4	**3'a**
		1b	27.6	**1b**
			30.3	**3'b**

Lesions indicate the disruption or deletion of specified gene; ***** indicates acetylation; and **'** indicates the lack of 5- or 5'-phosphate ester. [a] Data are from samples taken after 20 h of incubation in the presence of an organophosphonate. Due to uneven acidification of the growth media chemical shifts occasionally showed small differences among otherwise similar cultures. In particular 2-acetamidoethylphosphonate (**1g***) was prone to pH dependent chemical shifts (up to 0.6 ppm). [b] This signal was assigned as *N*-acetamidomethylphosphonate (**1f***) by spiking the NMR sample with the reaction product of aminoalkylphosphonate *N*-acetyltransferase with aminomethylphosphonate (**1f**) as the acetyl acceptor. [c] This signal was assigned as 2-acetamidoethylphosphonate (**1g***) by spiking the NMR sample with the reaction product of aminoalkylphosphonate *N*-acetyltransferase with 2-aminoethylphosphonate (**1g**) as the acetyl acceptor. [d] This signal was assigned as *N*-acetyl-(*S*)-1-aminoethylphosphonate (***S*-1h***) by

spiking the NMR sample with the reaction product of aminoalkylphosphonate *N*-acetyltransferase with (*S)*-1-aminoethylphosphonate (***S*-1h**) as the acetyl acceptor[31,35].

2.2.2.3 Accumulation of aminoalkylphosphonate catabolic intermediates in *phn* mutant strains of *E. coli*

There are limited studies that probe the growth of *phn* strains on aminoalkylphosphonates. Thus catabolic intermediates of aminoalkylphosphonate degradation in *E. coli phn* mutants were analyzed. The *phn*$^+$, *phnJ*, *phnO*, and *phnP* strains grown in the presence of 2-aminoethylphosphonate (**1g**), (*R*)-1-aminoethylphosphonate (***R*-1h**), (*S*)-1-aminoethylphosphonate (***S*-1h**) and aminomethylphosphonate (**1f**) were probed as above. The growth medium of strains grown in aminoalkylphosphonates was compared to that of the strains grown in ethylphosphonate (**1b**). A summary of the various ^{31}P-NMR chemical shifts obtained for the various strains along with their assignments is given in Table 2-3.

The *phn*$^+$ strain grown in the presence of **1b** did not display a ^{31}P-NMR spectroscopy signal other than that of **1b** and P_i, which is similar to that seen with growth in the presence of **1a**. This was also the case for growth in the presence of ***R*-1h**. However, when grown with other aminoalkylphosphonates two additional ^{31}P-NMR spectroscopy signals appeared, at δ 13.9 and δ 17.4 ppm for **1f**, δ 19.4 and δ 23.6 ppm for **1g**, and δ 18.1 and δ 20.6 ppm, for ***S*-1h**. The *phn*$^+$ strain grown with **1g** is shown as an example (Figure 2-11). The δ 16.8 ppm signal that corresponds to **1g** has greatly diminished after 20 h incubation with two additional signals (δ 19.4 and 23.6 ppm) appearing.

Analysis of the growth medium of the *phnJ* mutant revealed similar results to that of the *phn*$^+$ strain when grown with aminoalkylphosphonates. However, when grown in the presence of **1b** the *phnJ* mutant produced an additional signal at δ 30.3 ppm not seen in the *phn*$^+$ strain. This was similar to the δ 26 ppm, signal observed with **1a**. The *phnP* mutant exhibited an additional peak at δ 18.6 ppm for all organophosphonates added, with the exception of ***R*-1h**. The signal at

δ 18.6 ppm is therefore most likely an intermediate that is common to organophosphonate catabolism.

The growth medium of both *phnO* strains (HO2541 and HO3412) contained no additional ^{31}P-NMR spectroscopy signals beyond that of the added aminoalkylphosphonate and P_i. However, strain HO3412 in the presence of **1g** did exhibit a signal at δ 18.6 ppm seen in the growth medium of the *phnP* mutant. This indicates that the *phnO* gene product is responsible for forming the two additional signals seen in the growth medium of the *phnO*$^+$ strains in the presence of aminoalkylphosphonates. These peaks likely correspond to *N*-acetylated aminoalkylphosphonate intermediates in the CP-lyase pathway.

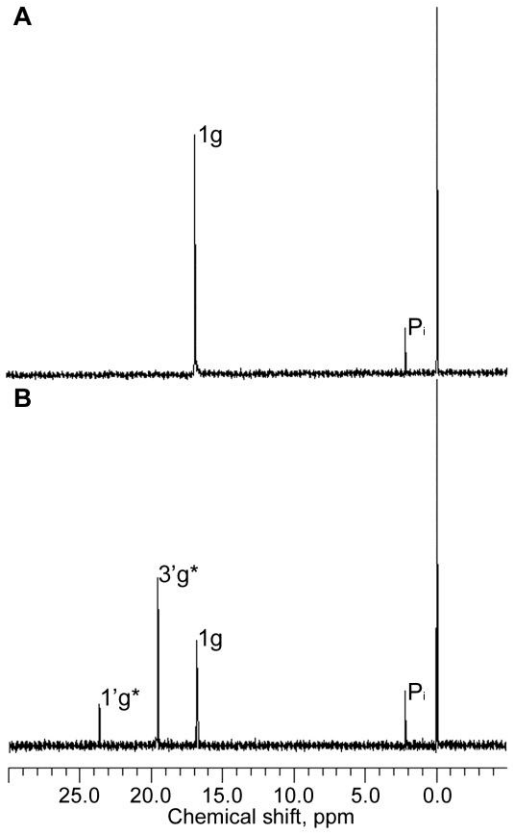

Figure 2-11. A representative ^{31}P-NMR spectroscopy of the conversion of aminoalkylphosphonates by the *E. coli phn*$^+$ strain using 2-aminoethylphosphonate (1g) as a substrate. The *phn*$^+$ strain (HO2568) was grown in 03P medium and the growth medium was analyzed as described in Material and Methods. (A) ^{31}P-NMR spectrum of growth medium

immediately after addition of **1g**, the signal at δ 16.8 ppm corresponds to **1g**. (B) ^{31}P-NMR spectrum of growth medium after 20 h of incubation with **1g**, two additional signals have appeared at δ 19.4 and δ 23.6 ppm corresponding to dephosphorylated **3g*** and **1g***, **3'g*** and **1'g***, respectively. The peaks at 2.3 ppm and 0.0 ppm correspond to P_i in the medium and the internal capillary standard, respectively. Figure adapted from reference 31.

2.2.2.4 Characterization of CP-lyase intermediates

The accumulating phosphorus-containing compounds were purified from the supernatants of larger cultures in order to determine their structure. The growth medium from a **1g**-grown culture of HO2542 (*phnP*) was clarified and applied to an ion-exchange column. The eluted phosphorus-containing compounds were separated and followed by ^{31}P-NMR spectroscopy as described in the methods section (Figure 2-12).

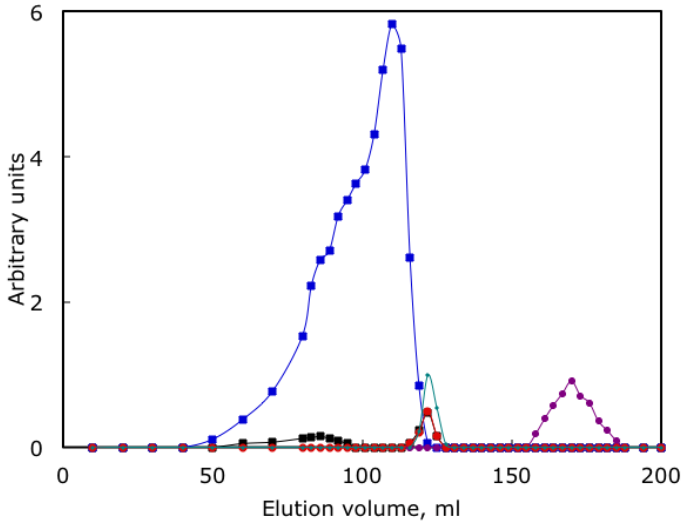

Figure 2-12. Elution profile of the ion-exchange chromatography of phosphorus-containing compounds from strain HO2542 after 24 h of incubation in the presence of 2-aminoethylphosphonate (1g). The clarified growth medium was applied to the ion-exchange column and the eluted fractions were monitored by ^{31}P-NMR spectroscopy. Relative amounts of the various compounds were estimated based on the 17 mM phosphoric acid external standard. The symbols correspond to the following signals: black squares, δ 24 ppm; blue squares, δ 19.5 ppm; purple circles, δ 18.6 ppm; red circles, δ 3.6 ppm; and green circles, δ 1.6 ppm (P_i). Figure from reference 31.

Fractions containing unique phosphorus-containing compounds were pooled and their structures were determined by NMR spectroscopy. The compound with a ^{31}P-NMR signal at δ 19.5 ppm (blue squares, Figure 2-12) was shown to be 2-*N*-acetamidoethylphosphonate (**1g***) by ^{1}H, ^{13}C and ^{31}P-NMR spectroscopy. The following data were obtained: ^{1}H-NMR (400 MHz, D_2O) δ 3.35 (dt, $^{2}J_{HH}$ = 7.6, $^{3}J_{HP}$ = 10.2 Hz, 2H), 1.96 (s, 3H), 1.82 (dt, $^{2}J_{HH}$ = 7.6, $^{2}J_{HP}$ = 16.1 Hz, 2H) (Figure 2-13A); ^{13}C-NMR (101 MHz, D_2O) δ 173.89 (s, CO, C3), 35.04 (s, CH_2, C2), 27.85 (d, $^{1}J_{CP}$ = 131 Hz, CH_2, C1), 22.03 (s, CH_3, C4) (Figure 2-13B). The protons were assigned to carbons by ^{1}H/^{13}C HSQC NMR (Figure 2-13C), and additional bond connectivities were assigned by ^{1}H/^{13}C HMBC NMR (Figure 2-13D). ^{1}H/^{13}C correlations from HSQC and HMBC NMR spectra are shown in Figure 2-14A.

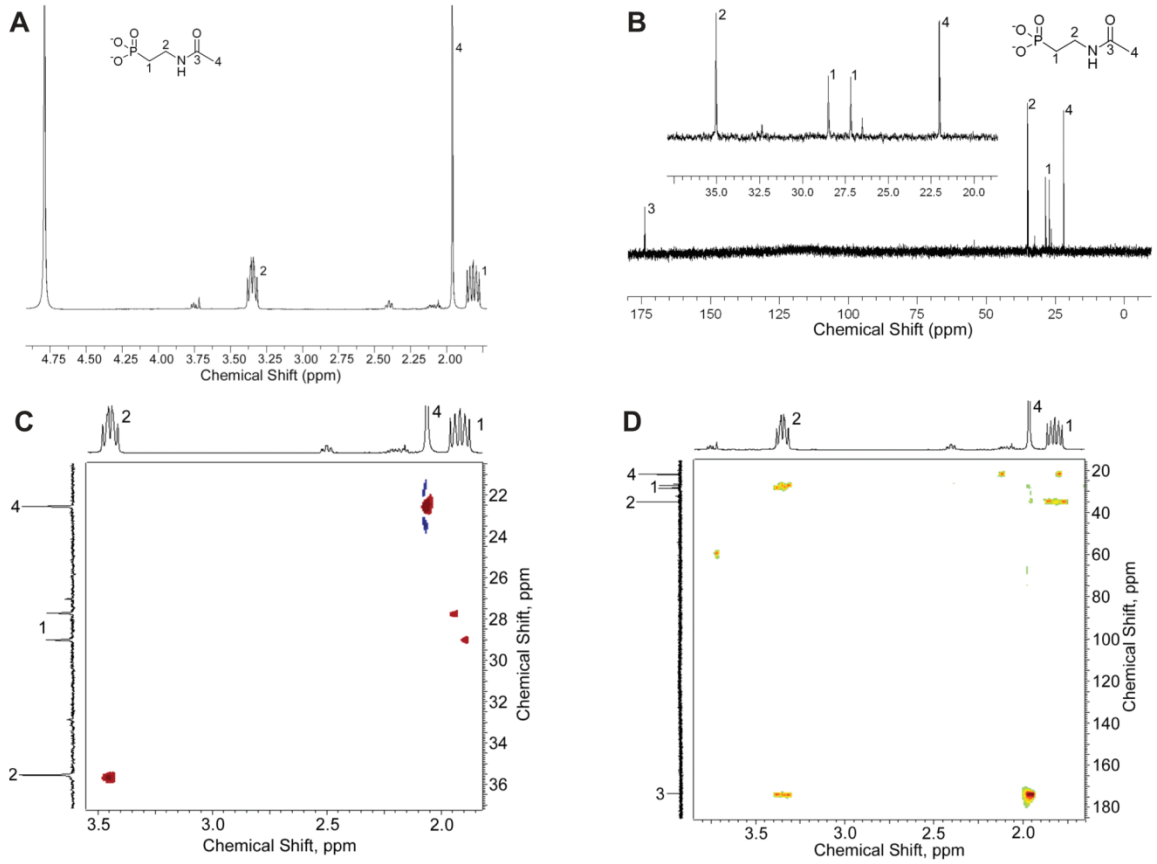

Figure 2-13. NMR spectra of 2-*N*-acetamidoethylphosphonate (1g*). (A) ^{1}H-NMR spectrum, (B) ^{13}C-NMR spectrum, (C) ^{1}H/^{13}C-HSQC NMR spectrum, and (D) ^{1}H/^{13}C-HMBC NMR spectrum[31].

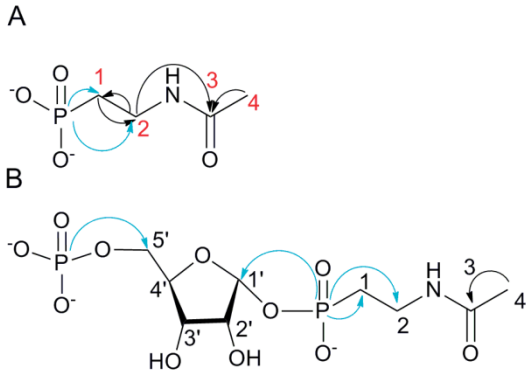

Figure 2-14. Summary of observed $^{1}H/^{13}C$ HSQC, $^{1}H/^{13}C$ HMBC and $^{1}H/^{31}P$ HMBC correlations for (A) 2-*N*-acetamidoethylphosphonate (1g*) and (B) 5'-phospho-α-D-ribosyl-1'-(2-*N*-acetamidoethylphosphonate) (3g*). The black arrows show the correlations observed by $^{1}H/^{13}C$ HSQC and $^{1}H/^{13}C$ HMBC spectroscopy; blue arrows show the correlation observed by $^{1}H/^{31}P$ HMBC spectroscopy[31].

In addition to 2-*N*-acetamidoethylphosphonate (**1g***), a compound was purified from the *phnP* growth medium that contained two ^{31}P-NMR shifts (δ 24 and δ 3.6 ppm). The chemical shift values of the phosphorus atoms suggest that one of the phosphorus atoms was bound to a carbon as an organophosphonate (δ 24 ppm) while the other was bond to oxygen as a phosphate ester (δ 3.6 ppm). Fractions containing these signals (elution volume 125 - 130 mL) were concentrated and analyzed by NMR spectroscopy. Although the sample also contained a small amount of **1g***, the structure of the second compound was assigned as 5'-phospho-α-D-ribosyl-1'-(2-*N*-acetamidoethylphosphonate) (**3g***). The following NMR data was obtained: ^{1}H-NMR (600 MHz, D_2O): δ 5.73 (H1', m, 1H), 4.41 (H4', m, 1H), 4.24 (H2'/H3', m, 3H), 4.04 (H5', m, 2H), 3.45 (H2 of **3g*** and **1g*** as well as a contaminating compound, m, 3.5H), 2.04 (H4 of **3g*** and **1g***, m, 5H), 1.89 (H1 of **3g*** and **1g*** as well as a contaminating compound, m, 7H) (Figure 2-15A); ^{13}C-NMR (125.7 MHz, D_2O) δ 173.9 (s, CO, C3), 97.4 (d, $^{2}J_{CP}$ = 5.8 Hz, CH, C1'), 84.3 (d, CH, C4'), 71.3 (s, CH, C2'), 69.4 (s, CH, C3'), 64.7 (d, $^{2}J_{CP}$ = 4.6 Hz, CH_2, C5'), 34.6 (s, CH_2, C2), 30.6 (d, $^{1}J_{CP}$ = 137 Hz, CH_2, C1), 22.0 (s, CH_3, C4) (Figure 2-15B); ^{31}P-NMR (161.9 MHz, D_2O) δ 23.7 (P1) and 0.55 (P5'), in addition to 21.7 ppm (P of **1g***) and 0.17 ppm P_i. The protons

were assigned to carbons on the basis of $^{1}H/^{1}H$ correlation spectroscopy (COSY), ^{13}C, ^{13}C distortionless enhancement by polarization transfer (DEPT) NMR, $^{1}H/^{13}C$ HSQC and $^{1}H/^{13}C$ HMBC NMR spectra, as well as $^{1}H/^{31}P$ HMBC NMR spectra. The two-dimensional $^{1}H/^{13}C$ HSQC and $^{1}H/^{31}P$ HMBC NMR spectra are shown in Figure 2-15C and D, respectively. The $^{1}H/^{1}H$ COSY spectrum and $^{1}H/^{13}C$ HMBC spectrum are seen in Figure 2-16 and Figure 2-17, respectively. The observed $^{1}H/^{13}C$ correlations from HSQC and HMBC NMR spectra as well as $^{1}H/^{31}P$ correlations from HMBC NMR spectra are shown in Figure 2-14B. In addition there is a list of chemical shifts of individual protons and their correlation with carbon and phosphorus atoms given in Table 2-4. High resolution ESI-MS (negative ion mode) revealed a molecular ion peak at *m/z* = 378.0351 corresponding to the expected value for the molecular ion of **3g*** ($C_9H_{18}NO_{11}P_2$; expect *m/z* = 378.0355).

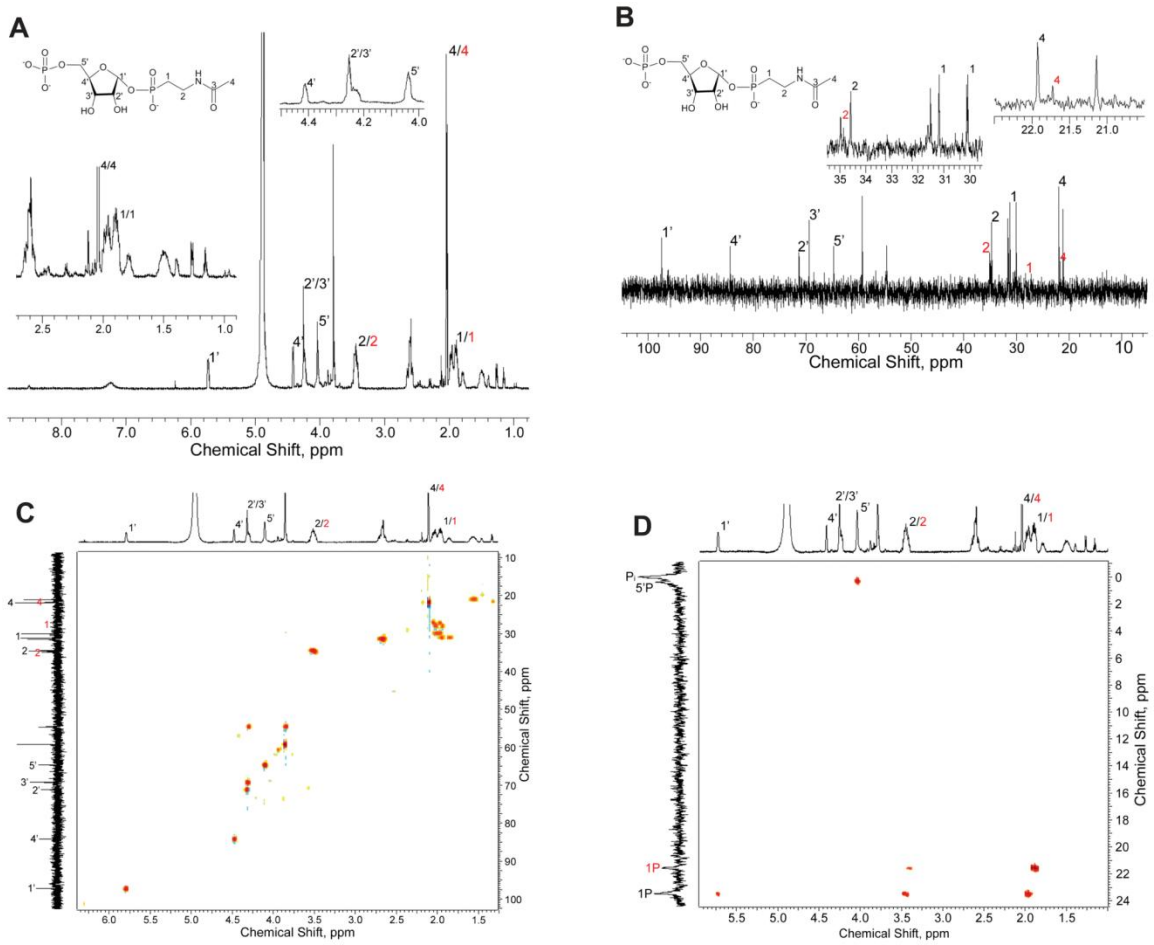

Figure 2-15. NMR spectroscopy of 5'-phospho-α-D-ribosyl-1'-(2-*N*-acetamidoethyl phosphonate) (3g*). (A) ^{1}H-NMR spectrum, (B) ^{13}C-NMR spectrum, (C), ^{1}H/^{13}C-HSQC NMR spectrum, and (D) ^{1}H/^{31}P HMBC-NMR spectrum. Protons and carbons of **1g*** are labelled in red[31].

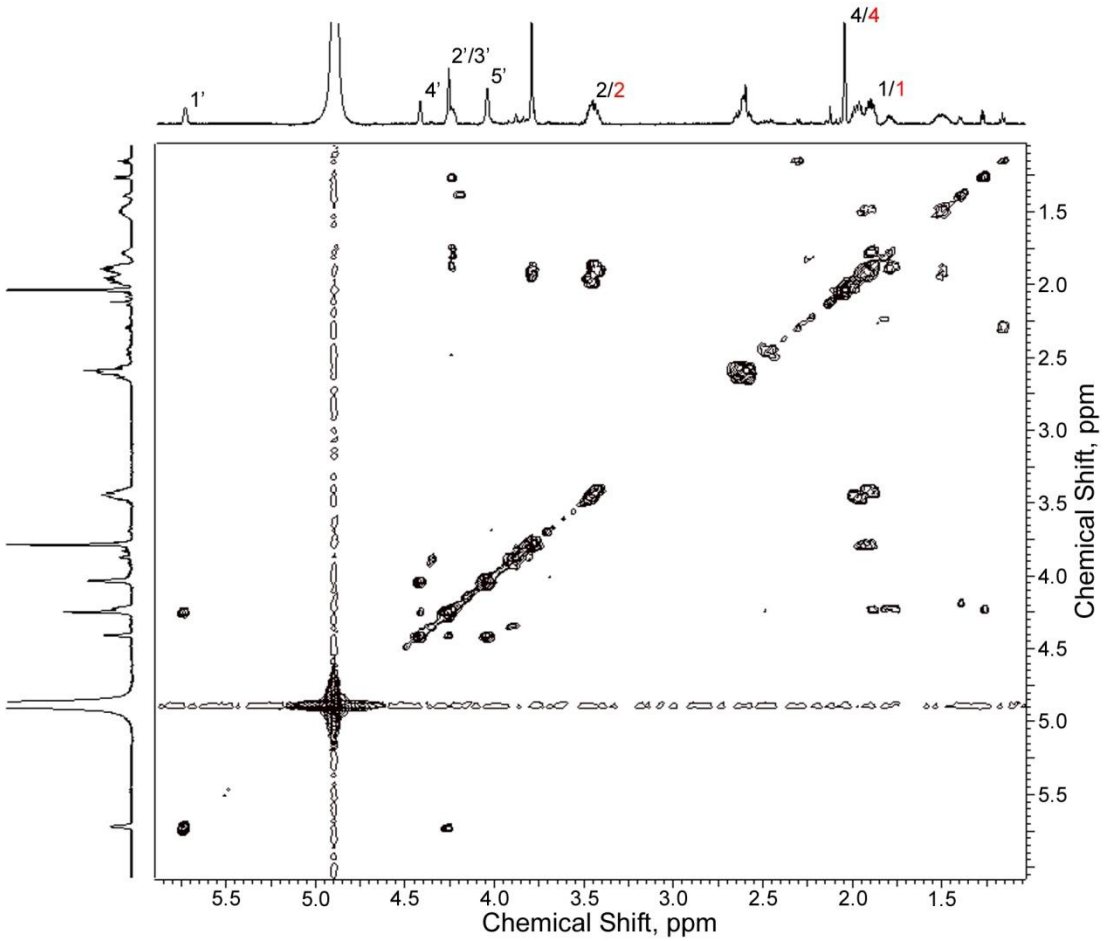

Figure 2-16. ^{1}H/^{1}H COSY spectrum of 5'-phospho-α-D-ribosyl-1'-(2-*N*-acetamidoethyl phosphonate) (3g*). Protons of **1g*** are labelled in red[31].

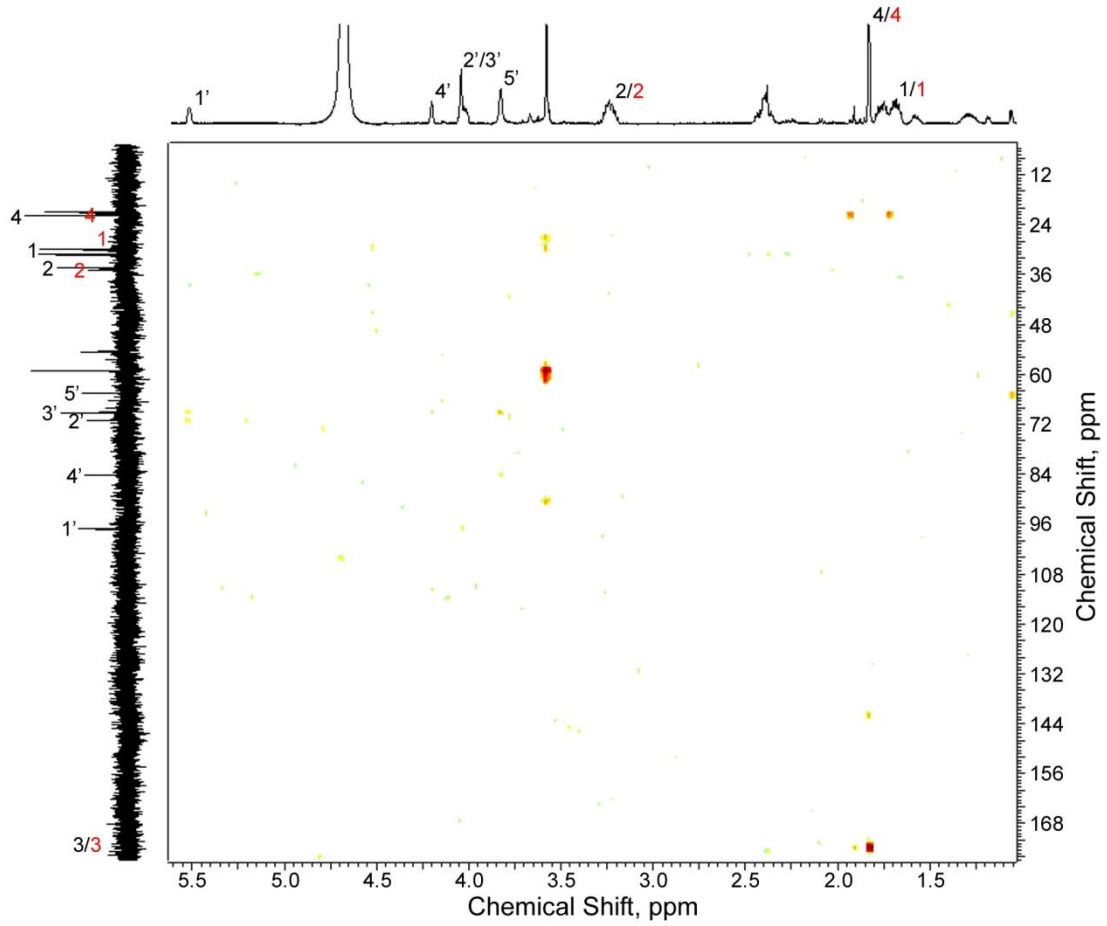

Figure 2-17. $^{1}H/^{13}C$ HMBC spectrum of 5'-phospho-α-D-ribosyl-1'-(2-*N*-acetamidoethyl phosphonate) (3g*). Carbons and protons of **1g*** are labelled in red[31].

Table 2-4. Assignment of NMR spectroscopy signals observed for 5'-phospho-α-D-ribosyl-1'-(2-*N*-acetamidoethylphosphonate) (3g*)[a,31]

C	*^{13}C-NMR (ppm)*	*^{1}H-NMR (ppm, multiplicity, integration)*	*^{1}H/^{13}C HMBC (ppm)*	*^{1}H/^{31}P HMBC (ppm)*
1	30.6	1.89, m, 7[b]		23.5, 21.6
2	34.6	3.45, m, 4		23.5, 21.6
3	173.9			
4	22.0	2.04, s, 5	172.1, 173.9	
1'	97.4	5.73, m, 1		23.5
2'	71.3	4.24, m, 3[c]		
3'	69.4	4.24, m, 3[c]		
4'	84.3	4.41, m, 1		
5'	64.7	4.04, m, 2		0.34
1[d]	27.7	1.89, m, 7[b]		23.5, 21.6
2[d]	34.9	3.45, m, 4		23.5, 21.6
3[d]	172			
4[d]	21.7	2.04, s, 5	172.1, 173.9	

[a] Preparation also contained 2-*N*-acetamidoethylphosphonate (**1g***) and small amounts of one or more contaminants. ^{13}C- and ^{1}H-NMR spectra were assigned to correlations observed in the COSY, HSQC and HMBC specra.

[b] 2H of 5'-phospho-α-D-ribosyl-1'-(2-*N*-acetamidoethylphosphonate) (**3g***) and 2-*N*-acetamidoethylphosphonate (**1g***) each, as well as 3H from a contaminating compound.

[c] H2' and H3' as well as H from a contaminating compound.

[d] Data for 2-*N*-acetamidoethylphosphonate (**1g***).

A third phosphorus-containing compound was isolated from the *E. coli phnP* growth medium with a ^{31}P-NMR signal at δ 24 ppm (black squares Figure 2-12). Based on the characterization of 5'-phospho-α-D-ribosyl-1'-(2-*N*-acetamidoethylphosphonate) (**3g***) and a similar compound from the growth medium of HO2542 grown in the presence of **1b** (see below), this third compound is likely α-D-ribosyl-1'-(2-*N*-acetamidoethylphosphonate), **3'g*** the 5'-

dephosphorylated derivative of **3g***, and for this reason the compound was not characterized further.

The unique downfield peak at δ 30.3 ppm found in the growth medium of HO2542 (*phnP*) grown in the presence of **1b** was also targeted for characterization. The clarified growth medium containing the compound with a ^{31}P-NMR spectroscopy peak at δ 30.3 ppm was purified by ion-exchange chromatography as described in the methods. The purified compounds ^{1}H and ^{31}P-NMR spectroscopic data corresponded to the previously reported α-D-ribosyl-1'-ethylphosphonate[42]. The following NMR data was obtained: ^{1}H-NMR (D_2O, 400 MHz): δ 5.57 (H1, dd, J_{H1-H2} = 4.0 Hz, J_{H1-P} = 6.5 Hz, 1H), 4.16 (H4, dd, J_{H4-H3} = 3.4 Hz, J_{H4-H5} = 7.6 Hz, 1H), 4.07 (H2, dd, J_{H2-H1} = 4.0 Hz, J_{H2-H3} = 6.4 Hz, 1H), 4.02 (H3, dd, J_{H3-H4} = 3.4 Hz, J_{H3-H2} = 6.5 Hz, 1H), 3.7 (H5ab, m, 2H), 1.60 (CH_2, dd, J_{H6-H7} = 7.6 Hz, J_{H6-P} = 17 Hz, 2H), 1.02 (CH_3, dt, J_{H7-H6} = 7.7 Hz, J_{H7-P} = 15 Hz, 3H). ^{31}P-NMR (161.9 MHz): δ 30.3 (ddd, J = 24, 18, and 6.2 Hz). By comparison, the structures of the varying downfield peaks in the growth medium of HO2542 when grown in the presence of different organophosphonates were then presumed to be α-D-ribosyl derivatives of the added organophosphonate (Table 2-3).

Finally, the common intermediate detected in the growth medium of HO2542 (*phnP*) in the presence of a variety of different organophosphonates and phosphite has a peak at δ 18.6 ppm. The chemical shift along with coupling constants $J_{P1,2-H1}$ = 17 Hz and $J_{P1,2-H2}$ = 4.3 Hz suggests that the compound is α-D-ribosyl-1,2-cyclic phosphate (**5'**) due to the similarity to the reported value for 5-phospho-α-D-ribosyl-1,2-cyclic phosphate (**5**) [55,56]. However, this compound lacks a phosphate ester peak at approximately 3 - 4 ppm indicating that the 5-phosphate ester is missing.

2.2.2.5 Activity of the *phnO* and *phnP* gene products

Based on the fact that the specified amino acid sequence from the *phnO* of *E. coli* and *phnO* of *S. enterica* are 77% identical, it is likely the specified enzymes perform similar

functions. The *phnO* gene product of *S. enterica* has been identified as an aminoalkylphophonate *N*-acetyltransferase that can acetylate a wide range of aminoalkylphosphonates. To confirm that the *phnO* gene product from *E. coli* also acetylates aminoalkylphosphoantes, a hexahistidine tagged variant of PhnO was purified. PhnO enzymatic activity was analyzed using aminomethylphosphonate (**1f**), 2-aminoethylphosphonate (**1g**), (*R*)-1-aminoethylphoshonate (***R*-1h**) and (*S*)-1-aminoethylphoshonate (***S*-1h**) as substrates and acetyl-CoA as the acetyl donor. The reactions were monitored with ^{31}P-NMR (Figure 2-18). PhnO was able to convert **1f**, ***S*-1h**, and **1g** to products with signals at δ 14.3, 18.1, and 20.5 ppm, respectively (Figure 2-18B-D). ***R*-1h** was only slowly converted to a product at δ 18.3 ppm (Figure 2-18E). Approximately 20% of ***R*-1h** was consumed in one hour; however further incubation or addition of more PhnO enzyme did result in more conversion to form a product appearing at δ 18.3 ppm. The product of the PhnO reaction with **1g** was mixed with the supernatant fluid of HO2542 grown in **1g** and the peak at δ 20.5 ppm enlarged. The chemical structure of this compound was shown by NMR spectroscopy to be, 2-*N*-acetamidoethylphosphonate (**1g***) with a signal at δ 20.5 ppm, this was confirmed by ^{1}H, ^{13}C ^{1}H/^{13}C HSQC and ^{1}H/^{13}C HMBC spectra, see above.

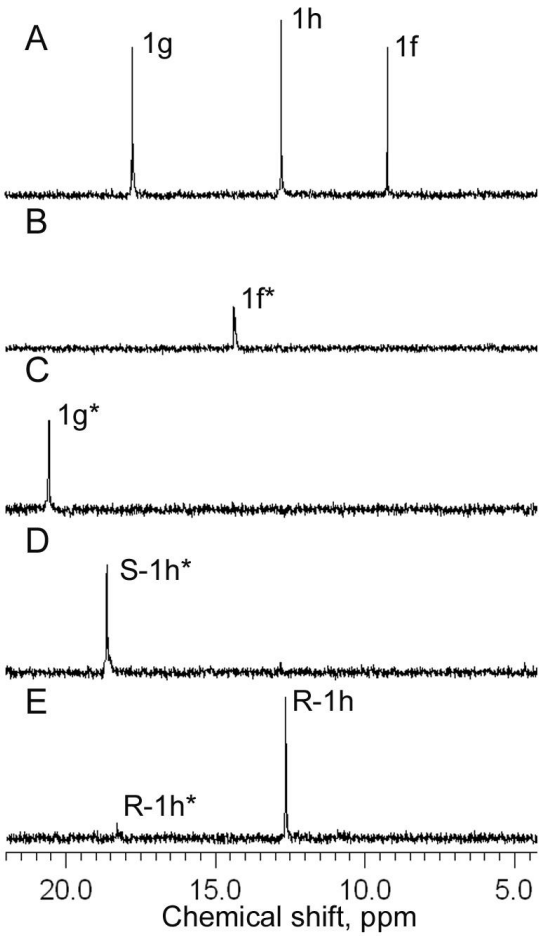

Figure 2-18. ^{31}P-NMR spectra of PhnO, an aminoalkylphosphonate *N*-acetyltransferase, reactions with a variety of aminoalkylphosphonates and acetyl-CoA. (A) Reaction mixture containing aminomethylphosphonate, **1f** (δ 9.2 ppm), 2-aminoethylphosphonate, **1g** (δ 17.7 ppm), (*R*)-1-aminoethylphosphonate, ***R*-1h** (δ 12.7 ppm) and (*S*)-1-aminoethylphoshonate, ***S*-1h** (δ 12.7 ppm). The ^{31}P-NMR signals of acetyl-CoA are not shown. (B) Product, **1f*** (δ 14.3 ppm) of reaction with **1f**, (C) product, **1g*** (δ 20.5 ppm) of reaction with **1g** (D) product, ***S*-1h*** (δ 18.3 ppm) of reaction with ***S*-1h** and (E) product, ***R*-1h*** (δ 18.3 ppm) of reaction with ***R*-1h**.

A common intermediate, α-D-ribosyl-1,2-cyclic phosphate (**5'**) (δ 18.6 ppm), accumulated in the HO2542 *phnP* strain when grown with a variety of organophosphonates. PhnP was previously shown to degrade 2',3'-cyclic phosphates, thus we hypothesized that the isolated α-D-ribosyl-1,2-cyclic phosphate was a PhnP substrate. When purified PhnP was added

to the growth medium of HO2542 grown with methylphosphonate (**1a**), the presence of the δ 18.6 ppm peak disappeared and a peak at δ 2.5 ppm appeared (Figure 2-10B). The PhnP product at δ 2.5 ppm was shown to be α-D-ribosyl-1-phosphate by spiking the sample with authentic material. However, the α-D-ribosyl-1,2-cyclic phosphate (**5'**) lacks a 5-phosphate ester, and the *phnN* gene product, an α-D-ribosyl-1,5-bisphosphate phosphokinase, is specific towards a 5-phosphorylated intermediate. Although most of the intermediates that accumulated in the HO2542 *phnP* strain lack this 5- or 5'-phosphate ester, a 5'-phosphorylated intermediate, 5'-phospho-α-D-ribosyl-1'-(2-*N*-acetamidoethylphosphonate) (**3g***) was isolated from the culture medium. It is likely that the 5- and 5'-dephosphorylated compounds in the growth medium arose by excretion from the cells with hydrolysis of the 5- and 5'-phosphate ester by a non-specific phosphatase. Therefore, it was hypothesized that the physiological substrate of PhnP was a 5-phosphorylated version of α-D-ribosyl-1,2-cyclic phosphate. To test this hypothesis, 5-phospho-α-D-ribosyl-1,2-cyclic phosphate (**5**) was synthesized by reaction of barium ion with PRPP (Figure 2-19). Upon addition of PhnP this compound was converted regioselectively to the expected α-D-ribosyl-1,5-bisphosphate (**6**) (Figure 2-19).

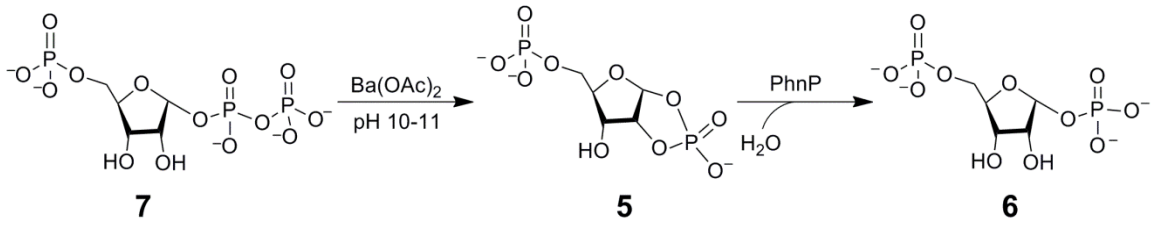

Figure 2-19. Synthesis of 5-phospho-α-D-ribosyl-1,2-cyclic phosphate (5) with barium acetate followed by conversion to α-D-ribosyl-1,5-bisphosphate (6) by PhnP.

To further verify that 5-phospho-α-D-ribosyl-1,2-cyclic phosphate is an intermediate in the CP-lyase pathway, a ^{32}P radiolabelled version of 5-phospho-α-D-ribosyl-1,2-cyclic phosphate

was synthesized by Bjarne Hove-Jensen. A radiolabelled physiological substrate of PhnP was also isolated by Bjarne Hove-Jensen from the growth medium of HO2542 *phnP*, as described[35]. The physiological substrate along with synthesized 5-phospho-α-D-ribosyl-1,2-cyclic phosphate and a mixture of the two were analyzed by TLC (Figure 2-20). The mixture of the two compounds afforded a single spot on the TLC plate, clearly showing that 5-phospho-α-D-ribosyl-1,2-cyclic phosphate is a physiological intermediate of the CP-lyase pathway and is therefore the substrate of the PhnP enzyme.

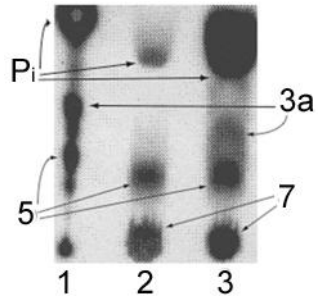

Figure 2-20. TLC on polyethyleneimine-cellulose of ^{32}P labelled organophosphonate metabolites. Lane 1, supernatant fluid of strain HO2542 (*phnP*) grown in the presence of $^{32}P_i$ and methylphosphonate (**1a**); lane 2, 5-phospho-α-D-ribosyl-1,2-cyclic phosphate (**5**) formed after incubation of [^{32}P] PRPP as described[35]; lane 3, a mixture of equal amounts of the solutions applied to lane 1 and 2. The identity of the remaining spot, **3a** is presumed to be 5'-phospho-α-D-ribosyl-1'-methylphosphonate. Figure adapted from reference 35.

2.2.2.6 Aminoalkylphosphonates as a P_i source

After examining the growth medium of some *phn* mutant strains grown in aminoalkylphosphonates it became apparent that the *phnO* gene is playing a role in the CP-lyase pathway. The question remains whether *N*-acetylation is important for CP bond cleavage or if it has an alternative physiological function. Many growth studies with *phn* mutants have been conducted[10,22,23]. However, these studies have not compared the growth of the strains on aminoalkylphosphonates. To analyze the importance of the *phnO* gene in the CP-lyase pathway, aminoalkyphosphonates were assessed as a P_i source for *E. coli* strains.

Isogenic *E. coli phn*$^+$ (HO3414) and *phnO* (BW17572 and HO3413 with altered *phnO38* and *ΔphnO789* alleles) strains were grown on solid medium with a variety of organophosphonates (**1a**, **1b**, **1c**, **1f**, **1g**, and **1i**, Figure 2-9). The growth response of the strains after 48 h was recorded (Table 2-5). The growth of the strains was compared to that of a *Δphn* strain (HO2578). As expected the *Δphn* strain lacking the *phnGHIJKLMNOP* genes could not grow on any of the added organophosphonates, indicating its inability to use organophosphonates as a P_i source. In contrast the *phn*$^+$ strain was able to utilize all the analyzed organophosphonates. Surprisingly, the two *phnO* strains were unable to utilize aminomethylphoshphonate (**1f**) as a P_i source, but were able to utilize all of the other organophosphonates assayed.

Aminomethylphosphonate (**1f**) is considered an analog of glycine and may inhibit biochemical reactions involving this amino acid. The addition of glycine did not restore the growth of the *phnO* strains, however the addition of P_i did. The data suggest that **1f** does not take the place of glycine in biochemical reactions but rather that the *phnO* gene product is obligatory for growth with **1f** as a P_i source. In contrast, the *phnO* gene product is not required for growth on other aminoalkylphosphonates, **1g** and **1i** or for growth with alkylphosphonates as P_i sources.

The two 1-aminoethylphosphonate enantiomers were also analyzed as P_i sources. (*S*)-1-Aminoethylphosphonate (***S*-1h**) is an analog of D-alanine and was found to be bactericidal. Cell lysis was initiated approximately 20 min upon its addition to the cultures. ***S*-1h** is a competitive inhibitor of alanine racemase[57], which is involved in the biosynthesis of the bacterial peptidoglycan cell wall. To overcome this effect the cells were grown with D-alanine or D/L-alanine as a supplement. The addition of D-alanine rescued the cells from lysis. The growth response of four strains on solid medium with 1-aminoethylphosphonate enantiomers as P_i sources is recorded in Table 2-6. None of the strains were capable of growing with only ***S*-1h** due to the bactericidal effect. All strains were able to grow with the addition of P_i and D-alanine, but only the *phn*$^+$ strain was capable of growing with just the addition of P_i. The addition of P_i to the

phnO and *Δphn* strains yielded small, heterogeneous colonies, indicative of the bactericidal effects of ***S*-1h**. The *phn*$^+$ strain would be capable of *N*-acetylating ***S*-1h** due to a functional *phnO* gene and therefore could be expected to detoxify the compound. When D-alanine was added, the toxic effect of ***S*-1h** was overcome, however the *phnO* strains were still unable to utilize ***S*-1h** as a sole P_i source. *N*-Acetylation is therefore required for growth on ***S*-1h**.

No toxic effects were observed with cells growing in the presence of ***R*-1h**. None of the strains grew with ***R*-1h** as the sole P_i source but all were capable of growing in the presence of ***R*-1h** and P_i. This indicates that ***R*-1h** is not an effective P_i source for *E. coli*.

Table 2-5. Growth response of *phnO* strains to various aminoalkyl- and alkylphosphonates

		Growth with phosphate source[a]								
					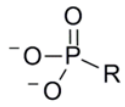		**1a**, R= -CH_3 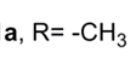 **1b**, R= 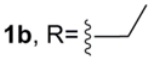	**1c**, R= 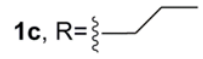 **1f**, R= 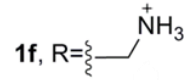	**1g**, R= 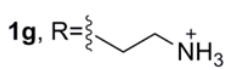 **1i**, R= 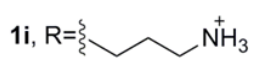	
Strain	***Lesion***	***None***	***1f***	***1f + P_i***	***1g***	***1i***	***1a***	***1b***	***1c***	***P_i***
BW17572	*phnO38*	-	-	+++	+++	++	+++	++	+	+++
HO3413	*ΔphnO789*	-	-	+++	++	+	++	++	+	+++
HO3414	*phn*$^+$	-	++	+++	+++	++	+++	++	+	+++
HO2578	*Δphn33-30*	-	-	+++	-	-	-	-	-	+++

[a] Growth was recorded after 48 h of incubation at 37 °C: -, no growth; + and ++, intermediate growth; +++, normal (wild-type-like) growth. Phosphorus-containing compounds were added at a concentration of 0.3 mM.

Table 2-6. Growth response of *phnO* strains to 0.3 mM 1-aminoethylphosphonate with and without additives

		Growth with[a] **(*S*)-1-aminoethylphosphonate** 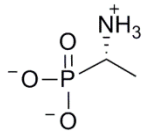				**(*R*)-1-aminoethylphosphonate** 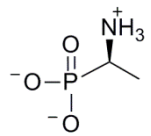	
Strain	***Lesion***	***None***	***P_i***	***D-alanine***	***P_i* + *D-alanine***	***No P_i***	***P_i***
BW17572	*phnO38*	-	-[b]	-	+++	-	+++
HO3413	*ΔphnO789*	-	-[b]	-	+++	-	+++
HO3414	*phn*$^+$	-	+++	++	+++	-	+++
HO2578	*Δphn33-30*	-	-[b]	-	+++	-	+++

[a] Growth was recorded after 48 h of incubation at 37 °C: -, no growth; + and ++, intermediate growth; +++, normal (wild-type-like) growth. The concentration of D-alanine was 100 mg L^{-1}.

[b] A few very small heterogeneous (in size and morphology) colonies were present.

2.2.3 Discussion

2.2.3.1 Intermediates of the CP-lyase pathway

Mutant strains of *E. coli* with a disrupted *pstSCAB-phoU* operon have proven to be useful for the detection of catabolic intermediates of organophosphonate degradation[43]. The mutant strains are unable to grow on organophosphonate as a sole P_i source due to the lack of one of the *phn* operon genes. However, the disrupted *pstSCAB-phoU* operon allows for the expression of the *phn* operon to be independent of the presence of P_i and therefore the cultures can be grown on P_i and an organophosphonate. This allows the catabolism of organophosphonates to be monitored. In earlier studies, Hove-Jensen grew these strains on a variety of organophosphonates in the presence of ^{32}P labelled P_i[43]. The results indicated that during the catabolic degradation of organophosphonates phosphorylation occurred at some point during the pathway. A labelled intermediate accumulated in *phnF*, *phnG*, *phnH*, *phnI*, *phnJ*, *phnK*, *phnL*, and *phnN* strains, whereas two compounds accumulated in the *phnP* strain. To further investigate these intermediates, the same mutants were grown with a variety of organophosphonates in the presence of P_i and culture mediums were monitored by ^{31}P-NMR spectroscopy. A similar pattern emerged for the *phnJ* and *phnP* strains, but no phosphorus-containing intermediates were detected in the growth medium of *phn*$^+$, *phnE*, *phnG*, *phnH*, *phnI*, *phnK*, *phnL*, *phnM*, *phnN* or *phnO* strains (Table 2-3).

The *phn*$^+$ strain is not expected to accumulate intermediates as it contains an intact CP-lyase pathway. Both *phnO* and *phnN* are dispensable for the breakdown of alkylphosphonates, and accumulation of intermediates is likewise not expected. The *Δphn* and *phnE* strains also are not expected to contain intermediates as the *phn* operon is completely missing from the *Δphn* strain and the *phnE* strain causes a disruption of the organophosphonate transport system, preventing alkylphosphonates from reaching other CP-lyase enzymes. Therefore, in these two

strains the supplied alkylphosphonates should be left untouched. One might expect the *phnG*, *phn*H, *phnI*, *phnK*, *phnL*, and the *phnM* strains to accumulate a phosphorus-containing intermediate as they have been shown to be necessary for cleavage of the CP bond. However, it is possible that one or more of these gene products are involved in the first step of organophosphonate catabolism, which was shown to be the case for PhnG, PhnH, PhnI and PhnL[28]. In addition, it is likely that the 5'-triphospho-α-D-ribosyl-1'alkylphosphonate formed by PhnI (Figure 2-9, step i.), in the presence of PhnG, PhnH, and PhnL, is unable to be secreted from the cell and this would be why the *phnM* strain does not yield an accumulation of a phosphorus-containing intermediate.

The ^{31}P-NMR signal at δ 18.6 ppm was observed in the growth medium of the *E. coli phnP* mutant in the presence of almost all organophosphonates and phosphite. It is likely that this signal represents a common CP-lyase pathway intermediate that is formed after CP bond cleavage. As the intermediate consistently accumulated in only the *phnP* strain it was hypothesized that this was the substrate of the *phnP* gene product. On the other hand, the chemical shift of the downfield signal found in both the *phnJ* and *phnP* strains varied according to the structure of the organophosphonate added to the medium. This downfield signal was therefore hypothesized to be a derivative of the added organophosphonate, and likely represents an intermediate in the pathway prior to CP bond cleavage. Due to the accumulation of these intermediates in the *phnJ* strain this would indicate that these organophosphonate derivatives are substrates of the *phnJ* gene product. In the case of the aminoalkylphosphonates two unique downfield signals were observed that vary depending on the structure of the aminoalkylphosphonate added to the medium. Neither of these unique downfield peaks are present in the *phnO* strains. This suggests that the corresponding intermediates are related to the activity of the *phnO* gene product. It was hypothesized that one of the downfield signals arose

from a product of *N*-acetylation by PhnO, whereas the second signal arises from further modification by one or more enzymes in the pathway.

The intermediates that were detected in the *phnP* strain were purified from growth medium of the *phnP* strain grown in the presence of ethylphosphosphonate (**1b**) and were characterized as α-D-ribosyl-1'-ethylphosphonate, previously isolated by Frost *et al.*[42], and α-D-ribosyl-1,2-cyclicphosphate (**5'**). Following our work Raushel and coworkers identified *in vitro* 5'-phosphorylated versions of these intermediates as substrates for CP-lyase enzymes[28]. In our studies both intermediates lack a 5- ot 5'-phosphate ester that is found in the radiolabelled studies by Hove-Jensen and in the work by Raushel, likely due to dephosphorylation by a non-specific phosphatase upon excretion from the cell. The physiological susbtrate of PhnP was confirmed using a ^{32}P radiolabelled substrate (Figure 2-19 and Figure 2-20), discussed in more detail below. Catabolic studies of aminoalkylphosphonates catabolism with the HO2568 *phn*$^{+}$ strain yielded a third intermediate, which was also observed in the *phnP* strain. Two *N*-acetylated intermediates were isolated from the growth medium of a *phnP* strain grown in the presence of **1g**. These intermediates were 2-*N*-acetamidoethylphosphonate (**1g***) and 5'phospho-α-D-ribosyl-1'-(2-*N*-acetamidoethylphosphonate) (**3g***).

2.2.3.2 Physiological role of PhnP

Two radioactive intermediates were previously shown to accumulate in a *phnP* strain grown in the presence of methylphosphonate (**1a**) and ^{32}P labelled P_i. The addition of PhnP converted one of the intermediates to a new compound, suggesting this was the physiological substrate of PhnP. In this study, α-D-ribosyl-1,2-cyclicphosphate was isolated from the *phnP* strain and was shown to be a competent substrate for PhnP yielding, α-D-ribosyl-1'-phosphate. The radiolabelled intermediates described above are phosphate esters. With this and the detection of 5'-phospho-α-D-ribosyl-1'-(2-*N*-acetamidoethylphosphonate) it appears that the detected α-D-

ribosyl-1'-ethylphosphonate (**3'b**) and α-D-ribosyl-1,2-cyclicphosphate (**5'**) are 5- and 5'-dephosphorylated versions of the *in vivo* intermediates of the organophosphonate degradation pathway. This was strengthened by the ability of PhnP to hydrolyze 5-phospho-α-D-ribosyl-1,2-cyclicphosphate (**5**) to α-D-ribosyl-1,5-bisphosphate (**6**), a substrate for α-D-ribosyl-1,5-bisphosphate phosphokinase, PhnN. The concentration of radiolabelled 5-phospho-α-D-ribosyl-1,2-cyclicphosphate was determined to be 15 μM by Bjarne Hove-Jensen[43] compared to 0.36 mM of α-D-ribosyl-1,2-cyclicphosphate[35]. Although both molecules were detected in the growth medium, the low concentration of the 5- and 5'-phosphate esters may be too low for detection by ^{31}P-NMR spectroscopy. On the other hand the dephosphorylated compounds would not be detected by the radiolabelled method. Luckily, with using **1g** as a substrate, 5'-phospho-α-D-ribosyl-1'-(2-*N*-acetamidoethylphosphonate) (**3g***) was detected directly by ^{31}P-NMR spectroscopy. This illustrates that the 5- or 5'-phosphate esters of the other compounds are likely the physiological substrates rather than the dephosphorylated versions.

PhnP is a metal ion-dependent phosphodiesterase of the β-lactamase superfamily[34]. It was previously shown to be active towards bis(*p*-nitrophenyl)phosphate as well as ribonucleoside-2',3'-cyclicphosphates. In this study α-D-ribosyl-1,2-cyclicphosphate and 5-phospho-α-D-ribosyl-1,2-cyclicphosphate were shown to be substrates of PhnP, with the later being proposed as the physiological substrate. PhnP is regioselective, converting ribonucleoside-2',3'-cyclicphosphates to ribonucleoside-3'-phosphates and α-D-ribosyl-1,2-cyclicphosphates to α-D-ribosyl-1-phosphate. The importance of hydrolysis of the α-D-ribosyl-1,2-cyclicphosphate intermediate is suggested by the strong conservation of genes within the *phn* operons of other bacteria that encode phosphodiesterase activity. Examination of 54 bacterial *phn* operons containing the essential *phnM* gene revealed that 27 contained *phnP*. In the *phn* operons that did not contain *phnP*, 16 contained the *rcsF* gene in its place[34,58]. The *rcsF* gene encodes a protein that is a member of the 2 histidine- (or 2H-) phosphodiesterase superfamily, which hydrolyzes

2',3'-cyclicnucleotides or ribosyl-1,2-cyclicphosphates[59]. It is plausible that 5-phospho-α-D-ribosyl-1,2-cyclicphosphate could be a substrate for the *rcsF* gene product. The *phnN* and *phnP* genes exhibit strong synteny in bacterial *phn* operons, where only 3 operons containing *phnN* do not contain either a *phnP* or *rcsF* gene[34]. There must be a biochemical link between the phosphorylation of α-D-ribosyl-1,5-bisphosphate and the hydrolysis of 5-phospho- α-D-ribosyl-1,2-cyclicphosphate.

2.2.3.3 *N*-acetylation by PhnO

Growth of the *phnP* strains in the presence of aminoalkylphosphonates accumulates another compound that was characterized as an *N*-acetylated aminoalkylphosphonate. *In vitro*, purified PhnO was shown to efficiently *N*-acetylate aminomethylphosphonate (**1f**), 2-aminoethylphosphonate (**1g**), and (*S*)-1-aminoethylphophonsate (***S*-1h**), whereas (*R)*-1-aminoethylphosphonate (***R*-1h**) was *N*-acetylated at a reduced rate. The *N*-acetylated intermediates **1g*** and **3g*** were isolated from *E. coli* cultures and therefore it appears that *N*-acetylation of aminoalkylphosphonates occurs before CP bond cleavage (Figure 2-21). Although PhnO *N*-acetylates **1g**, *N*-acetylation is not required for CP bond cleavage as *phnO* strains are still capable of growing on **1g** as the sole source of P_i. *N*-Acetylation is also not required for growth on 3-aminopropylphosphonate (**1i**). However, it is required for CP bond cleavage of and growth on **1f** and ***S*-1h**. ***R*-1h** is unable to act as a sole P_i source. It is possible that the reduced *N*-acetylation rate of ***R*-1h** does not supply enough *N*-acetyl-(*R*)-1-aminoethylphosphonate (***R*-1h***) to sustain growth on this aminoalkylphosphonate. It is not clear why acetylation is required for 1-aminoalkylphosphonates and not 2- or 3-aminoalkylphosphonates. The presence of an amino group at the α-carbon of a substrate could hinder one or more steps of the CP-lyase pathway. At physiological pH the amino group would be protonated with a formal charge of +1. This positive charge could negatively affect the binding and interaction of the aminoalkylphosphonate in the active site of one or more of the enzymes in the CP-lyase pathway. The electron withdrawing

effect of the ammonium group is known to destabilize an attached carbon centered radical by approximately 5 kcalmol[-1][60,61]. *N*-Acetylation of 1-aminoalkylphosphonates would neutralize the positive charge and eliminate the destabilizing effect, thereby facilitating CP bond cleavage.

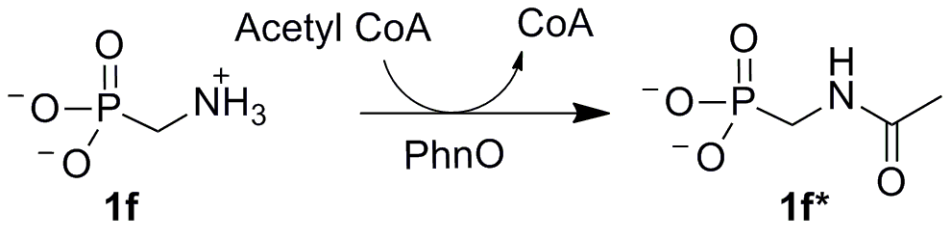

Figure 2-21. The reaction of PhnO, an aminoalkylphosphonate *N*-acetyl transferase, with aminomethylphosphonate (1f).

(*S*)-1-Aminoethylphosphonate (***S*-1h**) is an analog of D-alanine that has been shown to inhibit alanine racemase. This prevents the synthesis of D-alanine which is required for the synthesis of the peptidoglycan cell wall, leading to bacterial cell death[57]. Alaphosphin is a known 'Trojan horse' antibacterial agent that enters the bacterial cell through a dipeptide transport system. Upon entry into the cell, peptide bond hydrolysis yields ***S*-1h**, which exerts a bactericidal effect. It is possible to suppress cell lysis in the *phn*$^+$ strain by adding P_i and/or D-alanine. P_i eliminates the need for ***S*-1h** as a nutrient and PhnO presumably *N*-acetylates ***S*-1h**, inactivating this molecule and preventing cell lysis. Addition of excess D-alanine to cell cultures relieves the need for active alanine racemase, eliminating the toxic effect ***S*-1h**. Moreover, *N*-acetylation then allows ***S*-1h** to be used as a P_i source. The *phnO* strains were unable to overcome the toxic effects of ***S*-1h** in the presence of P_i and were also unable to utilize this compound as a P_i source in the presence of D-alanine. This demonstrates that *N*-acetylation is required for both detoxification and utilization of ***S*-1h** as a P_i source. It is odd that the *phn*$^+$ strain was unable to grow on ***S*-1h** in the absence of P_i or D-alanine. The expression of *phnO* must not be high enough to allow *E. coli* to overcome the toxic effect and allow for this compound to be utilized as a sole P_i source.

Growth of the *phn*$^{+}$, *phnJ* and *phnP* strains in the presence of **1g** revealed the accumulation of *N*-acetylated compounds. In contrast, no such accumulation was detected in the *phnO* strains. **1g** was determined to be an excellent source of P_i regardless of the presence of the *phnO* gene. It is possible that both *N*-acetylated and non-acetylated compounds may be concurrently degraded in the pathway. The *phnO* strains do not accumulate any detectable *N*-acetylated or non-acetylated compounds were the *phn*$^{+}$, *phnJ* and *phnP* strains only accumulate *N*-acetylated compounds. This indicates that when the *phnO* gene is present the *N*-acetylated compounds are dominant. This does not eliminate the possibility that non-acetylated compounds are not being simultaneously used. It is possible that the non-acetylated intermediates formed are at a level of concentration that is too low for detection by ^{31}P-NMR spectroscopy.

There are many bacterial *phn* operons that lack the *phnO* gene. One prominent example is *Pseudomonas stutzeri*[4], which contains two *phn* operons. Although **1g** is a competent P_i source for *P. stutzuri*, the growth on **1f** and ***S*-1h** has not been reported. Based on the findings in this thesis it is expected that *P. stutzuri* is incapable of utilizing either **1f** or ***S*-1h** as a P_i source. If it can utilize one of these 1-aminoalkylphosphonates then there may be a *phnO* homolog located outside the *phn* operon. Alternatively, *S. enterica* possesses a *phnO* gene but not a complete *phn* operon. In this case, *phnO* may serve as a detoxifying enzyme, as previously stated[32], or performs an unknown physiological function. The results presented here indicate that a physiological role of PhnO is to *N*-acetylate aminoalkylphosphonate such as **1f** and ***S*-1h**. Though **1f** is a major product of the catabolism of the synthetic herbicide glyphosphate[62] and is frequently found in the environment, neither of the 1-aminoalkylphosphonate compounds has been recognized as natural products. Therefore, *N*-acetylation of **1f** and ***S*-1h** may be a fortuitous coincidence and other naturally occurring 1-aminoalkylphosphonates are the true natural substrates of PhnO. It is still not clear what role the *phnO* gene plays in *E. coli* and the *phn* operon or what role it plays in other bacterial strains and if these roles are the same.

2.2.3.4 Deciphering the CP-lyase pathway

The catabolic intermediates described in this chapter helped piece together a major part of the CP-lyase pathway. The front end of the pathway involves PhnO if an aminoalkylphosphonate is being supplied as the P_i source. PhnO, an aminoalkylphosphonate *N*-acetyltransferase, *N*-acetylates the amino group of aminoalkylphosphonates neutralizing their positive charge that allows for CP bond cleavage (Figure 2-21). *N*-acetylation appears to be required for 1-aminoalkylphosphonates.

Ribosylation of organophosphonates yields a key intermediate, 5'-phospho-α-D-ribosyl-1'-alkylphosphonate, the dephosphorylated version was detected with a variety of substrates in this thesis using *E. coli phnJ* and *phnP* strains. We hypothesized that this was the substrate for CP-lyase (**3**, Figure 2-9), and that upon CP bond cleavage the capture of an electrophilic phosphoryl species by the nearby α-D-ribosyl-2-hydroxyl would yield 5-phospho-α-D-ribosyl-1,2-cyclicphosphate (**5**, Figure 2-9). Shortly after our work, this was confirmed *in vitro* by Raushel and coworkers. The CP-lyase product, as shown by our work, is the substrate for PhnP, a 1,2-cyclicphosphate phosphodiesterase. PhnP converts 5-phospho-α-D-ribosyl-1,2-cyclicphosphate (**5**) into α-D-ribosyl-1,5-bisphosphate (**6**) (step iv, Figure 2-9), the substrate for PhnN. Raushel and coworkers were also able to determine the functions of three other *phn* gene products. PhnI, a nucleosidase (glycosyltransferase) converts the organophosphonate to its corresponding 5'-triphospho-α-D-ribosyl-1'-alkylphosphonate (**2**) using MgATP as a glycosyl donor (step i. Figure 2-9). PhnM subsequently, catalyzes the hydrolysis of **2** to pyrophosphate and 5'-phospho-α-D-ribosyl-1'-alkylphosphonate (**3**) (step ii. Figure 2-9). This latter compound is the substrate for CP bond cleavage by PhnJ, a radical-S-adenosylmethionine (SAM) dependent enzyme with a [4Fe-4S] cluster. PhnJ converts **3** to its corresponding alkane product (**4**) and 5-phospho-α-D-ribosyl-1,2-cyclicphosphate (**5**) (step iii. Figure 2-9). Although the specific mechanism of CP bond cleavage by PhnJ is still not known the [4Fe-4S] cofactor is very capable

of initiating the radical chemistry that is predicted for this process[63]. After two decades of struggle, work from this thesis and by Raushel and coworkers has enabled many aspects of the pathway to be solved, however many details have yet to be established.

2.3 Discovery of protein complexes in the CP-lyase pathway

The sheer number of genes encoded by the *phn* operon suggests that in addition to comprising a catabolic pathway, some of the gene products may encode a protein complex. To test this hypothesis, a major objective of this thesis was to identify potential protein complexes in the CP-lyase pathway. Protein complex identification was attempted using an inducible expression plasmid encoding *phn* genes. A second sequential peptide affinity method was also pursued, but will not be discussed.

It was previously shown that expression of *phnGHJKLM* from a plasmid was sufficient to encode CP bond cleavage[19,43]. We hypothesized that expression of these genes in an *E. coli* strain lacking a *phn* operon would yield a soluble protein complex. The complex could then be purified and structurally analyzed using SDS-PAGE, amino acid sequencing by tandem mass spectrometry (ESI-MS/MS), size exclusion chromatography, and cross-linking experiments. Researchers have struggled for decades to isolate CP-lyase enzymes in soluble and active form therefore, isolation of a soluble CP-lyase complex, particularly if it were catalytically active, would represent a huge step forward in deciphering this enzyme system.

2.3.1 Methods

2.3.1.1 *E. coli* strains and growth conditions

A previously prepared strain, HO2735 F' (*Δ(lac)X74 Δ(phnCDEFGHIJKLMNOP)33-30*/F *lacI*^{q} *zzf*::Tn10)[29] was used as the host strain for plasmid expression and XL1-Blue (Agilent Technologies) was used for cloning and plasmid DNA production. Due to the sensitivity of restriction endonuclease *Sex*AI to methylation by the *dcm* gene product, the plasmid DNA for

digestion with *Sex*AI was propagated in the strain FM3392 (*dcm-6*/F *lacI*^{q} *zzf*::Tn*10*). FM3392 was constructed by conjugation of GM119 (*dcm-6*)[64], purchased from the Coli Genetic Stock Center (Yale University), with donor strain HO2814 *Δprs-5*/F *lacI*^{q} *zzf::*Tn*10*. Strain HO1429 (EcoK$^+$) is an *E. coli* K-12 derivative that is capable of growing on organophosphonates. HO1429 genomic DNA was isolated for use as a DNA template for the PCR amplification of *phn* genes. A table of the *E.* coli strains used, their genotype, as well as their origin is found in Appendix A.

Luria Bertani (LB) growth medium was used in most cases; however in some instances our collaborators used NZY broth[27]. For complementation assays, strains were grown at 37°C on solid P_i free MOPS buffered medium with 0.2% glucose as a carbon source and 1.8% agar[43,52]. As a P_i source, either 1 mM of P_i or **1a** were added. Glassware and agar were washed multiple times with deionized water (Milli-Q system) to reduce the P_i contamination. To the MOPS medium histidine and tryptophan were added to 40 mg L^{-1}, guanosine was added to 30 mg L^{-1}, uridine was added to 20 mg L^{-1}, and thiamine was added to 1 mg L^{-1}. The antibiotics tetracycline, chloramphenicol, and ampicillin were used as required at 10, 30 and 100 mg L^{-1}, respectively. Liquid cultures were grown overnight at 37°C with aeration for plasmid DNA isolation but for protein expression our collaborators chilled the cultures on ice for 30 min once they reached an OD_{600} between 0.4 and 0.6. Expression of *phn* genes were then induced with a final concentration of 0.5 mM isopropyl-β-D-1-thiogalactoside (IPTG), and cultures were grown for an additional 3 - 4 h at 26 - 28°C. Cells were then harvested, lysed and clarified prior to use[27].

2.3.1.2 Construction of *phn* plasmid DNA

The expression plasmid, pMN1 encoding genes *phnGHIJKLM*, was constructed by Mariah Nabi and Bjarne Hove-Jensen. They used the primers 5′- AGAATTCATTAAAGAGG-AGAAATTAACT*ATG*CACGCAGATACCGCGACCC-3′ (GupMN) and 5′- GGAAGCTTGCA-TGCTT*ATT*AGAACACCCTTTTACCCTGACGCC-3′ (Mdw) to amplify the *phnGHIJKLM* by

PCR from *E. coli* strain HO1429. Restriction endonuclease sites EcoRI and HindIII are underlined and the nucleotide sequences that specify the translation start and stop codons of *phnG* and *phnM*, respectively are italicized. The PCR product was digested by *Eco*RI and *Hind*III restriction endonucleases, yielding a 5,647-bp fragment that was ligated into a similarly digested pUHE23-2 plasmid forming pMN1. This plasmid was sequenced by Eurofins MWG Operon and indicates that five alterations that give rise to four point mutations and one silent mutation are present. The mutations are as follows: *phnH* codon 152 is altered from cag (Q) to cgg (R); *phnI* codon 322 is altered from gcc (A) to gtc (V); *phnK* codon 208 is altered from gtc (V) to gcc (A); *phnM* codons 107 is altered from cgg (R) to tgg (W) and 363 from aat (N) to aac (N). A method was devised to remove the alterations, and is described in Appendix B.

The pMN1 plasmid was altered by Bjarne Hove-Jensen to remove the *phnL* and *phnM* cistrons by treatment with the restriction endonucleases *Bst*EII and *Hind*III followed by incubation with Mung Bean nuclease. Ligation of the digested blunt ended plasmid formed pHO571 (*phnGHIJK*), which retained 228-bp of the *phnL* open reading frame. Another method was employed to remove *phnK*, *phnL*, and *phnM* cistrons that involved partial digestion of pMN1 with *Bss*HII, followed by digestion with *Hind*III. Again the digested plasmid was incubated with Mung Bean nuclease to give rise to blunt ends that were ligated to generate pHO572 (*phnGHIJ*), with the retention of 152-bp of the *phnK* open reading frame.

To individually delete the other cistrons from pHO571 a two-step overlap extension PCR method was used[65]. The method gave rise to in-frame deletions with seven codons of an upstream end and seven codons of a downstream end of a *phn* open reading frame fused together. The PCR programs used are given in Table 2-7, reactions contained 1 X Herculase II buffer, 500 μM of each dNTP, 2% DMSO, approximately 1 - 30 ng of DNA template (1 μL of isolated pMN1 plasmid DNA for the first round of PCR, the second round of PCR used 1 μL of a 10 fold dilution of two PCR products from round 1 as stated below), 0.2 μM of each primer, and 1 μL of

Herculase II polymerase (Stratagene). The PCRs were performed using a PTC-200 (MJ Research) or a Mastercycler epgradient (Eppendorf) thermol cycler and the reactions were initiated using a 'hot-start'. After analysis of PCR products by agarose gel electrophoresis the PCRs were subjected to an enzymatic clean-up protocol using the QIAquick gel extraction kit.

Using the deletion of the *phnG* cistron as an example, two PCRs were performed on pMN1 that gave rise to a 190-bp upstream PCR product (PCRDeGup) and a 1,252-bp downstream PCR product (PCRDEGdw). The primers used for PCRDeGup were UHE 5′-TAGGCGTATCACGAGGCCCTTTCG-3′, which anneals to the plasmid pUHE23-2, and DEphnGup 5′-*TCATGCGTTGTCTCCGCGAAC***GGTCGCGGTATCTGCGTGCAT**AG-3′ and the primers for PCRDEGdw were DEphnGdw 5′-**ATGCACGCAGATACCGCGACC***GTTCG-CGGAGACAACGCATGAC*-3′ and I 5′-GGAGTAGGCCAGCGCCAGCAAATAGC-3′, which anneals to the *phnI* cistron. In the primer sequences DEphnGup and DEphnGdw the nucleotides that are complementary to the first seven *phnG* coding strand codons are shown in bold and the nucleotides complementary to the terminal seven codons are italicized. The two PCR products, PCRDeGup and PCRDeGdw, are then used as the template DNA in the second round of PCR with oligonucleotides UHE and I. The second PCR resulted in a 1,400-bp product, PCRDeG. pHO571 and PCRDeG were digested with restriction endonuleases *Eco*RI and *Sac*II. The 512-bp fragment of PCRDeG was ligated into the digested pHO571 to create pFM31 (Δ*phnG phnH phnI phnJ phnK*).

For the deletion of *phnH*, the initial PCR products PCRDeHup (639-bp) and PCRdeHdw (671-bp) were created using the primers UHE and DEphnHup 5′-*TCAGCACACCTCCACATGA-GT***AAAAGCGGTTTCCAGGGTCATG**-3′, and with DEphnHdw 5′-**ATGACCCTGGAAAC-CGCTTTT***ACTCATGTGGAGGTG-TGCTGATG*-3' and I, respectively. The second PCR using primers UHE and I and the two PCR products above as templates, resulted in a 1,268-bp product, PCRDeH. pHO571 and PCRDeH were digested with restriction endonuleases *Eco*RI and *Psi*I.

The 838-bp fragment of PCRDeH was ligated into the digested pHO571 to create pFM32 (*phnG* Δ*phnH phnI phnJ phnK*).

For the deletion of *phnI* the PCR products PCRDeIup (417-bp) and PCRdeIdw (1537-bp) were created, respectively, using H 5′-CGATATCGTCAACCAGAGCCTGC-3′, which anneals to *phnH*, and DEphnIup 5′-*TTAGCCATGGTTCTGCTCCTG***CCCTTTCACGGCAACGTACA-TC**-3′, and with DEphnIdw 5′-**ATGTACGTTGCCGTGAAAGGG***CAGGAGCAGAACCATGG-CTAATC*-3′ and K2 5′-GCTTCATCACCAGCAAACGGTCCGCCAGCAGG-3′, which anneals to *phnK*. The second PCR, using primers H and K2 and the PCR products above as template, resulted in a 1,912-bp product, PCRDeI. pHO571 and PCRDeI were digested with restriction endonuleases *Sac*II and *Bsa*BI. The 525-bp fragment of PCRDeI was ligated into the digested pHO571 to create pFM33 (*phnG phnH* Δ*phnI phnJ phnK*).

Lastly, for the deletion of *phnJ* the PCR products, PCRDeJup (1,474-bp) and PCRdeJdw (699-bp) were created using H and DEphnJup 5′-*TCATTGGTTTTTTGCCTCGCT***GTAGCCGC-TCAGATTAGCCATG**-3′, and with DEphnJdw 5′-**ATGGCTAATCTGAGCGGCTAC***AGC-GAGGCAAAAAACCAATGAATC*-3′ and K2, respectively. The second PCR using primers H and K2 and the PCR products above as template resulted in a 2,131-bp product, PCRDeJ. pHO571 and PCRDeJ were digested with restriction endonuleases *Psi*I and *Sex*AI. The 1,245-bp fragment of PCRDeJ was ligated into the similarly digested pHO571 to create pFM34 (*phnG phnH phnI* Δ*phnJ phnK*). Plasmid DNA along with stab cultures of the host strain containing the different plasmids were sent to our collaborators Bjarne Hove-Jensen and Bjarne Jochimsen in Denmark.

Table 2-7. PCR programs used to create *phn* gene deletion plasmids.

Step	*Program 1*	*Program 2*	*Program 3*	*Program 4*	*Program 5*
1.	5 min at 95°C	5 min at 95°C	5 min at 95°C	5 min at 95°C	5 min at 95°C
2.	0.5 min at 95°C	0.5 min at 95°C	0.5 min at 95°C	0.5 min at 95°C	0.5 min at 95°C
3.	0.5 min at 64°C	0.5 min at 54°C	0.5 min at 57°C	0.5 min at 64°C	0.5 min at 62°C
4.	0.5 min at 72°C	1 min at 72°C	1.5 min at 72°C	1.5 min at 72°C	2 min at 72°C
5.	Go to step 2, 9 times	Go to step 2, 9 times	Go to step 2, 9 times	Go to step 2, 24 times	Go to step 2, 24 times
6.	0.5 min at 95°C	0.5 min at 95°C	0.5 min at 95°C	5 min at 72°C	5 min at 72°C
7.	1 min at 72°C	1.5 min at 72°C	2 min at 72°C		
8.	Go to step 6, 19 times	Go to step 6, 19 times	Go to step 6, 19 times		
9.		3 min at 72°C			

Program 1. used for amplification of PCRDeGup; Program 2. used for amplification of PCRDeHup, PCRDeHdw, PCRDeIup and PCRDeJdw; Program 3. used for amplification of PCRDeGdw, PCRDeIdw, and PCRDeJup; Program 4. used for amplification of PCRDeG and PCRDeH; and Program 5 used for amplification of PCRDeI and PCRDeJ.

In addition, Bjarne Hove-Jensen created a plasmid that encoded *phnGHIJK* where the *phnK* gene contained a sequence that specifies a C-terminal hexahistidine tag on PhnK, pHO575, and plasmids with individual *phn* cistrons possessing a specified C-terminal hexahistidine tag sequence in the pUHE23-2 plasmid. The constructed plasmids were pHO524 (*phnG*), pHO515 (*phnH*), pHO517 (*phnI*), pHO519 (*phnJ*), and pHO516 (*phnK*)[27,43].

Finally, a plasmid for a complementation assay was constructed by digesting the pMN1 plasmid with restriction endonucleases *Eco*RI and *Hind*III. The DNA fragment containing the *phnGHIJKLM* open reading frames was then ligated into a similarly digested pSU18 vector. The resulting plasmid was called pFM35. Ligation was confirmed by DNA digest with *Eco*RI and *Hind*III, the expected bands at 2289-bp and 5651-bp are seen in all 8 clones analyzed (Figure 2-22, lanes 2-9). All of the plasmid maps can be found in Appendix C.

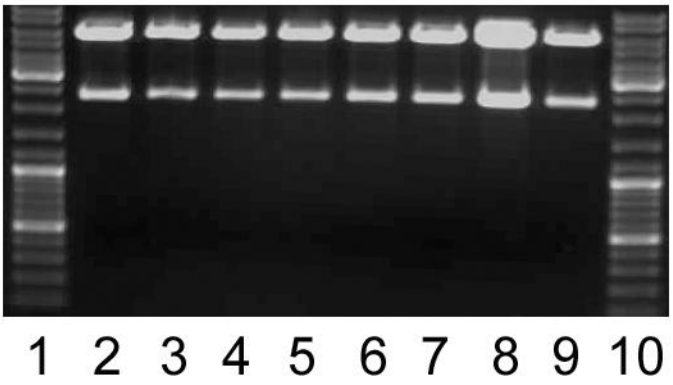

Figure 2-22. Analysis of pFM35 clones by agarose gel electrophoresis. 0.8% agarose gel of pFM35 clones digested with *Eco*RI and *Hind*III restriction enzymes to visualize inserted *phnGHIJK* fragment from pMN1. DNA ladder (SM0333, Fermentas) in Lane 1 and 10 (ladder contains 21 discrete fragments: 8000, 7000, 6000, 5000, 4000, 3500, **3000**, 2500, 2000, 1500, 1200, **1031**, 900, 800, 700, 600, **500**, 400, 300, 200, and 100-bp, there are larger quantities of the bolded fragments present in the mixture); lanes 2 to 9 contain digested pFM35 clones with expected bands at 2289-bp and 5651-bp.

2.3.1.3 Protein purification and analysis

Our collaborators Bjarne Hove-Jensen and Bjarne Jochimsen at Aarhus University, Denmark, performed the protein isolation and characterization portion of this work. For full details on these methods please refer to reference 27. In brief, ammonium sulfate, Vivaspin 6 columns (Sartorius Stedim Biotech) or in some instances for analytical analyses trichloroacetic acid (TCA) precipitation was used to concentrate the protein. Protein complexes PhnGHIJK, PhnGHIJ and PhnGI were purified at 4°C on a Q-Sepharose Fast Flow column on an ÄKTA Prime Plus platform (G.E. Healthcare) and analyzed using standard PAGE procedures. A LMW-SDS Marker Kit (G.E. Healthcare) was used as a molecular mass standard. Applicable fractions containing PhnG were pooled and concentrated, followed by further purification on a Sephacryl S-300 column (G.E. Healthcare). The eluted fractions were analyzed by SDS-PAGE.

Hexahistidine tagged proteins were purified by immobilized metal affinity chromatography using a Histrap FF crude column (G.E. Healthcare) on an ÄKTA Prime Plus

system. Size exclusion chromatography for molecular mass determination was performed using a Superdex 200 10/300 GL column (G.E. Healthcare) eluted at 0.5 mL min^{-1} with an ÄKTA Purifier system. Cross-linking was performed by adding glutaraldehyde (Sigma-Aldrich) to solutions of purified protein complexes at room temperature. At specified time intervals samples were removed and quenched with the addition of SDS-PAGE loading solution.

Peptide sequencing was perfomed at the Mass Spectrometry Core Facility, Department of Molecular Biology, Aarhus University, Denmark. In brief, purified protein complexes were resolved by SDS- or native-PAGE. Bands corresponding to individual proteins (or complexes in the case of native-PAGE) were excised from the gel and subjected to proteolysis. Digested peptides were analyzed by nano LC-MS/MS using a Micromass Q-TOF Ultima API MS (Waters) connected to a Proxeon nano LC system. The data was processed using MassLynx V4.0 and peak lists were used to query the Swiss-Prot database using Mascot search engine (version 2.2.06, Matrix Science)[66].

2.3.1.4 Complementation growth assay

The pSU18 and pFM35 plasmids were transformed into the *phn*$^{+}$ (HO2567) and *Δphn* (HO1647) strains, as well as mutant strains containing the *phnG35*, *phnH13*, *phnI40*, and *phnK6* alleles (HO1550, HO1547, HO1552 and HO1544, respectively). The strains were streaked out onto segments of comparable solid MOPS media containing no P_i source, 1 mM **1a** or 1 mM P_i. The strain growth was recorded after 90 h of incubation at 37°C.

2.3.2 Results

2.3.2.1 Expression of pMN1 and identification of gene products

A plasmid, pMN1 encoding the genes *phnGHIJKLM*, was constructed by our collaborators Bjarne Hove-Jensen and Mariah Nabi. pMN1 was transformed into *E. coli* strain HO2735 to give rise to HO3333. Co-expression of PhnGHIJKLM proteins was induced by the addition of IPTG to a HO3333 cell culture. The cell extract was analyzed by SDS-PAGE to confirm synthesis of Phn polypeptides (Figure 2-23A), the major bands were identified by MS/MS as PhnM (Figure 2-23 lane 1, band 1), PhnI (band 2), PhnJ (band 3 and 4), PhnK (band 5), PhnH (band 6), PhnL (band 7), and PhnG (band 8). It is apparent that each of the seven *phn* genes in pMN1 was expressed and the corresponding proteins synthesized. Some bands also contained other *E. coli* proteins. Elongation factor Tu was found in band 1. Outer membrane proteins C and F were found in band 3. Outer membrane proteins A and P were found in band 4 and ribosomal protein L3 was found in band 7. Interestingly PhnJ is found in two bands (3 and 4), suggesting that there may be a modification of this polypeptide. Additionally, both of the PhnJ bands had outer membrane proteins present.

2.3.2.2 Characterization of associated Phn polypeptides

The lysed cell supernatant contained approximately 50% of the synthesized Phn polypeptides with the remainder found in the insoluble fraction. The supernatant was treated with streptomycin sulfate to remove nucleic acids and subsequently applied to a Q-Sepharose anion exchange column and eluted with a NaCl gradient. PhnG is a small 17 kDa polypeptide that separates on the SDS-PAGE gel to a region with few other bands, allowing for its easy detection. Therefore, fractions containing PhnG were pooled, concentrated, redissolved in phosphate buffer and applied to a Sephacryl S-300 column. Fractions were analyzed by SDS-PAGE and five

polypeptides coeluted with equal intensities over the elution profile (Figure 2-23B). This coelution profile indicates that there is an association between these five proteins.

A fraction from the purification was concentrated and analyzed by SDS-PAGE, revealing seven protein bands. These were identified by MS/MS sequencing (Figure 2-23C). PhnG (band 7), PhnH (band 6), PhnK (band 5), and PhnI (band 1) all migrated as single bands around their expected molecular weights (Figure 2-23C, lane 2), compared to the marker (lane 3). However, PhnJ migrated as three distinct bands (Figure 2-23C, lane 2, bands 2, 3 and 4). PhnM, and PhnL were not detected as part of this protein complex and nor were any other *E. coli* proteins. A derivative of the pMN1 plasmid, pHO571, which lacks all of the *phnM* cistron and most of *phnL* cistron, was prepared. A similar PhnGHIJK complex was purified from a strain expressing the pHO571 plasmid (Figure 2-23D lane 1 and 2).

A variant of the pHO571 was constructed, pHO575 with an altered *phnK* allele that specifies a C-terminal hexahistidine tagged PhnK. Following expression in HO2735, a PhnGHIJK protein complex was purified by affinity chromatography using a Ni-chelate column (Figure 2-23D, lane 3). This complex was similar to those isolated from HO2735/pMN1 and HO2735/pHO571, with just the hexahistidine tagged PhnK migrating slightly above the native PhnK, as expected. The protein complex was analyzed by native-PAGE (Figure 2-23E). There is a predominant form of the complex found at band 2, with minor forms found above and below this band. The 5 bands marked were sent for MS/MS analysis. All the bands, with the exception of band 5, contained PhnG, PhnH, PhnI, PhnJ and PhnK, whereas band 5 lacked the PhnK protein.

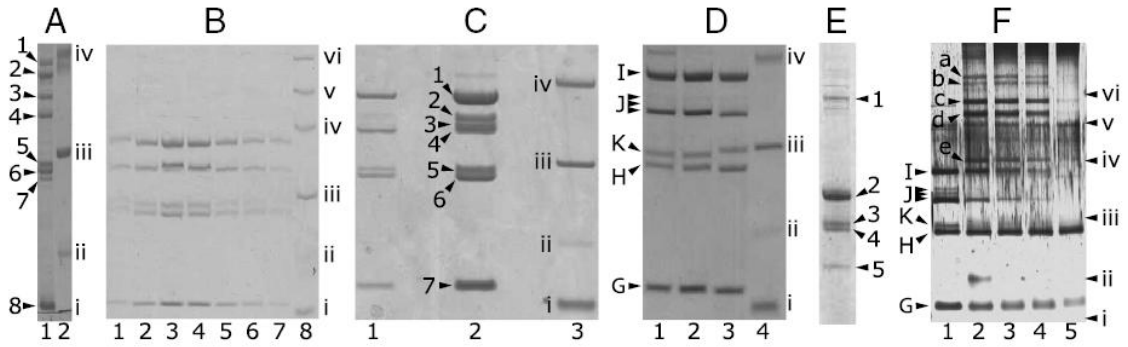

Figure 2-23. Characterization of the PhnGHIJK protein complex. (A) SDS-PAGE of polypeptides specified by pMN1 (*phnGHIJKLM*). Lane 1, pellet obtained by sonication and centrifugation of cells of strain HO2735/pMN1 followed by dissolving in 6 M urea. The polypeptides of the bands labelled 1 to 8 were identified by MS/MS; lane 2, molecular mass standard. (B) SDS-PAGE of selected fractions after elution of PhnGHIJK protein complex by size-exclusion chromatography on Sephacryl S-300. Lanes 1 to 7: fraction 18, 20, 22, 24, 26, 28, and 30, respectively. Lane 8: molecular mass standard. Analyzed protein was concentrated by precipitation with TCA. (C) SDS-PAGE of purified PhnGHIJK protein complex after size-exclusion chromatography and concentration. Lane 1, side fraction; lane 2, peak fraction; lane 3, molecular mass standard. Polypeptides of bands labelled 1 to 7 were identified by MS/MS: band 1, PhnI; band 2, PhnJ; band 3, PhnJ; band 4, PhnJ; band 5, PhnK; band 6, PhnH and band 7, PhnG. (D) SDS-PAGE of purified PhnGHIJK protein complex. Lanes 1 and 2, protein complex purified by ion-exchange and size-exclusion chromatography from strain HO2735/pMN1 and HO2735/pHO571, respectively; lane 3, histidine tagged protein complex purified by Ni-chelate affinity chromatography from HO2735/pHO575. Protein was concentrated by centrifugation through a Vivaspin column prior to analysis; lane 4, molecular mass standard. (E) Native-PAGE of purified PhnGHIJK protein complex. Polypeptides of the bands labelled 1 to 5 were identified by MS/MS. (F) Cross-linking of PhnGHIJK protein complex analyzed by SDS-PAGE followed by silver staining. Lanes 1 to 5, protein complex incubated with glutaraldehyde for 0, 1, 3.5, 7, and 24 h, respectively. Phn polypeptides are labelled I, J, K, H, and G; cross-linking products are labelled a, b, c, d, and e. Molecular mass standards are indicated by Roman numerals: i, 14.4; ii, 20.1; iii, 30; iv, 45; v, 66; and vi, 97 kDa. Figure from reference 27.

Two forms of the PhnGHIJK protein complex were eluted from a Superdex 200 size exclusion column to determine the molecular mass of the complex. The predominant form consisted of 80% of total protein complex with a molecular mass of approximately 260 kDa and

the remaining 20% of total protein complex eluted with a molecular weight of approximately 640 kDa. The minor form was reapplied to the size exclusion column and eluted as a single molecular form, again at approximately 640 kDa, suggesting that this is a stable complex rather than an equilibrium of two forms. Analysis by SDS-PAGE shows that both forms contained PhnG, PhnH, PhnI, PhnJ and PhnK.

The intensities of the polypeptides were determined using Quantity One software (BioRad). The relative intensity of Phn polypeptides from a typical lane (Figure 2-23B) after purification was: PhnG, 17%, PhnH, 13%, PhnI 36%, PhnJ (major form), 26%, and PhnK, 8%. Using these relative intensities, the 260 kDa complex observed by size exclusion chromatography would correspond to a quaternary structure of $PhnG_4H_2I_2J_2K$ (280 kDa). This calculation assumes PhnK is present as a single copy.

2.3.2.3 Cross-linking experiments with associated proteins

TCA precipitated fractions after the Sephacryl S-300 column were analyzed by SDS-PAGE (Figure 2-23B). The data revealed that polypeptides corresponding to PhnG, PhnH, PhnI, PhnJ and PhnK coeluted. This indicates that PhnGHIJK forms a potential putative CP-lyase protein complex. To further confirm complex formation, cross-linking experiments were performed with glutaraldehyde, which forms Schiff base linkages to lysine side chains that are in close proximity. The cross-linking reaction was monitored over time by SDS-PAGE (Figure 2-23F). Over time, three of the five Phn polypeptides PhnJ, PhnI, and PhnK (Figure 2-23F, bands J, I, and K) quickly disappeared with PhnG (Figure 2-23F, bands G) disappearing more slowly. The only band that did not disappear corresponded to PhnH, which only contains two lysine residues, one of which is embedded in the protein dimer, according to the X-ray crystal strucutre[29]. As the Phn protein bands disappeared the appearance of new bands of greater mass were detected (Figure 2-23F, bands a, b, c, d and e). The new bands (a to e) correspond to higher molecular weight complexes at 125, 115, 92, 78 and 47 kDa, respectively. After 24 hours of

incubation the Phn polypeptides (excluding PhnH and some PhnG) were found as large protein complexes.

2.3.2.4 Construction of deletion plasmids

Variant plasmids of pHO571 were created where each of the phnGHIJK cistrons were individually deleted (pFM31, pFM32, pFM33, pFM34, and pHO572). The first step in constructing the plasmids lacking *phnG*, *phnH*, *phnI*, or *phnJ* was to amplify fragments (PCRDeGup, PCRDeGdw, PCRDeHup, PCRDeHdw, PCRDeIup PCRDeIdw, PCRDeJup and PCRDeJdw) from pMN1 for the first-step of a two-step overlap extension PCR, as described in methods. Each PCR product was analyzed by agarose gel electrophoresis and were determined to have the expected length based on comparion to the DNA ladder (Figure 2-24).

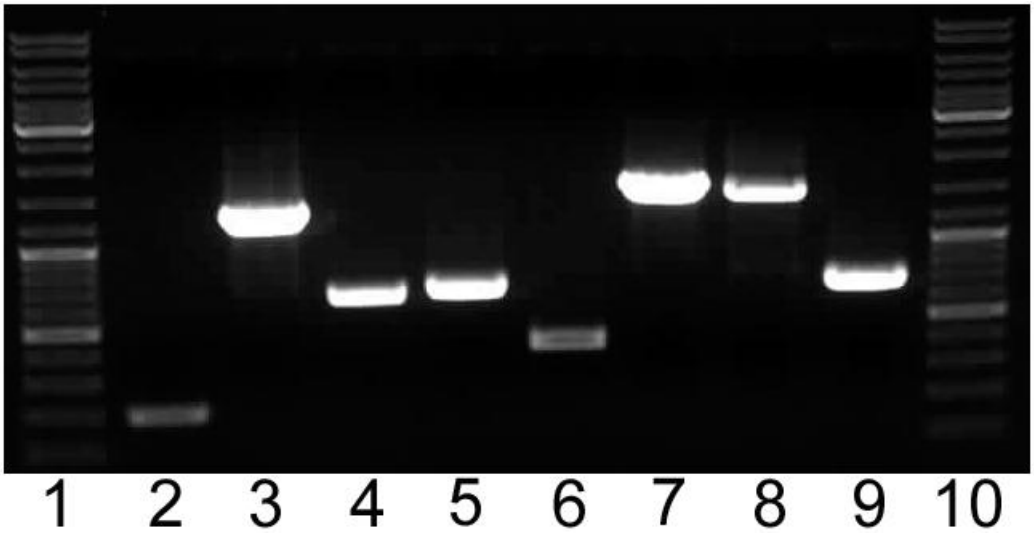

Figure 2-24. 1% agarose gel of round 1, initial PCR products. DNA ladder (SM0333, Fermentas) in Lanes 1 and 10 (ladder contains 21 discrete fragments: 8000, 7000, 6000, 5000, 4000, 3500, **3000**, 2500, 2000, 1500, 1200, **1031**, 900, 800, 700, 600, **500**, 400, 300, 200, and 100-bp, there are larger quantities of the bolded fragments present in the mixture). Lane 2 to 9 PCR products PCRDeGup (190-bp), PCRDeGdw (1252-bp), PCRDeHup (639-bp), PCRDeHdw (671-bp), PCRDeIup (417-bp), PCRDeIdw (1537-bp), PCRDeJup (1474-bp) and PCRDeJdw (699-bp) with size of DNA fragments amplified given in parentheses.

The overlapping pairs of PCR products were then assembled in a second round of PCR to to fuse together the front end of the gene to the back end of the gene for the formation of an in-frame deletion fragment (Figure 2-25). The assembly of PCRGeG (Lane 2) and PCRDeH (Lane 3) were successful as shown by the expected lengths in comparison to the marker (Lane 1). However the PCR reactions producing PCRDeI (Lane 4) and PCRDeJ (Lane 5) also contained contaminating nonspecific amplification products. Nevertheless, the desired PCR product is the most predominant band found in the each reaction. For this reason, the PCR products were not purified by agarose gel electrophoresis and gel extraction. However, all PCR reactions were subjected to enzymatic clean up using a QIAquick Extraction Kit (Qiagen).

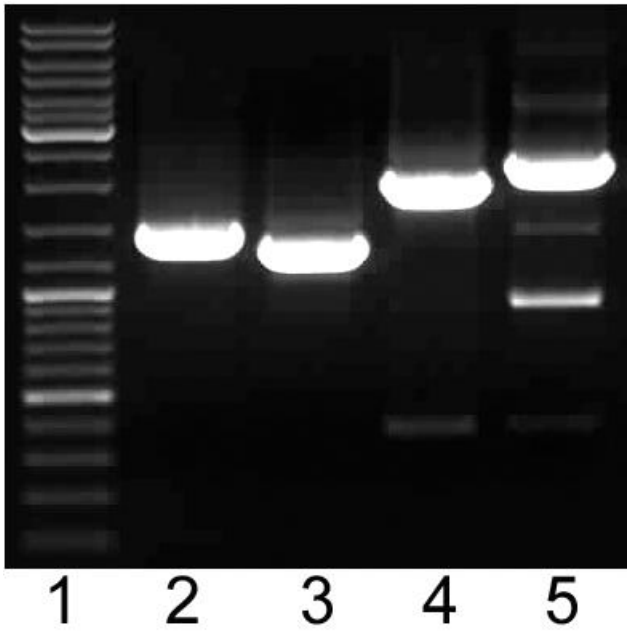

Figure 2-25. 1% agarose gel of assembly PCR products. DNA ladder in lane 1, as seen in Figure 2-24. Lane 2 to 5 PCR products PCRDeG (1400-bp), PCRDeH (1268-bp), PCRDeI (1912-bp), and PCRDeJ (2131-bp) with size of DNA fragments amplified in parenthesis.

PCR products were designed to be cloned into the pHO571 plasmid. Therefore, a large quantity of pHO571 plasmid DNA was isolated and its concentration was estimated by visualization on an agarose gel (Figure 2-26A). To obtain non-methylated pHO571 plasmid DNA for use with *Sex*AI a small quantity of the pHO571 plasmid DNA that was isolated was

transformed into FM3392. Non-methylated pHO571 plasmid DNA was isolated from FM3392/pHO571 and quantified. Four different double digests on pHO571 were performed to target various *phn* genes for deletion. pHO571 was digested with *Eco*RI and *Sac*II for deletion of *phnG* (Figure 2-26B, lane 2), *Eco*RI and *Psi*I, for deletion of *phnH* (Figure 2-26B, lane 3), and *Sac*II and *Bsa*BI for deletion of *phnI* (Figure 2-26B, lane 2). pHO571 propagated from FM3392 was digested with *Psi*I and *Sex*AI for deletion of *phnJ* (Figure 2-26C, lane 2). These digests gave rise to pHO571 plasmid DNA with DNA overhangs that allow for the correct insertion of constructed in-frame deletion assembly PCR products for each *phn* cistron. Ligation of the appropriate assembly PCR product into each digested plasmid afforded an in-frame deletion of the corresponding *phn* cistron (see below).

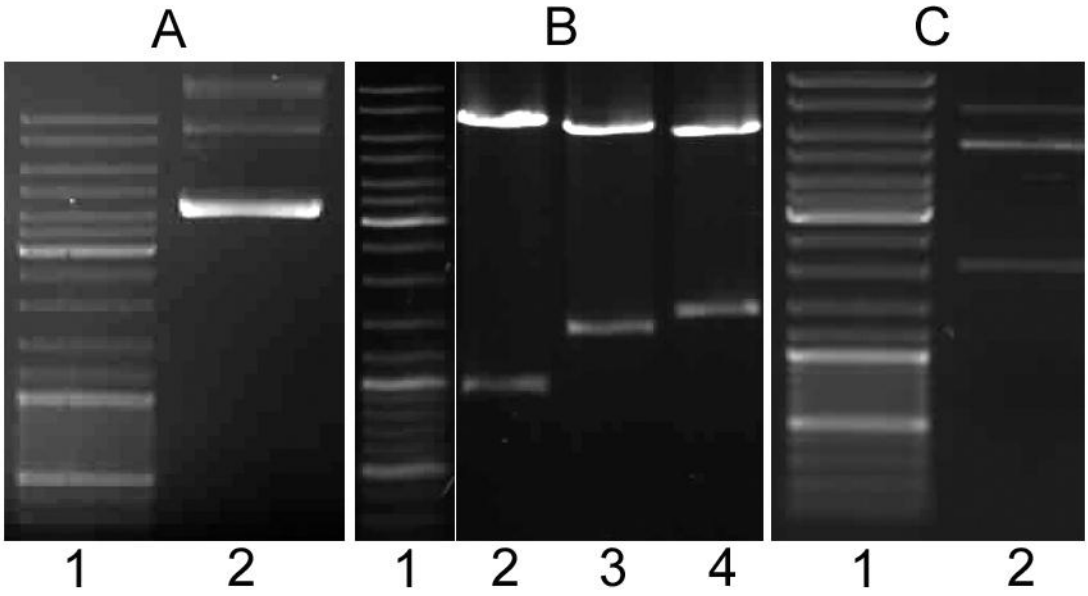

Figure 2-26. 1.5% agarose gels of pHO571 and digested pHO571. (A) Lane 1, DNA ladder, and lane 2 pHO571 plasmid DNA. (B) Lane 1, DNA ladder, lane 2 pHO571 digested with *Eco*RI and *Sac*II, lane 3 pHO571 digested with *Eco*RI and *Psi*I, and lane 4 pHO571 digested with *Sac*II and *Bsa*BI. (C) lane 1, DNA ladder and lane 2 *dcm*$^-$pHO571 digested with *Psi*I and *Sex*AI. DNA ladder annotated as seen in Figure 2-24.

The assembly PCR products were digested with the corresponding restriction endonucleases. PCRDeG was digested with *Eco*RI and *Sac*II (Figure 2-27A, lane 2), PCRDeH

was digested with *Eco*RI and *Psi*I (Figure 2-27A, lane 3), PCRDeI was digested with *Sac*II and *Bsa*BI (Figure 2-27B, lane 2) and finally PCRDeJ was digested with *Psi*I and *Sex*AI (Figure 2-27A, lane 4). Digested plasmids and PCR products were ethanol precipitated to concentrate the digested DNA for purification by agarose gel electrophoresis.

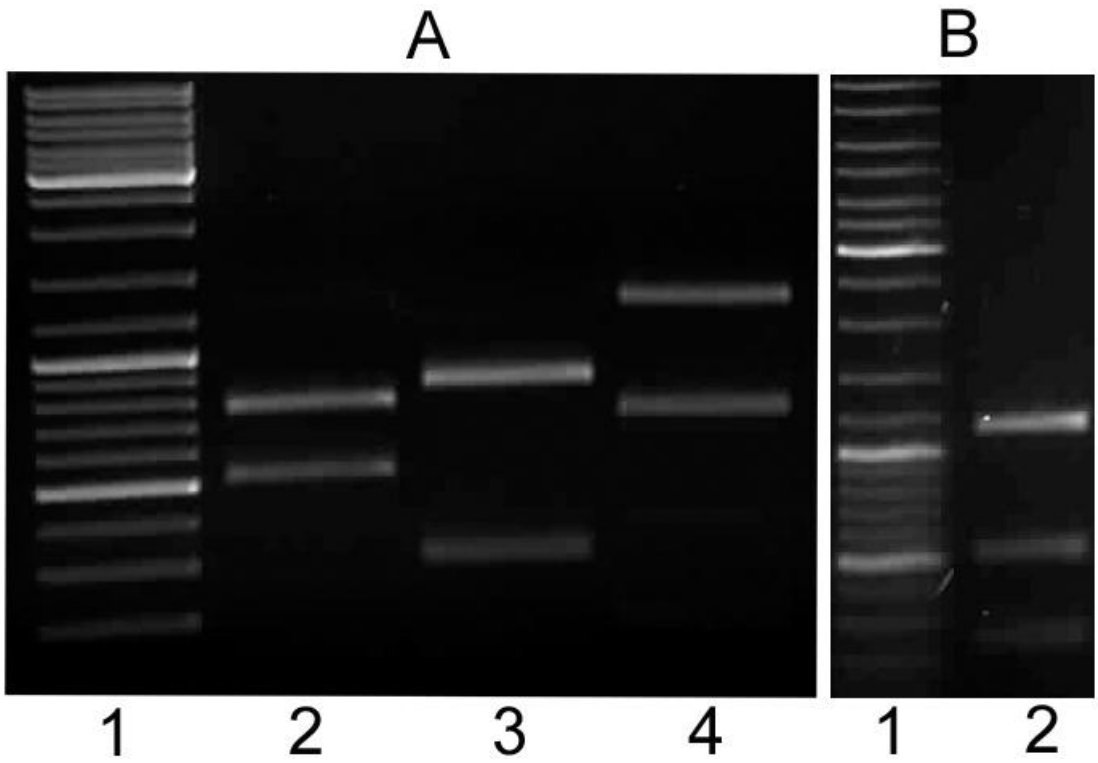

Figure 2-27. 1% agarose gels of digested assembly PCR products. (A) Lane 1, DNA ladder; lane 2, PCRDeG digested with *Eco*RI and *Sac*II; lane 3, PCRDeH digested with *Eco*RI and *Psi*I and lane 4, PCRDeJ digested with *Psi*I and *Sex*AI. (B) Lane 1, DNA ladder and lane 2, PCRDeI digested with *Sac*II and *Bsa*BI. DNA ladder annotated as seen in Figure 2-26.

Concentrated digested DNA was separated by agarose gel electrophoresis and desired DNA bands were excised. The excised agarose gel pieces containing desired DNA fragments were gel purified using the QIAquick Gel Extraction Kit (Qiagen), according to the manual. Following purification, the purity of the DNA was confirmed by agarose gel electrophoresis and the appropriately digested plasmids and assembly PCR products were ligated together with T4 DNA ligase. Ligation reactions were transformed into XLI-Blue cells and plated on LB agar

supplementated with tetracycline and ampicillin. Plasmid DNA was isolated from overnight cultures inoculated from single colonies off LB agar plates transformed with ligation reactions. The presence of the desired insert was confirmed by restriction enzyme digests (Figure 2-28). All pFM31 and pFM33 clones had the expected size change from 929-bp to 518-bp and 5264-bp to 4241-bp (Figure 2-28A and C). Only one pFM32 clone had the expected size change from 1385-bp to 842-bp (Figure 2-28B, lane 7) and all but one of the pFM34 clones had the expected size change form 2609-bp 1805-bp. Those lanes that did not contain the expected band size appear to be inefficiently digested. Nevertheless, at least one clone of each designed plasmid had the the desired sequence confirmed by DNA sequencing by Robarts Research Institute using primers UHE, I, H, K2 as well as UHERevseq 5'-CAACGGTGGTATATCCAGTG-3', I2DeGseq 5'-CCTTTCACG-GCAACGTACARC-3', JDEIseq 5'-CATTTACCTTCACCGGATAG-3'and I3DeJseq 5'-GAA-CAGCAGCTTAACCTCG-3' depending on insert being sequenced. The verified plasmids encoding *phn* cistron deletion mutants were finally transformed into HO2735 for analysis.

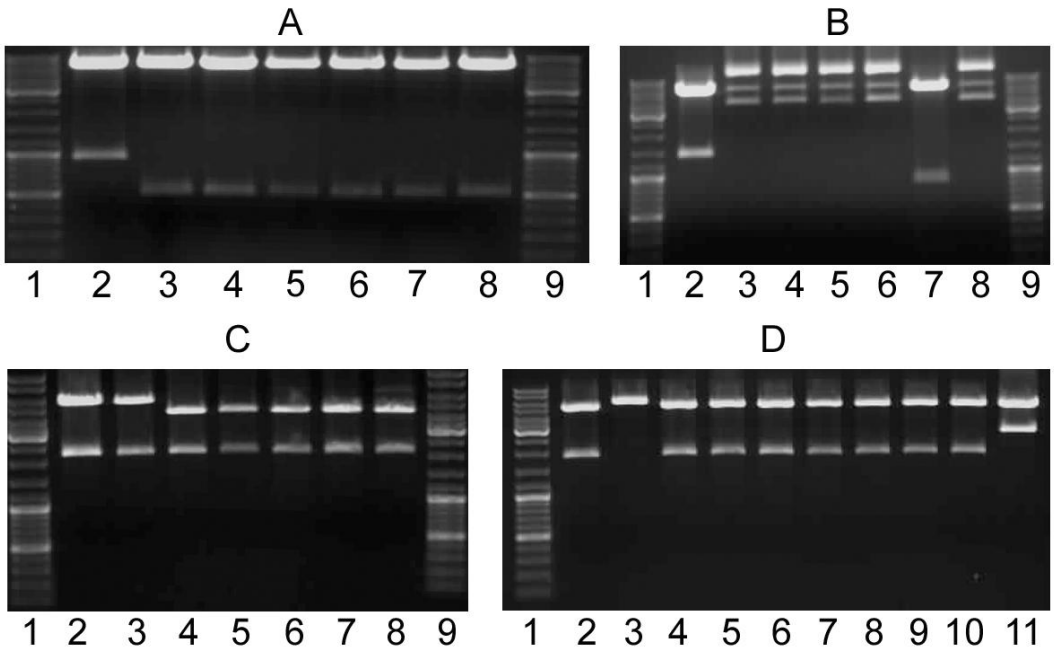

Figure 2-28. Analysis of deletion clones by agarose gel electrophoresis. (A) 0.8% agarose gel of pFM31 clones digested with *Eco*RI and *Sac*II restriction enzymes to visualize 518-bp product with *phnG* deleted. DNA ladder (SM0333, Fermentas) in Lane 1 and 9 (ladder contains 21 discrete fragments: 8000, 7000, 6000, 5000, 4000, 3500, **3000**, 2500, 2000, 1500, 1200, **1031**, 900, 800, 700, 600, **500**, 400, 300, 200, and 100-bp, there are larger quantities of the bolded fragments present in the mixture); lane 2, pHO571 control digested with *Eco*RI and *Sac*II with *phnG* present (929-bp fragment); lanes 3 to 8 contain digested pFM31 clones; (B) 0.8% agarose gel of pFM32 clones digested with *Eco*RI and *Psi*I restriction enzymes to visualize 842-bp product with *phnH* deleted. DNA ladder in Lane 1 and 9; lane 2, pHO571 control digested with *Eco*RI and *Psi*I with *phnH* present (1385-bp fragment); lanes 3 to 8 contain digested pFM32 clones; (C) 0.8% agarose gel of pFM33 clones digested with *Eco*RI and *Nde*I restriction enzymes to visualize change in vector size to 4241-bp with *phnI* deleted. DNA ladder in Lanes 1 and 9; lane 2, pHO571 control digested with *Eco*RI and *Nde*I with *phnI* present (5264-bp fragment); lanes 3 to 8 contain digested pFM33 clones; and (D) 0.8% agarose gel of pFM34 clones digested with *Nco*I restriction enzyme to visualize change in vector size to 1805-bp with *phnJ* deleted. DNA ladder in Lane 1; lanes 2 to 9 contain digested pFM34 clones; lane 11, pHO571 control digested with *Nco*I with *phnJ* present (2609-bp fragment).

2.3.2.5 Identification of partial CP-lyase complexes encoded by *phn* deletion plasmids

The deletion plasmids pFM31, pFM32, pFM33, pFM34 and pHO572 were expressed in the host strain, HO2735. The expression levels of the encoded Phn polypeptides were analyzed by SDS-PAGE (Figure 2-28). The expression of pFM32, pFM33, pFM34, and pHO572 led to the synthesis of the four polypeptides corresponding to the remaining intact *phn* cistrons present in the plasmids. For example, strain HO2735/pFM32 (*phnGΔHIJK*) synthesized PhnG, PhnI, PhnJ, and PhnK, but not PhnH. However, the strain harbouring pFM31 produced very little, if any, Phn polypeptides. Additional pFM31 clones were analyzed and gave identical results. DNA isolation of strains harbouring each of the deletion plasmids illustrated that the strains contained an equal content of each plasmid, therefore the expression of the *phn* genes in the strain harbouring pFM31 was not due to a low copy number of the plasmid. Upon further inspection of the plasmid DNA sequence, the sequence 5'-CCGCGAACGGTCGCGG-3' was observed on either side of the fusion point of the deleted *phnG* gene. This sequence could create an mRNA stem-loop with five GC pairs. This sort of stem-loop could affect translation of the downstream cistrons[67], explaining the poor yield of Phn proteins in strain HO2735/pFM31.

The purification of Phn complexes expressed from the deletion plasmids was performed by our collaborators Bjarne Hove-Jensen and Bjarne Jochimsen. pHO572, lacking the *phnK* cistron synthesized a PhnGHIJ protein complex (Figure 2-28B lane2). One or two copies of the PhnK protein is lost in comparison to the PhnGHIJK complex isolated from pMN1 and pHO571 (Figure 2-28B lane1). When the *phnH* cistron is absent a PhnGI complex is produced that has a molecular weight consistent with a $PhnG_2I_2$ heterotetramer (Figure 2-28B lane3). A Phn protein complex containing PhnG were not detected in extracts of HO2735 harbouring pFM31, pFM33 or pFM34, which lack the *phnG, phnI* and *phnJ* cistrons, respectively. Significant quantities of Phn proteins could not be purified from HO2735/pFM31 strain. However, PhnG could be identified

following ion-exchange chromatography of extracts from strains harbouring pFM33 and pFM34. In these latter cases, coelution of other Phn proteins with PhnG was not observed.

Additional cross-linking experiments were performed by Bjarne Hove-Jensen on the PhnGI complex. A PhnI-dimer rapidly formed (Figure 2-28C, lanes 2 to 7, band a) whereas PhnG only slowly reacted over time (Figure 2-28C, lanes 2 to 7). Both PhnGHIJ and PhnGI complexes were resolved by native-PAGE to examine their oligomeric states (Figure 2-28D, lanes 2 and 3, respectively). The PhnGHIJ complex had two bands similar to that of the PhnGHIJK complex (Figure 2-28D, bands 2 and 3) as well as bands above this. The PhnGI complex contained two bands (Figure 2-28D, bands 4 and 5). These bands were analyzed by MS/MS, revealing that bands 1, 2 and 3 each contained PhnG, PhnH, PhnI and PhnJ, whereas band 4 was elongation factor G and band 5 contained PhnG and PhnI.

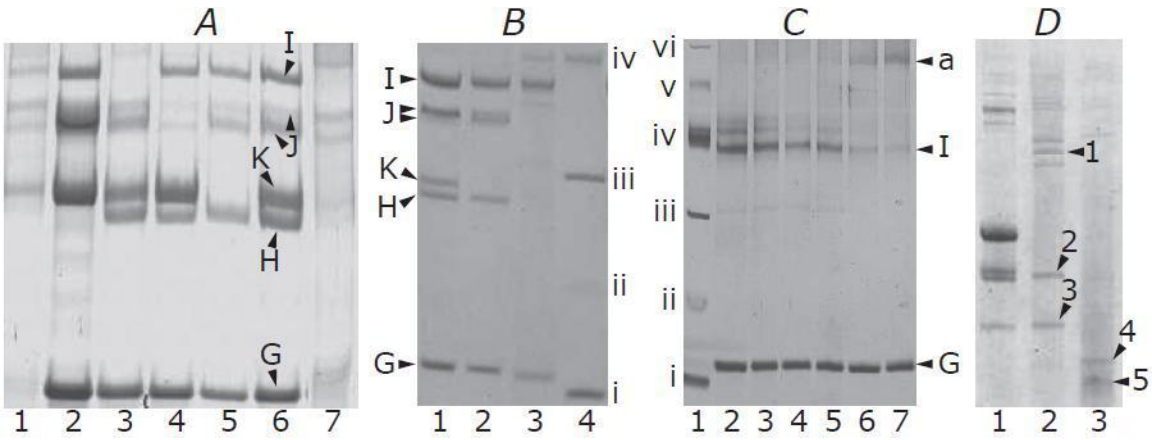

Figure 2-29. PAGE analysis of Phn protein complexes specified by *phn* deletion plasmids. (A) Synthesis of polypeptides specified by plasmids containing various *phn* deletions. After sonication and centrifugation of plasmid-harboring cells of strain HO2735, pellet was dissolved in 6 M urea and analyzed by SDS-PAGE. Cells contained: lane 1, pFM31 (*phnΔGHIJK*); lane 2, pFM32 (*phnGΔHIJK*); lane 3, pFM33 (*phnGHΔIJK*); lane 4, pFM34 (*phnGHIΔJK*); lane 5, pHO572 (*phnGHIJΔK*); lane 6, pHO571 (*phnGHIJK*); lane 7, pUHE23-2; i.e., empty vector. The position of each Phn polypeptide is indicated in lane 6. (B) PhnGHIJ and PhnGI protein complexes of *phnK* and *phnH* deletion plasmids, respectively, analyzed by SDS-PAGE. Lane 1, PhnGHIJK protein complex purified from strain HO2735/pHO571 (*phnGHIJK*); lane 2, PhnGHIJ protein complex purified from HO2735/pHO572 (*phnGHIJ*); lane 3, PhnGI protein complex purified from HO2735/pFM32 (*phnGΔHIJK*); lane 4, molecular mass standard. (C) Cross-linking of PhnGI protein complex analyzed by SDS-PAGE with silver staining. Lane 1, molecular mass standard; lanes 2 to 7, protein complex incubated with glutaraldehyde for 0, 2, 5, 30, 60, and 180 min, respectively. Phn polypeptides are indicated by I and G, cross-linking product is indicated by a. (D) Native-PAGE of PhnGHIJ and PhnGI protein complexes. Lane 1, PhnGHIJK protein complex identical to that shown in Figure 2-23E; lane 2, PhnGHIJ protein complex; lane 3, PhnGI protein complex. Polypeptides of bands labelled 1–5 were identified by MS/MS: band 1, PhnI, PhnJ, PhnH, and PhnG; band 2, PhnI, PhnJ, PhnH, and PhnG; band 3, PhnI, PhnJ, PhnH, and PhnG ; band 4, elongation factor G; band 5, PhnI, and PhnG[27]. DNA ladder annotated as seen in Figure 2-23. Figure from reference 27.

2.3.2.6 Expression of individually cloned *phnG*, *phnH*, *phnI*, *phnJ*, and *phnK* genes

Bjarne Hove-Jensen cloned each of the *phn* cistrons (*phnG*, *phnH*, *phnI*, *phnJ*, and *phnK*) individually into an expression plasmid, with each gene specifying a hexahistidine tag at the C-terminus. Isolation attempts of the Phn polypeptides from strain HO2735 (Δ*phn*) harbouring any one of the five plasmids revealed that only PhnH could be obtained in a soluble form. PhnG, PhnI, PhnJ, and PhnK were all found to be insoluble. Cross-linking experiments of PhnH with glutaraldehyde were conducted (Figure 2-30). The PhnH polypeptide reacted with glutaraldehyde quickly forming cross-linked products of approximately 52 and 110 kDa in size. The molecular mass of the cross-linked products are consistent with a $PhnH_2$ homodimer and a $PhnH_4$ homotetramer, respectively (Figure 2-30, lanes 1 to 5, band c and b). A larger cross-linked product also appeared (Figure 2-30, band a). The dimeric form of PhnH appeared almost immediately (compare Figure 2-30 lanes 1 and 7, time zero and untreated PhnH, respectively). This is a remarkable contrast to the cross-linking experiment involving the PhnGHIJK protein complex above where there was no visible band corresponding to a PhnH homodimer or tetramer (Figure 2-23F, lane 2 to 5).

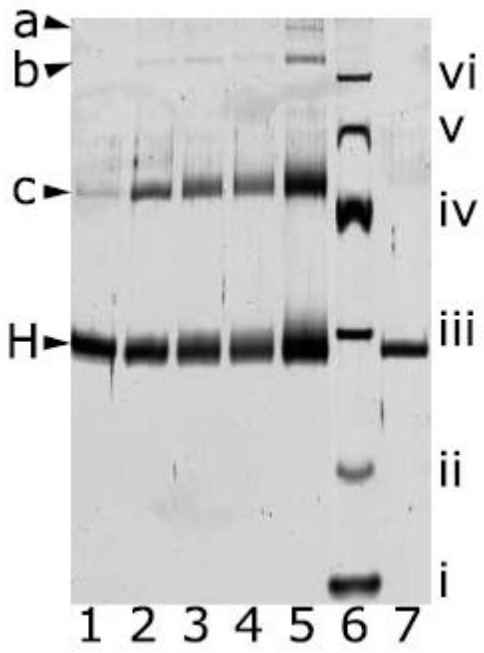

Figure 2-30. SDS-PAGE of PhnH cross-linking with glutaraldehyde. Lanes 1 to 4 contain PhnH incubated with glutaraldehyde at 0, 1, 3, and 8 h, respectively. Lane 5 and lane 4 are the same but there is a threefold higher loading in lane 5. Lane 6 contains the molecular mass standard. Lane 7 contains untreated PhnH. The PhnH monomer is labelled H and cross-linking products are labelled a, b, and c. Gel is stained with silver stain. DNA ladder annotated as seen in Figure 2-23. Figure from reference 27.

2.3.2.7 Complementation assay

A complementation assay was performed to determine if the point mutations found in the *phnG*, *phnH*, *phnI* and *phnK* genes of the pMN1 plasmid were detrimental to the gene products activity. Originally the growth assay was attempted in *ΔpstS* strains using the pMN1 plasmid but, the control sample with the empty pUHE23-2 plasmid rendered the *phn*$^+$ strain incapable of growth on **1a**. The *phnGHIJKLM* insert was hence transferred into a low copy plasmid pSU18 to give rise to pFM35. HO2567 (*phn*$^+$) strain was shown to grow on **1a** with either the pSU18 or pFM35 plasmids prior to attempting the assay. The pSU18 and pFM35 plasmid was then transformed into the various mutant strains HO1550 (*phnG*), HO1547 (*phnH*), HO1552 (*phnI*) and HO1544 (*phnK*). After 90 h of growth on solid media the results were recorded (Table 2-8).

The *phnG*, *phnH*, *phnI* and *phnK* mutants were unable to grow when transformed with pSU18 but all grew when transformed with pFM35 with the *phnK* mutant growing more efficiently than the others. However, none of the mutant strains grew as effectively as the *phn*$^+$ strain.

Table 2-8. Growth response of mutant strains complemented with the pFM35 plasmid.

Strain/plasmid	***Lesion***	***No P_i***	***1a***	***P_i***
HO1647/pFM35	*Δphn*	–	–	++
HO2567/pFM35	*phn*$^+$	–	+++	+++
HO1550/pSU18	*phnG35*	–	–	+++
HO1550/pFM35	*phnG35*	–	+	++
HO1547/pSU18	*phnH13*	–	–	+++
HO1547/pFM35	*phnH13*	–	+	+++
HO1552/pSU18	*phnI40*	–	–	+++
HO1552/pFM35	*phnI40*	–	+	+++
HO1544/pSU18	*phnK6*	–	–	+++
HO1544/pFM35	*phnK6*	–	++	+++

2.3.3 Discussion

Many studies over the past two decades have attempted to isolate CP-lyase without any success[35,36]. Attempts at cell-free CP-lyase reactions have also been fruitless[17,19,39,41,42]. Since the majority of individual Phn polypeptides are not soluble, a CP-lyase complex was proposed. As described in this thesis, coexpression of *phnGHIJKLM*, encoding Phn proteins, produced a soluble PhnGHIJK complex that remained intact after multiple purification steps. In addition a plasmid (pHO571) that allows for the coexpression of *phnGHIJK* also produces a soluble PhnGHIJK, therefore PhnM and PhnL are not required for the assembly of the PhnGHIJK complex. The PhnGHIJK complex is very likely directly involved in CP bond cleavage because *E. coli* strains lacking any one of the *phnG*, *phnH*, *phnI*, *phnJ*, or *phnK* genes is organophosphonate growth deficient[22,23] and cannot produce methane from methylphosphonate (**1a**)[19,29]. The production of a soluble CP-lyase complex consisting of enzymes that are essential

for CP bond cleavage represents an important step towards studying the biochemical and structural properties of this complex *in vitro*. A crystal structure of the PhnGHIJK protein complex is not yet available and hence a detailed picture of the complex's architecture is not available. Still, some conclusions can be drawn from the results obtained so far.

The PhnGHIJK protein complex has an approximate molecular weight of 260 kDa this is large enough to contain two or more copies of one or more of the five polypeptides present. Based on the relative amounts of the polypeptides, estimated by SDS-PAGE, this complex likely corresponds to a $PhnG_4H_2I_2J_2K$ quaternary structure. At the DNA level, translational coupling is observed for these five cistrons, which may help ensure the stoichiometry of the proteins in the complex. The *phn* genes known to be required for CP bond cleavage have all been individually cloned into expression plasmids. However, the only polypeptide to be synthesized in a soluble form was PhnH, consistent with previous attempts by the Zechel lab[29]. A PhnH crystal structure was previously reported[29], but no biochemical function could be determined. PhnH forms a homodimer with a novel protein fold. A small pocket formed at the dimer interface that contains several strictly conserved residues. Docking experiments failed in finding a natural ligand for PhnH, although the pocket appeared to be ideal for binding aromatic molecules.

It is possible that as PhnH is the only polypeptide that is soluble unaccompanied, that it forms a scaffold for the rest of the complex to form around. Cross-linking experiments with the PhnGHIJK complex left PhnH untouched, while PhnH readily reacted with glutaraldehyde when assayed alone. This implies that when PhnH is part of the complex the reactive lysine residues are hidden or inaccessible, whereas in PhnH alone these residues can react readily. It is very likely that PhnH is integrated and buried within the PhnGHIJK complex and this would explain the lack of reactivity towards the cross-linker. MS/MS analysis after native-PAGE clearly supports that PhnH is part of the protein complex. The *phnH* deletion plasmid gives rise to a PhnGI protein complex, demonstrating that PhnI and PhnG interact with one another. PhnK may

also interact with PhnG, as cross-linking pulls out a potential PhnGK cross-linked product. A small quantity of a PhnGHIJ complex is observed by native-PAGE analysis, which can also be isolated from the *phnK* deletion plasmid. It is possible that PhnK only weakly associates with PhnG and the rest of the complex, and therefore a stable complex of PhnGHIJ can also be formed. In the recent ground-breaking paper by Raushel and coworkers, with the knowledge of the PhnGHIJK complex the glycosyltransferase activity of PhnI was determined and was shown to require the presence of PhnG, PhnH and PhnL for activity. As PhnL rather than PhnK was required and both have similar traits it is possible that PhnK and PhnL proteins can be exchanged for one another on the complex. Both *phnK* and *phnL* genes have been suggested to encode an ATP-dependent permease component of a binding protein-dependent ABC transport system[22]. It is possible that PhnK and/or PhnL are involved in physically linking the complex to a membrane bound organophosphonate transport system.

Unfortunately, no CP bond cleaving activity could be detected with the PhnGHIJK complex as purified in our hands. Although 5'-phospho-α-D-ribosyl-1'-phosphonate has been determined as the substrate for CP-lyase (Section 2.2, published in references 31, and 35) it was unavailable in an appreciable quantity at a sufficient quality for analysis. However, it was later shown by Raushel and coworkers that PhnJ, the CP bond cleaving component of CP-lyase, is a SAM dependent enzyme that requires a [4Fe-4S] cluster for activity. The [4Fe-4S] cluster in PhnJ required anaerobic reconstitution conditions in order to obtain active enzyme, which has yet to be tested for the PhnGHIJK complex. In contrast, our purification conditions would have yielded PhnGHIJK with PhnJ in an inactive, oxidized form. In retrospect, it is not surprising that previous efforts by our lab and others to obtain CP bond cleaving activity in cell free extracts had failed, since cell lysis would immediately lead to oxidation and inactivation of the [4Fe-4S] cluster of PhnJ.

Shortly following our work Raushel and coworkers were able to reconstitute the enzyme activities for PhnI, PhnM and PhnJ. A major part of their success relied on the observation that a PhnGHIJK complex forms. Again, due to the poor solubility of the Phn polypeptides, a glutathione S-transferase (GST) fusion tag was used to express and isolate the individual proteins. The fusion enzymes were inactive; therefore removal of the GST tag by proteolysis *in situ* was needed to restore activity of PhnI, PhnJ, PhnL, and PhnM enzymes. Raushel's group observed that PhnI was distantly related to nucleosidases and began probing PhnI activity. PhnI alone was capable of converting ATP to adenine and 5-triphosphoribose. However, in the presence of PhnG, PhnH, and PhnL, PhnI was able to transfer the organophosonate to the 1' position of the ribose moiety, forming 5'-triphospho-α-D-ribosyl-1'-alkylphosphonate (step i, Figure 2-9). It was noted that during the assay the enzymes began to precipitate out of solution. With a 5'-triphospho-α-D-ribosyl-1'-alklylphosphonate (**2**) in hand, and noting our work that revealed 5'-phospho-α-D-ribosyl-1'-alkylphosphonate as a CP-lyase pathway intermediate (Section 2.2, published in reference 35), it was clear that another enzyme was required to remove the β and γ phosphate groups. Based on amino acid sequence homology, PhnM belongs to the amidohydrolase superfamily and seemed to be a good candidate for this role. Indeed. PhnM was shown to hydrolyze 5'-triphospho-α-D-ribosyl-1'-alkylphosphonate (**2**) to 5'-phospho-α-D-ribosyl-1'-alkylphosphonate (**3**) (Step ii. Figure 2-9).

At this point, in combination with our work on PhnP, only the CP bond cleaving reaction was missing from the CP-lyase pathway. The CP-lyase reaction has long been thought to be radical based[35,36]. PhnJ contains a $CX_2CX_{21}CX_3C$ sequence motif that resembles the conserved CX_3CX_2C motif of enzymes that utilize a [4Fe-4S] cluster and SAM to catalyze a wide spectrum of radical reactions. Thus PhnJ appeared to be a good candidate to catalyze CP bond cleavage through a radical process. With the CP-lyase substrate in hand, Raushel and coworkers were able to show CP bond cleavage by PhnJ after anaerobically reconstituting the [4Fe-4S] cluster and

cleaving the GST tag *in situ*. PhnJ was not stable after the GST tag was cleaved and they were only able to observe four turnovers before PhnJ precipitated out of solution.

In the analysis of the PhnGHIJK complex, PhnJ consistently migrated as either two or three polypeptide bands by SDS-PAGE. In most cases the fastest migrating band was the most abundant. This migration pattern suggests that one or more post-translational modification to PhnJ occurs. These post-translational modifications may have some relation to the [4Fe-4S] cluster that is required for activity of the PhnJ enzyme but have yet to be characterized. It is unlikely that these forms of PhnJ are active, as reconstitution of the [4Fe-4S] cluster under anaerobic conditions would be required to produce active PhnJ.

Although the pathway for CP-lyase has now been solved there are still many questions that remain, including several discrepancies that require further investigation. For example, the PhnL enzyme was found to be required for the activity of PhnI, but was not found in the CP-lyase complex. Likewise, although PhnK was detected in the complex there is no biochemical role assigned to this enzyme. PhnK seems to be somewhat loosely associated with the protein complex because a stable PhnGHIJ protein complex can also be detected. PhnK and PhnL have similar properties, both have a sequence that isrelated to nucleotide binding proteins[10,20] and have been suggested to encode an ATP-dependent permease component of a binding protein-dependent ABC transport system[22], which may suggest an association to the cell membrane. As PhnL is required for PhnI activity, it is likely that there is an association between PhnI and PhnL and potentally a PhnGHIJL complex might form in the absence of PhnK, or be induced in the presence of a specific substrate. As both proteins are required for CP bond cleavage *in vivo* then there must be a specific role for PhnK even though this enzyme is not required for CP bond cleavage *in vitro*. It is possible that PhnK may not play an enzymatic role but could aid in stabilizing the other Phn proteins that do perform enzymatic reactions. PhnK may also help with substrate recognition or funnel substrates to their corresponding enzyme.

The importance of protein-protein interactions to CP-lyase activity is emphasized by the detrimental effects of polypeptide tags. The work by Raushel and coworkers revealed that an N-terminal GST-tag (220 amino acids in length and approximately 26 kDa) renders PhnI, PhnJ, PhnL and PhnM proteins inactive. The N-terminal tag very likely prevents the formation of crucial protein-protein interactions, properly folded proteins and/or the formation of an active protein complex. In addition, although PhnI is active in the presence of PhnG, PhnH, and PhnL, the enzymes were not stable. This indicates that a stable soluble complex does not form *in vitro*, and suggests that an additional protein may be required, potentially PhnJ as seen in the isolated protein complex

The reaction of PhnJ was shown to proceed when the enzyme was present alone in solution, though PhnJ was unstable and quickly precipitated out of solution[28]. This could imply that the stability of PhnJ is dependent on one or more of the other Phn polypeptides, likely PhnG, PhnH, PhnI, or PhnK. Originally it was proposed[35] that the complex would perform the CP-lyase reaction and potentially additional pathway reactions. It is now known that within the CP-lyase complex PhnGHIJK, PhnI performs the ribosylation of the organophosphonate substrate and PhnJ cleaves the CP bond of 5'-phospho-α-D-ribosyl-1'-phosphonate. The product of the PhnI reaction, 5'-triphospho-α-D-ribosyl-1'-phosphonate, would have to leave the complex to be hydrolyzed by PhnM. The product of the PhnM reaction 5'-phospho-α-D-ribosyl-1'-phosphonate, would then have to reenter the PhnGHIJK complex for CP bond cleavage.

The *phn* operon encodes a large number of genes that forms a pathway for CP bond cleavage. This pathway is notable for its ability to cleave a wide range of structurally diverse organophosphonates. This is remarkable when one considers that the active site of every enzyme in the pathway must have relaxed specificity to recognize such a variety of substrates. Studies with the acetyltransferase PhnO reveal that a positive charge close to the organophosphonate moiety is detrimental to CP bond cleavge activity by the CP-lyase pathway. Neither **1f** nor **1h** is

a competent susbtrate when *N*-acetylation by PhnO is not performed. This implies that although the active sites are forgiving one or more of the later enzymes in the pathway cannot tolerate a positive charge near the active site. A prime candidate is the radical bond cleavage step catalyzed by PhnJ.

The addition of the organophosphonate to D-ribose by the pathway prior to CP bond cleavage is interesting from a mechanistic evolutionary perspective. There are at least two possible reasons for ribosylation. First, the addition of D-ribose places the organophosphonate on a direct pathway to synthesize an important metabolic molecule PRPP, which can be used to synthesize nucleotides, cofactors, and certain amino acids for cellular use. Secondly, D-ribose provides an opportunity to assist in the catalysis of CP bond cleavage. PhnJ is proposed to form a covalent ribosyl-1-phosphate ester intermediate following CP bond cleavage[28,68]. The 2-OH of D-ribose provides a convenient nucleophile that can be recruited by PhnJ to attack the adjacent phosphate ester thereby turning over the enzyme for another round of catalysis. The high effective molarity of the 2-OH would make this a faster reaction than direct attack by a water molecule. However, the α-D-ribosyl-1,2-cyclic phosphate product formed by this reaction cannot be used by the cell and is effectively a 'dead-end' metabolite. Thus the advantage gained with the 2-hydroxyl in the PhnJ reaction requires the addition of another enzyme to the pathway to recycle the α-D-ribosyl-1,2-cyclic phosphate, in this case the phosphodiesterase PhnP. This may not be the case in all CP-lyase pathways. In some instances neither PhnN nor PhnP are present in the pathway and therefore when PhnN and PhnP are lacking from the pathway there must be another method for recycling the α-D-ribosyl-1,2-cyclic phosphate.

Evidently there is strong selection pressure to use the 2-OH of ribose rather than water for turnover of PhnJ as virtually all CP-lyase pathways contain a phosphodiesterase to deal with the dead-end product. The use of the 2-OH of ribose for catalysis is not unique to PhnJ, however, as RNase A also uses the 2-OH to catalyze the hydrolysis of RNA phosphodiester bonds. The

fact that several of the CP-lyase enzymes and proteins form a complex adds another layer of complexity to this pathway. Structural analysis of the isolated CP-lyase protein complex is required to further understand the intricacies of the reactions performed and what the other Phn proteins contribute to the complex.

2.4 Conclusions

After the discovery of a 14 cistron operon in *E. coli* that is involved in organophosphonate metabolism back in the early 1990s[10,20,22,23] many attempts at determining the method of CP bond cleavage were conducted[19]. Initial *in vitro* studies were unsuccessful[17,19,39,41,42] and little information has shed light on the pathway since mutational and feeding experiments in the early 1990s. Until 2004 when a paper by Bjarne Hove-Jensen, involving the characterization of PhnN as a ribose 1,5-bisphosphokinase resurged an interest in CP-lyase. Since then, a series of publications that arose from this thesis and work by Kamat and Raushel has now solved the conundrum of organophosphonate catabolism by the CP-lyase pathway (Figure 2-9). This thesis describes the detection of CP-lyase catabolic intermediates and a CP-lyase protein complex, which has helped to shed light on the previously unknown CP-lyase pathway. Specifically, PhnP was shown to be a phosphodiesterase (EC 3.1.4.55) that cleaves 5-phospho-α-D-ribosyl-1,2-cyclic phosphate to 5-phospho-α-D-ribosyl-1-phosphate, which in turn is converted to PRPP by PhnN. PRPP can then be shuttled into the primary metabolism. Another important catabolic intermediate was isolated and characterized and was later shown to be the susbtrate for PhnJ, the CP bond cleaving enzyme. In addition, the use of aminoalkylphosphonates as a P_i source was probed, which revealed the surprising importance of *N*-acetylation of 1-aminoalkylphosphonates by the acetyl-CoA dependent enzyme PhnO. The function of PhnO is directly relevant to the microbial degradation of aminomethylphosphonate (**1f**), a metabolite of glyphosate degradation, and may also prove relevant to the degradation of 1-aminoalkylphosphonate natural products.

The PhnGHIJK complex represents an exciting opportunity to study the activities and structures of PhnI and PhnJ. This would include studying the activity of an anaerobically reconstituted [4Fe-4S] cluster of PhnJ while in the complex, as well as X-ray crystallographic studies of a five-polypeptide complex. Such structural and mechanistic studies would provide much needed insight into the mechanisms of the remarkable reactions performed by CP-lyase enzymes.

2.5 References

1. Villarreal-Chiu, J. F.; Quinn, J. P.; McGrath, J. W. The genes and enzymes of phosphonate metabolism by bacteria, and their distribution in the marine environment. *Front. Microbiol.* **2012**, *3*, 1-13.

2. Huang, J.; Su, Z.; Xu, Y. The evolution of microbial phosphonate degradative pathways. *J. Mol. Evol.* **2005**, *61*, 682-690.

3. Karl, D. M.; Beversdorf, L.; Björkman, K. M.; Church, M. J.; Martinez, A.; DeLong, E. F. Aerobic production of methane in the sea. *Nat. Geosci.* **2008**, *1*, 473-478.

4. White, A. K.; Metcalf, W. W. Two C-P Lyase operons in *Pseudomonas stutzeri* and their roles in the oxidation of phosphonates, phosphite, and hypophosphite. *J. Bacteriol.* **2004**, *186*, 4730-4739.

5. Dyhrman, S. T.; Chappell, P. D.; Haley, S. T.; Moffett, J. W.; Orchard, E. D.; Waterbury, J. B.; Webb, E. A. Phosphonate utilization by the globally important marine diazotroph *Trichodesmium*. *Nature* **2006**, *439*, 68-71.

6. Hsieh, Y.; Wanner, B. L. Global regulation by the seven-component P_i signaling system. *Curr. Opin. Microbiol.* **2010**, *13*, 198-203.

7. Baek, J. H.; Lee, S. Y. Novel gene members in the Pho regulon of *Escherichia coli*. *FEMS Microbiol. Lett.* **2006**, *264*, 104-109.

8. Murray, E. L.; Conway, T. Multiple regulators control expression of the Entner-Doudoroff aldolase (Eda) of *Escherichia coli*. *J. Bacteriol.* **2005**, *187*, 991-1000.

9. Gorelik, M.; Lunin, V. V.; Skarina, T.; Savchenko, A. Structural characterization of GntR/HutC family signaling domain. *Protein Sci.* **2006**, *15*, 1506-1511.

10. Metcalf, W. W.; Wanner, B. L. Involvement of the *Escherichia coli phn* (*psiD*) gene cluster in assimilation of phosphorus in the form of phosphonates, phosphite, P_i esters, and P_i. *J. Bacteriol.* **1991**, *173*, 587-600.

11. Metcalf, W. W.; Steed, P. M.; Wanner, B. L. Identification of phosphate starvation-inducible genes in *Escherichia coli* K-12 by DNA sequence analysis of psi::lacZ(Mu d1) transcriptional fusions. *J. Bacteriol.* **1990**, *172*, 3191-3200.

12. Makino, K.; Shinagawa, H.; Amemura, M.; Nakata, A. Nucleotide sequence of the *phoB* gene, the positive regulatory gene for the phosphate regulon of *Escherichia coli* K-12. *J. Mol. Biol.* **1986**, *190*, 37-44.

13. Bauer, K.; Benz, R.; Brass, J.; Boos, W. *Salmonella typhimurium* contains an anion-selective outer membrane porin induced by phosphate starvation. *J. Bacteriol.* **1985**, *161*, 813-816.

14. Kasahara, M.; Makino, K.; Amemura, M.; Nakata, A. Nucleotide sequence of the ugpQ gene encoding glycerophosphoryl diester phosphodiesterase of *Escherichia coli* K-12. *Nucleic Acids Res.* **1989**, *17*, 2854.

15. van Veen, H. W. Phosphate transport in prokaryotes: molecules, mediators and mechanisms. *A. van. Leeuw. J. Microb* **1997**, *72*, 299-315.

16. White, A. K.; Metcalf, W. W. Microbial metabolism of reduced phosphorus compounds. *Annu. Rev. Microbiol.* **2007**, *61*, 379-400.

17. Wackett, L. P.; Shames, S. L.; Venditti, C. P.; Walsh, C. T. Bacterial carbon-phosphorus lyase: products, rates, and regulation of phosphonic and phosphinic acid metabolism. *J. Bacteriol.* **1987**, *169*, 710-717.

18. Matys, S. V.; Laurinavichius, K. S.; Krupyanko, V. I.; Nesmeyanova, M. A. Optimization of degradation of methylphosphonate — analogue of toxic pollutants with direct C-P bond by *Escherichia coli*. *Process Biochemistry* **2001**, *36*, 821-827.

19. Yakovleva, G. M.; Kim, S.; Wanner, B. L. Phosphate-independent expression of the carbon-phosphorus lyase activity of *Escherichia coli*. *Appl. Microbiol. Biotechnol.* **1998**, *49*, 573-578.

20. Chen, C.; Ye, Q.; Zhu, Z.; Wanner, B. L.; Walsh, C. T. Molecular biology of carbon-phosphorus bond cleavage. Cloning and sequencing of the *phn* (*psiD*) genes involved in alkylphosphonate uptake and C-P lyase activity in *Escherichia coli* B. *J. Biol. Chem.* **1990**, *265*, 4461-4471.

21. Wanner, B. L.; Metcalf, W. W. Molecular genetic studies of a 10.9-kb operon in *Escherichia coli* for phosphonate uptake and biodegradation. *FEMS Microbiol. Lett.* **1992**, *100*, 133-140.

22. Metcalf, W. W.; Wanner, B. L. Mutational analysis of an *Escherichia coli* fourteen-gene operon for phosphonate degradation, using Tn*phoA'* elements. *J. Bacteriol.* **1993**, *175*, 3430-3442.

23. Metcalf, W. W.; Wanner, B. L. Evidence for a fourteen-gene, *phnC* to *phn*P locus for phosphonate metabolism in *Escherichia coli*. *Gene* **1993**, *129*, 27-32.

24. Rizk, S. S.; Cuneo, M. J.; Hellinga, H. W. Identification of cognate ligands for the *Escherichia coli phnD* protein product and engineering of a reagentless fluorescent biosensor for phosphonates. *Protein Sci.* **2006**, *15*, 1745-1751.

25. Alicea, I.; Marvin, J. S.; Miklos, A. E.; Ellington, A. D.; Looger, L. L.; Schreiter, E. R. Structure of the *Escherichia coli* phosphonate binding protein PhnD and rationally optimized phosphonate biosensors. *J. Mol. Biol.* **2011**, *414*, 356-369.

26. Gebhard, S.; Cook, G. M. Differential regulation of high-affinity phosphate transport systems of *Mycobacterium smegmatis*: identification of PhnF, a repressor of the *phnDCE* operon. *J. Bacteriol.* **2008**, *190*, 1335-1343.

27. Joshimsen, B.; Lolloe, S.; McSorley, F. R.; Nabi, M.; Stougaard, J.; Zechel, D. L.; Hove-Jensen, B. Five phosphonate operon gene products as components of a multi-subunit complex of the carbon-phosphorus lyase pathway. *Proc. Natl. Acad. Sci. U. S. A.* **2011**, *108*, 11393-11398.

28. Kamat, S. S.; Williams, H. J.; Raushel, F. M. Intermediates in the transformation of phosphonates to phosphate by bacteria. *Nature* **2011**, *480*, 570-572.

29. Adams, M. A.; Luo, Y.; Hove-Jensen, B.; He, S.; van Staalduinen, L. M.; Zechel, D. L.; Jia, Z. C. Crystal structure of PhnH: an essential component of carbon-phosphorus lyase in *Escherichia coli*. *J. Bacteriol.* **2008**, *190*, 1072-1083.

30. Hove-Jensen, B.; Rosenkrantz, T. J.; Haldimann, A.; Wanner, B. L. *Escherichia coli phnN*, encoding ribose 1,5-bisphosphokinase activity (phosphoribosyl diphosphate forming): dual role in phosphonate degradation and NAD biosynthesis pathways. *J. Bacteriol.* **2003**, *185*, 2793-2801.

31. Hove-Jensen, B.; McSorley, F. R.; Zechel, D. L. Catabolism and detoxification of 1-aminoalkylphosphonic acids: N-Acetylation by the *phnO* gene product. *Plos One* **2012**, *7*, e46416.

32. Errey, J. C.; Blanchard, J. S. Functional annotation and kinetic characterization of PhnO from *Salmonella enterica*. *Biochemistry-US* **2006**, *45*, 3033-3039.

33. He, S.; Wathier, M.; Podzelinska, K.; Wong, M.; McSorley, F. R.; Asfaw, A.; Hove-Jensen, B.; Jia, Z.; Zechel, D. L. Structure and mechanism of PhnP, a phosphodiesterase of the carbon-phosphorus lyase pathway. *Biochemistry* **2011**, *50*, 8603-8615.

34. Podzelinska, K.; He, S.; Wathier, M.; Yakunin, A.; Proudfoot, M.; Hove-Jensen, B.; Zechel, D. L.; Jia, Z. Structure of PhnP, a phosphodiesterase of the carbon-phosphorus lyase pathway for phosphonate degradation. *J. Biol. Chem.* **2009**, *284*, 17216-17226.

35. Hove-Jensen, B.; McSorley, F. R.; Zechel, D. L. Physiological role of *phnP*-specified phosphoribosyl cyclic phosphodiesterase in catabolism of organophosphonic acids by the carbon−phosphorus lyase pathway. *J. Am. Chem. Soc.* **2011**, *133*, 3617-3624.

36. Frost, J. W.; Loo, S.; Cordeiro, M. L.; Li, D. Radical-based dephosphorylation and organophosphonate biodegradation. *J. Am. Chem. Soc.* **1987**, *109*, 2166-2171.

37. Berlin, K. D.; Taylor, H. A. The reactions of aroyl halides wit phosphites. Esters of aroylphosphonic acids. *J. Am. Chem. Soc.* **1964**, *86*, 3862-3866.

38. Engel, R. Phosphonates as analogues of natural phosphates. *Chem. Rev.* **1977**, *77*, 349-367.

39. Cordeiro, M. L.; Pompliano, D. L.; Frost, J. W. Degradation and detoxification of organophosphonates: cleavage of the carbon to phosphorus bond. *J. Am. Chem. Soc.* **1986**, *108*, 332-334.

40. Shames, S. L.; Wackett, L. P.; LaBarge, M. S.; Kuczkowski, R. L.; Walsh, C. T. Fragmentative and stereochemical isomerization probes for homolytic carbon to phosphorus bond scission catalyzed by bacterial carbon-phosphorus lyase. *Bioorg. Chem.* **1987**, *15*, 366-373.

41. Avila, L. Z.; Loo, S. H.; Frost, J. W. Chemical and mutagenic analysis of aminomethylphosphonate biodegradation. *J. Am. Chem. Soc.* **1987**, *109*, 6758-6764.

42. Avila, L. Z.; Draths, K. M.; Frost, J. W. Metabolites associated with organophosphonate C-P bond cleavage: chemical synthesis and microbial degradation of [^{32}P]-ethylphosphonic acid. *Bioorg. Med. Chem. Lett.* **1991**, *1*, 51-54.

43. Hove-Jensen, B.; Rosenkrantz, T. J.; Zechel, D. L.; Willemoes, M. Accumulation of intermediates of the carbon-phosphorus lyase pathway for phosphonate degradation in *phn* mutants of *Escherichia coli*. *J. Bacteriol.* **2010**, *192*, 370-374.

44. Quiocho, F. A.; Ledvina, P. S. Atomic structure and specificity of bacterial periplasmic receptors for active transport and chemotaxis: variation of common themes. *Mol. Microbiol.* **1996**, *20*, 17-25.

45. Rigali, S.; Derouaux, A.; Giannotta, F.; Dusart, J. Subdivision of the helix-turn-helix GntR family of bacterial regulators in the FadR, HutC, MocR and YtrA subfamilies. *J. Biol. Chem.* **2002**, *277*, 12507-12515.

46. He, S.; Luo, Y.; Hove-Jensen, B.; Zechel, D. L. A fluorescent substrate for carbon-phosphorus lyase: towards the pathway for organophosphonate metabolism in bacteria. *Bioorg. Med. Chem. Lett.* **2009**, *19*, 5954-5957.

47. Harkness, D. R. Bacterial growth on aminoalkylphosphonic acids. *J. Bacteriol.* **1966**, *92*, 623-627.

48. Strong, M.; Sawaya, M. R.; Wang, S.; Phillips, M.; Cascio, D.; Eisenberg, D. Toward the structural genomics of complexes: crystal structure of a PE/PPE protein complex from *Mycobacterium tuberculosis*. *Proc. Natl. Acad. Sci. U. S. A.* **2006**, *103*, 8060-8065.

49. Silhavy, T. J.; Berman, M. L.; Enquist, L. W. *Experiments with gene fusions;* Cold Spring Harbor Laboratory Press: Cold Spring Harbor, NY, 1984; , pp 303.

50. Iqbal, S.; Parker, G.; Davidson, H.; Moslehi-Rahmani, E.; Robson, R. L. Reversible phase variation in the *phnE* gene, which is required for phosphonate metabolism in *Escherichia coli* K-12. *J. Bacteriol.* **2004**, *186*, 6118-6123.

51. Makino, K.; Kim, S.; Shinagawa, H.; Amemura, M.; Nakata, A. Molecular analysis of the cryptic and functional *phn* operons for phosphonate use in *Escherichia coli* K-12. *J. Bacteriol.* **1991**, *173*, 2665-2672.

52. Neidhardt, F. C.; Bloch, P. L.; Smith, D. F. Culture medium for enterobacteria. *J. Bacteriol.* **1974**, *119*, 736-747.

53. Khorana, H. G.; Fernandes, J. F.; Kornberg, A. Pyrophosphorylation of ribose 5-phosphate in the enzymatic synthesis of 5-phosphorylribose 1-pyrophosphate. *J. Biol. Chem.* **1958**, *230*, 941-948.

54. Surin, B. P.; Rosenberg, H.; Cox, G. B. Phosphate-specific transport system of *Escherichia coli*: nucleotide sequence and gene-polypeptide relationships. *J. Bacteriol.* **1985**, *161*, 189-198.

55. Fathi, R.; Jordan, F. Certain novel ribofuranosyl phosphates derived from phospho-a-D-ribofuranosyl-1-pyrophosphate: Synthesis, structure, and alkaline hydrolytic reactivities. *J. Org. Chem.* **1988**, *53*, 1997-2001.

56. Meola, M.; Yamen, B.; Weaver, K.; Sandwick, R. K. The catalytic effect of Mg^{2+} and imidazole on the decomposition of 5-phosphoribosyl-α-1-pyrophosphate in aqueous solution. *J. Inorg. Biochem.* **2003**, *93*, 235-242.

57. Atherton, F. R.; Hall, M. J.; Hassall, C. H.; Lambert, R. W.; Lloyd, W. J.; Ringrose, P. S. Phosphonopeptides as antibacterial agents: mechanism of action of alaphosphin. *Antimicrob. Agents. Ch.* **1979**, *15*, 696-705.

58. Overbeek, R.; Begley, T.; Butler, R. M.; Choudhuri, J. V.; Chuang, H. Y.; Cohoon, M.; de Crecy-Lagard, V.; Diaz, N.; Disz, T.; Edwards, R.; Fonstein, M.; Frank, E. D.; Gerdes, S.; Glass, E. M.; Goesmann, A.; Hanson, A.; Iwata-Reuyl, D.; Jensen, R.; Jamshidi, N.; Krause, L.; Kubal, M.; Larsen, N.; Linke, B.; McHardy, A. C.; Meyer, F.; Neuweger, H.; Olsen, G.; Olson, R.; Osterman, A.; Portnoy, V.; Pusch, G. D.; Rodionov, D. A.; Ruckert, C.; Steiner, J.; Stevens, R.; Thiele, I.; Vassieva, O.; Ye, Y.; Zagnitko, O.; Vonstein, V. The subsystems approach to genome annotation and its use in the project to annotate 1000 genomes. *Nucleic Acids Res.* **2005**, *33*, 5691-5702.

59. Mazumder, R.; Iyer, L. M.; Vasudevan, S.; Aravind, L. Detection of novel members, structure-function analysis and evolutionary classification of the 2H phosphoesterase superfamily. *Nucleic Acids Res.* **2002**, *30*, 5229-5243.

60. Bordwell, F. G.; Zhang, X. Effects of anions and radicals of alpha-quaternary ammonium substituents. *J. Org. Chem.* **1990**, *55*, 6078-6079.

61. Bordwell, F. G.; Zhang, X.; Alanjjar, M. S. Effects of adjacent acceptors and donors on the stabilities of carbon-centered radicals. *J. Am. Chem. Soc.* **1992**, *114*, 7623-7629.

62. Rueppel, M. L.; Brightwell, B. B.,; Schaefer, J.; Marvel, J. T. Metabolism and degradation of glyphosphate in soil and water. *J. Agric. Food Chem.* **1977**, *25*, 517-528.

63. Shisler, K. A.; Broderick, J. B. Emerging themes in radical SAM chemistry. *Curr. Opin. Struc. Biol.* **2012**, *22*, 701-710.

64. Arraj, J. A.; Marinus, M.,G. Phenotypic reversal in *dam* mutants of *Escherichia coli* K-12 by a recombinant plasmid containing the *dam*$^+$ gene. *J. Bacteriol.* **1983**, *153*, 562-565.

65. Ho, S. N.; Hunt, H. D.; Horton, R. M.; Pullen, J. K.; Pease, L. R. Site-directed mutagenesis by overlap extension using the polymerase chain reaction. *Gene* **1989**, *77*, 51-59.

66. Perkins, D. N.; Pappin, D. J. C.; Creasy, D. M.; Cottrell, J. S. Probability-based protein identification by searching sequence databases using mass spectrometry data. *Electrophoresis* **1999**, *20*, 3551-3567.

67. Hall, M. N.; Gabay, J. D.,M.; Schwartz, M. A role for mRNA secondary structure in the control of translation initiation. *Nature* **1982**, *295*, 616-618.

68. Zhang, Q.; van der Donk, W. A. Answers to the Carbon-Phosphorus lyase conundrum. *ChemBioChem* **2012**, *13*, 627-629.

Chapter 3

A new oxidative pathway for CP bond cleavage

3.1 Introduction

One of the most predominant organophosphonates in nature is 2-aminoethylphosphonate (**1g**, Figure 1-2)[1-4]. In many organisms, **1g** and its *N*-methylated derivatives are used to replace phosphoethanolamine in phosphonolipids or are incorporated into glycolipids[3,5]. The precise role of phosphonolipids is not known, but incorporation of organophosphonates into lipids may be in response to phosphate (P_i) limitation, or the carbon-phosphorus (CP) bond may play a significant function. For example, the CP bond may protect the organism against hydrolytic enzymes, and / or contribute to intercellular communication[6]. In general, biosynthesis of organophosphonates occurs through intramolecular rearrangement of phosphoenolpyruvate to phosphonopyruvate, which is catalyzed by phosphoenolpyruvate mutase[6-8]. In addition to synthesizing organophosphonates, many more microorganisms are capable of degrading them. Genes that encode pathways for biosynthesis of organophosphonates are found in 10% of available whole-genome bacterial sequences, whereas 40% contain one or more phosphonate degradation pathways[9]. As discussed previously in Chapter 2, there were until recently only two known general enzyme mechanisms for cleaving a CP bond[2,10], the hydrolytic 'electron-sink' mechanism, and the radical based CP-lyase pathway. A screen of marine metagenomic DNA recently hinted at a third potential CP cleavage mechanism[11]. Two genes, *phnY* and *phnZ*, were capable of restoring the ability of a Δ*phn E. coli* mutant strain to grow on **1g** as a P_i source. Neither *phnY* nor *phnZ* showed any similarity to known organophosphonate utilizations genes, suggesting a novel process for degrading phosphonates.

3.1.1 Discovery and distribution of *phnY* and *phnZ* genes

Organophosphonate utilization by marine bacteria has recently been explored. *Trichodesmium erythraeum* is known to contain a complete CP-lyase operon that is expressed in P_i-limited cultures as well as *in situ* in the Sargasso Sea. It is therefore likely that they are capable of utilizing organophosphonates as a P_i source[12]. Other organophosphonate utilization pathways have been found in metagenomic libraries in the Sargasso Sea[10]. Also, in Station ALOHA in the North Pacific Subtropical Gyre, methane was released upon addition of methylphosphonate (**1a**), indicating the likely presence of bacteria containing a CP-lyase pathway[13]. With this in mind Martinez *et al.* screened marine metagenomic DNA libraries (created from a 130 m depth sample) for genes that could complement the ability of an *E. coli* strain lacking a CP-lyase pathway (Δ*phn*) to grow on **1g** as a sole source of P_i.

This approach identified two unique clones that allowed the *E. coli* Δ*phn* strain to grow on **1g**[11]. One of the isolated clones, HF130_AEPn_2, was found to contain three genes required for **1g** utilization that were similar to the previously characterized phosphonatase pathway: *phnW*, encoding a pyruvate aminotransferase, *phnX*, encoding phosphonoacetaldehyde hydrolase, and a gene that encodes the LysR transcriptional regulator. This pathway was interesting in that it was not regulated by P_i levels and allowed *E. coli* to use **1g** as a source of nitrogen in addition to P_i. This was also the first time a phosphonatase pathway had been observed in a marine microbe[11]. The other isolated clone, HF130_AEPn_1, allowed for growth on **1g** as a P_i source but not as a nitrogen or carbon source. Poor growth on **1g** as a P_i source in a copy up experiment indicated that one or more of the genes on the HF130_AEPn_1 fosmid were toxic at high expression levels. Intriguingly, HF130_AEPn_1 did not contain a gene similar to that of any known CP bond-cleaving pathway. Transposon insertion mutants were created and their phenotypic analysis revealed two genes that were required for **1g** utilization, *phnY* and *phnZ*[11]. Based on the sequence

it is not clear what phyla these genes come from but analyses suggested that it may have come from a *Deltaproteobacteria* representative[11].

The distribution of *phnY* and *phnZ* genes in microorganism genomes strongly suggests a marine bias for this pathway. The average abundance of *phnY* and *phnZ* in the Global Ocean Survey database was 2% and 8% compared to 6% and 8% of *phnI* and *phnJ*, respectively[11]. The distribution of *phnY* and *phnZ* in the water column was also examined. In the ALOHA samples *phnZ* was found in 10% or less microorganisms throughout the column whereas *phnY* only appears after the 125 m mark[11]. The full pathway is therefore more prevalent below surface water. The Sargasso Sea, which has two orders of magnitude lower P_i levels contained larger quantities of *phnZ* at 24% of the sample, these genes were commonly linked to *Prochlorococcus marinus*. It is also interesting that CP-lyase genes were not detected at 500 m but *phnZ* genes were still present in a significant fraction of the microorganisms at that depth[11]. A more recent study of phosphonate utilization gene distribution showed that *phnY* and *phnZ* were present in 0.4% of fully sequenced bacterial genomes. However, this is biased towards terrestrial bacteria. If only marine bacterial genomes are considered, the frequency of *phnY* and *phnZ* increases to 2.1%[9]. Moreover, in 83 oceanic sites sampled by the Global Ocean Survey, *phnZ* was found in 77.1%[9] of the metagenomic DNA samples, indicating that *phnZ* likely plays an important role in the marine environment.

3.1.2 Fe^{2+} / α-ketoglutarate dependent dioxygenases

Neither *phnY* nor *phnZ* genes had any sequence similarity to known phosphonate utilization genes. However, PhnY belongs to a catalytically diverse class of Fe^{2+} and α-ketoglutarate dependent dioxygenases (family code: pfam05721, Figure 3-1). This family includes diverse enzyme activitities, including phytanoyl-CoA dioxygenases and halogenases[14,15]. In particular, PhnY shares a high homology to EpoA and HtxA, which catalyze the epoxidation of *cis*-propenylphosphonic acid and the oxidation of hypophosphite, respectively[16,17]. Non-heme

Fe^{2+} / α-ketoglutarate dependent dioxygenases feature a mononuclear Fe^{2+} bound in the active site by two histidine residues and either an aspartate or glutamate residue. The α-ketoglutarate co-substrate binds to the Fe^{2+} along with O_2. The α-keto acid is then oxidatively cleaved into CO_2 and succinate, with the later acquiring one oxygen atom from O_2. This drives the formation of a highly reactive ferryl Fe(IV)=O intermediate that incorporates the second oxygen atom of O_2 into the substrate[14]. This chemistry is remarkable in its ability to cleave unactivated C-H bonds. Interestingly, well studied Fe^{2+} / α-ketoglutarate dependent dioxygenases, TauD[18] and DhpA[19], hydroxylate the C1 position of taurine and 2-hydroxyethylphosphonate, both molecules are structurally similar to **1g**.

3.1.3 HD family enzymes

PhnZ shares sequence similarity to metal ion dependent phosphohydrolases of the HD superfamily. PhnZ belongs to a large subclass of uncharacterized enzymes that have been associated with the *phn* operon in many bacterial species (family codes; pfam01966 and TIGR03276, Figure 3-2). The HD superfamily has three highly conserved motifs (I, II and V) and two less significant unique motifs (III and IV)[21]. Motif II contains the HD signature that coordinates to an active site metal-ion and motifs I and V contain other conserved histidine and aspartate residues. Within motifs III and IV additional conserved histidines are observed in some members of the HD-superfamily. It was noted that mutations to the HD signature and the aspartate residue in motif V cause the most severe effects on enzyme activity[22].

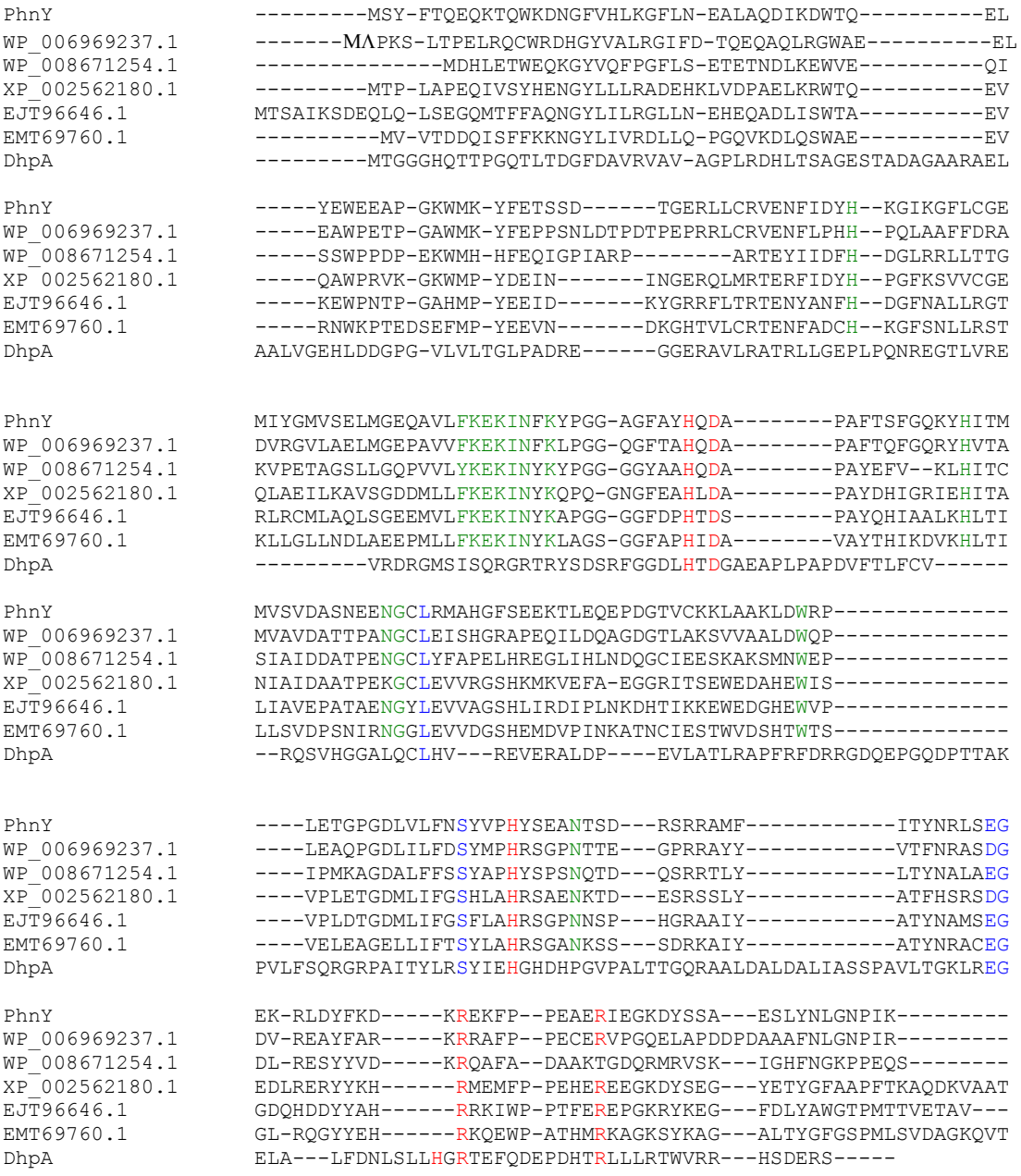

Figure 3-1. Alignment of PhnY to similar α-ketoglutarate / Fe^{2+} dependent enzymes. PhnY was aligned to similar enzymes from the PhyH superfamily and to DhpA using Clustal Omega[20]. GenBank accession numbers are given for members of the PhyH superfamily. Conserved residues are in red, similarly conserved residues are in blue, and conserved residues specific to the PhyH superfamily are in green.

```
PhnZ              ------------------------------------------------------------
WP_009283152.1    ------------------------------------------------------------
WP_008202132.1    ------------------------------------------------------------
YP_003388204.1    ------------------------------------------------------------
WP_007976432.1    ------------------------------------------------------------
WP_005792319.1    ------------------------------------------------------------
MIOX              GAMGMKVDVGPDPSLVYRPDVDPEMAKSKDSFRNYTSGPLLDRVFTTYKLMHTHQTVDFV

PhnZ              ----------------------MSLSNSSKVSVLISLLEKSRDLDYIG---EAINQLEHS
WP_009283152.1    ------------------------MIEQTISDISTLFERSGNDAYFG---EPVTQLEHA
WP_008202132.1    -----------------MKPTFIEKSKNKRLALIFDLYEKYGDDDYIG---EPVSQIEHM
YP_003388204.1    ------------------------------METIANLFAQGGDDAYFG---EPITQLEHA
WP_007976432.1    ----------------------MRSNEQTVAKVFALYERFGDSDYIG---EPVSQIEHM
WP_005792319.1    ----------------------MSPEQAIAQVFGLYEQHGTADYIG---EPVSQIEHM
MIOX              SRKRIQYGSFSYKKMTISRKRIQYGSFSYKKMTIMEAVGMLDDLVDESDPDVDFPNSFHA

PhnZ              LQCAYFAQ-RSGADNEMVLAALLHDLGHYCND-TSFEDMGGYGV-----------------
WP_009283152.1    LQCAGLAE-RAGADDETIIAAFLHDIGHLLPPDMAGGYMDGYGT-----------------
WP_008202132.1    CQSAQLAE-KEGYDEEVILAAFFHDIGHLCVHLGSFESMNGYGI-----------------
YP_003388204.1    LQCAQLAE-EAGADDDTIVAAFLHDIGHLLPPDLAGGYMDGYGT-----------------
WP_007976432.1    SQAAQCAM-AEGFDDEVVLAAFFHDIGHICAE--GAENMGGYGV-----------------
WP_005792319.1    SQAAQLAM-AEGFDDEVVLAAFFHDIGHLCGQ--GAENMGGYGV-----------------
MIOX              FQTAEGIRKAHPDKDWFHLVGLLHDLGKI--M-ALWGEP-QWAV-----VGDTFPVGCRP

PhnZ              ------------------------------------------WQHEKVGADYLRGLGF--S
WP_009283152.1    ------------------------------------------VDHERLGADYLRQRGF--S
WP_008202132.1    ------------------------------------------KSHEKIGGDFLRDMFG--P
YP_003388204.1    ------------------------------------------VDHERLGADYLRERGF--S
WP_007976432.1    ------------------------------------------VSHERLGADYLRNAGF--S
WP_005792319.1    ------------------------------------------VSHERLGADYLRRAGF--S
MIOX              QASVVFCDSTFQDNPDLQDPRYSTELGMYQPHCGLENVLMSWGHDEYLYQMMKFNKFSLP

PhnZ              ERVACLIEGHVAAKRYLVSSKASYLKNLSDASRKTLEYQGGPMDEGERRL-FEEREDFKD
WP_009283152.1    EKVAQLIEHHVNAKRYLVAKKPEYLARLSEASLKTLEFQGGPMTVDETES-FEKNPYFRQ
WP_008202132.1    ERIAKLVENHVQAKRYLTFKNPAYFDKLSEASRKTLEFQGGKMNESEAKE-FENDPLFEV
YP_003388204.1    EKVAQLIENHVNAKRYLVYKNPAYFARLSEASLKTLEFQGGPMTAAEAML-FETNPYFKG
WP_007976432.1    ERMARLVEYHVQAKRYLTLREPGYYERLSEASRRTLEYQGGVMTEAEADA-FEQDPLCNV
WP_005792319.1    ERMAKLVEYHVPAKRYLTFSQPGYYAGLSEASRRTLGYQGGVMTAEEAQI-FEQDPLCQI
MIOX              SEAFYMIRFHSF-YPWHTGG----------------------DYR-QLCSQQDLD--MLPW

PhnZ              CLKIRAWDEKGKQTDLKVP--GPEHYRKMMEEHLSENQN--------
WP_009283152.1    ILQVRGWDEQAKETGMVLP--DPIHYLEKCYNHLESRLS--------
WP_008202132.1    SIKMRNWDELAKLENVPLP--DLGVYRKIAERLIA------------
YP_003388204.1    ILLMRTWDEQAKIPGLPTP--GIDYYMAIVE-RNANRVD--------
WP_007976432.1    SLRMRQWDEQAKEMHVPVI--DLEVLKRKAASLLTGDPIPAAGTV--
WP_005792319.1    SLRMRHWDEQAKETQVPVL--DLQILKSKAARLLAT-----------
MIOX              VQEFNKFDLYTKCPDLPDVESLRPYYQGLIDKYCP-GTLSW
```

Figure 3-2. Alignment of PhnZ to similar Phn-HD enzymes and MIOX. PhnZ was aligned to similar enzymes from the Phn-HD sub-clade using Clustal Omega[20], a structural alignment of PhnZ to MIOX by Dali was used to compare Phn-HD enzymes to MIOX. GenBank accession numbers are given for members of the Phn-HD sub-clade. Conserved HD residues are in red, with the fifth H of the Phn-HD sub-clade in green and other conserved residues in the Phn-HD sub-clade in blue.

3.1.4 Rationale and objectives

PhnY and PhnZ potentially represent a new enzymatic pathway for cleavage of a CP bond. It is possible that PhnY reacts with **1g** to introduce a hydroxyl group at the C1 position, analogous to the reaction performed by TauD on taurine[23]. The hydroxylation of taurine weakens the carbon-sulfur bond leading to non-enzymatic cleavage of the bond. Hydroxylation of **1g** could similarly weaken the CP bond making it susceptible to hydrolytic cleavage by PhnZ. The HD domain is known to coordinate to divalent metal ions that could stabilize a CP bond cleavage transition state. The objective is to investigate the PhnY and PhnZ reactions to determine how this novel pathway allows for the utilization of **1g** as a P_i source.

3.2 Methods

3.2.1 Materials and equipment

Restriction endonucleases and T4 DNA ligase were purchased from New England Biolabs. Luria-Bertani (LB) broth and agar were obtained from Fisher Scientific or Bio-Shop. *E. coli* BL21 (DE3) cells (Novagen) were used for protein production. XL1-Blue cells (Stratagene) were used as the recipient strain for transformations of ligated DNA and for plasmid DNA isolation. The *phnY* and *phnZ* genes were codon optimized for expression in *E. coli* and synthesized by DNA 2.0 (California, USA). The genes were provided in expression plasmids as pJexpress401_*phnY* and pJexpress401_*phnZ*. The expression plasmids pET21a and pET28a were obtained from Novagen. Nickel-nitrilotriacetic acid (NTA) agarose resin and the QIAquick Extraction Kit were obtained from Qiagen. Streptactin Superflow resin was obtained from IBA Life Sciences GmbH (Göttingen, Germany). Nucleospin plasmid DNA extraction kit was obtained from Macherey-Nagel. 2-Aminoethylphosphonate was purchased from Acros Organics (Geel, Belgium), and phosphite was purchased from Riedel-deHaën (Buchs, Switzerland). Racemic 2-amino-1-hydroxyethylphosphonate (**8**) and the *R*-enantiomer were obtained from Peter Wyatt (Queen Mary, University of London), with other aminophosphonates, 2-amino-(*S*)-1-

hydroxyethylphosphonate and (*R*,*R*)- and (*R*,*S*/*S*,*R*)-2-amino-1-hydroxypropylphosphonates (**11**) were obtained from Friedrich Hammerschmidt (Institute of Organic Chemistry, University of Vienna). 1-Hydroxyethylphosphonate (**12**) was obtained from Wilfred van der Donk (Department of Chemistry, University of Illinois). Methyl-, ethyl-, and aminomethylphosphonates, phosphoethanolamine, Chelex-100 and all other chemicals were purchased from Sigma-Aldrich and used without any further purification. The antibiotics ampicillin and kanamycin were purchased from either Sigma-Aldrich or BioShop and used at a final concentration of 100 μg L^{-1} and 50 μg L^{-1}, respectively.

All NMR spectra were recorded on Bruker Avance 400 MHz spectrometers at Queen's University. The ^{1}H NMR chemical shifts (δ) are relative to HDO, and ^{31}P chemical shifts are relative to 85% phosphoric acid at 0 ppm. HPLC analysis was performed on a Varian 920-LC system. ICP-MS analysis was performed using a Varian 820-MS ICP mass spectrometer. The X-ray crystal structure of PhnZ was solved by Laura van Staalduinen and Margaret Kim in the lab of Professor Zongchao Jia (Department of Biomedical and Molecular Sciences, Queen's University). The extinction coefficients for PhnY and PhnZ were calculated from their respective amino acid sequences using the web based tool ProtParam (http://web.expasy.org/protparam/)[24].

3.2.2 Expression of *phnY* in *E. coli* and purification of the p*hnY* gene product[25]

The *phnY* gene (GenBank ID: ACU83549) followed by a C-terminal Strep-tag (WSHPQFEK) encoding sequence was codon optimized for expression in *E. coli* using GeneDesigner (DNA 2.0). The optimized *phnY* coding sequence, with NdeI and HindIII restriction endonuclease sites underlined, is as follows: 5'-<u>CATATG</u>GGC AGCTACTTCACGCAAGAGCAGAAAACGCAATGGAAAGACAATGGTTTCGTTCATTTG AAAGGTTTTCTGAACGAGGCGCTGGCGCAGGACATCAAAGATTGGACGCAGGAATT GTACGAGTGGGAAGAGGCACCGGGTAAATGGATGAAGTATTTCGAGACTAGCTCTG ACACCGGTGAGCGCCTGCTGTGCCGCGTTGAGAATTTCATCGACTACCATAAAGGCA

TTAAGGGCTTTCTGTGTGGCGAGATGATTTACGGTATGGTTAGCGAGTTGATGGGTG
AACAAGCTGTGCTGTTTAAAGAGAAAATCAACTTCAAATATCCGGGTGGCGCAGGCT
TCGCCTACCACCAGGATGCGCCTGCATTCACCAGCTTTGGCCAAAAGTATCACATCA
CCATGATGGTCAGCGTCGACGCGAGCAACGAAGAGAATGGTTGCCTGCGCATGGCA
CACGGTTTCAGCGAAGAGAAAACGCTGGAGCAAGAACCGGACGGTACCGTGTGTAA
AAAGCTGGCGGCGAAGCTGGACTGGCGTCCGCTGGAAACCGGTCCAGGTGATCTGG
TCCTGTTTAACTCGTATGTGCCGCATTACTCTGAAGCCAATACCTCCGATCGTTCGCG
TCGTGCTATGTTTATCACCTATAACCGTCTGAGCGAGGGTGAAAAACGCTTGGATTA
CTTCAAGGATAAGCGTGAAAAGTTTCCGCCGGAGGCCGAGCGTATTGAAGGTAAGG
ACTATAGCAGCGCGGAGAGCCTGTACAACCTGGGCAATCCGATTAAGTGGTCCCACC
CGCAGTTTGAAAAGTAAAAGCTT-3'. The synthetic *phnY* gene was ligated into the pJ401 expression plasmid, yielding pJexpress401_*phnY*. However, production of PhnY in *E. coli* from this plasmid was poor (described below in the Results). Consequently, the *phnY* gene was excised from pJexpress401_*phnY* using restriction endonucleases *Nde*I and *Hind*III and ligated into the corresponding sites of pET21a, yielding pFM36. In addition three other clones were constructed using PCR. The following primers were used: ForPhnY 5'-gataa*catatg*ggcagctacttc-3' encoding an NdeI site, RevPhnY 5'-gctc*aagctt*atta cttaatcggattgcccaggttg-3' encoding a HindIII site, RevHisPhnY 5'-gctc*aagctt*atta**gtgatgatggtgatgatg**cttaatcggattgcccaggttg-3' encoding a HindIII site, and ForStrepPhnY 5'-gctc*ccatgg*gc**tggtctcatccgcagttcgaaaag**atgggcagctacttcacgc-aag-3' encoding a NcoI site. Restriction endonuclease sites are italicized, altered stop codons are underlined, and nucleotide sequences encoding purification tags are in bold. PCR was performed with 1 X Herculase II buffer, 250 μM of each dNTP, 5% DMSO, approximately 1 - 30 ng of DNA template (1 μL of isolated pJexpress401_*phnY* plasmid DNA), 0.25 μM of each primer, and 1 μL of Herculase II polymerase (Stratagene) in a 50 μL reaction volume. The PCR was performed using a PTC-200 theromal cycler (MJ Research) as per programs seen in Table 3-1.

All PCR products were then analyzed on a 1.5% agarose gel electrophoresis and purified using the QIAquick Gel Extraction Kit (following the enzymatic clean-up protocol) prior to digestion. ForPhnY and RevHisPhnY were used to amplify the *phnY* gene from pJexpress401_*phnY* and replace the C-terminal Strep-tag with a C-terminal histidine tag. The amplified PCR product, *phnYhis*, along with the pET21a plasmid, was digested with *Nde*I and *Hind*III and ligated to create pFM37. ForPhnY and RevPhnY were used to amplify the *phnY* gene from pJexpress401_*phnY* and replace the C-terminal Strep-tag with a stop codon. The resulting PCR product, *phnY*, was digested with *Nde*I and *Hind*III and ligated into the similarly digested pET28a plasmid. The resulting plasmid, pFM38, encodes *phnY* with an N-terminal histidine tag followed by a thrombin site. ForStrepPhnY and RevPhnY primers were used to amplify the *phnY* gene from pJexpress401_*phnY* and replace the C-terminal Strep-tag with a stop codon and insert an N-terminal Strep-tag, creating PCR product *strepphnY*. The amplified PCR, *strepphnY*, product along with the pET28a plasmid was digested with *Nco*I and *Hind*III. The corresponding DNA fragments were ligated to create pFM39. Prior to ligation, all digest reactions were separated by agarose gel electrophoresis and desired DNA fragments were excised from gel and extracted using the QIAquick Gel Extraction Kit according to the manufacturer's instructions. The purity and concentration of the DNA fragments were then analyzed by agarose gel electrophoresis and ligation reactions were set up based on the approximate DNA concentrations of the digested PCR product and its corresponding digested plasmid backbone.

E. coli XL1-Blue was transformed with ligation reactions of pFM36, pFM37, pFM38 and pFM39 and were then grown overnight at 37°C on LB-agar supplemented with ampicillin or kanamycin, as required. Single colonies were used to inoculate 4 mL LB liquid cultures supplemented with the required antibiotic. Plasmid DNA was isolated using the Nucleospin kit and digested to confirm the presence of the *phnY* fragment. A select number of positive clones were sent for DNA sequencing by Robarts Research Laboratories.

Table 3-1. PCR programs used to create *phnY* gene alteration.

Step	*Program 1*	*Program 2*
1.	5 min at 95°C	5 min at 95°C
2.	0.5 min at 95°C	0.5 min at 95°C
3.	0.5 min at 61°C	0.5 min at 63°C
4.	40 s at 72°C	40 s at 72°C
5.	Go to step 2, 24 times	Go to step 2, 24 times
6.	5 min at 72°C	5 min at 72°C

Program 1 used for amplification of *phnYHis* and *phnY*; Program 2 used for amplification of *strepphnY*.

E. coli BL21 (DE3) transformed with pJexpress401_*phnY*, pFM36, pFM37, pFM38 and pFM39 were grown at 37°C on LB-agar supplemented with ampicillin or kanamycin, as required. A single colony was used to inoculate 5 mL of LB, which was then incubated in an air shaker at 37°C, 240 rpm, for 16 h. This pre-culture was used to inoculate 500 mL of LB. The cultures were induced with various IPTG concentrations and were grown at varying temperatures to determine the optimized expression conditions (described below). Uninduced and induced samples were lysed chemically with B-PER II Bacterial Protein Extraction Reagent (Thermo Scientific, Rockford, IL, USA) as per manual and soluble and insoluble samples of each were analyzed by SDS-PAGE to determine protein production levels.

3.2.3 Optimization of PhnY protein production

Protein production of PhnY was not optimal and varying conditions were attempted to increase the amount of soluble PhnY being produced. Production of PhnY form BL21 (DE3) / pJexpress401_*phnY* in different media were compared. LB, LB supplemented with 100 μM $Fe(SO_4)_2(NH_4)_2$, and autoinduction media (Overnight Express Instant TB Medium, Novagen, Darmstadt, Germany) were inoculated with BL21 (DE3) / pJexpress401_*phnY*. The LB and iron supplemented LB cultures were induced at OD_{600} = 0.6-0.8 with 200 μM IPTG and grown for a remaining 4 h at 30°C, whereas the autoinduction media was grown as per manual for 24 h after

inoculation at 30°C. Uninduced and induced cell pellets from each media were B-PER treated and the insoluble and soluble fractions were separated and analyzed by SDS-PAGE.

The production of PhnY from an LB culture of BL21 (DE3) / pJexpress401_*phnY* at a reduced growth temperature was compared to production from standard conditions. Two 500 mL LB cultures were inoculated with BL21 (DE3) / pJexpress401_*phnY* and induced at OD_{600} = 0.5 with 200 μM ITPG. The cultures were grown for 20 h at 15°C after induction with IPTG. Uninduced and induced cell pellets were B-PER treated and the insoluble and soluble fractions were separated and analyzed by SDS-PAGE. A similar reduced temperature comparison was performed using autoinduction media. A culture of PhnY in autoinduction media was grown at 15°C for 40 h with the production of soluble PhnY compared to that of PhnY produced in autoinduction media under standard conditions.

Attempts to increase production of PhnY from BL21 (DE3) / pJexpress401_*phnY* were unsuccessful. Therefore the *phnY* gene was subcloned into a plasmid with an alternate promoter (as described above). The production of PhnY from these newly constructed plasmids was then optimized. Three LB cultures were inoculated with BL21 (DE3) cells containing pJexpress401_*phnY*, pFM36, or pFM37 plasmids and induced at OD_{600} = 0.5 - 0.7 with 200 μM IPTG and grown for an additional 4 h at 30°C. Uninduced and induced samples were treated with B-PER and soluble and insoluble portions were compared by SDS-PAGE. A larger quantity of PhnY was being produced but in the insoluble fraction, therefore reduced growth temperatures and IPTG concentrations were compared. BL21 (DE3) cells containing pFM36 or pFM37 were induced with different IPTG concentrations (200 μM vs. 40 μM) and grown at different temperatures (15°C for 20 h).

The optimized conditions for *phnY* expression with pFM36 transformed *E. coli* cultures were incubation at 37°C and 240 rpm until the optical density at 600 nm reached 0.5-0.7. After chilling the culture on ice for 30 min IPTG was added to a final concentration of 40 μM. The

culture was then incubated at 15°C, 240 rpm, for 24 h. The cells were harvested by centrifugation at 10,000 x g for 30 min at 4°C, washed with 0.9% NaCl, and then stored at -20°C until use.

3.2.4 Purification of the *phnY* gene product[25]

To lyse cells containing PhnY with a strep-tag, the cell pellet was thawed on ice for 15 min then resuspended in 3 - 5 mL of NP buffer (50 mM NaH_2PO_4, 300 mM NaCl, pH 8.0) per 1 g of cell pellet. The cell suspension was sonicated on ice using eight cycles of 20 s sonication (output power of 15 watts) alternating with 20 s of rest. Cell debris was removed by centrifugation at 40,000 x g for 30 min at 4°C, followed by passage of the supernatant fluid through a 0.45 μm filter. The supernatant containing strep-tagged PhnY was applied to a 2 mL Streptactin Superflow column previously equilibrated in NP buffer. After washing the column with 10 column volumes of NP buffer PhnY was eluted with 5 - 6 column volumes of NPD buffer (50 mM NaH_2PO_4, 300 mM NaCl, 2.5 mM desthiobiotin, pH 8.0).

To lyse cells containing PhnY with a hexahistidine-tag, the cell pellet was thawed on ice for 15 min and then resuspended in 3 - 5 mL of 20 mM Tris-HCl, 300 mM NaCl, 20 mM imidazole, pH 7.5, per 1 g of cell pellet. The cell suspension was lysed as above using sonication and the cell debris was removed by centrifugation at 40,000 x g for 30 min at 4°C, followed by passage of the supernatant fluid through a 0.45 μm filter. The supernatant was applied to a 2 mL Ni-NTA column previously equilibrated in 20 mM Tris-HCl, 300 mM NaCl, 20 mM imidazole, pH 7.5. After washing the column with 10 column volumes of 20 mM Tris-HCl, 300 mM NaCl, 40 mM imidazole, PhnY was eluted with 5 - 6 column volumes of 20 mM Tris-HCl, 300 mM NaCl, 500 mM imidazole.

In both cases, purification fractions were analyzed by SDS-PAGE. Fractions containing PhnY were pooled and dialyzed against 50 mM Tris-HCl, 10% (wt/vol) glycerol, pH 7.5. The final purified yield of PhnY was approximately 15 mg L^{-1} from BL21 (DE3)/pFM36 cultures.

The concentration of PhnY was determined by measuring the absorbance at 280 nm using the extinction coefficient 54,110 M^{-1} cm^{-1}.

3.2.5 Expression of *phnZ* in *E. coli* and purification of the *phnZ* gene product[25]

The *phnZ* gene (GenBank ID: ACU83550) followed by a C-terminal hexahistidine tag specifying sequence was optimized for expression in *E. coli* using GeneDesigner (DNA 2.0). The optimized *phnZ* sequence, with *Nde*I and *Hind*III restriction endonuclease sites underlined, is as follows: 5'-CATATGAGCCTGAGCAATAGCA GCAAAGTGAGCGTCCTGATCTCCCTGCT GGAGAAGTCTCGCGACTTGGACTACATCGGTGAGGCGATTAACCAACTGGAACACA GCCTGCAGTGTGCCTATTTTGCACAACGCAGCGGTGCGGACAACGAGATGGTGCTGG CGGCACTGCTGCACGATCTGGGCCACTATTGCAATGACACCTCTTTCGAGGATATGG GCGGCTACGGTGTCTGGCAGCACGAGAAGGTTGGTGCAGACTACTTGCGTGGCTTGG GTTTTTCCGAGCGTGTTGCCTGCCTGATCGAAGGCCATGTCGCGGCGAAACGTTATCT GGTTAGCTCCAAGGCTAGCTATCTGAAAAACCTGAGCGATGCTAGCCGTAAAACCTT GGAATACCAGGGTGGCCCGATGGATGAGGGTGAACGTCGCCTGTTCGAAGAGCGTG AGGATTTCAAGGACTGTCTGAAGATTCGCGCGTGGGATGAGAAAGGTAAGCAGACG GACCTGAAAGTGCCGGGTCCGGAACATTACCGTAAAATGATGGAAGAGCACCTGTC GGAAAATCAAAACCATCATCACCATCACCACTAAAAGCTT-3'. The optimized *phnZ* sequence was synthesized by DNA 2.0 and provided as the plasmid pJexpress401_*phnZ*. *E. coli* BL21 (DE3) cells transformed with pJexpress401_*phnZ* were grown at 37°C on LB-agar plates supplemented with kanamycin. A single colony was used to inoculate 5 mL LB supplemented with kanamycin, which was then incubated in an air shaker at 37°C, 240 rpm, for 16 h. This pre-culture was used to inoculate 500 mL LB supplemented with kanamycin, which was subsequently incubated at 37°C, 240 rpm, until the optical density at 600 nm reached 0.5 - 0.7. After chilling the culture on ice for 30 min, expression of the *phnZ* gene was induced by adding IPTG to a final concentration of 200 μM. The culture was then incubated at 30°C, 240 rpm, for 4 h. Cells were

harvested by centrifugation and a crude extract was prepared as described for PhnY with the exception that the cell pellet was resuspended in 3 - 5 mL of buffer A (20 mM Tris-HCl, 300 mM NaCl, pH 7.5) containing 4% buffer B (20 mM Tris-HCl, 300 mM NaCl, 500 mM imidazole, pH 7.5) per 1 g of cell pellet. The crude extract was applied to a 5 mL Ni-NTA column pre-equilibrated with 96:4 buffer A / buffer B. After washing the column with 10 column volumes of 96:4 buffer A / buffer B, the column was attached to an ÄKTA FPLC system and PhnZ was eluted with an imidazole gradient of 4% to 100% buffer B over 20 column volumes (5 mL min^{-1}) at 4°C. The eluent was monitored at 280 nm. Collected fractions were analyzed by SDS-PAGE and those containing PhnZ were pooled and dialyzed against 25 mM Tris-HCl, 150 mM NaCl, 10% (wt/vol) glycerol, pH 7.5 at 4°C. The yield of PhnZ was typically 8 - 15 mg L^{-1} of culture. The concentration of PhnZ was determined by measuring the absorbance at 280 nm and using the extinction coefficient 24,660 M^{-1} cm^{-1}.

3.2.6 Generation of *phnZ* variants and *E. coli* growth conditions for protein production

The QuickChange site-directed mutagenesis protocol (Stratagene, Cedar Creek, TX, USA) was used to introduce the following substitutions to the PhnZ active-site: Y24E, Y24F, E27A, N30A, H34A, H58A, D59A, H62A, H80A, H104A, K108A, and D161A. Histidine and aspartate residues were changed by the author and other residues were changed by Laura van Staalduinen (Jia lab, Department of Biomedical and Molecular Sciences, Queen's University). PCR contained 1 X *pfu* Ultra buffer, 200 μM of each dNTP, approximately 1 - 30 ng of DNA template (0.5 - 10 μL of 100-fold diluted pJexpress401_*phnZ* plasmid DNA isolated from *E. coli*), 0.25 μM of each primer, and 1 μL of pfu Ultra polymerase (Stratagene) in a 50 μL reaction volume. The author used a 'hot-start' initiation for PCR mutagenesis with the following thermocycler program: initial denaturation step at 96°C for 5 min, 18 cycles of 96°C for 0.5 min, 55°C for 1 min and 68°C for 4.5 min, and a final elongation step at 68°C for 10 min. The *Dpn*I restriction enzyme was then added to the PCR and left for 1 h at 37°C. The mutagenic primers

used to introduce active site substitutions can be found in Table 3-2. PCR products were analyzed on agarose gels to confirm amplification of the plasmid and then were transformed into XL1-Blue cells. Single colonies were obtained on LB-agar supplemented with the appropriate antibiotic after incubation overnight at 37°C. Isolated clones were used to generate plasmid DNA that was sequenced using pJexpress_Seqfor2 5'-cgagcttcatgcacagtgaaatc-3' and pJexpress_Seqrev2 5'-cgaaaggctcagtcgaaa-gactgg-3' to confirm modified codon.

Expression of all active site variants were the same as the native PhnZ, however purification was done on a 5 mL gravity Ni-NTA column using a stepwise elution consisting of 5 mL of 50 mM, 100 mM, 150 mM, 200 mM, 250 mM and 300 mM imidazole in 20 mM Tris-HCl, 300 mM NaCl, pH 7.5, at room temperature. Collected fractions were analyzed by SDS-PAGE and those containing PhnZ were pooled and concentrated using an Amicon Ultra-4 or -15 (Millipore Ireland Ltd, Cork, Ireland) filtration devise. Imidazole was removed by adding 20 mM Tris-HCl, 300 mM NaCl, pH 7.5 at 4°C and concentrating the PhnZ variants multiple times with repeated dilutions with 20 mM Tris-HCl, 300 mM NaCl, pH 7.5.

Table 3-2. PhnZ QuickChange mutagenic primers

Substitution	*Mutagenic Primer (5'-3')*
Y24E	For: ctcgcgacttggacGAGatcggtgaggcg
	Rev: cgcctcaccgatCTCgtccaagtcgcgag
Y24F	For: ctcgcgacttggacTTCatcggtgaggcg
	Rev: cgcctcaccgatGAAgtccaagtcgcgag
E27A	For: ggactacatcggtGCGgcgattaaccaactg
	Rev: cagttggttaatcgcCGCaccgatgtagtcc
N30A	For: cggtgaggcgattGCCcaactggaacacagc
	Rev: gctgtgttccagttggGCAatcgcctcaccg
H34A	For: cgattaaccaactggaaGCCagcctgcagtgtgc
	Rev: gcacactgcaggctGGCttccagttggttaatcg
H58A	For: ctggcggcactgctgGCCgatctgggccactattgcaatg
	Rev: cattgcaatagtggcccagatcGGCcagcagtgccgccag
D59A	For: gcactgctgcacGCActgggccactattgcaatgac
	Rev: gtcattgcaatagtggcccagTGCgtgcagcagtgc
H62A	For: ctgctgcacgatctgggcGCCtattgcaatgacacctc
	Rev: gaggtgtcattgcaataGGCgcccagatcgtgcagcag
H80A	For: ctacggtgtctggcagGCCgagaaggttggtgcagactac
	Rev: gtagtctgcaccaaccttctcGGCctgccagacaccgtag
H104A	For: ctgcctgatcgaaggcGCGgtcgcggcgaaacgttatc
	Rev: gataacgtttcgccgcgacCGCgccttcgatcaggcag
K108A	For: gcgatgctagccgtGCAaccttggaataccaggg
	Rev: ccctggtattccaaggtTGCacggctagcatcgc
D161A	For: gaagattcgcgcgtggGCAgagaaaggtaagc
	Rev: gcttacctttctcTGCccacgcgcgaatcttc

Modified codons are in uppercase. For: forward primer; Rev: reverse primer.

3.2.7 ^{31}P-NMR spectroscopic analysis of PhnY and PhnZ reactions[25]

PhnY reactions consisted of 1 mM **1a**, **1b**, **1f** or **1g**, 0.1 mM $Fe(SO_4)_2(NH_4)_2$ (from a freshly prepared stock solution), 2 mM α-ketoglutarate, 0.2 mM ascorbate, and 10 μM PhnY in 25 mM Tris-HCl, pH 7.5, in a total reaction volume of 500 μL. The reaction mixture was

incubated at 30°C for 16 h. The combined PhnY and PhnZ reaction was performed similarly with the addition of 5 μM PhnZ. The PhnZ reactions with phosphite (**1e**), phosphoethanolamine (**10**), synthetically produced aminophosphonates (**8** and **11**) and 1-hydroxyethylphosphonate (**12**) consisted of 1 mM substrate, 0.1 mM $Fe(SO_4)_2(NH_4)_2$ and 5 μM PhnZ in 25 mM Tris-HCl, pH 7.5. To determine the metal ion dependence, PhnZ was incubated with 10 mM EDTA for 16 h immediately after purification, followed by dialysis as above. Reactions utilizing apo-PhnZ consisted of 1 mM **8** (generated enzymatically by PhnY as described above, or with synthetic **8**, 0.1 mM metal ion, 5 μM PhnZ, 25 mM Tris-HCl, pH 7.5, in a total volume of 500 μL. PhnZ activity was assayed in the presence of the following metal ion salts: $MgCl_2$, $MnCl_2$, $Fe(SO_4)_2(NH_4)_2$, $FeCl_3$, $NiCl_2$, $CoCl_2$, $CaCl_2$, $CuSO_4$, and $ZnCl_2$. PhnY and PhnZ reactions were stopped by the addition of sodium dithionite, EDTA and D_2O to final concentrations of 10 mM, 50 mM and 20% (vol/vol), respectively. The reaction mixtures were centrifuged and the supernatant fluids were analyzed by ^{31}P-NMR spectroscopy. The chemical shifts (ppm) are referenced to 85% phosphoric acid at 0 ppm.

3.2.8 Enzymatic synthesis of 2-amino-1-hydroxy-ethylphosphonate (8)[25]

Enzymatic synthesis of **8** was performed by incubation 10 μM PhnY with 1 mM **1g** in 25 mM Tris-HCl, pH 7.5, along with 0.1 mM $Fe(SO_4)_2(NH_4)_2$, 2 mM α-ketoglutarate, and 0.2 mM ascorbate in a total reaction volume of 5 mL. ^{31}P-NMR spectroscopic analysis of a reaction aliquot indicated full conversion after 16 h with a single ^{31}P-NMR signal at 14.3 ppm. The remainder of the reaction was heated for 10 min at 95°C and precipitated PhnY was removed by centrifugation. The supernatant containing **8** (~1 mM) was concentrated four-fold using a rotary evaporator and used for reactions with PhnZ.

3.2.9 ICP-MS analysis of metal ion content in PhnZ[25]

Purified PhnZ was dialyzed against 25 mM Tris-HCl, 35 mM NaCl, pH 7.5, and concentrated using an Amicon ultrafiltration device. The dialysis buffer (4 L) was previously treated with Chelex-100 for 4 h, to remove residual metal ions, followed by filtration for the removal of the Chelex resin. ICP-MS analysis was performed by Alemayehu Asfaw from Diane Beauchemin lab (Department of Chemistry, Queen's University) with the following settings: plasma flow, 18.0 L min^{-1}; auxiliary flow, 1.75 L min^{-1}; nebulizer flow, 0.90 L min^{-1}; sheath gas flow, 0.04 L min^{-1}; sampling depth, 6.0 mm; horizontal alignment, - 0.8 mm; vertical alignment, 0.2 mm; RF power, 1.36 kW; pump rate, 12 rpm. Five replicates of three different samples at various enzyme concentrations were corrected for residual metal content by analyzing the used dialysis buffer alone. Two isotopes of each element were used for detection of iron and calcium. The average values for iron were 1.24 ± 0.14 mol ^{54}Fe and 1.18 ± 0.12 mol ^{57}Fe per mol PhnZ, whereas the values for calcium were 0.57 ± 0.07 mol ^{43}Ca and 0.51 ± 0.15 mol ^{44}Ca per mol PhnZ.

3.2.10 Detection of product formation of the PhnY / PhnZ reaction

Glycine was detected following reaction with phenyl isothiocyanate as described by Gunawan *et al.*[25,26]. PhnY and PhnZ reactions consisted of 1 mM racemic **1g**, 0.1 mM $Fe(SO_4)_2(NH_4)_2$ (from a freshly prepared stock solution), 2 mM α-ketoglutarate, 0.2 mM ascorbate, with either 10 μM PhnY and / or 5 μM PhnZ in 25 mM Tris-HCl, pH 7.5, in a total reaction volume of 500 μL. The reaction mixture was incubated at 30°C for 16 h. PhnY and PhnZ reactions were stopped by the addition of sodium dithionite, EDTA and D_2O to final concentrations of 10 mM, 50 mM, and 20% (vol/vol), respectively. The reaction mixtures were centrifuged and the supernatant fluids were analyzed by ^{31}P-NMR (as described above) to verify the reaction had proceeded. A 50 μL aliquot of the reaction (prior to addition of sodium dithionite, EDTA and D_2O) was dried under vacuum, and once ^{31}P-NMR confirmed the reaction

had proceeded it was re-dissolved in 20 μL of 2:2:1 ethanol-water-triethylamine, dried a second time under vacuum, and then re-dissolved with 30 μL of 7:1:1:1 ethanol-water-triethylamine-phenyl isothiocyanate. The sample was allowed to react for 20 min at room temperature. After drying the sample under vacuum the residue was dissolved in 300 μL of solvent A (0.1 M sodium acetate, pH 5.7). HPLC analysis was performed using a Polaris C18-A 150 mm × 4.6 mm column. A 20 μL sample was injected onto the column and separated using a gradient consisting of solvent A and solvent B (60:40 acetonitrile-water) as described[26] with a flow rate of 1 mL min^{-1} and detection at 254 nm. A solution of 1 mM glycine was reacted with phenyl isothiocyanate as described above to create a standard for HPLC analysis.

3.2.11 Circular dichroism spectral analysis of PhnY, PhnZ and PhnZ variants

Circular dichroism (CD) spectra were collected for assessing potential changes in the secondary structural content of PhnY and PhnZ. The spectra were acquired by Kim Munro in the Protein Function Discovery facility, Queen's University, using a Chirascan CD Spectrometer (Applied Photophysics Ltd., Leatherhead, Surrey. U.K.). Prior to measurement, the purified enzymes were buffer exchanged five times with 20 mM Tris-HCl, pH 6.8 using an Amicon ultrafiltration device. The concentrations of the enzymes were determined by measuring the absorbance at 280 nm and using the calculated extinction coefficients. To assess their structural stability in response to changes in temperature or the presence of iron, spectra were collected at 4°C, 15°C, and 25°C in the presence or absence of a 10 or 5 times molar excess of iron based on one or two iron ion(s) per mol of PhnY and PhnZ, respectively. Potential secondary structural changes resulting from a series of single-point mutations to PhnZ were evaluated by comparison of spectra collected at 25°C. For each PhnY or PhnZ sample, six replicate CD scans were collected with 1 nm increments and 1.0-second integration time, and raw spectra were corrected with reference spectra for corresponding buffer and temperature conditions.

Preliminary data processing and reference subtraction were performed with Chirascan ProViewer software. Secondary structural deconvolutions of reference-corrected spectra were performed using OLIS SpectralWorks software (On-line Instrument Systems, Bogart, Georgia).

3.2.12 Kinetic analysis of PhnZ and its variants

PhnZ activity was measured using the EnzChek Phosphate Assay Kit (Molecular Probes, Invitrogen) based on the coupled enzyme assay by Webb[27]. The kit utilizes a shift of maximal absorbance from 330 to 360 nm when the substrate 2-amino-6-mercapto-7-methylpurine riboside (MESG) and P_i are converted to ribose-1-phosphate and 2-amino-6-mercapto-7-methylpurine by purine nucleoside phosphorylase (PNP). The kit allows for the continuous detection of P_i as it is generated by PhnZ. Experiments were performed using a final concentration of 50 mM MOPS at pH 6.8 following the EnzChek manual. The following reagent concentrations were used: 1 mM, $MgCl_2$; 200 μM, MESG; 200 μM, freshly prepared $Fe(SO_4)_2(NH_4)_2$; 1 U, PNP; and 2 - 10 μM of PhnZ (or PhnZ variant). The reaction components were combined and incubated for 10 min at 25°C to deplete any free P_i in the reaction components. The reaction was then initiated by addition of the substrate. The reaction was monitored every 0.1 s at 360 nm at 25°C using a Cary UV-Vis Bio 300 spectrophotometer (Varian). The initial reaction rate was determined using the molar extinction coefficient ε_{360} = 11,200 M^{-1} cm^{-1} for the 2-amino-6-mercapto-7-methylpurine product. To determine kinetic parameters k_{cat} and K_M the initial velocities measured at various substrate concentrations (between 0 and 10 mM) were fitted to the Michaelis-Menten equation using GraFit 7.0 (Erithacus Software Limited, UK).

3.2.13 Crystallization, X-ray data collection, structure solution and refinement[28]

A selenomethionine derivative of PhnZ was produced and purified by Laura van Staalduinen. *E. coli* DL41 (DE3) transformed with pJexpress401_*phnZ* were grown in LeMaster media and purified on a Ni–NTA column. Protein fractions were pooled and further purified by

size-exclusion chromatography using a Superdex 200 column. Protein was concentrated to 16 mg mL^{-1} by centrifugation in an Amicon ultrafiltration device.

The selenomethionine derivative crystals of PhnZ were grown by Laura van Staalduinen using hanging drop vapour diffusion method. The final crystal forming conditions in the well were 2.4 M ammonium sulfate and 0.15 M potassium sodium tartrate. The reservoir solution was mixed in a 1:1 ratio (5 μL plus 5 μL) with 740 μM PhnZ (16 mg ml^{-1}) and 1 μL of 5% *n*-octyl-β-D-glucoside was added to the drop. For co-crystallization with substrate, PhnZ was mixed with a racemic mixture of **8** in a 1:20 molar ratio. Crystal were grown using a sitting drop vapour diffusion method with a 1:1 ratio of protein : substrate complex to well (1 μL + 1 μL). The final crystallization condition contained 0.1 M Bis-Tris, pH 6.5 and 20% (w/v) polyethelyne glycol 5000 monomethylether.

Diffraction data were collected at 100 K, using the well solution in 20 % glycerol. The data were indexed and scaled using XDS by Laura van Staalduinen. Laura van Staalduinen solved the PhnZ structure using the multiple anomalous dispersion (MAD) method with a single selenomethionine crystal, which diffracted to 1.7 Å resolution. The substrate-bound PhnZ structure was solved by molecular replacement using MOLREP by Laura van Staalduinen. The Dali server (http://ekhidna.biocenter.helsinki.fi/dali_server/) was used to search for structural homologues for PhnZ in the protein data bank (PDB). For more details please see Laura van Staalduinen's Ph.D. thesis[28].

3.3 Results

3.3.1 Heterologous expression of *phnY* and *phnZ* genes and purification of their gene products

The *phnY* and *phnZ* genes were derived from a marine bacterium and for this reason it was decided at the outset to optimize the sequences for expression in *E. coli*. The sequences were changed to have codons that are typically used in *E. coli*, as well as to minimize the formation of

secondary structures in mRNA following transcription. This is relatively simple to predict using web-based algorithms or software provided by DNA synthesis companies. The *phnY* and *phnZ* genes were synthesized by DNA 2.0 and were provided in a T5 promoter based plasmid (pJexpress401), plasmid constructs can be found in Appendix C. To confirm that the correct genes were present on the plasmid a digest with *Nde*I and *Hind*III restriction endonucleases was performed and analyzed by agarose gel electrophoresis (Figure 3-3). The 813-bp and 588-bp, *phnY* and *phnZ* genes encoding C-terminal tagged PhnY and PhnZ were clearly present in their corresponding plasmids.

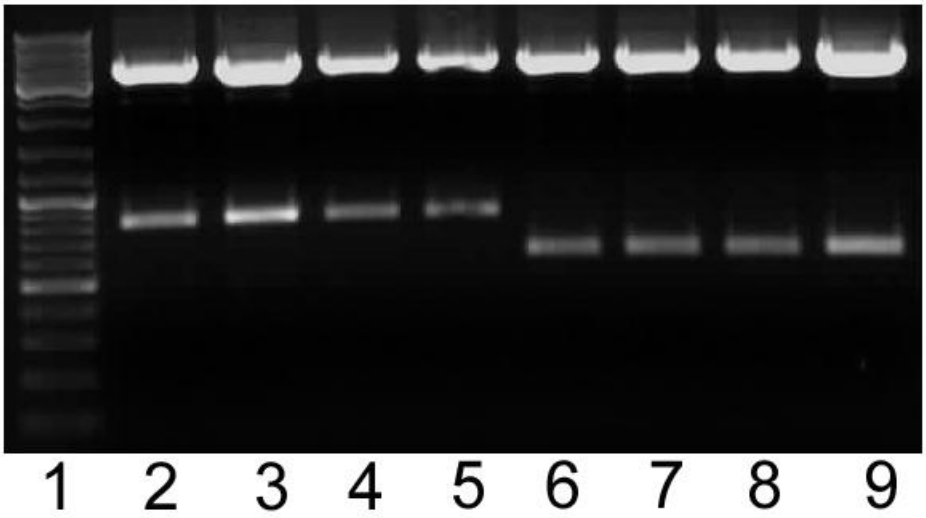

Figure 3-3. 1% agarose gel of pJ401express_*phnY* and pJ401express_*phnZ* digests. DNA ladder (SM0333, Fermentas) in Lane 1 (ladder contains 21 discrete fragments: 8000, 7000, 6000, 5000, 4000, 3500, **3000**, 2500, 2000, 1500, 1200, **1031**, 900, 800, 700, 600, **500**, 400, 300, 200, and 100-bp, there are larger quantities of the bolded fragments present in the mixture). Lane 2 to 4 contains *Nde*I and *Hind*III digested pJexpress_*phnY*, the 813-bp fragment corresponds to the desired *phnY* gene. Lane 5 to 9 contains *Nde*I and *Hind*III digested pJexpress_*phnZ*, the 588-bp fragment corresponds to the desired *phnZ* gene.

The *phnY* and *phnZ* genes encoded by these plasmids were expressed in *E. coli* BL21 (DE3) cells following induction with IPTG. Lysed cells were separated into soluble and insoluble fractions and analyzed by 12% SDS-PAGE (Figure 3-4). Bands of 31.4 kDa and 22.4

kDa were expected for PhnY and PhnZ, respectively. A prominent band corresponding to PhnZ was observed in the induced soluble fraction (boxed in lane 7, Figure 3-4). However a band corresponding to PhnY was not present in either the induced soluble or insoluble fractions (Lanes 3 and 5, respectively Figure 3-4).

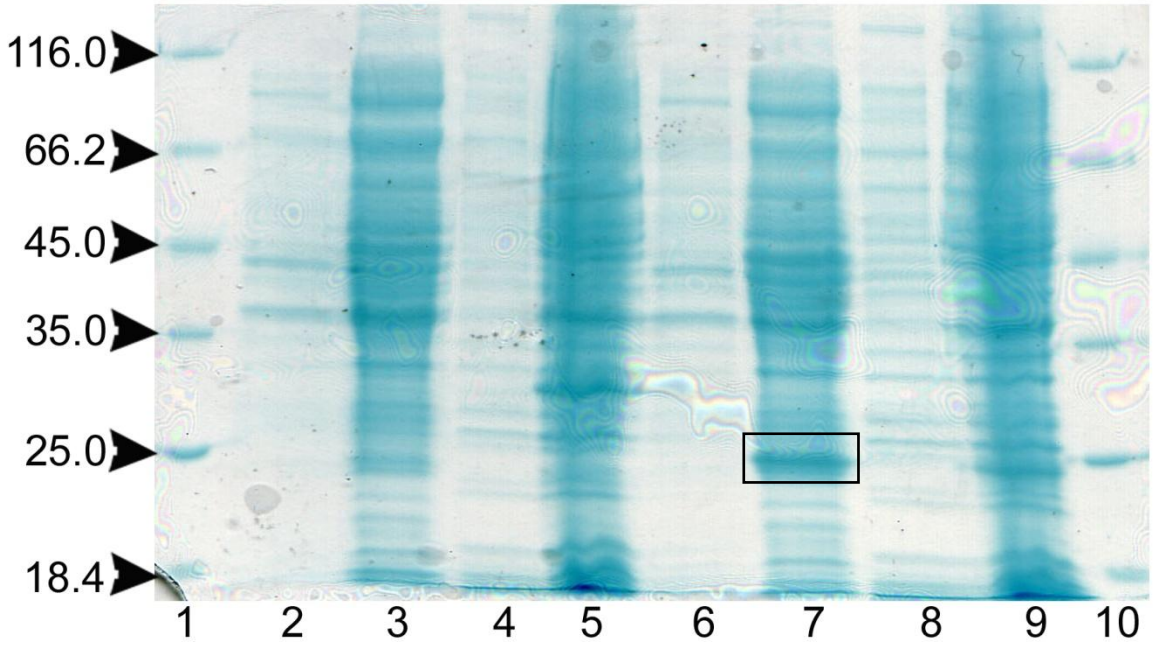

Figure 3-4. SDS-PAGE (15%) analysis of protein production from BL21 (DE3) / pJexpress401_*phnY* and BL21 (DE3) / pJexpress401_*phnZ*. Lanes 1 and 10, molecular weight marker SM0431 (Fermentas) the size of the marker bands in kDa are labelled to the left of the gel; lane 2, soluble cell lysate of B-PER treated uninduced BL21 (DE3) / pJexpress401_*phnY*; lane 3, soluble cell lysate of B-PER treated induced BL21 (DE3) / pJexpress401_*phnY*; lane 4, insoluble cell lysate of B-PER treated uninduced BL21 (DE3) / pJexpress401_*phnY*; lane 5, insoluble cell lysate of B-PER treated induced BL21 (DE3) / pJexpress401_*phnY*; lane 6, soluble cell lysate of B-PER treated uninduced BL21 (DE3) / pJexpress401_*phnZ*; lane 7, soluble cell lysate of B-PER treated induced BL21 (DE3) / pJexpress401_*phnZ* over produced PhnZ protein (22.4 kDa) outlined with a black box; lane 8, insoluble cell lysate of B-PER treated uninduced BL21 (DE3) / pJexpress401_*phnZ*; lane 9, insoluble cell lysate of B-PER treated induced BL21 (DE3) / pJexpress401_*phnZ*.

Although production of PhnY in cell extracts was not directly visible by SDS-PAGE (Figure 3-4), this could simply indicate that expression levels are low. Indeed, taking advantage

of the strep-tag sequence, small quantities of relatively pure PhnY could be isolated (Figure 3-5). The purified yield of PhnY was approximately 1.5 mg of enzyme per 1 L of culture. However, some unspecifically bound proteins coeluted with PhnY from the column. It was reasoned that if more PhnY protein could be produced there would be less chance of unspecific binding and the purity of PhnY would improve.

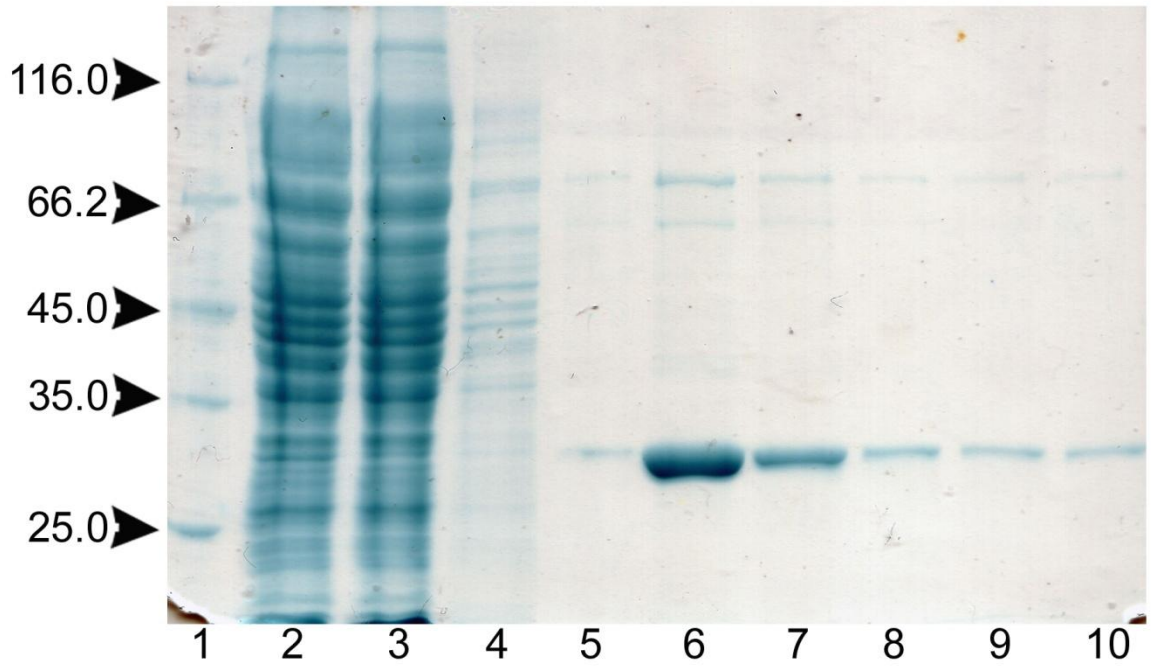

Figure 3-5. SDS-PAGE (15%) analysis of the purification of PhnY bearing a C-terminal strep-tag sequence on a Streptactin superflow affinity column. Lane 1, molecular weight marker SM0431 (Fermentas) the size of the marker bands in kDa are labelled to the left of the gel; lane 2, crude cell extract; lane 3, flow-through upon loading column with cell extract; lane 4, flow-through upon washing the column with NP buffer; lanes 5 to 10, fractions collected upon elution is NPD buffer. PhnY has a predicted molecular weight of 31.5 kDa.

To attempt to increase protein production, protein production from BL21 (DE3) / pJexpress401_*phnY* was compared in LB, LB supplemented with 100 μM $Fe(SO_4)_2(NH_4)_2$, and autoinduction media. Uninduced and induced cells grown in each medium were lysed, centrifuged, separated into soluble and insoluble fractions, and then analyzed by SDS-PAGE (Figure 3-6). Although the soluble fraction of the autoinduction sample (Lane 5, Figure 3-6) is

different to that of the LB samples (Lanes 3 and 4, Figure 3-6), there was still no PhnY visible. However, there was a marked increase in the level of PhnY, in the insoluble fraction obtained from the autoinduction culture (Lane 9, Figure 3-6). After purification of PhnY from the lysed cell pellet of PhnY produced in the autoinduction media less than 2 mg of PhnY was isolated per 1 L of culture, which is not a noteworthy increase from that previously isolated from LB grown cells.

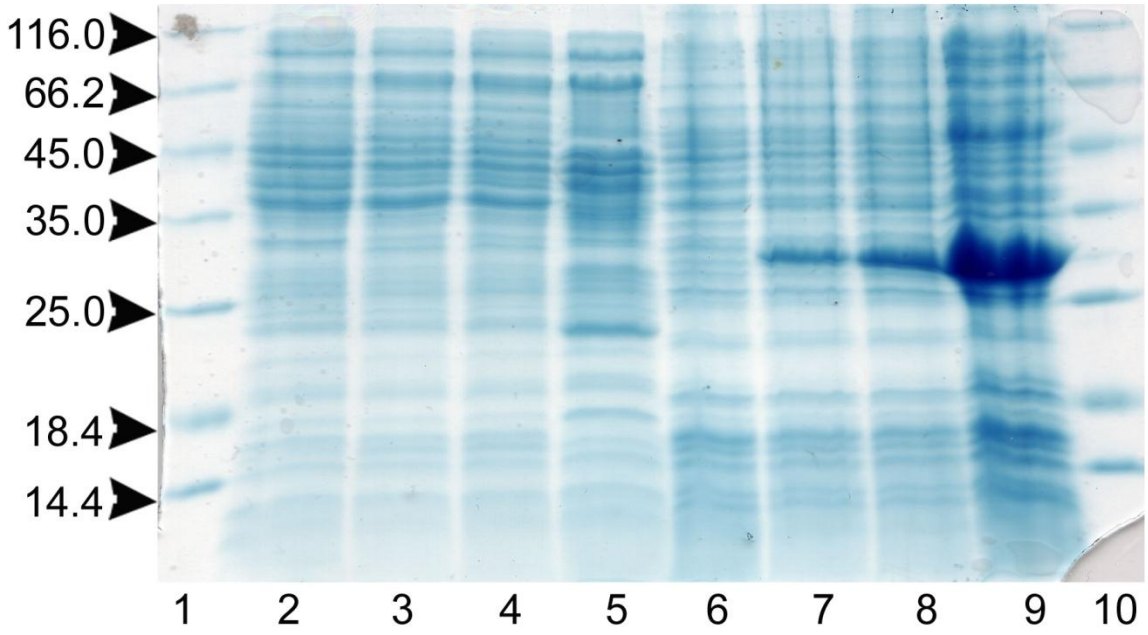

Figure 3-6. SDS-PAGE (15%) analysis of protein production from BL21 (DE3) / pJexpress401_*phnY* grown cells in varying media. Lanes 1 and 10, molecular weight marker SM0431 (Fermentas) the size of the marker bands in kDa are labelled to the left of the gel; lane 2, soluble cell lysate of B-PER treated uninduced BL21 (DE3) / pJexpress401_*phnY* grown in LB media; lane 3, soluble cell lysate of B-PER treated induced BL21 (DE3) / pJexpress401_*phnY* grown in LB media; lane 4, soluble cell lysate of B-PER treated induced BL21 (DE3) / pJexpress401_*phn Y* grown in LB media supplemented with iron; lane 5, soluble cell lysate of B-PER treated induced BL21 (DE3) / pJexpress401_*phn* grown in autoinduction media *Y*; lane 6, insoluble cell lysate of B-PER treated uninduced BL21 (DE3) / pJexpress401_*phnY* grown in LB media; lane 7, insoluble cell lysate of B-PER treated induced BL21 (DE3) / pJexpress401_*phnY* grown in LB; lane 8, insoluble cell lysate of B-PER treated induced BL21 (DE3) /

pJexpress401_*phnY* grown in LB media supplemented with iron; lane 9, insoluble cell lysate of B-PER treated induced BL21 (DE3) / pJexpress401_*phnY* grown in autoinduction media.

The effect of reduced culture temperature and increased growth time on PhnY production was explored next. Duplicate cultures of BL21 (DE3) / pJexpress401_*phnY* were grown for 20 h at 15°C after induction with IPTG. Lysed cells were separated into soluble and insoluble fractions and analyzed by SDS-PAGE (Figure 3-7A). Very little PhnY was observed in both the induced soluble and insoluble fractions (Lanes 3, 5, 7 and 9, Figure 3-7A). The purified yield of PhnY was 3 mg / L culture (Figure 3-7B), which is not a substantial improvement compared to previous attempts. Reduced temperature growth in autoinduction media also did not increase the production of PhnY.

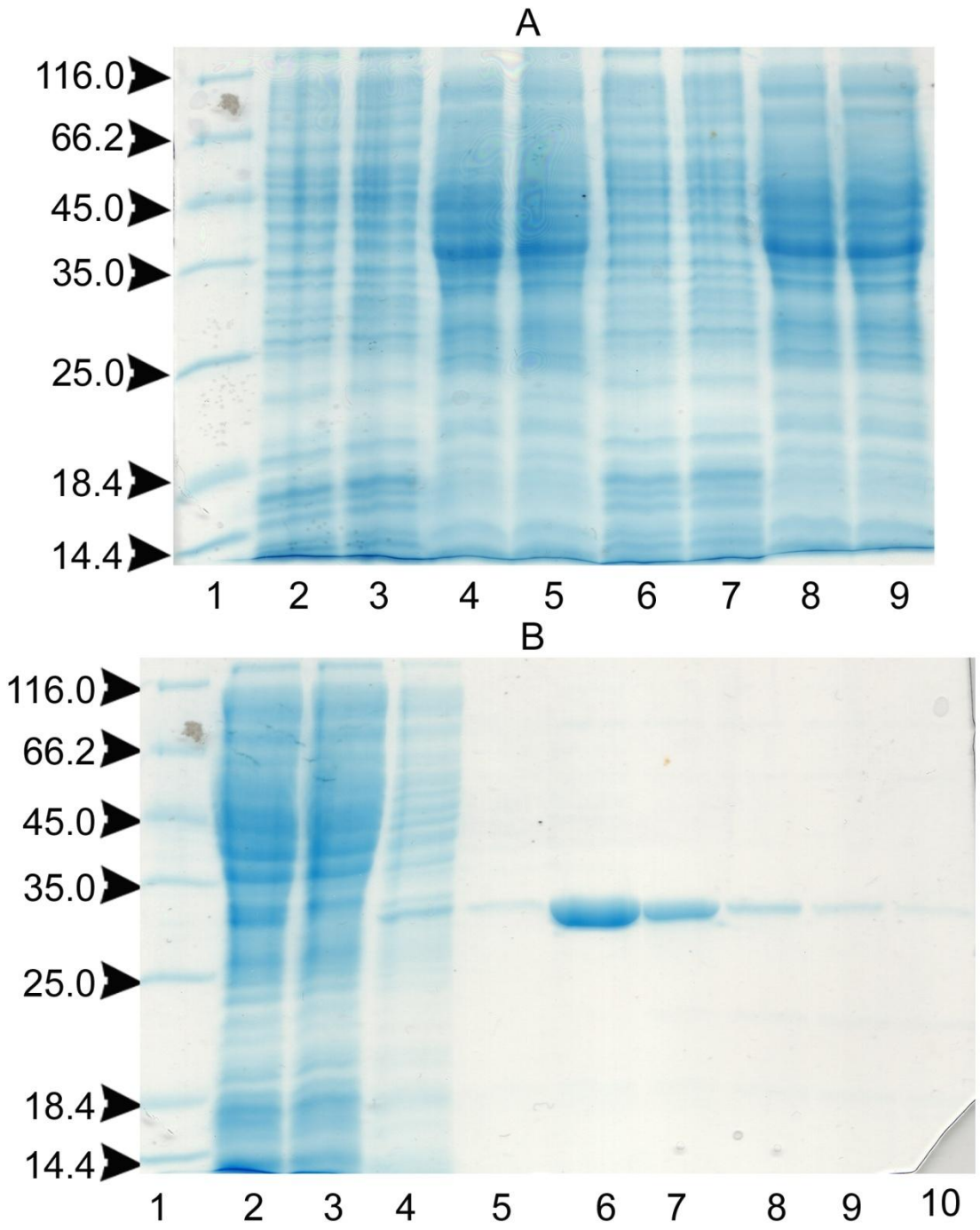

Figure 3-7. SDS-PAGE (15%) analysis of the production and purification of PhnY from BL21 (DE3) / pJexpress401_phnY grown in LB. (A) Lane 1, molecular weight marker SM0431 (Fermentas) the size of the marker bands in kDa are labelled to the left of the gel; lane 2 and 6, uninduced soluble cell lysate; lane 3 and 7, induced soluble cell lysate; lane 4 and 8, uninduced insoluble cell lysate; lane 5 and 9, induced insoluble cell lysate. (B) Lane 1, molecular

weight marker SM0431 (Fermentas) the size of the marker bands in kDa are labelled to the left of the gel; lane 2, crude cell extract; lane 3, flow-through upon loading column with cell extract; lane 4, flow-through upon washing the column with NP buffer; lanes 5 to 10, fractions collected upon elution is NPD buffer.

3.3.2 DNA manipulation of *phnY* gene for enhanced protein production

The generally poor production of PhnY may arise from the T5 promoter used in the pJexpress401_*phnY* plasmid. It was hypothesized that expression of the *phnY* gene from the stronger T7 promoter would increase transcription and subsequent protein synthesis. In addition to poor production, it was also noted that purified PhnY was unstable and precipitated out of solution at room temperature. It was hypothesized that the location and sequence of the tag had an impact on the stability of PhnY. Therefore, with the aim to increase protein production and protein stability, variants of PhnY were designed and encoded in pET plasmids with a T7 promoter (plasmid maps can be found in Appendix C). The clones specified PhnY with a C-terminal strep tag, pFM36; a C-terminal hexahistidine tag, pFM37; an N-terminal hexahistidine tag followed by a thrombin recognition site, pFM38; and an N-terminal strep tag, pFM39.

To create pFM37, pFM38, and pFM39 PCR amplification of the gene with specific primers was required. The PCR primers ForPhnY and RevHisPhnY were used to create the *phnYhis* PCR product; ForPhnY and RevPhnY were used to create the *phnY* PCR product; and ForStrepPhnY and RevPhnY were used to create the *strepphnY* PCR product. The PCR was performed in duplicate for each PCR product as described in methods, and the PCR products were analyzed by 1.5% agarose gel electrophoresis (Figure 3-8). All PCR products were successfully amplified (lane 2 to 7, Figure 3-8).

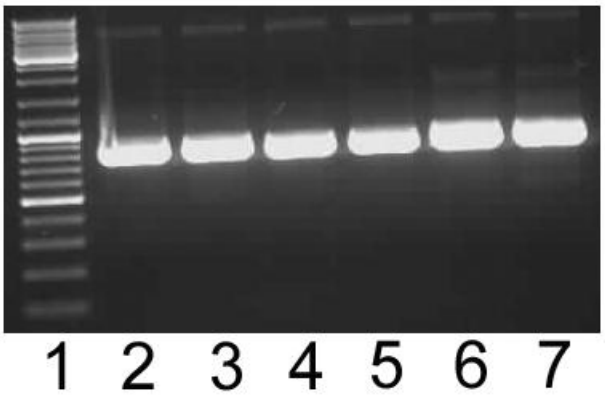

Figure 3-8. 1.5% agarose gel of pJ401express_*phnY* PCR. DNA ladder (SM0333, Fermentas) in Lane 1 (ladder contains 21 discrete fragments: 8000, 7000, 6000, 5000, 4000, 3500, **3000**, 2500, 2000, 1500, 1200, **1031**, 900, 800, 700, 600, **500**, 400, 300, 200, and 100-bp, there are larger quantities of the bolded fragments present in the mixture). Lane 2 and 3 contain PCR product *phnYhis*. Lane 4 and 5 contain PCR product *phnY*. Lane 6 and 7 contain PCR product *strepphnY*.

The T7 promoter was introduced simply by subcloning the *phnY* gene into appropriate pET plasmids. The PCR products along with pET21a, pET28a and pJexpress401_*phnY* were digested, separated by agarose gel, gel extracted and then ligated together to create pFM36, pFM37, pFM38 and pFM39 as described in methods. Single clones of each construct were analyzed by restriction enzyme digests (Figure 3-9A-D). The expected *phnY* insert was observed for pFM36, pFM37 and pFM39 (Figure 3-9A, B and D). However, no *phnY* insert was observed for pFM38 clones (Figure 3-9C). Either the digest or the ligation reaction was ineffective, therefore a second round of digests and ligation reactions were performed. This time no colonies were observed on the ligation transformation plates. Consequently, further attempts to make this *phnY* construct were abandoned. The sequence of the *phnY* gene and its tag in pFM36, pFM37 and pFM39 were confirmed by DNA sequencing.

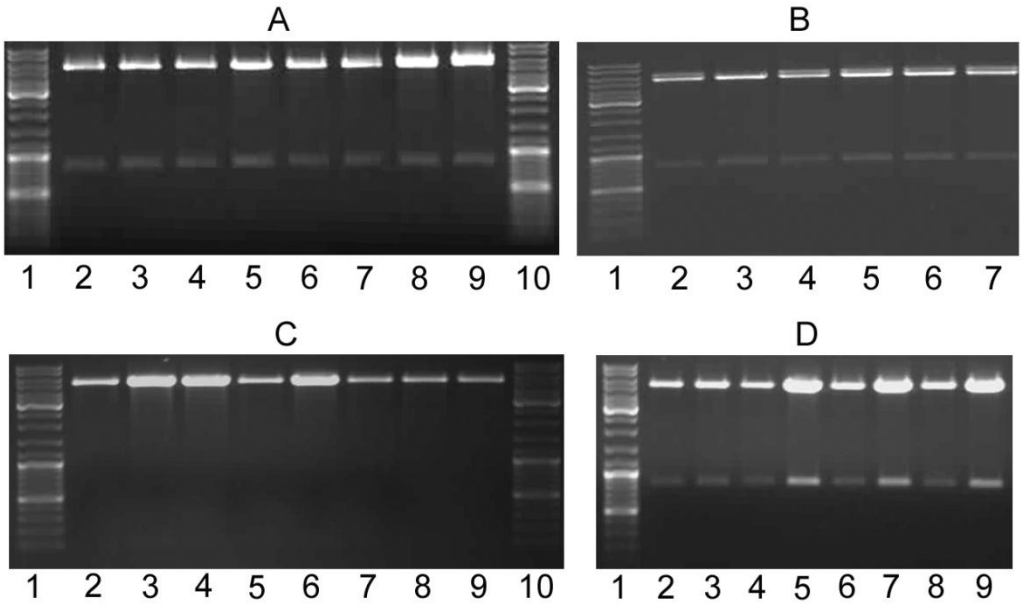

Figure 3-9. Analysis of *phnY* subclones by agarose gel electrophoresis. (A) 1.5% agarose gel of pFM36 clones digested with *Nde*I and *HindIII* restriction enzymes to visualize inserted *phnYstrep* fragment from pJexpress_*phnY* into pET21a. DNA ladder (SM0333, Fermentas) in Lane 1 and 10 (ladder contains 21 discrete fragments: 8000, 7000, 6000, 5000, 4000, 3500, **3000**, 2500, 2000, 1500, 1200, **1031**, 900, 800, 700, 600, **500**, 400, 300, 200, and 100-bp, there are larger quantities of the bolded fragments present in the mixture), lanes 2 to 9 contain digested pFM36 clones; (B) 1.5% agarose gel of pFM37 clones digested with *Nde*I and *HindIII* restriction enzymes to visualize inserted *phnYhis* fragment into pET21a. DNA ladder (SM0333, Fermentas) in Lane 1; lanes 2 to 7 contain digested pFM37 clones; (C) 1.5% agarose gel of pFM38 clones digested with *Nde*I and *HindIII* restriction enzymes to visualize inserted *phnY* fragment into pET28a. DNA ladder (SM0333, Fermentas) in Lanes 1 and 10; lanes 2 to 9 contain digested pFM38 clones; and (D) 1.5% agarose gel of pFM39 clones digested with *Nco*I and *HindIII* restriction enzymes to visualize inserted *strepphnY* fragment into pET28a. DNA ladder (SM0333, Fermentas) in Lane 1; lanes 2 to 9 contain digested pFM39 clones.

The T7 based *phnY* encoding plasmids were then transformed into BL21 (DE3) for protein production. LB cultures of BL21 (DE3) cells containing pJexpress401_*phnY*, pFM36, or pFM37 plasmids were analyzed by SDS-PAGE (Figure 3-10A-B). The analysis clearly illustrates that there is a major increase in PhnY production from the T7 promoter based plasmids pFM36 and pFM37 (lanes 6 and 7 verses lane 5, Figure 3-10A). However, the enzyme is found only in

the insoluble portion. To increase the fraction of soluble PhnY, BL21 (DE3) cells containing pFM36 or pFM37 were induced with different IPTG concentrations and grown at different temperatures, as described in methods. The uninduced and induced samples were treated as above and analyzed by SDS-PAGE. Analysis of cell extracts by SDS-PAGE revealed a dramatic improvement in the amount of PhnY produced in the soluble fraction (see lane 3 of Figure 3-10C). Thus, the optimized PhnY protein production method involved induction at OD_{600} = 0.5 - 0.7 with 40 μM IPTG and growth for an additional 20 h at 15°C with either pFM36 (or pFM37) plasmids. These optimized conditions were used for all future PhnY production cultures. Approximately 16 mg of strep-tagged PhnY and 64 mg of hexahistidine tagged PhnY was isolated from 1 L of LB culture.

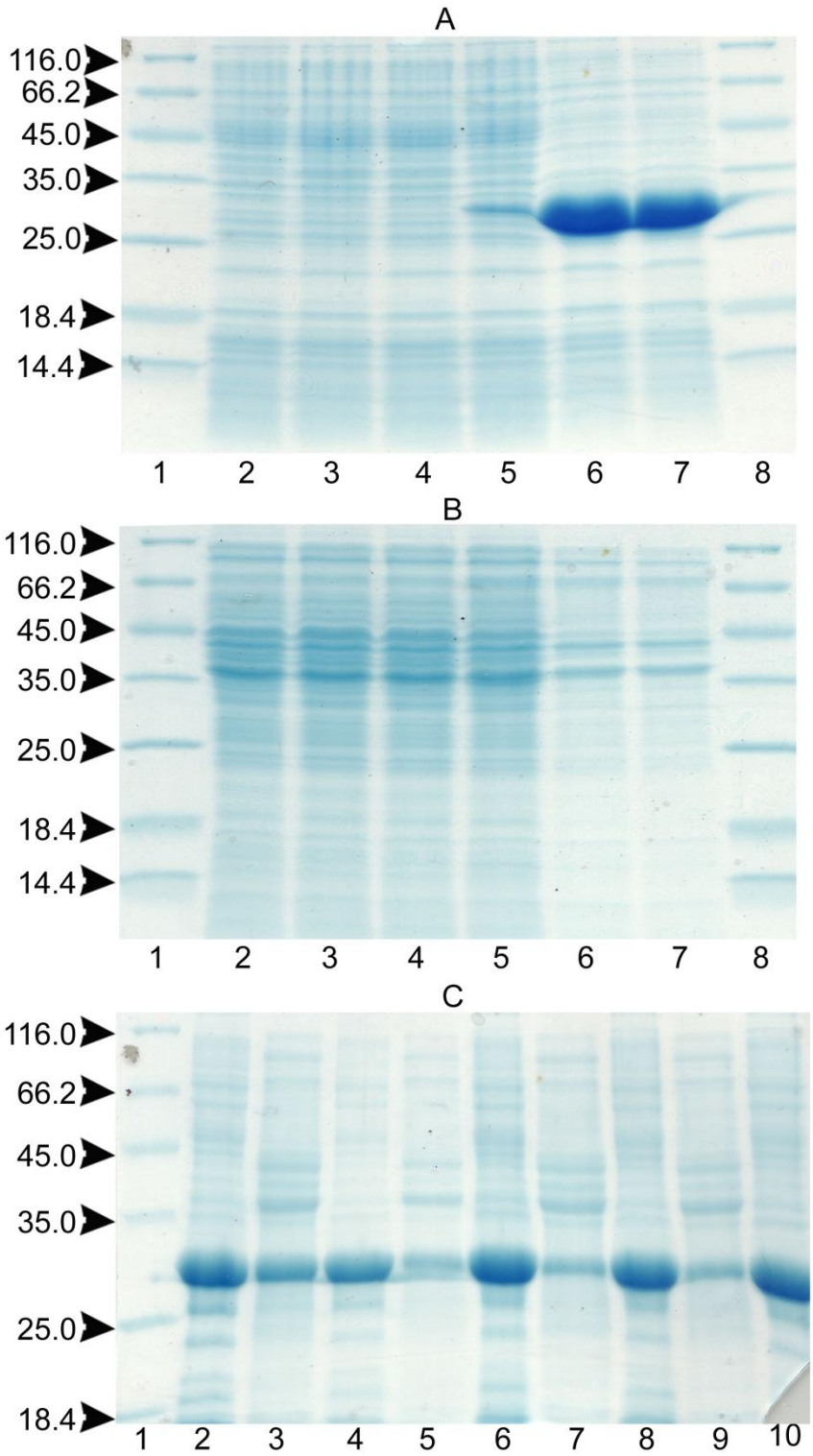

Figure 3-10. SDS-PAGE (15%) analysis of the production of PhnY from different clones and varying conditions. (A) SDS-PAGE of PhnY B-PER treated insoluble cell lysates from three different clones. Lanes 1 and 8, molecular weight marker SM0431 (Fermentas) the size of

the marker bands in kDa are labelled to the left of the gel; lane 2 and 5, insoluble cell lysate of B-PER treated uninduced and induced BL21 (DE3) / pJexpress401_*phnY*, respectively; lane 3 and 6, insoluble cell lysate of B-PER treated uninduced and induced BL21 (DE3) / pFM36, respectively; lane 4 and 7, insoluble cell lysate of B-PER treated uninduced and induced BL21 (DE3) / pFM37, respectively. (B) SDS-PAGE of PhnY B-PER treated soluble cell lysates from three different clones. Lanes 1 and 8, molecular weight marker SM0431 (Fermentas) the size of the marker bands in kDa are labelled to the left of the gel; lane 2 and 5, soluble cell lysate of B-PER treated uninduced and induced BL21 (DE3) / pJexpress401_*phnY*, respectively; lane 3 and 6, soluble cell lysate of B-PER treated uninduced and induced BL21 (DE3) / pFM36, respectively; lane 4 and 7, soluble cell lysate of B-PER treated uninduced and induced BL21 (DE3) / pFM37, respectively. (C) SDS-PAGE of PhnY B-PER treated cell lysates from two different clones induced with varying IPTG concentrations. Lane 1, molecular weight marker SM0431 (Fermentas) the size of the marker bands in kDa are labelled to the left of the gel; lanes 2 and 10, insoluble cell lysate of B-PER treated 40 μM IPTG induced Bl21 (DE3) / pFM36; lane 3, soluble cell lysate of B-PER treated 40 μM IPTG induced Bl21 (DE3) / pFM36; lane 4, insoluble cell lysate of B-PER treated 200 μM IPTG induced Bl21 (DE3) / pFM36; lane 5, soluble cell lysate of B-PER treated 200 μM IPTG induced Bl21 (DE3) / pFM36; lane 6, insoluble cell lysate of B-PER treated 40 μM IPTG induced Bl21 (DE3) / pFM37; lane 7, soluble cell lysate of B-PER treated 40 μM IPTG induced Bl21 (DE3) / pFM37; lane 8, insoluble cell lysate of B-PER treated 200 μM IPTG induced Bl21 (DE3) / pFM37; and lane 9, soluble cell lysate of B-PER treated 200 μM IPTG induced Bl21 (DE3) / pFM36.

3.3.3 Purification of PhnY and PhnZ

After optimizing protein production conditions, at least 15 mg of PhnY and PhnZ protein could be isolated from 1 L of culture. The enzymes were purified in a single affinity chromatography step. The elution fractions were analyzed by SDS-PAGE to determine the purity of the enzymes (Figure 3-11A-B). Fractions containing minimally contaminated protein were combined and dialyzed. It was observed that dialysis with Snake Skin pleated dialysis tubing (Thermo Scientific, Rockford, IL, USA) rendered PhnY inactive and therefore Slide-A-Lyzer dialysis cassettes (Thermo Scientific, Rockford, IL, USA) were used for PhnY and Snake Skin

tubing was used for PhnZ. After dialysis the purity of PhnY and PhnZ was estimated by SDS-PAGE to be > 95% (Figure 3-12).

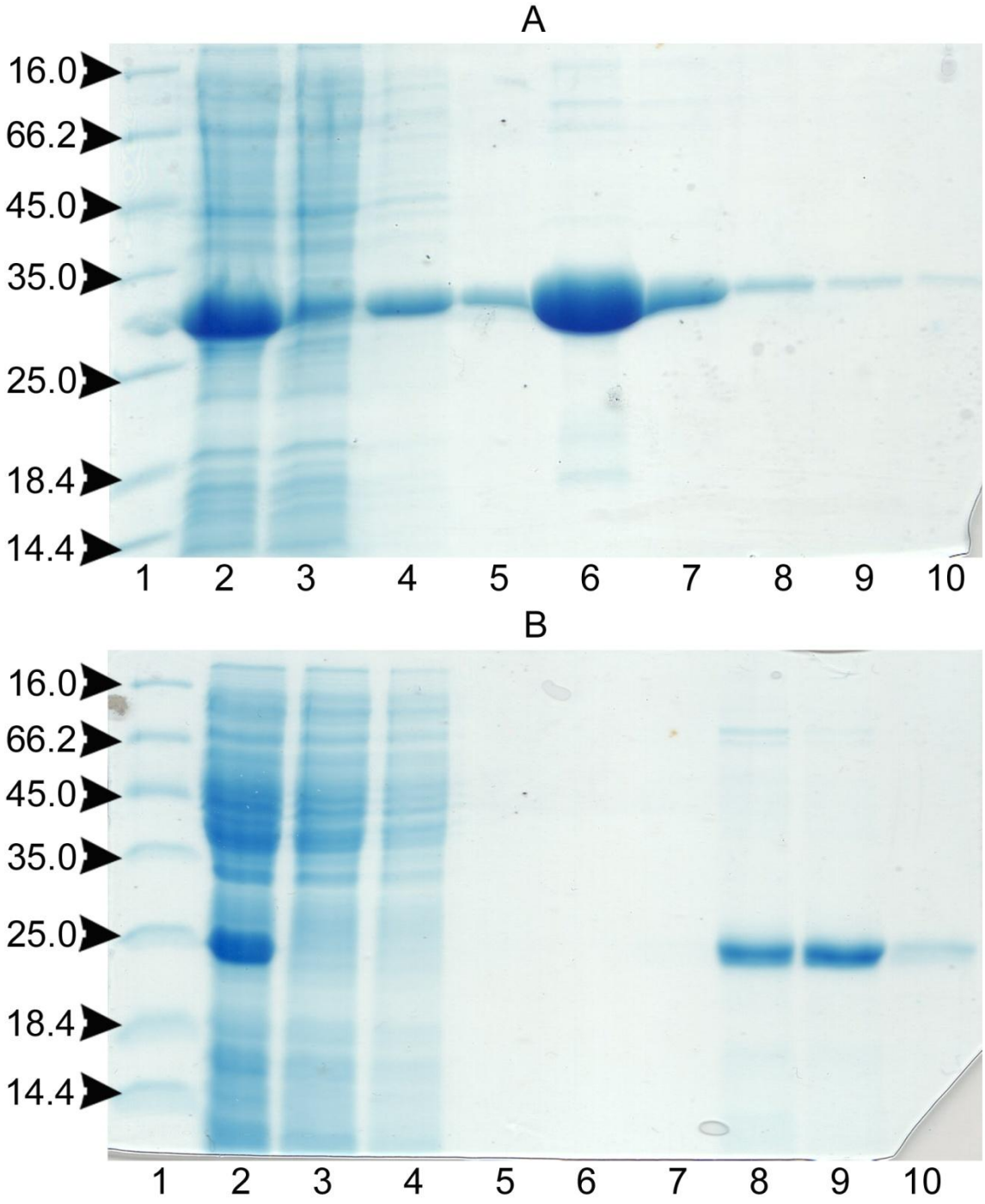

Figure 3-11. SDS-PAGE analysis of PhnY and PhnZ purification. (A) SDS-PAGE (15%) analysis of the purification of PhnY bearing a C-terminal Strep-Tag: Lane 1, molecular weight

marker SM0431 (Fermentas) the size of the marker bands in kDa are labelled to the left of the gel; Lane 2, crude cell extract; Lane 3, flow-through upon loading column with cell extract; Lane 4, flow-through upon washing the column with NP buffer; Lanes 5 to 10, fractions collected upon elution with NPD. (B) SDS-PAGE (15%) analysis of the purification of PhnZ bearing a C-terminal hexahistidine tag: Lane 1, molecular weight marker SM0431 (Fermentas) the size of the marker bands in kDa are labelled to the left of the gel; Lane 2, crude cell extract; Lane 3, flow-through upon loading column with cell extract; Lane 4, flow-through upon washing the column; Lanes 5 to 10, elution of PhnZ with an increasing imidazole gradient.

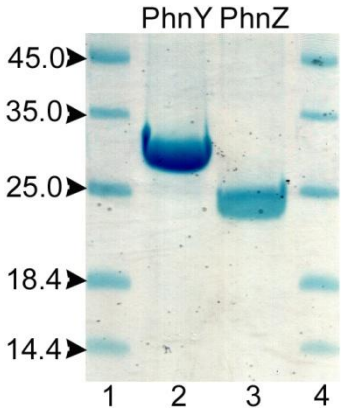

Figure 3-12. SDS-PAGE analysis of purified PhnY and PhnZ after dialysis. Lanes 1 and 4, molecular weight marker SM0431 (Fermentas) the size of the marker bands in kDa are labelled to the left of the gel; Lane 2, purified PhnY; Lane 3, purified PhnZ.

3.3.4 Effect of temperature and addition of iron to PhnY and PhnZ

The genes *phnY* and *phnZ* are from an unknown marine species. In deep sea ocean environments the average temperature is well below room temperature. CD analysis was used to analyze the effect of temperature on the structure of PhnY and PhnZ. CD was run at three different temperatures (4°C, 15°C and 25°C) to observe any structural alterations caused by the differences in temperature. PhnY displayed a spectrum that was consistent with a structure comprised of 19% α-helices, with 30% β-strands, 22 % turns, and 29% unordered polypeptide. In contrast the spectrum for PhnZ suggested a structure that was comprised of 52% α-helices, 8% β-strands, 15 % turns, and 24% unordered polypeptide. The CD spectra also revealed that the structures of PhnY and PhnZ were not altered significantly by temperature (Figure 3-13).

Secondary structure values for PhnY were not altered at all and a decrease of only 1% in α-helical content (with a corresponding increase of 1 % of turns) was observed for PhnZ upon reducing the temperature from 25°C to 4°C.

PhnY and PhnZ require Fe^{2+} for activity (described later in this chapter). It was hypothesized that the Fe^{2+} cofactor could be important for maintaining the structure of the enzyme in addition to facilitating catalysis. However, CD spectra revealed that there are limited alterations in the structure upon adding Fe^{2+} to PhnY or PhnZ. With the addition of iron to PhnY there was a 1% decrease of α-helical content with a corresponding increase in the fraction of unstructured polypeptide (Figure 3-13).

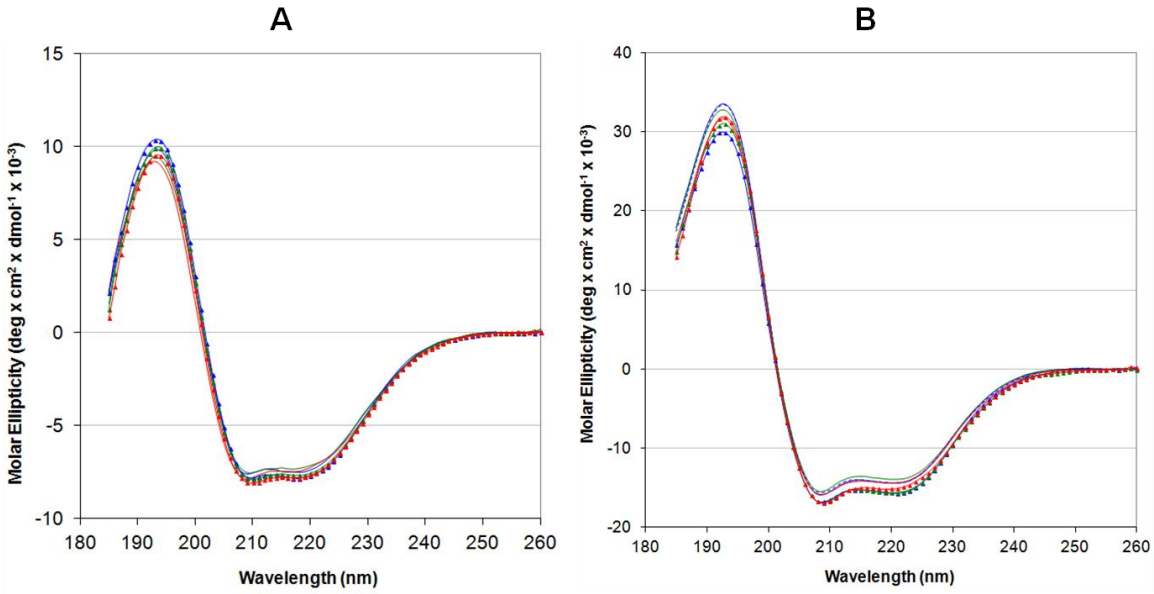

Figure 3-13. The effect of temperature and the presence of iron on the CD spectra of (A) PhnY and (B) PhnZ. Spectra are coloured according to temperature with the spectra run at 4°C, 15°C and 25°C seen in blue, green, and red, respectively. The spectra of PhnZ containing Fe^{2+} have triangles along the line.

3.3.5 Analysis of the PhnY / PhnZ reaction using ^{31}P-NMR spectroscopy

^{31}P-NMR spectroscopy is an ideal technique for monitoring reactions involving organophosphonates due to the sensitivity of the technique and the far downfield chemical shifts displayed by most organophosphonates. The hypothesized substrate for PhnY, **1g,** has a distinct chemical shift at δ 17.3 ppm as shown by the ^{31}P-NMR spectrum of a control reaction lacking PhnY (Figure 3-14A-i.). No change was observed upon addition of PhnY alone and α-ketoglutarate (Figure 3-14A-ii. and iii.). However, upon adding PhnY, α-ketoglutarate, and $Fe(SO_4)_2(NH_4)_2$ a new signal appeared at δ 14.3 ppm (Figure 3-14A-iv.). Ascorbate, a reducing agent known to enhance the activity of α-ketoglutarate / Fe^{2+} dependent dioxygenases by maintaining the iron cofactor in the catalytically active ferrous form[29], was then added to the reaction mixture. This reducing agent dramatically improved the PhnY mediated conversion of **1g** to the compound appearing at δ 14.3 ppm (Figure 3-14A-v.).

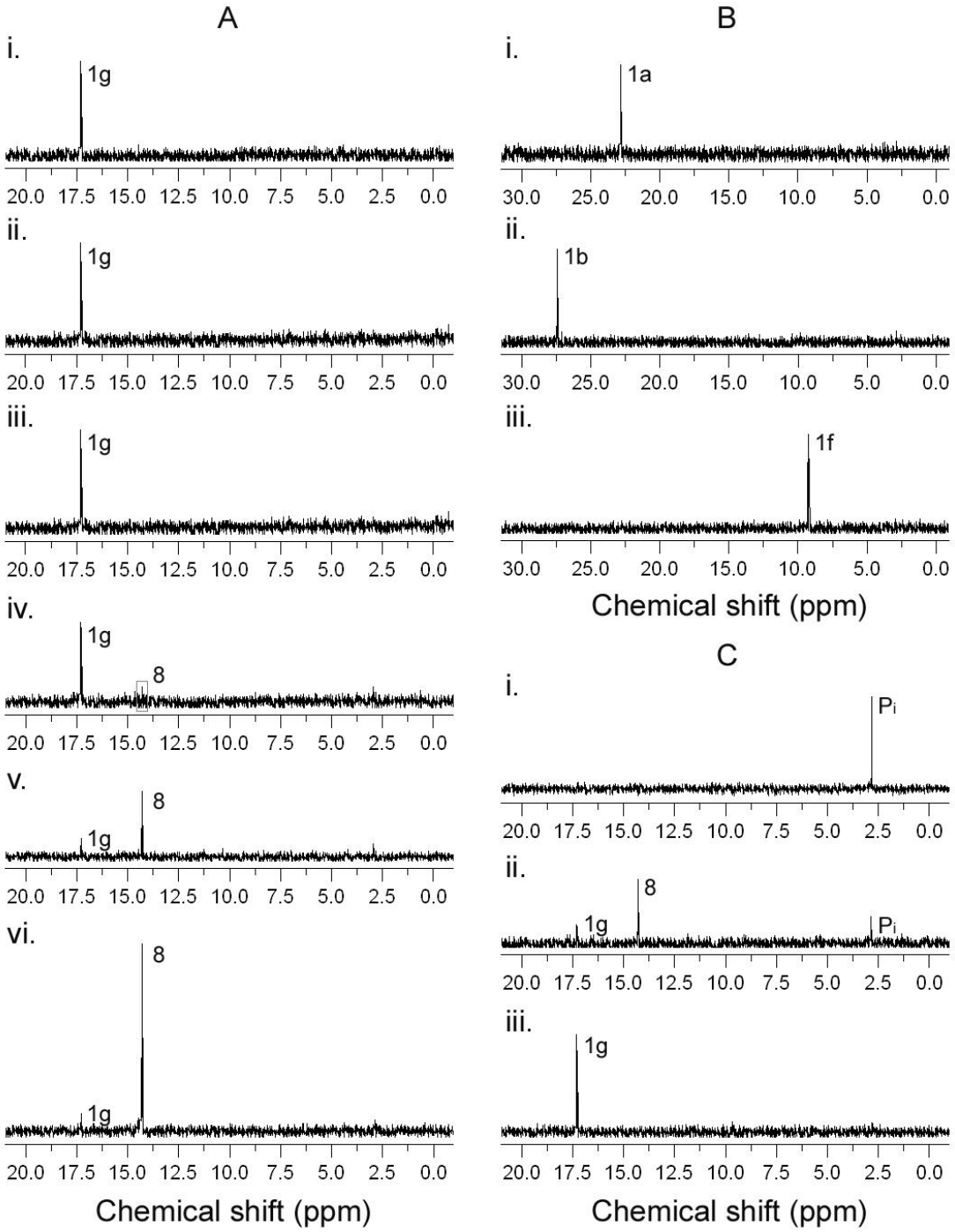

Figure 3-14. ^{31}P-NMR spectroscopic analysis of *in vitro* reactions of PhnY and PhnZ. (A) Spectra of PhnY reactions with **1g**: i. Spectrum of **1g** (δ 17.29 ppm); ii. Spectrum of the reaction of **1g** with PhnY; iii. Spectrum of the reaction of **1g** with PhnY and α-ketoglutarate; iv. Spectrum of the reaction of **1g** with PhnY and α-ketoglutarate in the presence of Fe^{2+}; v. Spectrum of the reaction of **1g** with PhnY and α-ketoglutarate in the presence of Fe^{2+}, and ascorbate; vi. Spectrum

of the reaction seen in v. with the addition of ***R*/*S*-8**. (B) Spectra of PhnY reactions with i. **1a**, ii. **1b**, and iii. **1f**, in the presence of α-ketoglutarate, Fe^{2+}, and ascorbate. (C) Spectra of PhnY and PhnZ reactions with **1g**. i. Spectrum of the reaction of **1g** with PhnY and PhnZ in the presence of α-ketoglutarate, Fe^{2+}, and ascorbate; ii. Addition of PhnZ to a solution of **8** as prepared in Figure3-12A-v. after removal of PhnY by denaturation (95°C for 10 min) and centrifugation of precipitated enzyme; iii. Spectrum of the reaction of **1g** with PhnZ alone.

Given that the α-ketoglutarate / Fe^{2+} dependent dioxygenases TauD[18] and DhpA[19] hydroxylate the C1 position of structurally similar substrates, it was predicted that PhnY would perform a similar reaction to give 2-amino-1-hydroxyethylphosphonate (**8**) (Figure 3-15). This was confirmed by adding synthetic ***R*/*S*-8** to the PhnY reaction and observing an increase in the signal at δ 14.3 ppm (Figure 3-14A-vi.). Methylphosphonate (**1a**) and ethylphosphonate (**1b**) were not substrates of PhnY (Figure 3-14B-i. and ii.), which agrees with the observation that these compounds do not sustain growth of *E. coli* Δ*phn* transformed with *phnY* and *phnZ* genes[11]. Aminomethylphosphonate (**1f**) was also not a substrate for PhnY (Figure 3-14B-iii.).

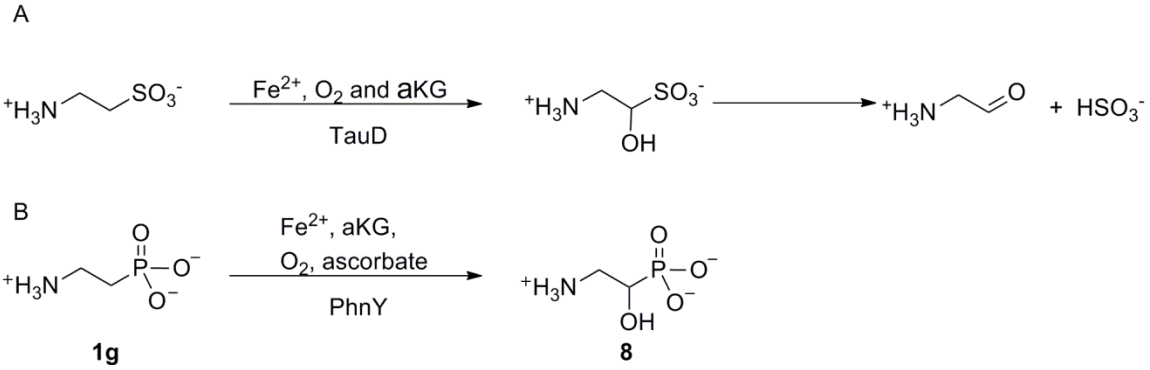

Figure 3-15. Scheme of the (A) TauD and (B) PhnY reactions. aKG, α-ketoglutarate.

PhnZ was subsequently added to the PhnY reaction and the resulting products analyzed by ^{31}P-NMR spectroscopy. In this case, complete conversion of **1g** to P_i was obtained (Figure 3-14C-i). A sequential reaction, where PhnY was denatured (95°C, 10 min) after forming **8**, followed by the addition of PhnZ, also afforded P_i (Figure 3-14C-ii.). Incubation of **1g** with PhnZ alone did not produce a new product (Figure 3-14C-iii.). The reaction of PhnZ directly with

synthetically derived ***R*/*S*-8** resulted in only 50% conversion (Figure 3-16A-ii.). This suggests that PhnZ is stereospecific. Because PhnZ fully converts **8** produced by PhnY to P_i, therefore PhnY is likely stereospecific as well.

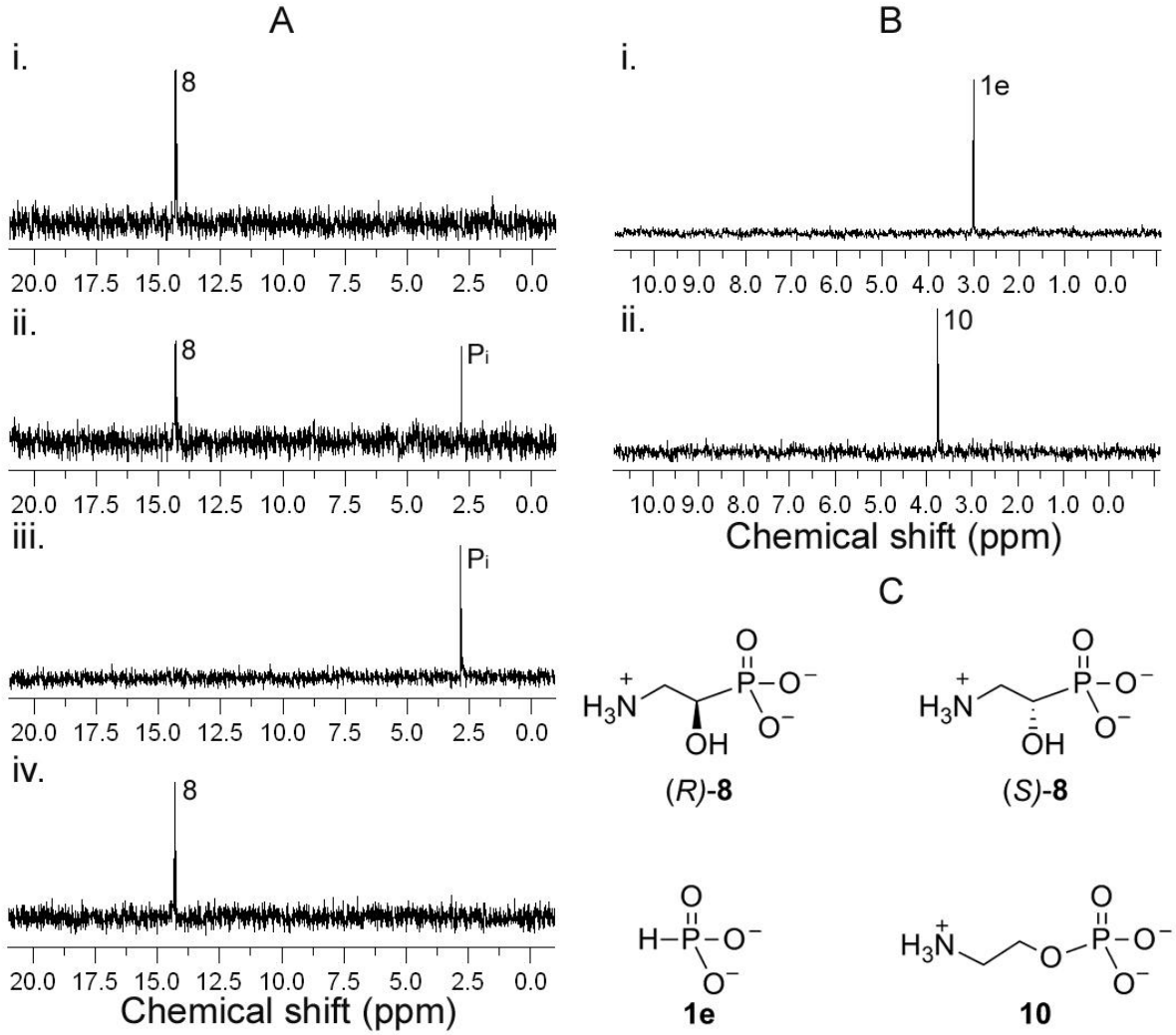

Figure 3-16. ^{31}P-NMR spectroscopic analysis of *in vitro* reactions of PhnZ. (A) Spectra of PhnZ reactions with **8**: i. Spectrum of ***R*/*S*-8** (δ 14.30 ppm); ii. Spectrum of the reaction of ***R*/*S*-8** with PhnZ in the presence of Fe^{2+}; iii. Spectrum of the reaction of ***R*-8** with PhnZ in the presence of Fe^{2+}; iv. Spectrum of the reaction of ***S*-8** with PhnZ in the presence of Fe^{2+}; v. (B) Spectra of PhnZ reactions with i. **1e**, and ii. **10**. (C) Structures of molecules 2-amino-*R*-1-hydroxyethylphosphonate, ***R*-8**; 2-amino-(*S*)-1-hydroxyethylphosphonate, ***S*-8**; phosphite, **1e**; and phosphoethanolamine, **10** tested as PhnZ substrates.

3.3.6 Analysis of the PhnZ reaction

3.3.6.1 Stereospecificity of PhnZ

The fact that only 50% of a racemic mixture of **8** was converted by PhnZ to P_i implies that both PhnY and PhnZ are stereospecific. The *R*- and *S*-enantiomer of **8** were tested for conversion to P_i by PhnZ. PhnZ was only capable of converting the *R*-enantiomer to P_i, whereas the *S*-enantiomer was left untouched (Figure 3-16A-iii and iv.). In addition, crystallization of PhnZ with a racemic mixture of **8** afforded a PhnZ complex bound to the *R*-enantiomer (Section 3.3.7.2).

3.3.6.2 Detection of PhnZ CP bond cleavage intermediates and products

Potential mechanisms of CP bond cleavage of **8** by PhnZ could lead to intermediates such as phosphite (**1e**) or phosphoethanolamine (**10**). Both **1e** and **10** were tested as substrates for PhnZ with various metal ions and neither was converted to P_i according to ^{31}P-NMR spectroscopy (Figure 3-16B-i. and ii.). Potential products of the PhnZ reaction such as acetaldehyde, ammonia, aminoacetaldehyde, and aminoethanol were assayed enzymatically or by HPLC after derivatization. Three different methods were used to search for the presence of an acetaldehyde product. One involved the use of an enzyme assay using acetaldehyde dehydrogenase that converts acetaldehyde and NAD^+ to acetic acid and NADH where an increase in absorbance caused by NADH is monitored at 340 nm. Other attempts to detect acetaldehyde included ^{1}H-NMR spectroscopy and the detection of dinitrophenylhydrazine (DNPH) adducts by HPLC. All methods yielded negative results implying that an aldehyde was not a product of the PhnZ reaction. This corresponded with the observation that no ammonia was detected using a glutamate dehydrogenase assay that converts α-ketoglutarate to glutamate in the presence of ammonia and NADH or NADPH. Subsequently the production of aminoacetaldehyde was assayed. To look for aminoacetaldehyde the reactions were first subjected to an enzymatic reaction with alcohol dehydrogenase that would convert any aminoacetaldehyde produced to

aminoethanol, which was then subsequently derivatized by phenylisothiocyanate (PITC). However, there was no peak present in the HPLC chromatogram that corresponded to derivatized aminoethanol. Finally the PhnZ reaction was directly derivatized with PITC. The derivatized reactions were analyzed using HPLC as stated in methods. HPLC analysis (Figure 3-17) indicated that a control that contained only **1g** afforded a peak at 7.2 min that corresponds to derivatized **1g** (Figure 3-17 i.). In contrast the PhnY reaction contained some residual **1g** in addition to a new peak at 6.7 min that likely corresponds to derivatized **8** (Figure 3-17 ii.). Finally the PhnY / PhnZ coupled reaction affords a new peak at 8.2 min (Figure 3-17 iii.). The PITC adduct of glycine also affords a peak at 8.2 min (Figure 3-17 iv.), indicating that glycine is the aminoalkyl product of the PhnZ reaction.

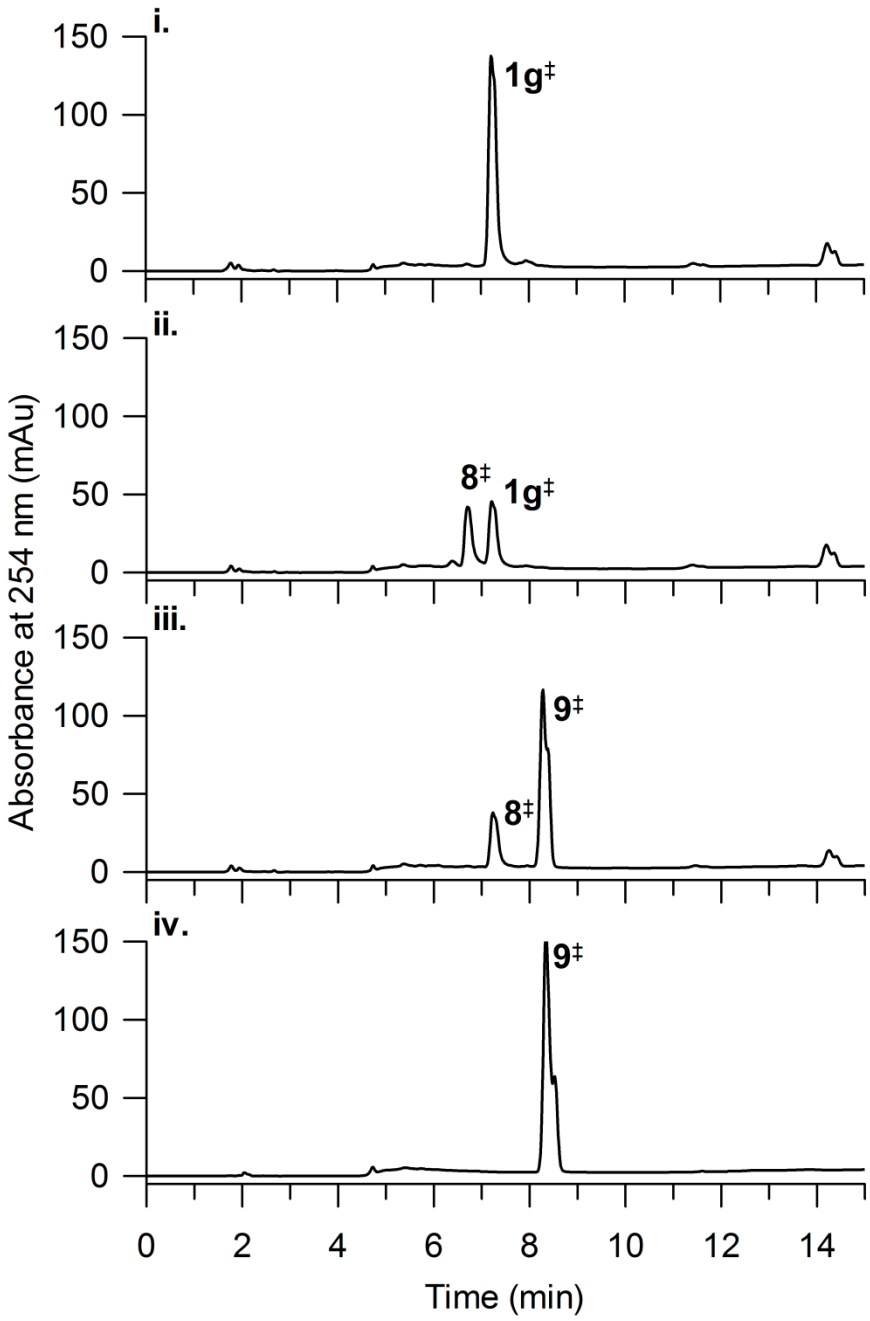

Figure 3-17. HPLC analysis of PhnY and PhnZ reaction products. All reactions were treated with phenylisothiocyanate prior to HPLC analysis and the phenylisothiocyanate adducts are denoted with a double dagger (‡). i. HPLC chromatogram of **1g**; ii. HPLC chromatogram of PhnY reaction with **1g** in the presence of α-ketoglutarate, Fe^{2+} and ascorbate that gives rise to **8**; iii. HPLC chromatogram of the addition of PhnZ to the PhnY reaction described in ii.; iv. HPLC chromatogram of phenylisothiocyanate adduct of glycine **9**.

3.3.6.3 Metal ion dependence of PhnZ

The activity of PhnZ is abolished by the addition of EDTA (Figure 3-18A-i. and B-i.), suggesting that PhnZ requires a metal ion cofactor. To determine which metal ion is required, the PhnZ enzyme was treated with EDTA to remove all metal ions present following purification from *E. coli*. EDTA was then removed from the enzyme sample by dialysis as described in the Methods section. PhnZ was then incubated with PhnY generated **8** in the presence of various metal ions (Fe^{2+}, Fe^{3+}, Mn^{2+}, Ni^{2+}, Ca^{2+}, Cu^{2+}, Zn^{2+}, or Mg^{2+}, 0.1 mM each). The reactions were analyzed by ^{31}P-NMR spectroscopy and it was revealed that only the addition of Fe^{2+} enabled PhnZ to completely convert **8** to P_i (Figure 3-18A-vi.). Partial activity was observed with other metal ions (Figure 3-18A-iv.), presumable due to the presence of residual Fe^{2+} from the PhnY reaction. The exception was Mg^{2+}, where no conversion was observed, suggesting that this metal ion is inhibitory (Figure 3-18A-v.). This analysis was repeated using synthetic ***R*/*S*-8** in the presence of Fe^{2+}, Fe^{3+}, and Ca^{2+}, which confirmed that PhnZ requires Fe^{2+} for activity (Figure 3-18B). ICP-MS analysis of the metal ion content of PhnZ as purified from *E. coli* revealed the presence of 1.25 ± 0.14 mol ^{54}Fe and 1.18 ± 0.12 mol ^{57}Fe per mol of PhnZ and 0.57 ± 0.07 mol ^{43}Ca and 0.51 ± 0.15 mol ^{44}Ca per mol of PhnZ.

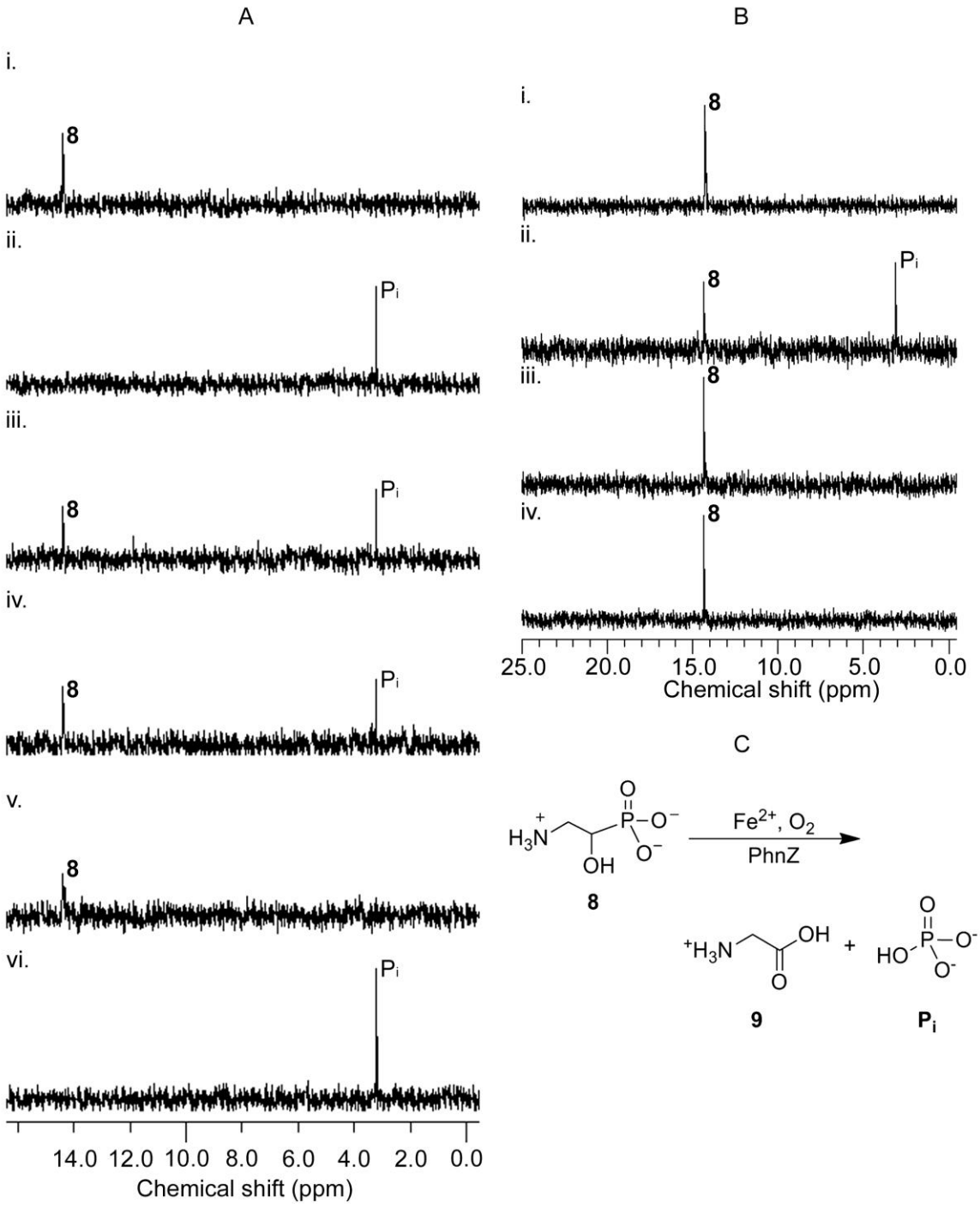

Figure 3-18. ^{31}P-NMR spectroscopic analysis of the metal ion dependence of PhnZ. (A) PhnZ reactions with PhnY generated **8**: i. Spectrum of the PhnY product **8** (δ 14.30 ppm). PhnY was reacted with **1g** in the presence of α-ketoglutarate, Fe^{2+} and ascorbate. The enzyme was then denatured (95°C for 10 min); ii. Addition of PhnZ as purified from *E. coli* to a solution of **8** as prepared in i. (P_i appears at δ 2.9 ppm); iii. Addition of apo-PhnZ (treated with EDTA after

purification, followed by dialysis) to a solution of **8** as prepared in i.; iv. Spectrum arising from the addition of 0.1 mM $CoCl_2$ to the solution described in iii. The addition of other metal ion salts (MnCl2, $FeCl_3$, $NiCl_2$, $CalCl_2$, $CuSO_4$ and $ZnCl_2$) afforded essentially identical spectra; v. Spectrum of the addition of $MgCl_2$ to the solution described in iii.; vi. Spectrum of the addition of $Fe(SO_4)_2(NH_4)_2$ to the solution described in iii. (B) PhnZ reactions with synthetic ***R*/*S*-8**: i. Spectrum of ***R*/*S*-8** (δ 14.30 ppm) reaction with apo-PhnZ, ii. Spectrum of the addition of $Fe(SO_4)_2(NH_4)_2$ to the solution described in i.; iii. Spectrum of the addition of $FeCl_3$ to the solution described in i.; and iv. Spectrum of the addition of $CaCl_2$ to the solution described in i. (C) Scheme of the PhnZ reaction.

3.3.7 Crystal structure of PhnZ

3.3.7.1 PhnZ crystal bound to L-tartrate

The crystal structure of PhnZ was solved to 1.7 Å, by Laura van Staalduinen using the multiple anomalous dispersion method (Figure 3-19A)[28]. Although PhnZ is a monomer in solution as determined by size-exclusion chromatography[28], two almost identical molecules of PhnZ were seen in the asymmetric unit, likely caused by crystal packing. The crystal structure reveals one domain composed of 11 α-helices with two bound metal-ions and a bound L-tartrate molecule in the active site (Figure 3-19A). The metal ion density was modeled as Fe ions based on PhnZ activity and ICP-MS data. The L-tartrate molecule, which was present in the crystallization buffer, bound to one of the Fe ions in the active site of PhnZ. The active site is surrounded by two pairs of antiparallel α-helices (α2, α3, α5 and α6) and a fifth α-helix (α10) that all supply residues for co-ordinating the metal ions. The iron ion denoted Fe1 is coordinated by the side chains of Y24, H34, H58, and D161. D59 and a water molecule each form a bridge from Fe1 to the second iron ion, Fe2 (Figure 3-19B and C). Fe2 is additionally coordinated by the side chains of H80, H104, and two oxygen atoms of L-tartrate. L-tartrate also interacts with a polar region in the active site that includes K108, S126, T129, Q133 and R158 (Figure 3-19B and C).

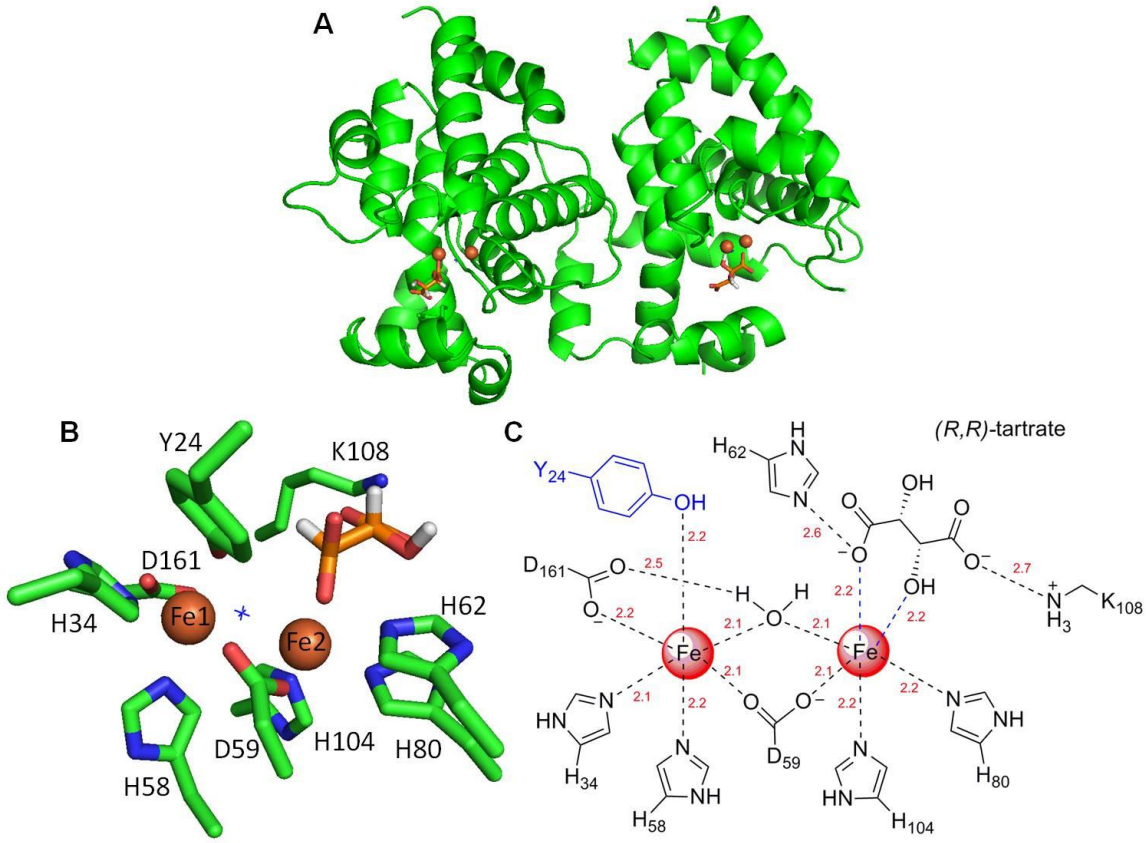

Figure 3-19. Crystal structure of PhnZ bound to L-tartrate. (A) A topology representation of the overall dimeric structure of PhnZ bound to L-tartrate. Iron ions are shown as orange spheres. (B) The active site of PhnZ with catalytic side chains shown in green sticks. L-tartrate bound to Fe2 is shown in orange sticks. (C) A schematic representation of the active site of PhnZ with key interatomic distances given in Å.

3.3.7.2 PhnZ crystal bound to ***R*-8**

Using new crystallization conditions with a racemic mixture of **8**, Laura van Staalduinen solved a second crystal structure of PhnZ to 2.1 Å. Two similar molecules were found in the asymmetric unit (Figure 3-20A and B), however there was a significant difference to a loop conformation resulting in closure of the active site in molecule A compared to that of molecule B (Figure 3-20A and B) and the L-tartrate bound structure (Figure 3-21B and C). In both molecule A and B there was density for the *R*-enantiomer of **8**, rather than the *S*-enantiomer, which correlates with activity assays that show the *S*-enantiomer left untouched and the *R*-enantiomer

cleaved to yield P_i. The active site of molecule B more closely represents that of the L-tartrate bound structure with both found in the open conformation with the Y24 side chain directed into the active site as a ligand for Fe1 (Figure 3-19B and C for L-tartrate and Figure 3-20B and D for molecule B). However, in molecule A the loop undergoes a large (17 Å) conformational change where E27 enters the active site, causing Y24 to depart from the active site and be replaced by a water molecule (Figure 3-20A and C). E27 forms an electrostatic interaction with the amine group of ***R*-8** which is likely protonated (pk_a = 11) at physiological pH and would be positively charged. The same residues (K108, S126, T129, Q133 and R158) that interact with L-tartrate also interact with the phosphonyl oxygens of ***R*-8**. The substrate also makes a bidentate interaction to Fe2 through the α-hydroxyl group and one of the phosphonyl oxygen atoms. The phosphono group of ***R*-8** reveals similar interactions in both molecule A and B.

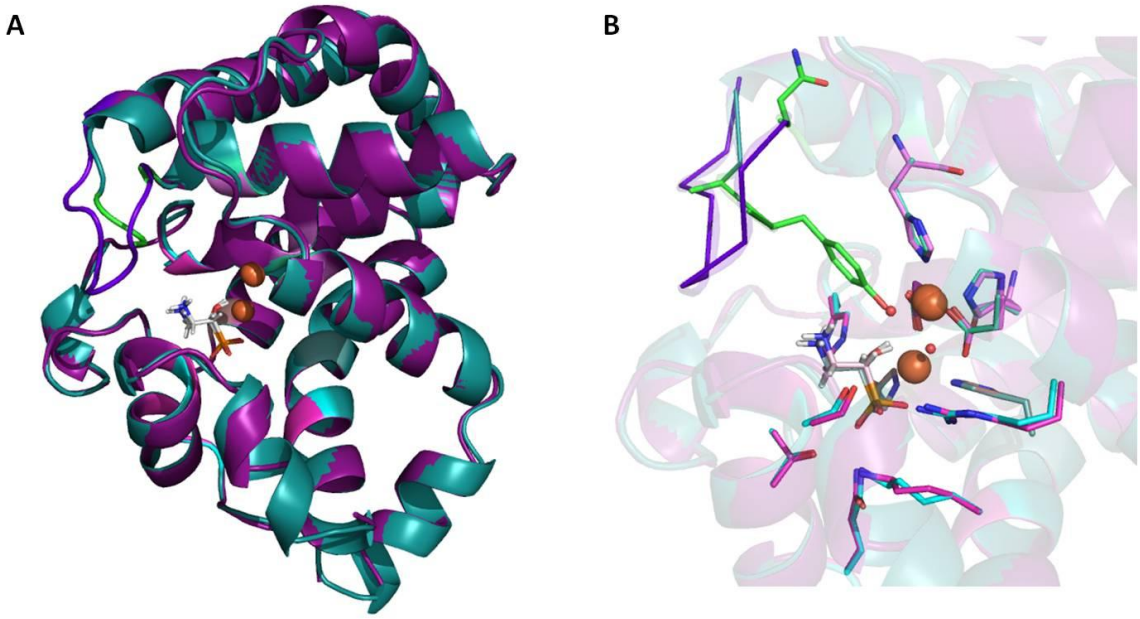

Figure 3-20. X-ray crystal structure of PhnZ bound to the substrate *R*-8. (A) A topological representation of overlaid molecule A and molecule B monomers of PhnZ bound to ***R*-8**. (B) A close up of the superimposed molecule A and B active site. Molecule A is coloured in light blue and molecule B is coloured in purple. Iron ions are shown as orange spheres. The loop regions are highlighted in dark purple and green for molecule A and B.

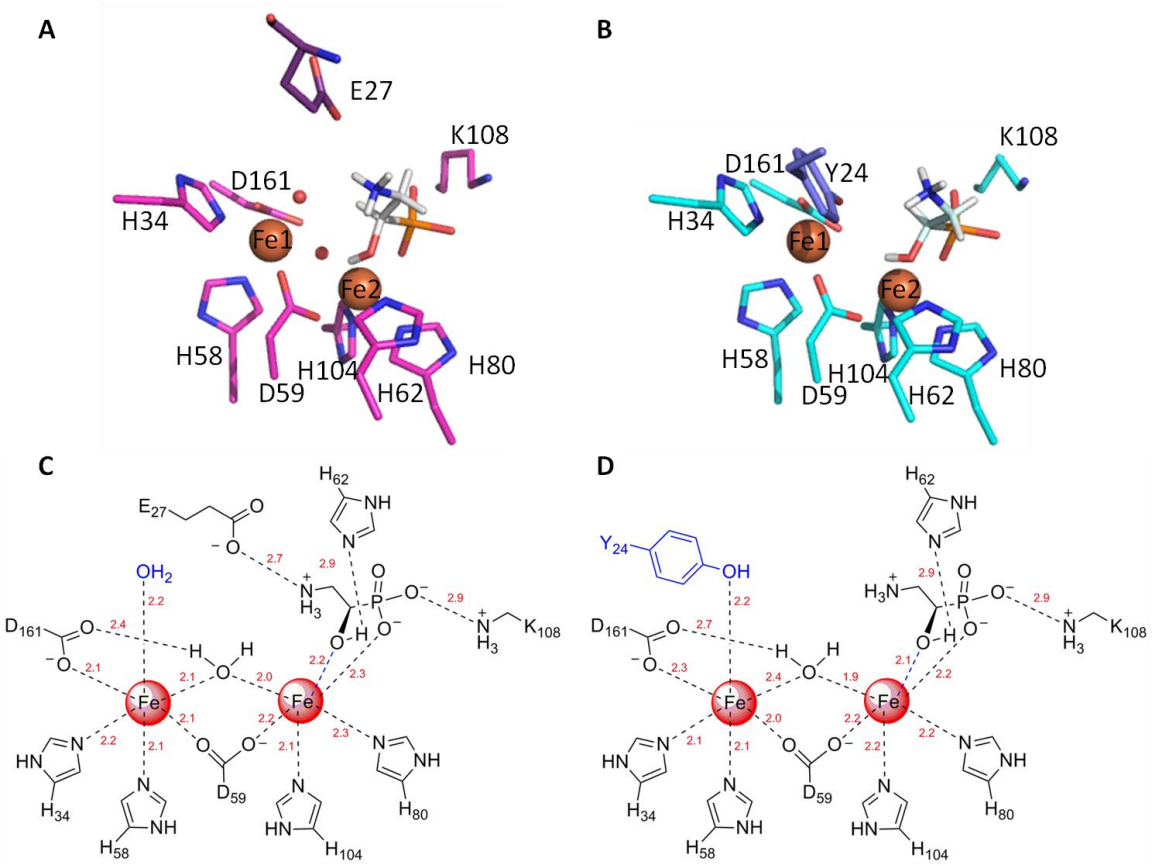

Figure 3-21. The active site of PhnZ. PhnZ crystallized as a dimer. (A) Active site of molecule A of the PhnZ structure. (B) Active site of molecule B of the PhnZ structure. (C) A schematic of the active site of PhnZ molecule A, with key interatomic distances noted in Å. (D) A schematic of the active site of PhnZ molecule B, with key interatomic distances noted in Å.

3.3.7.3 Alignment of PhnZ to MIOX

Structural homology searches using Dali[30] performed by Laura van Staalduinen revealed that the closest structural homologue to PhnZ is mouse *myo*-inositol oxygenase (MIOX, PDB ID: 2HUO, RMSD = 2.7 Å). This is a notable result because the two enzymes have very poor overall sequence homology (10% identity). MIOX is also a member of the HD superfamily, albeit a distant one based on sequence homology, and is one of the few members with a characterized biochemical reaction. MIOX converts *myo*-inositol to D-glucuronic acid in an Fe^{2+} dependent manner. The X-ray crystal structure along with extensive biochemical studies have revealed that MIOX catalyzes oxidative carbon-carbon bond cleavage using two active-site bound Fe ions,

which are proposed to be in mixed oxidation states, Fe^{2+}/Fe^{3+}, at the beginning of the reaction cycle[31-33]. The structural cores and active sites of PhnZ and MIOX align very well with one another (Figure 3-22A). One noteworthy difference is that PhnZ lacks the loops found in MIOX that are used to interact with an enzyme in the *myo*-inositol catabolic pathway. Additionally, the intriguing interaction of Y24 with Fe1 observed in molecule B of the PhnZ structure is not present in MIOX, a water molecule is observed instead. However, in molecule A of PhnZ bound to ***R*-8**, a similar water molecule is observed bound to Fe1. This form of the PhnZ structure also shares a similar active site loop conformation with MIOX, with the active site more closed off from the solvent.

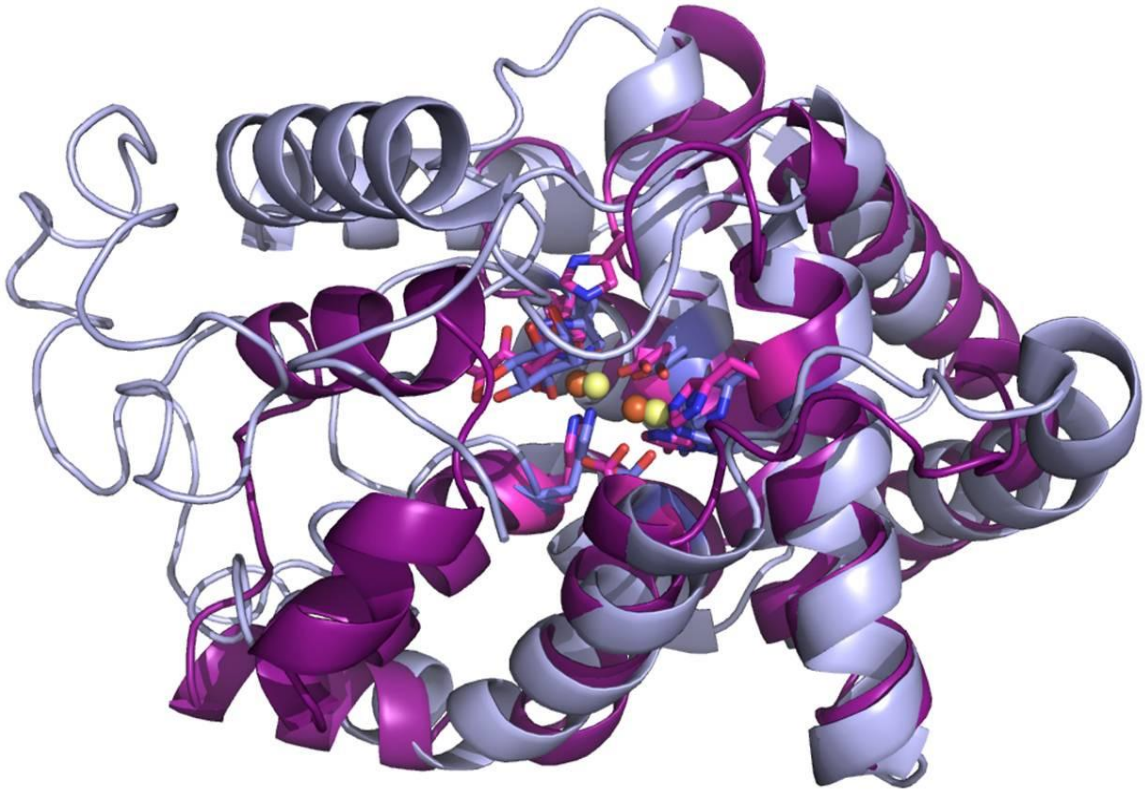

Figure 3-22. PhnZ shares structural homology with myo-inositol oxygenase (PDB: 2HUO). PhnZ is coloured in purple with active site residues in pink, whereas MIOX is coloured in grey with active site residues coloured in blue. The iron ions are shown as orange (PhnZ) and yellow (MIOX) spheres.

3.3.8 Probing the roles of PhnZ active site residues

3.3.8.1 Generation of PhnZ variants

Active site amino acids that coordinate the metal ions and interact with the substrate were altered to probe their roles in the PhnZ reaction. QuickChange PCR was utilized to alter the DNA sequence of Y24, E27, N30, H34, H58, D59, H62, H80, H104, and K108 as described in the methods section. QuickChange PCR uses double-stranded plasmid DNA that contains the gene of interest as a template. After denaturation, the mutagenic primers anneal to the plasmid and are extended by the polymerase. This will generate a mutated plasmid containing staggered nicks. To remove the parent plasmid that was used as the template, the reaction is treated with *Dpn*I. The *Dpn*I exonuclease is specific for methylated DNA, which is only present on the parent plasmid synthesized by cells, and not the PCR product. The mutated PCR product is then transformed into *E. coli* which repairs the nicked plasmid generated by the PCR.

The PCR products were resolved on a 1% agarose gel to confirm amplification of the plasmid. Three different PCRs were set up for generation of D59A (Lanes 1-3, Figure 3-23A) and D161A variants (Lanes 4-6, Figure 3-23A), with varying amounts of the pJexpress401_*phnZ* plasmid as template. In addition, two reactions were set up without polymerase to ensure that the *Dpn*I restriction endonuclease was working effectively (Lanes 7-8, Figure 3-23A). *Dpn*I was only added to one control. Transformations of XL1-Blue with the control reactions yielded the expected results, with the reaction lacking *Dpn*I yielding colonies while the reaction with *Dpn*I did not. Analysis of the PCR by agarose gel electrophoresis showed that in all cases small levels of DNA were successfully amplified (Lanes 1-6, Figure 3-23A). Along with the *Dpn*I reaction, there is no visible plasmid DNA left in the positive *Dpn*I control (lane7, Figure 3-23A) while there is a slight band from the template DNA seen in lane 8, which is *Dpn*I negative. As the PCR product is nicked it runs at the expected size (4526-bp) based on the DNA ladder, however, the template DNA will be found mainly in a supercoiled fashion and will run slightly faster on the gel

than that of the nicked DNA and will therefore appear smaller. To increase the amount of DNA amplified, the PCR for generation of the H34A variant was set up with six different amounts of template DNA and an increased amount of primer. Agarose gel electrophoresis analysis confirmed that all six amounts different quantities of DNA yielded positive amplification of the 4526-bp plasmid DNA(Figure 3-23B). PCRs for generating H58A, H62A, H80A and H104A variants were set up using the optimal conditions determined with the D59A, D161A, and H34A PCRs. Agarose gel electrophoresis analysis (Figure 3-24A and B) confirmed that all remaining mutated plamids were successfully amplified.

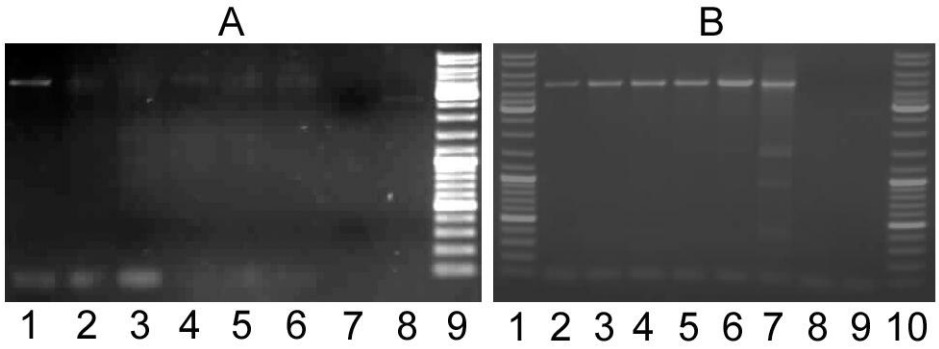

Figure 3-23. 0.8% agarose gel of QuickChange PCR for generation of PhnZ D59A, D161A and H34A variants. (A) Lane 1 to 3 contain QuickChange PCR product *phnZD59A* (4526-bp) amplified using different quantities of 10-fold diluted template DNA (2, 3, and 5 μL, respectively); lane 4 to 6 contain QuickChange PCR product *phnZD161A* (4526-bp) amplified using different quantities of 10-fold diluted template DNA (2, 3, and 5 μL, respectively), lanes 7 and 8 contains PCR controls with no polymerase with and without *Dpn*I, respectively; lane 9, DNA ladder (ladder contains 21 discrete fragments: 8000, 7000, 6000, 5000, 4000, 3500, **3000**, 2500, 2000, 1500, 1200, **1031**, 900, 800, 700, 600, **500**, 400, 300, 200, and 100-bp, there are larger quantities of the bolded fragments present in the mixture). (B) Lanes 1 and 10, DNA ladder; lane 2 to 6 contain QuickChange PCR product *phnZH34A* (4526-bp) amplified using different quantities of 100-fold diluted template DNA (0.5, 1, 2, 5, and 10 μL, respectively); lane 7 contains QuickChange PCR product *phnZH34A* (4526-bp) using 1 μL undiluted template DNA; lanes 8 and 9 contains PCR controls with no polymerase with and without *Dpn*I, respectively.

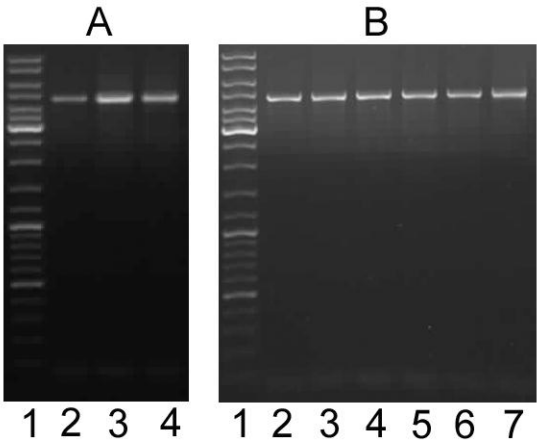

Figure 3-24. 0.8% agarose gel of QuickChange PCR for generation of PhnZ H58A, H62A, H80A and H104A variants. (A) DNA ladder (ladder contains 21 discrete fragments: 8000, 7000, 6000, 5000, 4000, 3500, **3000**, 2500, 2000, 1500, 1200, **1031**, 900, 800, 700, 600, **500**, 400, 300, 200, and 100-bp, there are larger quantities of the bolded fragments present in the mixture) in lane 1. Lane 2 to 4 contain QuickChange PCR product *phnZH58A* (4526-bp) amplified using different quantities of 100-fold diluted template DNA (2, 5, and 10 μL, respectively); (B) Lane 1, DNA ladder; lane 2 and 3 contain QuickChange PCR product *phnZH62A* (4526-bp) amplified using 5 and 10 μL of 100-fold diluted template DNA, respectively; lane 4 and 5 contain QuickChange PCR product *phnZH80A* (4526-bp) amplified using 5 and 10 μL of 100-fold diluted template DNA, respectively; lane 6 and 7 contain QuickChange PCR product *phnZH104A* (4526-bp) amplified using 5 and 10 μL of 100-fold diluted template DNA, respectively.

The PCR products were transformed into XL1-Blue to obtain single colonies on LB-agar plates. Plasmid DNA from at least one clone of each variant was confirmed to have the desired modified codon by DNA sequencing. Additional PhnZ variants Y24E, Y24F, E27A, K108A and N30A were generated by Laura van Staalduinen[28].

3.3.8.2 Substitutions within the active site of PhnZ changes the colour of the enzyme solution

Solutions of PhnZ are distinctively pink in colour when the enzyme is concentrated to 2 mg mL^{-1} or greater. The colour increases in intensity as the concentration of PhnZ is increased implying that the pink colour is associated with the enzyme itself. The PhnZ crystal generated by

Laura van Staalduinen was also pink in color. However upon the addition of 20 times molar excess of racemic **8**, a colour change from pink to yellow was observed[28].

Alterations of active site residues also affected the colour of the enzyme preparation (Table 3-3.). The H58A and D59A variants were unstable and could not be concentrated sufficiently to determine their colour. However, substitution of the other metal ion histidine ligands for alanine, as well as substitution of Y24 for phenylalanine, created variants that were either yellow or colourless. In contrast, substitution of substrate binding residues gave variants that remained pink in colour. This shows that the pink colour of PhnZ is associated with the ligand environment of one or both of the metal ions. The colour of the variants is summarized in Table 3-3.

Table 3-3. Summary of PhnZ variant colour.

Variant	*Colour of enzyme solution*
WT	Pink
Y24E	Yellow
Y24F	Yellow
E27A	Pink
N30A	Pink
H34A	Yellow
H58A	Clear[a]
D59A	Clear[a]
H62A	pink
H80A	Clear
H104A	Clear
K108A	Pink
D161A	Clear

[a] Enzymes precipitated upon concentration.

3.3.8.3 CD spectroscopy of PhnZ variants

CD spectroscopy was utilized to analyze the effect of active site substitutions on the structure of PhnZ. The PhnZ variants Y24E, Y24F, E27A, N30A K108A and D161A exhibited essentially the same CD spectra as wild type PhnZ, indicating that these substitutions had a minimal impact on the overall structure of the enzyme (Figure 3-25). Analysis of the spectra revealed a minor 2% difference in the amount of α-helical content with these substitutions. The CD spectra of PhnZ variants H34A, H62A, H80A and H104A appear to be different than wild type PhnZ with a decreased peak at 192 nm and a smaller valley seen at both 208 and 220 nm which points towards a more unstructured enzyme (Figure 3-25). Analysis of the data revealed an increase in the percentage of turns, β-strands and unordered polypeptide, with a corresponding decrease in α-helical content. The spectra of H58A and D59A were not obtained properly due to the instability of the enzymes. It appears that substitution of residues that coordinate a metal ion (H34, H58, D59, H80 and H104) as well as the substrate binding residue H62 have an impact on the structure of PhnZ, while alteration of substrate binding residues (E27 and K108), metal coordinating residues (Y24 and D161) and the open loop stabilizing residue, N30 leave the structure unaffected.

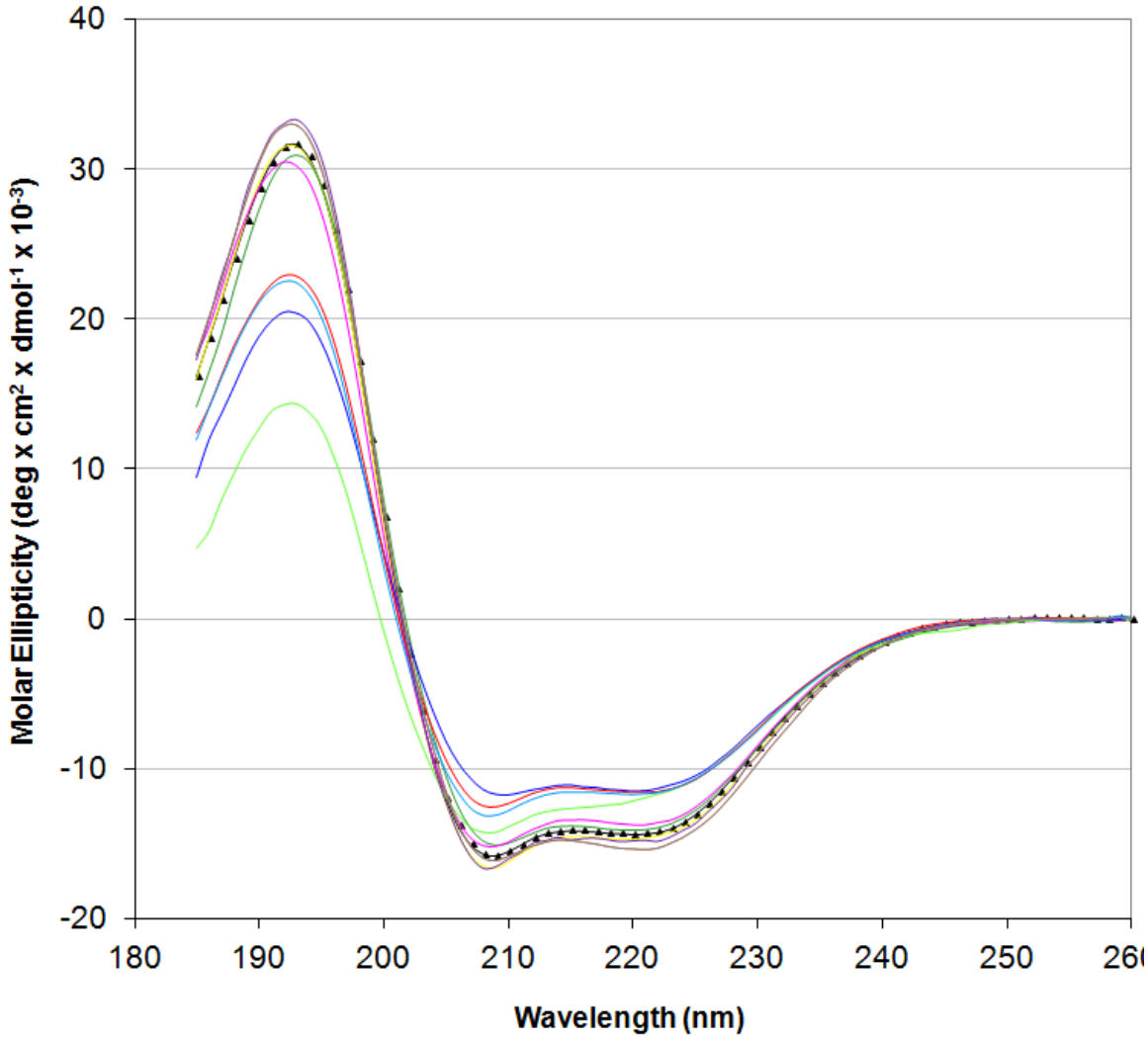

Figure 3-25. The effect of active site substitutions on the CD spectra of PhnZ at 25°C. Spectra are coloured according to the PhnZ variant: WT PhnZ in black with triangles, PhnZ Y24E in yellow, PhnZ Y24F in green, PhnZ E27A in pink, PhnZ N30A in orange, PhnZ H34A in light green, PhnZ H62A in blue, PhnZ H80A in red, PhnZ H104A in light blue, PhnZ K108A in purple, and PhnZ D161A in grey.

3.3.8.4 Kinetic analysis of PhnZ and PhnZ variants

To establish the importance of the PhnZ active site residues to catalysis, kinetic analysis of PhnZ and PhnZ variants was performed using ***R*-8** as a substrate (k_{cat} = 11 ± 1 min^{-1}, K_M = 0.17 ± 0.05 mM). The production of P_i was monitored using a coupled enzyme assay[27]. During the PhnZ reaction, a nucleoside phosphorylase uses the P_i product as a nucleophile to convert a

synthetic nucleoside to α-D-ribose 1-phosphate and 2-amino-6-mercapto-7-methylpurine. The 2-amino-6-mercapto-7-methylpurine leaving group is chromophoric and its production can be monitored at 360 nm. The initial reaction rates were plotted as a function of the concentration of ***R*-8** and the data was fitted with the Michaelis-Menten equation. Michaelis-Menten curve of PhnZ WT can be seen in Figure 3-26, all other curves are in Appendix D. The kinetic parameters k_{cat} and K_M for each variant are given in Table 3-4.

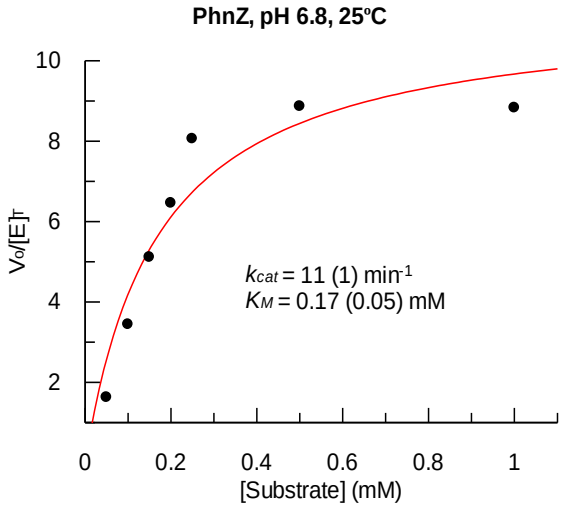

Figure 3-26. Michaelis-Menten plots for WTPhnZ.

Table 3-4. Kinetic parameters of PhnZ variants with *R*-8

Variant	k_{cat} *(min^{-1})*	K_M *(mM)*	k_{cat}/K_M *(min^{-1} · mM^{-1})*	$(k_{cat}/K_M)^{var}/(k_{cat}/K_M)^{WT}$
WT	11± 1	0.17 ± 0.05	65 ± 20	1.0
Y24E	8 ± 1	0.22 ± 0.08	36.0 ± 14	0.53
Y24F	11 ± 1	0.26 ±0.07	42.3 ± 12	0.62
E27A	3.0 ± 0.1	1.1 ± 0.1	2.7 ± 0.3	0.04
N30A	7.4 ±0.3	0.07 ± 0.01	106 ± 16	1.6
H62A	2 ± 1	0.4 ± 0.2	5.0 ± 3.5	0.06
H80A	4.0 ± 0.2	0.6 ± 0.1	6.7 ± 1.2	0.10
K108A	11 ± 1	0.12 ± 0.04	92 ± 32	1.4

The kinetic data for PhnZ variants H34A, H58A, H104A and D161A were not determined because their activities were non-existent or too low to measure accurately. The variant D59A was found to be too unstable to measure its activity accurately.

Alteration of the metal ion binding residues found in the HD motif (H58 and D59) created variants of PhnZ that were unstable and were essentially inactive. This was also the case for the other conserved histidine and aspartic acid residues found in the active site that coordinate the metal ions (H34, H80, H104 and D161). The only metal ion coordinating variant that had detectable activity was H80A, which had a 10 times lower activity than that of the WT enzyme. The K_M value for this variant was also more than 3 times greater than that of WT PhnZ.

The role of Y24 in the PhnZ reaction is of great interest as its location in the active site is coupled to the interaction of E27 with the substrate ***R*-8.** The hydroxyl group of Y24 forms a ligand interaction with Fe1 in the 'open active-site' form of PhnZ bound to ***R*-8**. Upon interaction of E27 with the amino group of ***R*-8,** which produces the 'closed active-site' form of PhnZ, the Y24 side chain is removed from the active site. Two variants, Y24E and Y24F, were analyzed. Both substitutions had a minimal effect on the PhnZ reaction rate with k_{cat}/K_M values that are only half that of the WT enzyme, indicating that Y24 does not play a crucial role in the rate of CP bond cleavage. In contrast, the E27A variant has extremely low activity, with a 4-fold reduction in k_{cat} and a 6-fold increase in K_M that gives a k_{cat} / K_M of 2.6 ± 0.1 $min^{-1} \cdot mM^{-1}$, which is about 4 %) of the WT enzyme (k_{cat} / K_M of 66 ± 0.3 $min^{-1} \cdot mM^{-1}$*)*. This data indicates that E27 plays an important role in cleaving the CP bond of ***R*-8**.

It was hypothesized that Y24 may coordinate to Fe1 to prevent premature oxidation of the iron ion in the absence of the substrate. This was tested by replacing the active site metal ions of purified WT and Y24F variants with Fe^{2+}, then monitoring the residual activity as a function of time. No additional Fe^{2+} was added to the assay solution; therefore the enzymes had to rely on Fe^{2+} that remained bound to the active site. As shown in Figure 3-27, the activity of WT PhnZ and the Y24F variant both decrease similarly over time. Because PhnZ requires Fe^{2+} for activity, this decrease is likely due to autooxidation of $Fe^{2+}$to Fe^{3+}. The similar rates of loss of activity suggest that Y24 does not protect Fe1 from autooxidation.

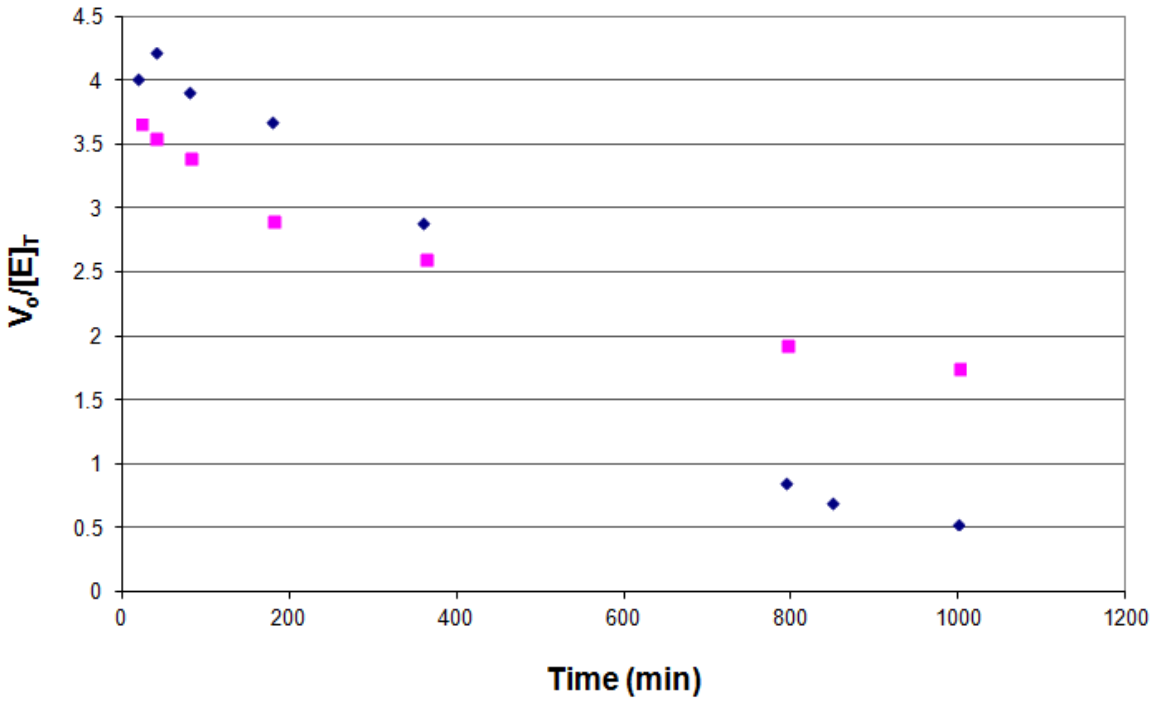

Figure 3-27. Autooxidation of PhnZ and a corresponding loss of activity. The initial rate of PhnZ and the PhnZ Y24F variant were compared over time after loading both enzymes with Fe^{2+}. PhnZ initial rates are denoted with blue diamonds while PhnZ Y24F rates are denoted with pink squares.

The contributions of other substrate binding residues to catalysis were also determined. The H62 side chain is of great interest due to its observed interaction with the α-hydroxyl group of ***R*-8** when bound to Fe2 in the active site of PhnZ. The H62A variant had significantly lower activity in comparison to that of the WT PhnZ. The K_M value (0.17 ± 0.05 mM) was more than 2-fold greater than the WT value (0.4 ± 0.2 mM) and the k_{cat} value (2 ± 1 min^{-1}) was 5.5 times lower than WT PhnZ (11 ± 1 min^{-1}). This resulted in an almost 16-fold drop in k_{cat}/K_M. K108 interacts with phosphonyl oxygens of ***R*-8**. Surprisingly, a K108A variant had a slightly higher k_{cat}/K_M value than WT PhnZ, the result of a slight decrease in K_M.

3.3.9 The activity of PhnZ towards modified substrates

The specifity of PhnZ was probed using synthetically modified versions of the native substrate ***R*-8**. The diastereomers of a slightly larger substrate analogue, 2-amino-1-hydroxypropylphosphonate (**11**), were assessed by ^{31}P-NMR spectroscopy. The **1*R*,2*R*-11** stereoisomer was found to be a competent substrate for PhnZ whereas only 50% of the racemic mixture **1*R*,2*S*/1*S*,2*R*-11** was converted (Figure 3-29A-ii. And iii.), which parallels the specificities towards ***R*-8** and racemic **8**. Kinetic analysis of the reaction of PhnZ with **1*R*,2*R*-11** revealed kinetic parameters that were similar to ***R*-8** (k_{cat}/K_M = 46.3 ± 0.3 $mM^{-1} \cdot min^{-1}$). The role of the 2-amino group of **8** to the PhnZ reaction was also probed. WT PhnZ and the variants E27A and Y24F were analyzed by ^{31}P-NMR spectroscopy for the ability to convert racemic 1-hydroxyethylphosphonate (**12**) to P_i (Figure 3-29B). Neither the WT PhnZ nor the E27A variant was able to convert racemic **12** to P_i (Figure 3-29B-ii. and iii.). In contrast, PhnZ Y24F converted nearly 50% of racemic **12** to P_i Figure 3-29B-iv.).

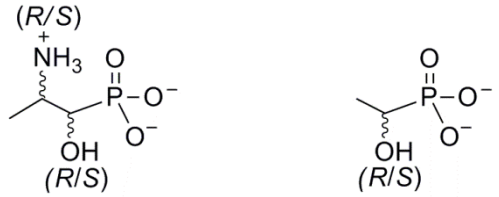

Figure 3-28. Chemical structures of PhnZ substrate analogues, 2-amino-1-hydroxypropylphosphonate (11) and 1-hydroxyethylphosphonate (12).

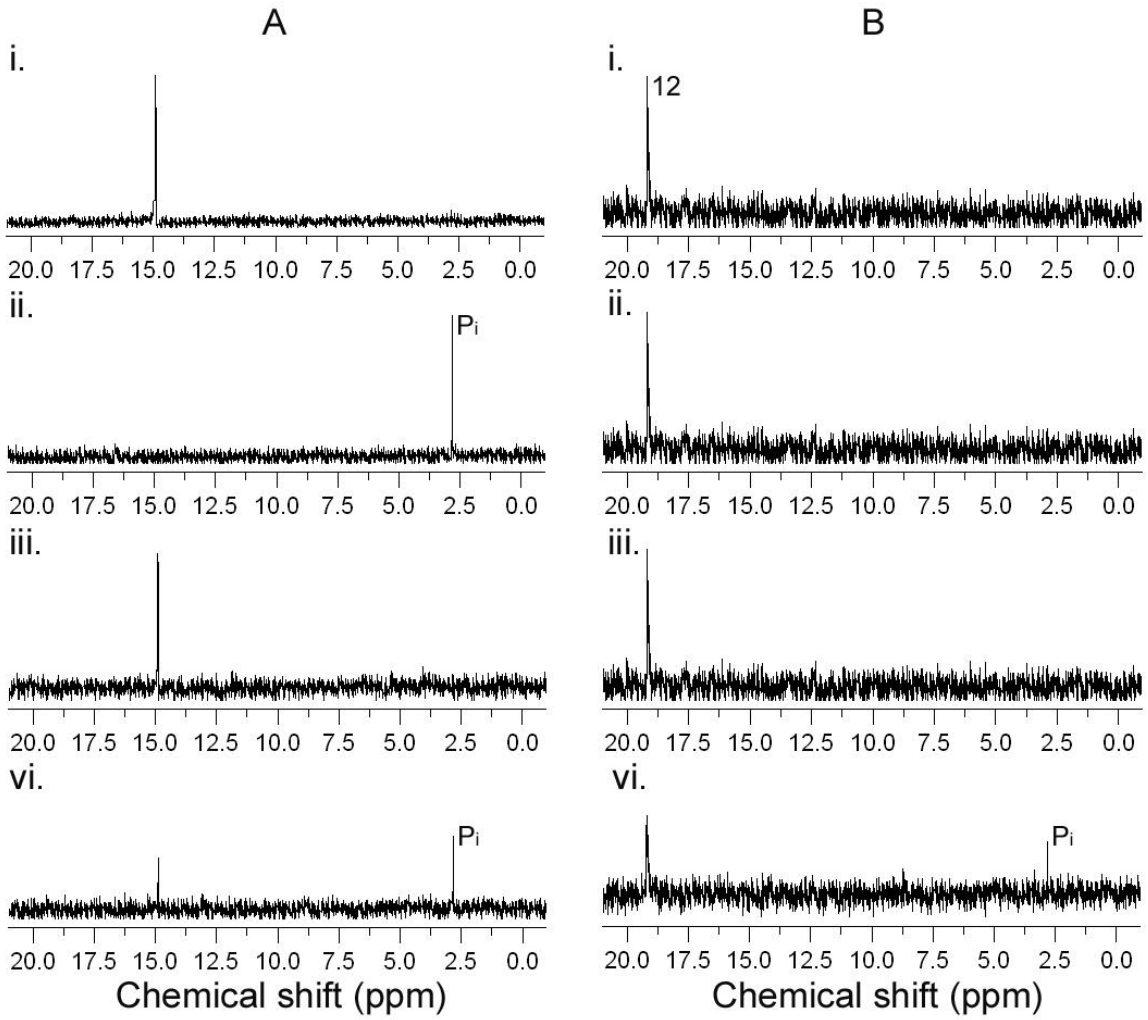

Figure 3-29. ^{31}P-NMR spectroscopic analysis of the reaction of PhnZ and active site variants with substrate analogues. (A) Spectra of PhnZ reactions with **11**: i. Spectrum of (1*R*,2*R*)-**11** (δ 14.89 ppm); ii. Spectrum of the reaction of (1*R*,2*R*)-**11** with PhnZ; iii. Spectrum of the reaction of (1*R*,2*S*/1*S*,2*R*)-**11** (δ 14.89 ppm); iv. Spectrum of the reaction of (1*R*,2*S*/1*S*,2*R*)-**11** with PhnZ. (B) Spectra of PhnZ and PhnZ variant reactions with **12**: i. Spectrum of **12** (δ 19.13 ppm); ii. Spectrum of the reaction of **12** with PhnZ; iii. Spectrum of the reaction of **12** with PhnZ E27A; ii. Spectrum of the reaction of **12** with PhnZ Y24F.

3.4 Discussion

Martinez *et al.*[11] recently demonstrated that the genes *phnY* and *phnZ*, which are derived from an unknown marine bacterium, encode a new pathway for the conversion of the natural organophosphonate 2-aminoethylphosphonate (**1g**) to P_i. In this thesis, synthetic and codon

optimized versions of *phnY* and *phnZ* were successfully expressed in *E. coli* and the encoded enzymes were purified by affinity chromatography. Amino acid sequence analysis reveals that PhnY belongs to a catalytically diverse class of non-heme Fe^{2+} / α-ketoglutarate dependent dioxygenases and that PhnZ is a member of a largely uncharacterized subfamily (TIGR03276), of HD phosphohydrolases that are often associated with organophosphonate degradation pathways. In the work described by this thesis, PhnY and PhnZ were determined to comprise a new oxygenase pathway for cleavage of a CP bond.

Non-heme Fe^{2+} / α-ketoglutarate dependent dioxygenases are known to have potent oxidizing abilities. A member of this family, TauD, is known to hydroxylate the C1 position of taurine, which strongly resembles the structure of **1g** with a sulfonate taking the place of the phosphonate group. Therefore PhnY seemed the best candidate for initial modification of **1g**. ^{31}P-NMR spectroscopy revealed that PhnY converts **1g** to a new phosphorus-containing compound with a ^{31}P-NMR shift that is more upfield than that of **1g**. This phosphorus-containing compound was confirmed to be 2-amino-1-hydroxyethylphosphonate (**8**), indicating that PhnY does indeed hydroxylate the C1 position of **1g**. Based on the similarity of the PhnY and TauD[18,34,35] substrates and products, the reaction likely proceeds through a similar mechanism[18,34,35]. In this mechanism α-ketoglutarate and **1g** enter the active site of PhnY first, followed by molecular oxygen. The active site Fe^{2+} ion catalyzes the reduction of O_2 and subsequent oxidative decarboxylation of α-ketoglutarate to form succinate. This drives the formation of a powerful oxidant in the form of an Fe(IV)=O intermediate. This potent oxidant is capable of abstracting the relatively non-reactive C1-hydrogen of **1g** to form a C1 carbon centered radical. Following rebound of a hydroxyl radical from the subsequent Fe(III)-OH intermediate, which would regenerate the Fe(II) oxidation state for another catalytic cycle, the hydroxylated product **8** would be formed (Figure 3-30). The role of PhnY in this pathway is now

clear because, as shown by this thesis, the α-hydroxy group of **8** is required for CP bond cleavage by PhnZ.

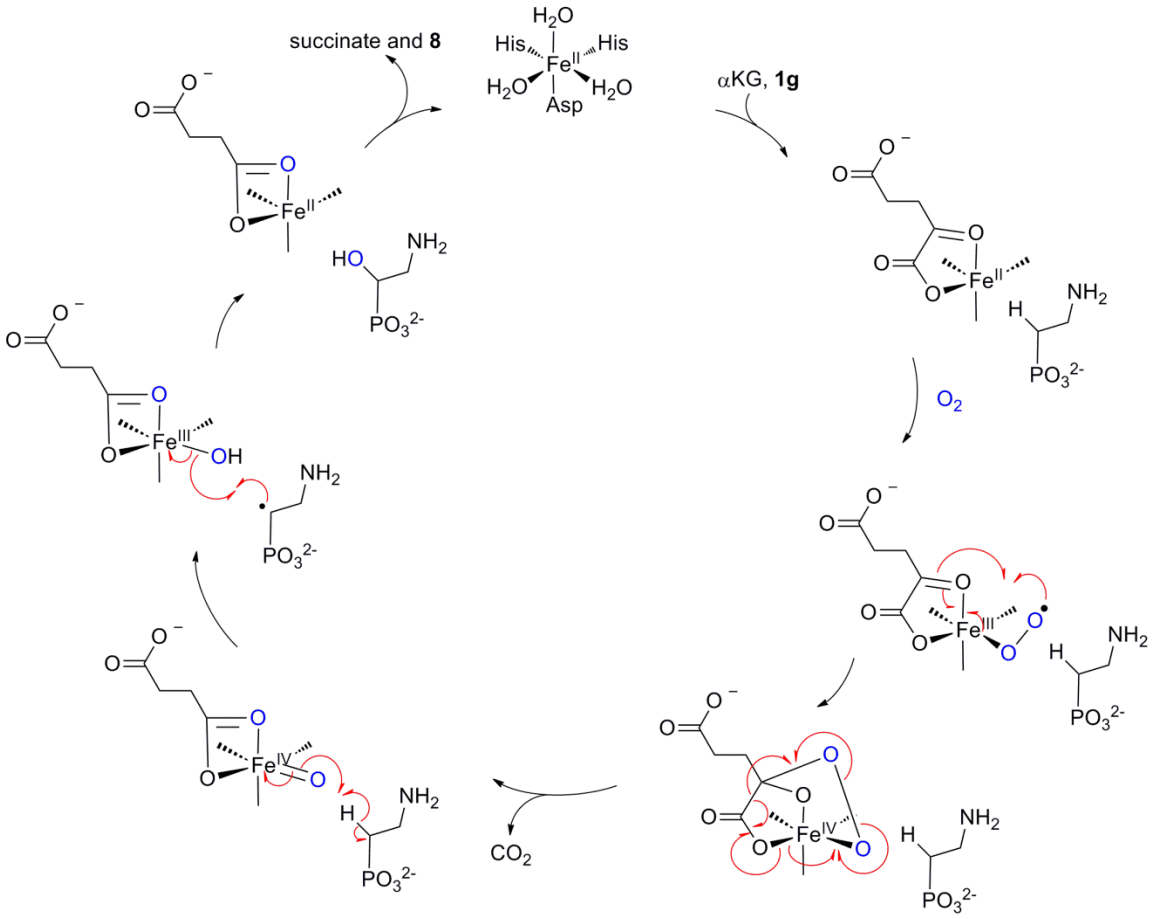

Figure 3-30. Scheme of the proposed PhnY reaction mechanism. aKG, α-ketoglutarate.

Since **8** was confirmed as the intermediate in the PhnY / PhnZ pathway the mechanism for CP bond cleavage by PhnZ was probed further. A few hypotheses for CP bond cleavage were tested. It was predicted that a retro-Abramov reaction could occur to form 2-aminoethanal and phosphite. The latter intermediate may undergo hydrolysis to yield P_i and H_2, analogous to the promiscuous reaction reported for *E. coli* alkaline phosphatase[36]. However, PhnZ did not convert phosphite to P_i in the presence of various metal ions, indicating that this is not a competent intermediate. Likewise aminoacetaldehyde was not detected in the reaction. An alternative mechanism may involve a α-hydroxylphosphonate – phosphate rearrangement where PhnZ

catalyzes an intramolecular attack of the α-hydroxyl on the phosphonyl group. This would lead to a phosphorane intermediate with a strained 3 membered ring, which upon pseudorotation[37] would expel C1 as a carbanion. Following protonation of C1 phosphoethanolamine (**10**) would be formed. Phosphoethanolamine would be subsequently hydrolyzed by PhnZ to form aminoethanol and P_i. However, PhnZ in the presence of various metal ions was incapable of hydrolyzing **10** to form P_i, implying that it is not an intermediate in the reaction. An alternative route of the α-hydroxylphosphonate – phosphate rearrangement would expel ammonia to form vinyl phosphate. Vinyl phosphate spontaneously degrades into acetaldehyde and P_i[38]. However, aldehyde was not detected as a product of the PhnZ reaction using an enzymatic assay, ^{1}H-NMR spectroscopy, or through derivatization with DNPH. Additionally, a glutamate dehydrogenase assay did not detect the formation of ammonia.

The above experiments were fixated on testing hypotheses that are based on heterolytic mechanisms for CP bond cleavage, and illustrate the danger in relying too heavily on the prediction of enzyme function based on sequence homology alone. Although PhnZ belongs to what is largely a 'hydrolase' family of enzymes, CP bond cleavage by PhnZ was shown to be dependent on Fe^{2+}, which suggested that PhnZ might cleave the CP bond through an oxidative mechanism. There is some precedent for such chemistry. For example, the Fe^{2+} dependent enzyme 2-hydroxyethylphosphonate dioxygenase (HEPD) catalyzes the oxidative cleavage of the carbon-carbon bond in 2-hydroxyethylphosphonate[39]. However, with 1-hydroxyphosphonates as substrates, which resemble the PhnZ substrate ***R*-8** in having an α-hydroxyl group, HEPD cleaves the CP bond[40,41]. More revealing is the similarity of the structure of PhnZ to MIOX[28], which oxidatively cleaves the C1-C6 bond of *myo*-inositol to form D-glucuronic acid. Unlike HEPD, MIOX is distantly related to the HD hydrolase family[42] and shares the same active site amino acids as PhnZ, although the overall sequence homology of the two enzymes is weak (10% identity, 19% similarity). MIOX is also dependent on Fe^{2+} for activity and, like PhnZ, does not

require external reducing equivalents for a full catalytic cycle. If PhnZ catalyzed a reaction analogous to HEPD and MIOX, the CP bond of **8** would be oxidatively cleaved to form P_i and glycine (Figure 3-31A). This was indeed confirmed to be the case by the detection of a glycine as a product of the PhnZ reaction (Figure 3-17).

Due to the resemblance of the active site of PhnZ with MIOX, the mechanism of PhnZ likely follows a similar mechanism for oxidative cleavage of a CP bond[25]. MIOX has been shown biochemically and structurally to utilize a diiron active site for catalysis[42]. Likewise, the X-ray crystal structure of PhnZ clearly showed electron density in the active site for a pair of metal ions that were modeled as Fe ions. PhnZ co-purifies with approximately one equivalent of iron rather than two[25], therefore the active site is not fully loaded with metal ion after purification from *E. coli*. MIOX is proposed to use the two Fe ions in differing oxidation states to catalyze the oxidative cleavage of the carbon-carbon bond of *myo*-inositol[31,32]. The first Fe ion, Fe1, is proposed to be in the ferrous (Fe^{2+}) state and initiates oxidation by binding and reducing molecular oxygen. The second Fe ion, Fe2, is proposed to be in the ferric (Fe^{3+}) state and has been structurally observed to bind the substrate *myo*-inositol in a bidentate mode. The structure of PhnZ bound to ***R*-8** reveals a similar bidentate binding interaction between the substrate and Fe2. In both enzymes, the C-H bond of the substrate is directed towards the apical position of Fe1, where molecular oxygen is proposed to bind and be reduced to form a reactive superoxide species. The stereospecificity of PhnZ is clear in this context as binding of ***S*-8** in the active site would project the C1-H bond away from where the superoxide would form, thus preventing abstraction of this hydrogen.

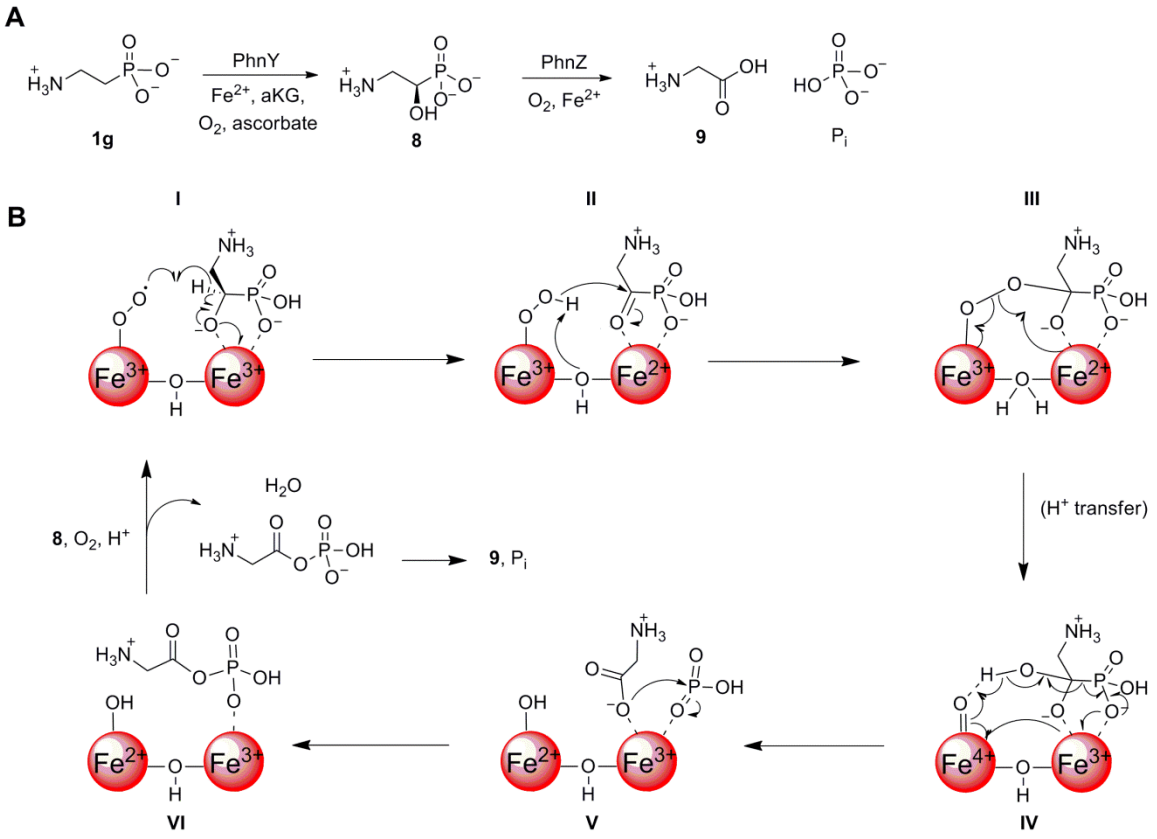

Figure 3-31. (A) Scheme of the overall PhnY and PhnZ reaction. (B) Proposed mechanism for PhnZ. aKG, α-ketoglutarate.

Calculations on the reaction path of MIOX performed by the Hirao and Morokuma provide a template for CP bond cleavage mechanism of PhnZ[43]. Analogous to MIOX, PhnZ likely uses Fe1 in the ferrous state to reduce molecular oxygen to form a superoxo-Fe^{3+} species (**I** in Figure 3-31) [32,43]. Fe2 would likely be in the ferric Fe^{3+} state to bind the substrate **8** in a bidentate mode. The greater positive charge of Fe2 would be ideal for stabilizing the negatively charged phosphonyl group and facilitate formation of an alkoxide at the C1 position of the substrate. The superoxo-Fe^{3+} species at Fe1 would abstract the α-hydrogen of **8,** which would be accompanied by a single electron oxidation of the substrate to form an acylphosphonate intermediate and concomitant reduction of Fe2 to the ferrous state (**II** in Figure 3-31)[43,44]. This step would be facilitated by H62 (and the Lewis acidic Fe2) by stabilizing formation of a C1

alkoxide, as the negatively charged oxygen could help delocalize the single electron formed at C1 in the transition state for bond cleavage. It is conceivable that H62 acts as a general base in this step, abstracting the C1-OH proton as the C1-H bond is being cleaved. In either scenario, this would explain why H62 is conserved in the PhnZ family. It is also noteworthy that MIOX uses a conserved Lys side chain at the same position, which is proposed to perform a similar alkoxide stabilizing role during the oxidation of *myo*-inositol[42].

The subsequent steps of the mechanism involve oxidative cleavage of the CP bond using a highly reactive Fe(IV)=O intermediate. The metal ion bridging hydroxide is thought to provide general base catalysis to facilitate nucleophilic attack of the Fe^{3+}-hydroperoxide on the α-carbonyl of intermediate **II**. In the case of PhnZ this would lead to the peroxide-hemiketal, **III**. Calculations for MIOX favour homolytic cleavage of the peroxide-hemiketal oxygen-oxygen bond[43,44], leading to the formation of the Fe(IV)=O species and the diolate intermediate **IV**. CP bond cleavage would be initiated by abstraction of the hydroxyl hydrogen by the Fe(IV)=O oxygen leading to glycine (**9**) and metaphosphate. Metaphosphate may be attacked by water to form P_i directly, or alternatively be captured by the glycine α-carboxylate to form glycyl phosphate, **VI**. The glycyl phosphate would then be hydrolyzed to **9** and P_i. It is not clear whether this latter reaction would occur spontaneously or be catalyzed by PhnZ because ^{31}P-NMR signals corresponding to this intermediate have not been detected in the PhnZ reaction.

The structure of PhnZ also reveals a novel induced fit mechanism for binding the substrate ***R*-8** in a specific fashion. An active site loop composed of residues 24 to 30 is observed in open and closed configurations when bound to ***R*-8**[28]. Two key amino acids, Y24 and E27, which are conserved in the PhnZ sub-clade of the HD superfamily, reside within this loop. In the open structure E27 is exposed to solvent and the hydroxyl of Y24 is coordinated to Fe1 with only the N30 residue stabilizing the loop conformation by H-bonding to the main chain. In the closed structure the loop flips the orientation of E27 and Y24. The E27 residue moves inwards and

interacts with the amine group of the substrate, which is likely protonated (pK_a = 11)[45] at physiological pH and would contain a formal charge of +1. The Y24 residue flips out of the active site and is replaced by a water molecule that sits in an analogous position to the expected O_2 binding site of MIOX[42]. It is proposed in this thesis that the closed structure represents the active form of PhnZ at the beginning of its catalytic cycle because the open structure would prevent binding of O_2 through the interaction of Y24 with Fe1. The closed structure is also more similar to the MIOX structure.

Active site substitutions of Y24 and E27 along with the loop-stabilizing residue, N30, were analyzed to determine the importance of these residues to catalysis. A phenylalanine substitution of Y24 did not substantially change the kinetic parameters of the enzyme with only a 1.5 fold decrease of k_{cat} observed. This is not consistent with Y24 participating directly in oxidative CP bond cleavage, such as through formation of a tyrosyl radical. Y24 was also shown to not provide protection to Fe1 against oxidation in the absence of substrate. The N30A substitution is slightly more active than that of the WT enzyme, this is likely caused by a more mobile loop as the H-bond stabilizing the open form is lacking. The loop movement, in particular the Y24 residue, appears to correlate with the colour of PhnZ. The pink colour likely arises from a charge transfer complex formed by Fe1 and Y24, which has also been observed to arise from a tyrosyl-iron interaction in the enzyme Dr0930, which is a member of the amidohydrolase superfamily that catalyzes the hydrolysis of δ- and γ-lactones[46]. In both cases a substitution of the tyrosine residue (Y24 in PhnZ, Y97 in Dr0930) to phenylalanine results in loss of colour. Additionally, it is observed that concentrated PhnZ solutions and crystals become yellow upon adding substrate, which may correspond to the loop movement that occurs upon substrate binding and removal of Y24 from the active site during catalysis.

In contrast to substitution of Y24, an alanine substitution of E27 was almost completely inactive with a K_M almost 6 times greater than the WT enzyme and a 4-fold reduction in k_{cat}. This

indicates that E27 plays a direct role in catalysis of CP bond cleavage. The most obvious role is binding of the substrate, which would lead to an increase in K_M upon disrupting this interaction (if K_M is treated as a simple binding constant). However, some of this binding energy may also be used to stabilize the rate determining transition state of the reaction in order to account for the large drop in k_{cat} upon removing this side chain. Alternatively, without E27 the mechanism for removing Y24 from Fe1 would be eliminated. This would prevent binding of O_2, oxidation of the substrate would not proceed, and a low k_{cat} value would be observed.

Further analysis using substrate analogues confirmed the importance of the E27 and Y24 in dictating substrate specificity and access of molecular oxygen to the active site. The substrate (1*R*, 2*R*)-2-amino-1-hydroxypropylphosphonic acid (**11**) proved to be a competent substrate for PhnZ, indicating that the active site has sufficient space in the closed form to accommodate a substrate that is longer by one methyl group than the native one. However, PhnZ did not convert racemic 1-hydroxyethylphosphonate, (**12**) a substrate analogue that lacks the 2-amino group. Presumably when the amino group of the substrate is missing, an electrostatic interaction cannot form between the substrate and E27, which prevents the flip of the active site loop and expulsion of Y24 from the active site. Consequently, the hydroxyl of Y24 would remain as an apical ligand for Fe1 and prevent molecular oxygen from binding and forming a superoxide species. Remarkably, the Y24F variant of PhnZ converted approximately 50% of racemic 1-hydroxyethylphosphonate. When Y24 is altered to phenylalanine, the interaction of the side chain hydroxyl with Fe1 is eliminated. It is most likely that this small change in the active site allows access of molecular oxygen to Fe1 irrespective of an interaction between E27 and the substrate. Although Y24 is conserved in the Phn-HD sub-clade, there is not a counterpart to Y24 in MIOX. It is possible that PhnZ has developed the need for substrate recognition to prevent the breakdown of phosphonate natural products produced by the organism or to prevent analogous phosphate molecules from binding and inhibiting the PhnZ enzyme. These experiments confirm

the need for substrate recognition to induce oxidation of the substrate by PhnZ, and also indicate that it is possible to manipulate the active site of PhnZ to allow for recognition of other substrates.

Other active site residues involved in metal ion coordination and substrate binding were targeted for substitution. Metal ion coordinating residues H34A, H80A, H104A and D161A had little to no activity with only the H80A variant having enough activity to determine kinetic parameters. The H80A variant has a 10-fold lower k_{cat}/K_M than that of WT PhnZ. Substitutions of the other two metal coordinating residues H58 and D59, which comprise the HD motif, rendered the enzyme unstable. The metal binding residues are therefore critical for the stability and activity of the PhnZ enzyme. The amino acids H62 and K108 are found to interact with the substrate through the α-OH and one of the phosphonyl oxygens, respectively. In comparison to WT PhnZ the H62A variant exhibits a 16-fold decrease in k_{cat}/K_M, whereas the K108A variant activity is almost identical to that of the WT enzyme (0.7 fold increase in k_{cat}/K_M). It is surprising that the substitution to the substrate interacting residue K108 has little impact on the activity of the enzyme. However, there are multiple polar interaction with enzyme residues and the phosphonyl oxygens of the substrate, therefore the interaction with K108 may be redundant. The major impact of the substitution of H62 strengthens the proposal, noted above, that this side chain assists formation of a negative charge on the C1 hydroxyl of **8** during catalysis (Figure 3-31, I). It is also noteworthy that substitution of the Lys residue (K127) that plays a similar role in MIOX leads to an inactive enzyme[42].

In summary, a new pathway for the degradation of **1g** has been elucidated that involves a new mechanism for CP bond cleavage. The pathway begins with hydroxylation of the α-carbon of **1g** by an α-ketoglutarate / Fe^{2+} dependent enzyme, PhnY. The introduction of this hydroxyl group facilitates the CP bond cleaving step of the reaction catalyzed by PhnZ. PhnZ, a diiron oxygenase, uses molecular oxygen to catalyze a 4 electron oxidative cleavage of the CP bond without the need for external reducing equivalents. This represents a new mechanism for

cleavage of a CP bond, and extends the range of reactions catalyzed by members of the HD hydrolase family. Interestingly, in surface waters (above 125 m) microbial genomes encoding PhnZ are found without a gene encoding PhnY[11]. Therefore hydroxylation of the C1 position of **1g** must be performed by another enzyme. However, **8** is also a natural product that is found in phosphonolipids[6], and in some ecosystems may represent a major source of P_i. In such environments bacteria would only need PhnZ to acquire P_i. PhnZ may also be capable of degrading other 1-hydroxyalkylphosphonates that are present in marine environments.

There are still many details of both PhnY and PhnZ that require study. Mechanistic studies, such as KIE analysis of both enzymes to determine the rate limiting steps as well as studying additional active site variants of PhnZ will further our understanding of the mechanisms. Crystallization of PhnY will help confirm if PhnY exhibits a similar active site to that of TauD and follows a similar mechanism. A structure of PhnY will also allow for the important active site substitutions to be probed. So far the crystal structure of PhnZ and analysis of some key active site residues has enabled a mechanistic proposal for PhnZ and has opened the door for engineering the active site of the enzyme to accept alternative substrates. Engineering of PhnZ may lead to a catalyst that is capable of degrading toxic organophosphonates in the environment.

3.5 References

1. Quin, L. D.; Quin, G. S. Screening for carbon-bound phosphorus in marine animals by high-resolution ^{31}P-NMR spectroscopy: coastal and hydrothermal vent invertebrates. *Comp. Biochem. Physiol. B:Biochem. Mol. Biol.* **2001**, *128*, 173-185.

2. White, A. K.; Metcalf, W. W. Microbial metabolism of reduced phosphorus compounds. *Annu. Rev. Microbiol.* **2007**, *61*, 379-400.

3. Hilderbrand, R. L. *The role of phosphonates in living systems;* CRC: 1983; .

4. Hori, T.; Sugiyama, M. Use of hydrous iron(III) oxide in a concentration step for the determination of trace amounts of organophosphorus compounds in aqueous solutions. *Analyst* **1992**, *117*, 893-897.

5. Van Mooy, B. A. S.; Fredricks, H. F.; Pedler, B. E.; Dyhrman, S. T.; Karl, D. M.; Koblízek, M.; Lomas, M. W.; Mincer, T. J.; Moore, L. R.; Moutin, T.; Rappé, M. S.; Webb, E. A. Phytoplankton in the ocean use non-phosphorus lipids in response to phosphorus scarcity. *Nature* **2009**, *458*, 69-72.

6. Metcalf, W. W.; van der Donk, W. A. Biosynthesis of phosphonic and phosphinic acid natural products. *Annu. Rev. Biochem.* **2009**, *78*, 65-94.

7. Bowman, E.; McQueney, M.; Barry, R. J.; Dunaway-Mariano, D. Catalysis and thermodynamics of the phosphoenolpyruvate/phosphonopyruvate rearrangement. Entry into the phosphonate class of naturally occuring organophosphorus compounds. *J. Am. Chem. Soc.* **1988**, *110*, 5575-5576.

8. Seidel, H. M.; Freeman, S.; Seto, H.; Knowles, J. R. Phosphonate biosynthesis: isolation of the enzyme responsible for the formation of a carbon–phosphorus bond. *Nature* **1988**, *335*, 457-458.

9. Villarreal-Chiu, J. F.; Quinn, J. P.; McGrath, J. W. The genes and enzymes of phosphonate metabolism by bacteria, and their distribution in the marine environment. *Front. Microbiol.* **2012**, *3*, 1-13.

10. Quinn, J. P.; Kulakova, A. N.; Cooley, N. A.; McGrath, J. W. New ways to break an old bond: the bacterial carbon-phosphorus hydrolases and their role in biogeochemical phosphorus cycling. *Environ. Microbiol.* **2007**, *9*, 2392-2400.

11. Martinez, A.; Tyson, G. W.; DeLong, E. F. Widespread known and novel phosphonate utilization pathways in marine bacteria revealed by functional screening and metagenomic analyses. *Environ Microbiol.* **2010**, *12*, 222-238.

12. Dyhrman, S. T.; Chappell, P. D.; Haley, S. T.; Moffett, J. W.; Orchard, E. D.; Waterbury, J. B.; Webb, E. A. Phosphonate utilization by the globally important marine diazotroph *Trichodesmium*. *Nature* **2006**, *439*, 68-71.

13. Karl, D. M.; Beversdorf, L.; Björkman, K. M.; Church, M. J.; Martinez, A.; DeLong, E. F. Aerobic production of methane in the sea. *Nat. Geosci.* **2008**, *1*, 473-478.

14. Kovaleva, E. G.; Lipscomb, J. D. Versatility of biological non-heme Fe(II) centers in oxygen activation reactions. *Nat. Chem. Biol.* **2008**, *4*, 186-193.

15. Bollinger, J. M.,Jr.; Krebs, C. Stalking intermediates in oxygen activation by iron enzymes: Motivation and method. *J. Inorg. Biochem.* **2006**, *100*, 586-605.

16. Watanabe, M.; Sumida, N.; Murakami, S.; Anzai, H.; Thompson, C. J.; Tateno, Y.; Murakami, T. A phosphonate-induced gene which promotes *Penicillium*-mediated bioconversion of *cis*-propenylphosphonic acid to fosfomycin. *Appl. Environ. Microbiol.* **1999**, *65*, 1036-1044.

17. White, A. K.; Metcalf, W. W. Isolation and biochemical characterization of hypophosphite/2-oxoglutarate dioxygenase. A novel phosphorus-oxidizing enzyme from *Psuedomonas stutzeri* WM88. *J. Biol. Chem.* **2002**, *277*, 38262-38271.

18. Price, J. C.; Barr, E. W.; Tirupati, B.; Bollinger, J. M.; Krebs, C. The first direct characterization of a high-valent iron intermediate in the reaction of an alpha-ketoglutarate-dependent dioxygenase: A high-spin Fe(IV) complex in taurine/alpha-ketoglutarate dioxygenase (TauD) from *Escherichia coli*. *Biochemistry-US* **2004**, *43*, 7497-7508.

19. Circello, B. T.; Eliot, A. C.; Lee, J.; van der Donk, W. A.; Metcalf, W. W. Molecular cloning and heterologous expression of the dehydrophos biosynthetic gene cluster. *Chemistry & Biology* **2010**, *17*, 402-411.

20. Sievers, F.; Wilm, A.; Dineen, D. G.; Gibson, T. J.; Karplus, K.; Li, W.; Lopez, R.; McWilliam, H.; Remmert, M.; Söding, J.; Thompson, J. D.; Higgins, D. G. Fast, scalable generation of high-quality protein multiple sequence alignments using Clustal Omega. *Molecular Systems Biology* **2011**, *7*, 539-doi:10.1038/msb.2011.75.

21. Aravind, L.; Koonin, E. V. The HD domain defines a new superfamily of metal-dependent phosphohydrolases. *Trends Biochem. Sci.* **1998**, *23*, 469-472.

22. Turko, I.; Francis, S. H.; Corbin, J. D. Potential roles of conserved amino acids in the catalytic domain of the cGMP-binding cGMP-specific phosphodiesterase. *J. Biol. Chem.* **1998**, *270*, 6460-6466.

23. Eichhorn, E.; van der Ploeg, J. R.; Kertesz, M. A.; Leisinger, T. Characterization of alpha-ketoglutarate-dependent taurine dioxygenase from *Escherichia coli*. *J. Biol. Chem.* **1997**, *272*, 23031-23036.

24. Gasteiger, E.; Hoogland, C.; Gattiker, A.; Duvaud, S.; Wilkins, M.; Appel, R.; Bairoch, A. In *Protein identification and analysis tools on the Expasy Server;* Walker, J., Ed.; The Proteomics Protocols Handbook; Humana Press: 2005; pp 571-607.

25. McSorley, F. R.; Wyatt, P. B.; Martinez, A.; DeLong, E. F.; Hove-Jensen, B.; Zechel, D. L. PhnY and PhnZ comprise a new oxidative pathway for enzymatic cleavage of a Carbon-Phosphorus bond. *J. Am. Chem. Soc.* **2012**, *134*, 8364-8367.

26. Gunawan, S.; Walton, N. Y.; Treiman, D. M. High-performance liquid-chromatographic determination of selected amino-acids in rat-brain by precolumn derivatization with phenylisothiocyanate. *J. Chromatogr.* **1990**, *503*, 177-187.

27. Webb, M. R. A continuous spectrophotometric assay for inorganic-phosphate and for measuring phosphate release kinetics in biological-systems. *Proc. Natl. Acad. Sci. U. S. A.* **1992**, *89*, 4884-4887.

28. van Staalduinen, L. M. Structural insights into novel microbrial metalloenzymes, Queen's University, Kingston, ON, Canada, 2013.

29. Costas, M.; Mehn, M. P.; Jensen, M. P. Q.,L.Jr. Dioxygen activation at mononuclear nonheme iron active sites: enzymes, models, and intermediates. *Chem. Rev.* **2004**, *104*, 939-986.

30. Holm, L.; Rosenstrom, P. Dali server: conservation mapping in 3D. *Nucleic Acids Res.* **2010**, *38*, W535-W549.

31. Xing, G.; Barr, E. W.; Diao, Y.; Hoffart, L. M.; Prabhu, K. S.; Arner, R. J.; Reddy, C. C.; Krebs, C.; Bollinger, J. M. Oxygen activation by a mixed-valent, diiron(II/III) cluster in the glycol cleavage reaction catalyzed by myo-inositol oxygenase. *Biochemistry-US* **2006**, *45*, 5402-5412.

32. Xing, G.; Diao, Y.; Hoffart, L. M.; Barr, E. W.; Prabhu, K. S.; Arner, R. J.; Reddy, C. C.; Krebs, C.; Bollinger, J. M. Evidence for C–H cleavage by an iron–superoxide complex in the glycol cleavage reaction catalyzed by myo-inositol oxygenase. *Proc. Natl. Acad. Sci. U. S. A.* **2006**, *103*, 6130-6135.

33. Xing, G.; Hoffart, L. M.; Diao, Y.; Prabhu, K. S.; Arner, R. J.; Reddy, C. C.; Krebs, C.; Bollinger, J. M. A coupled dinuclear iron cluster that is perturbed by substrate binding in myo-inositol oxygenase. *Biochemistry-US* **2006**, *45*, 5393-5401.

34. McCusker, K. P.; Klinman, J. P. Modular behavior of *tauD* provides insight into the origin of specificity in alpha-ketoglutarate-dependent nonheme iron oxygenases. *Proc. Natl. Acad. Sci. U. S. A.* **2009**, *106*, 19791-19795.

35. McCusker, K. P.; Klinman, J. P. An active-site phenylalanine directs substrate binding and C-H cleavage in the alpha-ketoglutarate-dependent dioxygenase TauD. *J. Am. Chem. Soc.* **2010**, *132*, 5114-5120.

36. Yang, K.; Metcalf, W. W. A new activity for an old enzyme: *Escherichia coli* bacterial alkaline phosphatase is a phosphite-dependent hydrogenase. *Proc. Natl. Acad. Sci. U. S. A.* **2004**, *101*, 7919-7924.

37. Westheimer, F. H. Pseudo-rotation in hydrolysis of phosphate esters. *Acc. Chem. Res.* **1968**, *1*, 70-78.

38. Baer, E.; Ciplijauskas, L. J.; Visser, T. Synthesis of vinyl phosphate, a possible intermediate in carbohydrate metabolism and photosynthesis. *J. Biol. Chem.* **1959**, *234*, 1-4.

39. Cicchillo, R. M.; Zhang, H.; Blodgett, J. A. V.; Whitteck, J. T.; Li, G.; Nair, S. K.; van der Donk, W. A.; Metcalf, W. W. An unusual carbon–carbon bond cleavage reaction during phosphinothricin biosynthesis. *Nature* **2009**, *459*, 271-875.

40. Peck, S. C.; Cooke, H. A.; Cicchillo, R. M.; Malova, P.; Hammerschmid, F.; Nair, S. K.; van der Donk, W. A. Mechanism and substrate recognition of 2-hydroxyethylphosphonate dioxygenase. *Biochemistry (N. Y.)* **2011**, *50*, 6598-6605.

41. Whitteck, J. T.; Cicchillo, R. M.; van der Donk, W. A. Hydroperoxylation by hydroxyethylphosphonate dioxygenase. *J. Am. Chem. Soc.* **2009**, *131*, 16225-16232.

42. Brown, P. M.; Caradoc-Davies, T. T.; Dickson, J. M. J.; Cooper, G. J. S.; Loomes, K. M.; Baker, E. N. Crystal structure of a substrate complex of myo-inositol oxygenase, a di-iron oxygenase with a key role in inositol metabolism. *Proc. Natl. Acad. Sci. U. S. A.* **2006**, *130*, 15032-15037.

43. Hirao, H.; Morokuma, K. Insights into the (superoxo)Fe(III)Fe(III) intermediate and reaction mechanism of myo-Inositol oxygenase: DFT and ONIOM(DFT:MM) study. *J. Am. Chem. Soc.* **2009**, *131*, 17206-17214.

44. Hirao, H.; Morokuma, K. Ferric superoxide and ferric hydroxide are used in the catalytic mechanism of hydroxyethylphosphonate dioxygenase: A density functional theory investigation. *J. Am. Chem. Soc.* **2010**, *132*, 17901-17909.

45. Gosset, G.; Satre, M.; Blaive, B.; Clément, J.; Martin, J.; Culcasi, M. P.,S. Investigation of subcellular acidic compartments using a-aminophosphonate ^{31}P nuclear magnetic resonance probes. *Anal. Biochem.* **2008**, *380*, 184-194.

46. Xiang, D. F.; Kolb, P.; Fedorov, A. A. M.,M.M.; Fedorov, L. V.; Nguyen, T. T.; Sterner, R.; Almo, S. C.; Shoichet, B. K.; Raushel, F. M. Functional annotation and three-dimensional structure of Dr0930 from D*einococcus radiodurans*, a close relative of phosphotriesterase in the amidohydrolase superfamily. *Biochemistry-US* **2008**, *48*, 2237-2247.

Chapter 4

Conclusions

The work presented in this thesis has contributed to solving the pathway for the breakdown of CP bonds by CP-lyase as well as a new CP bond degradation pathway, PhnY / PhnZ. For over 20 years the CP-lyase pathway remained an enigma. Many obstacles hindered the determination of the CP-lyase pathway, such as the inability to obtain soluble protein and isolate pathway intermediates. However through perseverance these obstacles were overcome. The isolation of catabolic intermediates and a soluble protein complex that are presented in this thesis, along with studies by Raushel and coworkers have facilitated in solving the mystery of the CP-lyase pathway.

^{31}P-NMR spectroscopy and mutated E. coli strains have proven to be useful for tracking CP-lyase pathway intermediates. These techniques can likely be applied to characterizing other CP bond degrading or synthetic routes. ^{31}P-NMR spectroscopy was also a valuable technique for monitoring the purification of CP-lyase pathway intermediates that allowed for their characterization. Knowing the catabolic intermediates enabled us to determine the function of two enzymes from the catabolic pathway. PhnO was determined to be an aminoalkylphosphonate N-acetyltransferase that is required for CP bond cleavage of 1-aminoalkylphosphonates. Whereas PhnP was shown to convert 5-phospho-α-D-ribosyl-1,2-cyclicphosphate to α-D-ribosyl-1,5-bisphosphate. In addition the substrate for the CP bond cleavage step was proposed by our work, and was later confirmed by Raushel and coworkers, to be 5'-phospho-α-D-ribosyl-1'-phosphonate.

It was hypothesized that members of the phn operon are encoded to form a CP-lyase complex. By coexpressing phn genes potentially involved in the formation of the CP-lyase complex a PhnGHIJK complex was successfully isolated. However, no CP bond cleaving

activity could be detected with the isolated complex. The production of a soluble CP-lyase complex consisting of enzymes essential for CP bond cleavage represented an important step towards studying CP-lyase biochemical and structural properties. The CP-lyase enzyme was recently determined to be PhnJ, which is also a member of the isolated complex. PhnJ was shown to require anaerobic reconstitution of a [4Fe-4S] cluster and SAM for activity. During these studies, the PhnJ enzyme was unstable and precipitated out of solution. The isolated PhnGHIJK complex is soluble and stable showing the importance of protein-protein interactions to CP-lyase activity. Therefore, future studies should attempt to reconstitute the complex with the [4Fe-4S] cluster and monitor the enzyme activity. In addition a crystal structure of the PhnGHIJK protein complex would give a detailed picture of the complex's architecture and aid in the significance of each member of the complex. Studying the PhnGHIJK complex will not only reveal interesting aspects of the CP-lyase pathway but will also allow for better understanding of the general importance of protein complexes.

Furthermore a new CP bond cleaving pathway, PhnY / PhnZ was characterized. This pathway is unique to other known CP bond cleaving pathways. This new pathway allows for the degradation of 2-aminoethylphosphonate (**1g**). Firstly, PhnY, an α-ketoglutarate / Fe^{2+} dependent enzyme, hydroxylates the α-carbon of **1g**. This hydroxyl group facilitates the CP bond cleaving step by a diiron oxygenase, PhnZ. PhnZ uses molecular oxygen and two Fe ion cofactors to catalyze the 4 electron oxidative cleavage of the CP bond without the need for external reducing equivalents. The WT PhnZ enzyme was also capable of degrading other substrates and one substitution in the active site allowed PhnZ to degrade 1-hydroxyethylphosphonate. There are still many details of both PhnY and PhnZ that are unknown. Mechanistic studies of both enzymes are still required. In addition, crystallization of PhnY will allow for important active site substitutions to be probed. Crystallization of PhnZ and analysis of some key active site residues has enabled a mechanistic proposal for this new CP bond cleaving enzyme.

Genomic analyses suggest that not all organophosphonate degradation pathways have been discovered. Techniques employed during these studies along with metagenomic DNA searches used by DeLong and coworkers could help in discovering and characterizing these new pathways. In summary six enzymatic pathways for the cleavage of CP bonds have been established to date: i. phosphonoacetaldehyde hydrolase, ii. phosphonoacetate hydrolase, iii. phosphonopyruvate hydrolase; iv. PEP phosphomutase, as well as the two pathways studied in this thesis, v. CP-lyase, and vi. PhnY / PhnZ. With better understanding of the CP-lyase pathway and knowledge of a new CP bond cleaving pathway, PhnY / PhnZ, it is possible that future work with enzyme engineering may allow for the detoxification of harmful man-made organophosphonates.

Appendix A

Strains used in this thesis

Strain	*Genotype*	Source / reference / construction
FM3392	(*dcm-6*/F *lacI*^{q} *zzf*::Tn*10*)	conjugation of GM119 (*dcm-6*)[1] with HO2814 *Δprs-5*/F *lacI*^{q} *zzf::*Tn*10*
HO1429	F$^-$ *deoD gsk-3 udp phnE*(EcoK$^+$)[b]	[2]
HO1440	F$^-$ *deoD gsk-3 udp phnE*(EcoK$^+$) *Δprs-4::*Kan^R[b]	[2]
HO1544	F$^-$ *Δ(lac)X74 ΔphoA532 phnK6::*Tn*5-112* Kan^R	Constructed by Bjarne Hove-Jensen
HO1547	*phnH13::*Tn*phoA´-9* Kan^{Ra}	Constructed by Bjarne Hove-Jensen
HO1550	*phnG35::*Tn*phoA´-9* Kan^{Ra}	Constructed by Bjarne Hove-Jensen
HO1552	*phnI40::*Tn*phoA´-9* Kan^{Ra}	Constructed by Bjarne Hove-Jensen
HO1647	F$^-$ *Δ(lac)X74 Δ(phnC?DEFGHIJKLMNOP)33-30*	Constructed by Bjarne Hove-Jensen
HO2531	F$^-$ *phnE15::*Tn*phoA'-9 ΔpstS605::cat*[a]	[3]
HO2533	F$^-$ *phnE*(EcoK$^+$) *phnG35::*Tn*phoA'-9 ΔpstS605::cat*[a]	[3]
HO2534	F$^-$ *phnE*(EcoK$^+$) *phnH13::*Tn*phoA'-9 ΔpstS605::cat*[a]	[3]
HO2535	F$^-$ *phnE*(EcoK$^+$) *phnI40::*Tn*phoA'-9 ΔpstS605::cat*[a]	[3]
HO2536	F$^-$ *phnE*(EcoK$^+$) *phnJ14::*Tn*phoA'-9 ΔpstS605::cat*[a]	[3]
HO2537	F$^-$ *phnE*(EcoK) *Δ(lac) χ74 ΔphoA532 phnK6::*Tn*5-112 ΔpstS605::cat*	[3]
HO2538	F$^-$ *phnE*(EcoK$^+$) *phnL39::*Tn*phoA'-9 ΔpstS605::cat*[a]	[3]
HO2539	F$^-$ *phnE*(EcoK$^+$) *phnM28::*Tn*phoA'-1*	[2]

	ΔpstS605::cat[a]	
HO2540	F⁻ *phnE*(EcoK⁺) *ΔuidA5 phnN45::*Tn*phoA'-3* *ΔpstS605::cat*[a]	[4]
HO2541	F⁻ *phnE*(EcoK⁺) *phnO38::*Tn*phoA'-9* *ΔpstS605::cat*[a]	[4]
HO2542	F⁻ *phnE*(EcoK⁺) *phnP54::*Tn*phoA'-1* *ΔpstS605::cat*[a]	[4]
HO2568	F⁻ *phnE*(EcoK⁺) *ΔuidA5 rph-1 rpoS396*$_{am}$ *ΔpstS605::cat*[a]	[3]
HO2678	*Δ(lac)χ74 ΔphoA532* *Δ(phnC?DEFGHIJKLMNOP)33-30*	[5]
HO2680	F⁻ *Δ(lac)χ74 Δ(phnCDEFGHIJKLMNOP)33-30* *ΔpstS605::cat*	[3]
HO2735	*Δ(phnC?DEFGHIJKLMNOP)33-30*/F *lacI*^{q} *zzf::*Tn*10*	[6]
HO3342	F⁻ *deoD gsk-3 udp phnE*(EcoK⁺) *Δprs-4::*Kan^{R} *ΔpstS605::cat*[b]	[2]
HO3372	*F⁻ Δ(lac)X74 ΔphoA532 Δ (phnHIJKLMNOP)4/2::Tn5-112/* F *lacI*^{q} Tet^{R}	[HO1488 conjugated with HO2735, selected for Kan^{R}Tet^{R}]
HO3412	*Δ(lac)χ74 ΔphoA532 rph-1 rpoS396*$_{am}$ *ΔpstS605::cat phn*(EcoK⁺) or *phn*(EcoB) *ΔphnO789::kan*	[2]
HO3413	*phn*(EcoK⁺) *ΔphnO789::kan*[c]	[2]
HO3414	*phn*(EcoK⁺)[c]	[2]
HO3417	*phn*(EcoK⁺) *ΔpstS605::cat*[c]	[2]
HO3418	*phn*(EcoK⁺) or *phn*(EcoB) *phnO38::TnphoA'-9*	[2]

[a] Also contains *Δ(lac)χ74 ΔphoA532 phn-10::uidA2-aadA Δ(fumCA manA uidA add)*.

[b] Also contains *araC*$_{am}$ *araD Δ(lac)U169 trp*$_{am}$ *mal*$_{am}$ *rpsL relA thi supF*.

[c] Also contains *Δ(araD-araB)567 ΔlacZ4787(::rrnH-3) rph-1 Δ(rhaD-rhaB568) hsdR514*.

Tet^R, tetracyclin-resistance; Kan^R, kanamycin-resistance.

A.1 References

1. Arraj, J. A.; Marinus, M.,G. Phenotypic reversal in *dam* mutants of *Escherichia coli* K-12 by a recombinant plasmid containing the *dam*$^+$ gene. *J. Bacteriol.* **1983**, *153*, 562-565.

2. Hove-Jensen, B.; McSorley, F. R.; Zechel, D. L. Physiological role of *phnP*-specified phosphoribosyl cyclic phosphodiesterase in catabolism of organophosphonic acids by the carbon−phosphorus lyase pathway. *J. Am. Chem. Soc.* **2011**, *133*, 3617-3624.

3. Adams, M. A.; Luo, Y.; Hove-Jensen, B.; He, S.; van Staalduinen, L. M.; Zechel, D. L.; Jia, Z. C. Crystal structure of PhnH: an essential component of carbon-phosphorus lyase in *Escherichia coli*. *J. Bacteriol.* **2008**, *190*, 1072-1083.

4. Hove-Jensen, B.; Rosenkrantz, T. J.; Zechel, D. L.; Willemoes, M. Accumulation of intermediates of the carbon-phosphorus lyase pathway for phosphonate degradation in *phn* mutants of *Escherichia coli*. *J. Bacteriol.* **2010**, *192*, 370-374.

5. Hove-Jensen, B.; McSorley, F. R.; Zechel, D. L. Catabolism and detoxification of 1-aminoalkylphosphonic acids: N-Acetylation by the *phnO* gene product. *Plos One* **2012**, *7*, e46416.

6. Hove-Jensen, B.; Rosenkrantz, T. J.; Haldimann, A.; Wanner, B. L. *Escherichia coli phnN*, encoding ribose 1,5-bisphosphokinase activity (phosphoribosyl diphosphate forming): dual role in phosphonate degradation and NAD biosynthesis pathways. *J. Bacteriol.* **2003**, *185*, 2793-2801.

Appendix B

Method to convert all point mutation in *phnGHIJKLM* fragment of pFM35 back to that of the wild type cistrons

B.1 PhnM mutation (5053)

Revert a C to T mutation back to a C; there are two unique enzyme sites on either side of the mutation, *MfeI* (5024/5028) and *BclI* (5075/5079).

Therefore use designed oligos with desired overhangs to insert into the digested plasmid:

5'-A A T T G G C G A C G T G C G C G A C G G C G G C G A T **C** G G C T G G A G

C C G C T G C A C G C G C T G C C G C C G C T A **G** C C G A C C T C

A A T C T G G A G A A G A *T-3'*

T T A G A C C T C T T C T *A C T A G*

PMupPhnM

*5'-aattg*gcgacgtgcgcgacggcggcgat**c**ggctggagaatctggagaaga*t*

PMdwPhnM

*5'-gatca*tcttctccagattctccagcc**g**atcgccgccgtcgcgcacgtcgc*c*

Both oligos are 51 bases long and T_m = 168°C

1) Transform pFM35 into dam strain, FM3992

2) Digest plasmid with *MfeI* in Buffer 4 at 37°C, raise temperature to 50°C and add *BclI*

3) Anneal oligos by heating the combined oligos to 95°C and then allowing mixture to cool to room temperature

4) Ligate annealed oligos into digested pFM35 to create pFM40

5) Transform pFM40 into XL1-Blue.

6) Sequence with: phnM_seq_rev in Primer Box 1, 6G (tacttctcgcggttggcgaac) and PhnMseq_for (gagctgcataccgataatctg)

B.2 PhnK mutation (3811)

Revert a T to C mutation back to a T; there are two restriction enzymes close by, *BaeGI* (3533/3529) and *RsrII* (3827/3830). Do four-primer-PCR to eliminate the mutation.

PhnK-NheI-Rev in Primer Box 1 (Phn primers), 9E

CGCC***GCTAGC***ATTCTGCAAAACCGATGACA 30 bp long T_m = 68°C

PMphnKup

cacccatgatttaggcg**t**cgcccgcctgctgg 32 bp long T_m = 104°C

PhnJ-HindIII-For in Primer Box 1 (Phn primers), 1E

AGGGC***AAGCTT***ATGGCTAATCTGAGCGGCT 30 bp long T_m = 62/58°C

PMphnKdw

ccagcaggcgggcg**a**cgcctaaatcatgggtg T_m = 104°C

1) PCR with pFM35 as a template

a) PhnK-NheI-Rev and PMphnKup to get PCRpmKup.

b) PhnJ-HindIII-For and PMphnKdw to get PCRpmKdw.

2) Secondary PCR with PCRpmKup and PCRpmKdw as template and PhnK-NheI-Rev and PhnJ-HindIII-For, resulting in a 1618-bp PCR product, PCRpmK.

3) Digest PCRpmK and pFM40 with *BaeGI* and *RsrII* in Buffer 4 at 37°C.

4) Ligate the 294-bp fragment into pFM40 to give you pFM41.

5) Transform pFM41 into XL1-Blue.

6) Sequence with: PhnK_seq_for (gaagaccacgctgctgaagtcg) and PhnK_seq_rev (gcatttgtaggccggataag).

B.3 PhnI mutation (2254)

Revert a C to T mutation back to a C; there are two restriction enzymes on either side of the mutation, *BstYI* (1960/1964) and *AvaI* (2728/2732). Do four-primer-PCR to eliminate the mutation.

PhnJ Hind in Primer Box 1 (Phn primers), 9D

CCGC***AAGCTT***TTGGTTTTTTGCCTCGCTCTG 31 bp long T_m = 62°C

PMphnIup

cgacaacgtcgaag**c**cgcaggctttgtctc 30 bp long T_m = 92°C

PhnI-HindIII-For in Primer Box 1 (Phn primers), 9C

GGGCAAGCTTATGTACGTTGCCGTGAAAGG 30 bp long, 20 anneal T_m = 60°C

PhnI NdeI in Primer Box 1 (Phn primers), 2D

TATA*CAT**ATG***TACGTTGCCGTGAAAGG 27 bp long T_m = 60°C

PMphnIdw

gagacaaagcctgcg**g**cttcgacgttgtcg 30 bp long T_m = 92°C

1) PCR with pFM35 as a template:

a) PhnJ Hind and PMphnIup to get PCRpmIup.

b) PhnI-HindIII-For or PhnI NdeI and PMphnIdw to get PCRpmIdw.

2) Secondary PCR with PCRpmIup and PCRpmIdw as template and PhnJ Hind and PhnI-HindIII-For/PhnI NdeI, resulting in a 1920 or 1917 bp PCR product, PCRpmI. PCR product size depends on primer selected in 1b.

3) Digest PCRpmI and pFM41 with *AvaI* in Buffer 4 at 37°C then add *BstYI* and raise the temperature to 60°C.

4) Ligate the 768-bp fragment generated into pFM41 to give you pFM42.

5) Transform pFM41 into XL1-Blue

6) Sequence with: H in Primer Box 6, 9A (cgatatcgtcaaccagagcctgc) and J (gatatcttcatacagtttcacctgc).

B.4 PhnH mutation (1160)

Revert an A to G mutation back to an A; there are two restriction on either side of the mutation, *SfcI* (496/500) and *PsiI* (1615). Do four-primer-PCR to eliminate the mutation.

phnI seq rev 2 in Primer Box 1 (Phn primers), 5D

AAACTTCGCCAGCCCCTGAC 20 bp long T_m = 64°C

I in Primer Box 6, 1B

GGAGTAGGCCAGCGCCAGCAAATAGC 26 bp T_m = 84/76°C

PMphnHup

cgaatgatcgctccgc**a**gctgccggagtgcattc 34 bp T_m = 108°C

PhnG-HindIII For in Primer Box 1 (Phn primers), 5A

AGGGCAAGCTTATGCACGCAGATACCGCGAC 31 bp long 20 anneal T_m = 64°C

PhnG-NdeI-forward in Primer Box 1 (Phn primers), 7A

TATA*CATATG*CACGCAGATACCGCGACC 28 bp long T_m = 68°C

PMphnHdw

gaatgcactccggcagc**t**gcggagcgatcattcg 34 bp T_m = 108°C

1) PCR with pFM35 as a template:

a) phnI seq rev 2/I and PMphnHup to getPCRpmHup.

b) PhnG-HindIII/PhnG-NdeI-forward and PMphnHdw to get PCRpmHdw.

2) Secondary PCR with PCRpmHup and PCRpmHdw as template and phnI seq rev 2/I and PhnG-HindIII/PhnG-NdeI-forward, resulting in a ~1663-bp PCR product, PCRpmH. PCR product size depends on primer selected in 1a and b.

3) Digest PCRpmH and pFM42 with *SfcI* and *PsiI* in Buffer 4 with BSA at 37°C.

4) Ligate the 1119-bp fragment into pFM42 to give you pFM43.

5) Transform pFM43 into XL1-Blue

6) Sequence with: M13 rev and I in Primer Box 6, 1B (ggagtaggccagcgccagcaaatagc)

Appendix C

Plasmid constructs used in this thesis

Below are images of the plasmid maps from plasmids used in this thesis. The plasmid name and size, in bp, are found in the centre of the plasmid map. The plasmid backbone is in black with unique characteristics of the plasmid such as the origin site and resistence gene labelled with a green arrows. Unique restricition enzyme sites within the plasmid are labelled in red font with other restricition enzyme sites and all other regions labelled in black. Genes that encode for proteins to be expressed are found as red arrows.

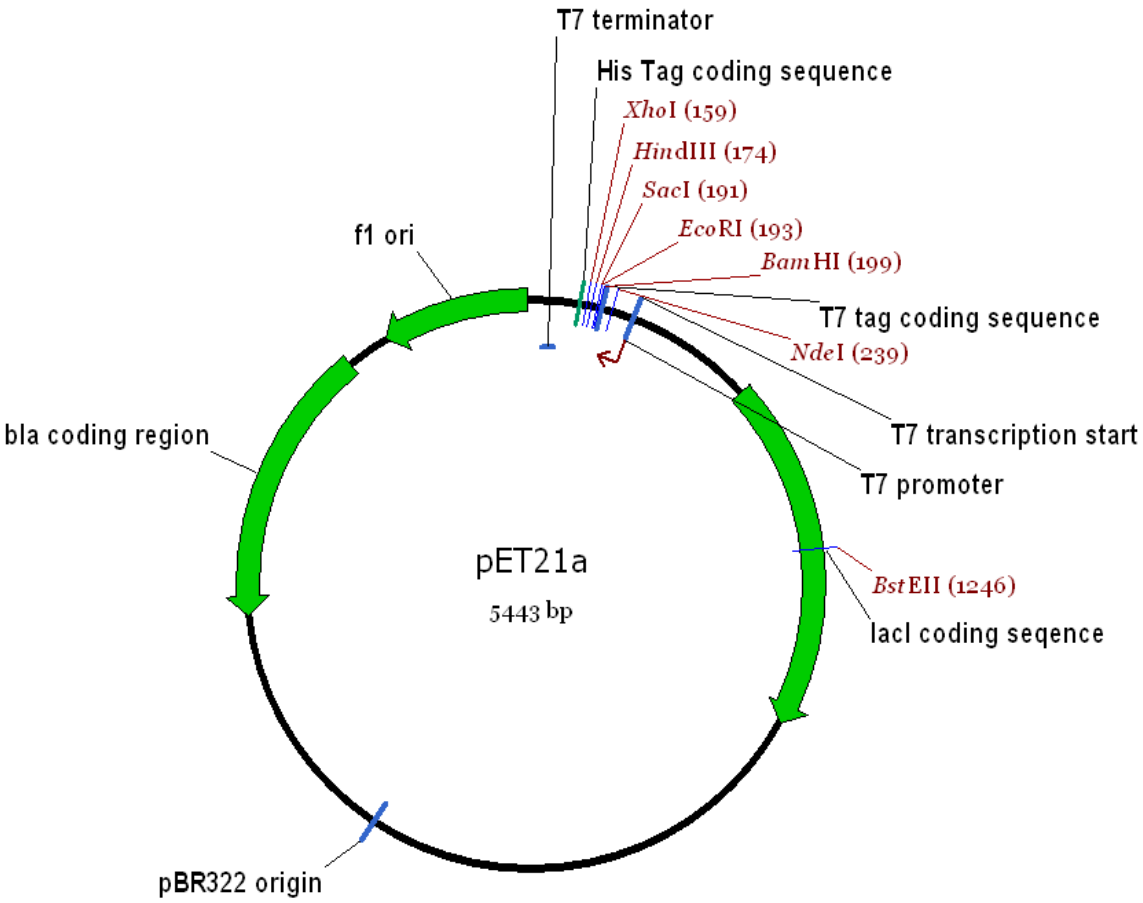

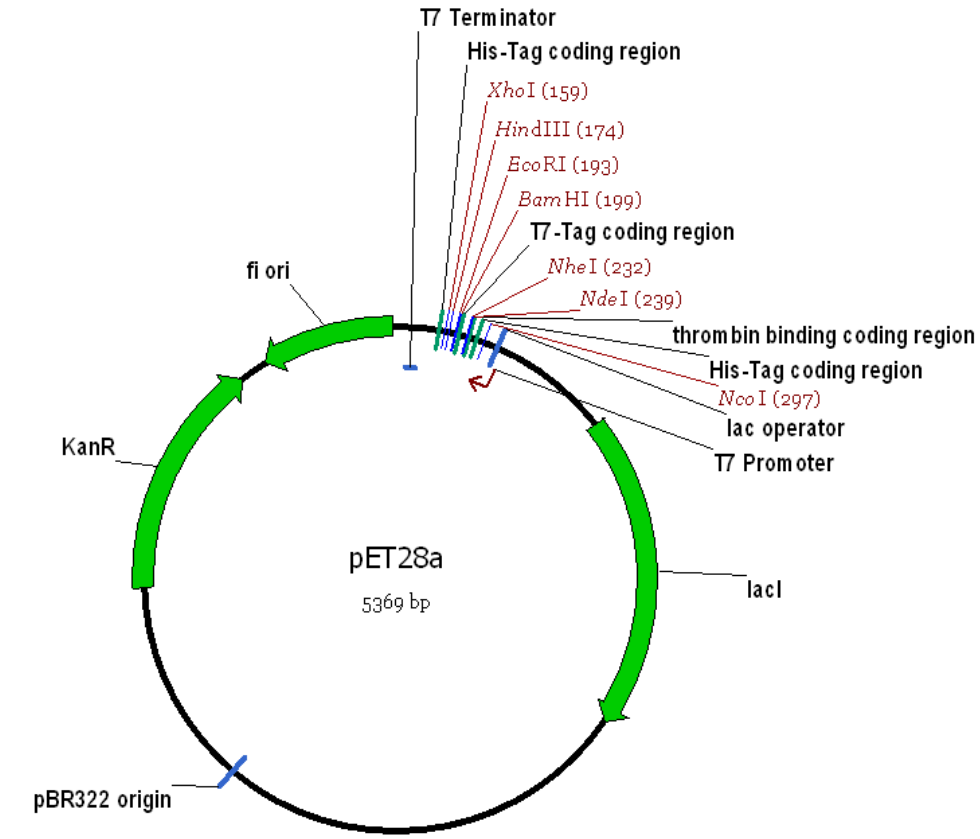
T7 Terminator
His-Tag coding region
XhoI (159)
HindIII (174)
EcoRI (193)
BamHI (199)
T7-Tag coding region
NheI (232)
NdeI (239)
thrombin binding coding region
His-Tag coding region
NcoI (297)
lac operator
T7 Promoter
fi ori
KanR
pET28a
5369 bp
lacI
pBR322 origin

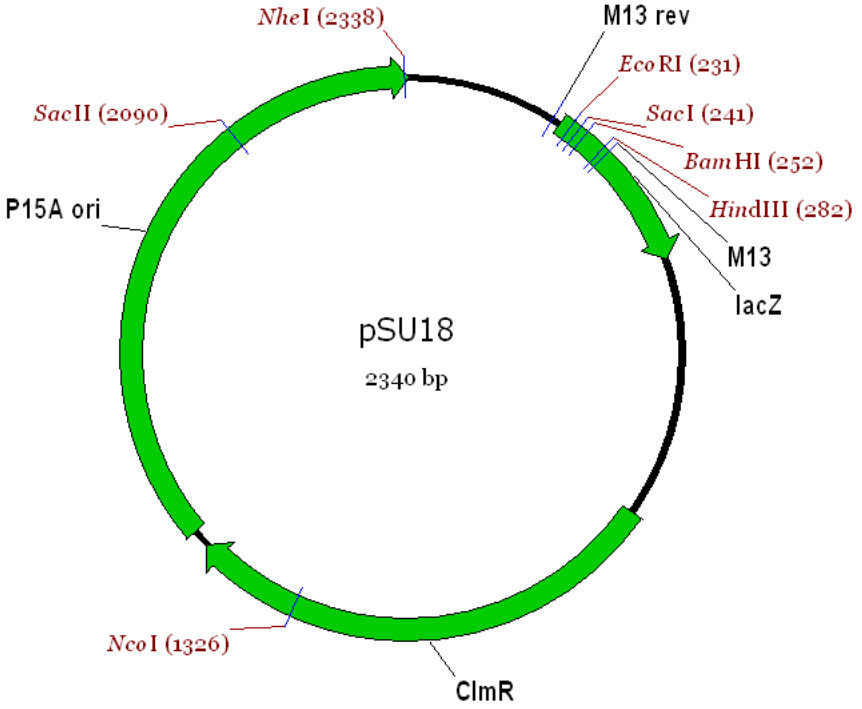
NheI (2338)
M13 rev
EcoRI (231)
SacII (2090)
SacI (241)
BamHI (252)
HindIII (282)
P15A ori
M13
lacZ
pSU18
2340 bp
NcoI (1326)
ClmR

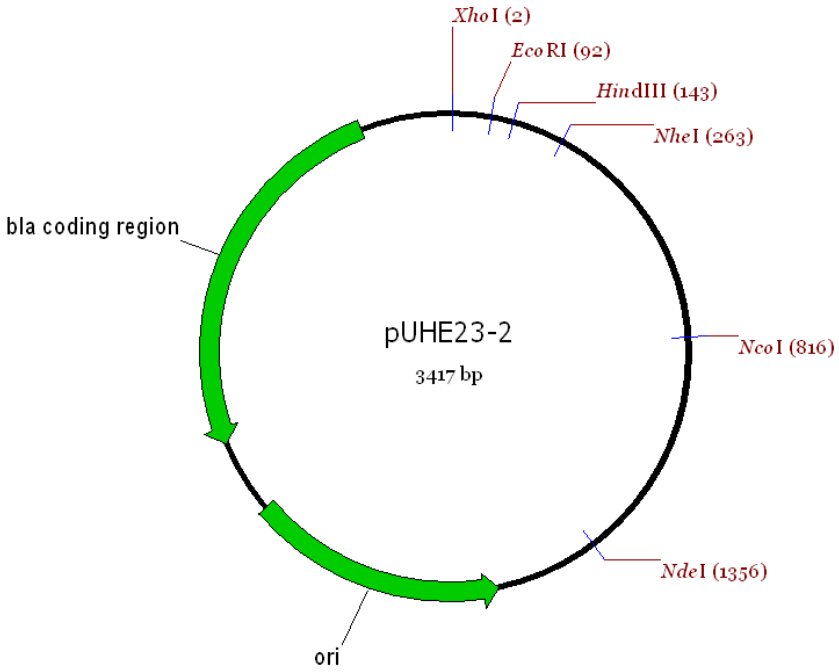
XhoI (2)
EcoRI (92)
HindIII (143)
NheI (263)
bla coding region
pUHE23-2
3417 bp
NcoI (816)
NdeI (1356)
ori

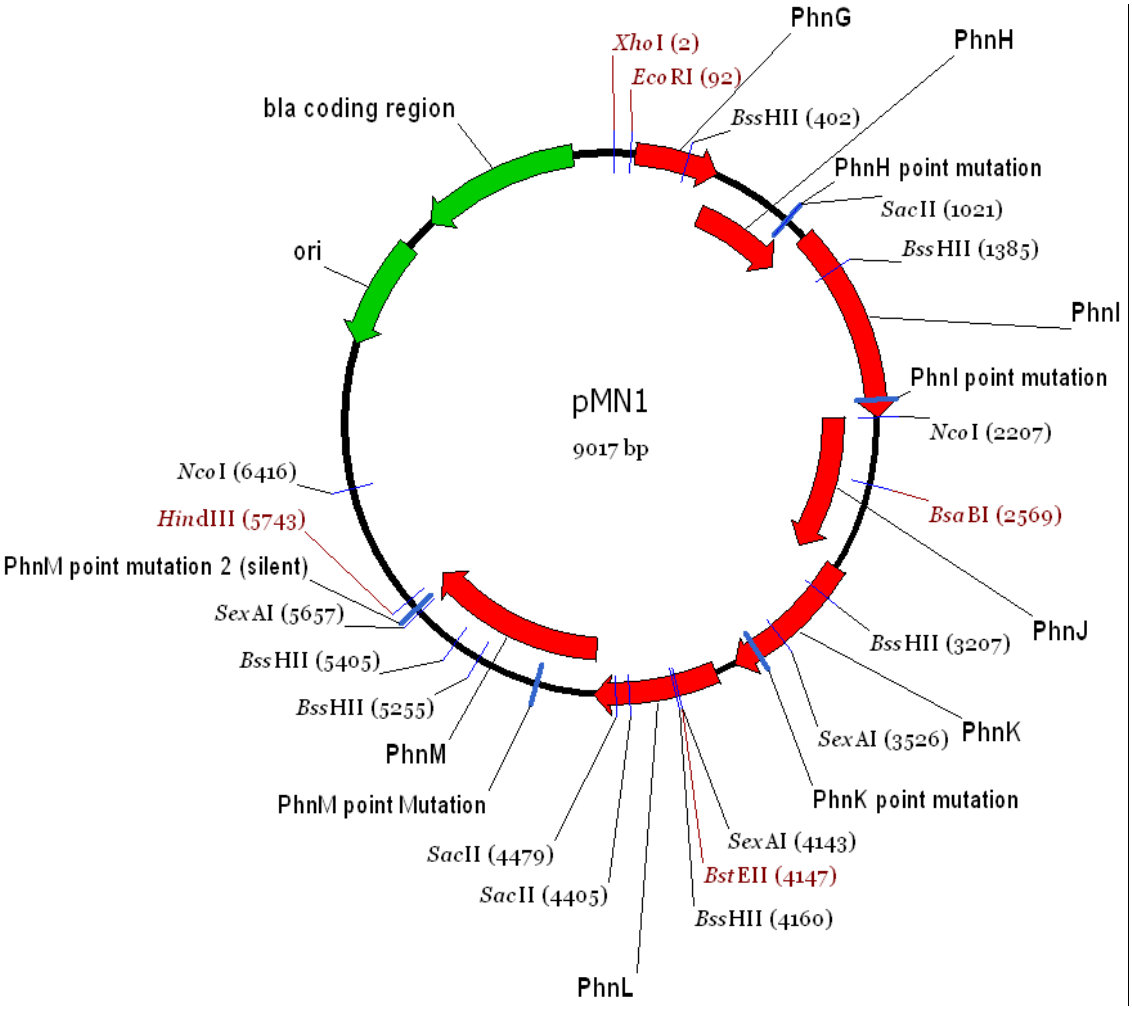
PhnG
PhnH
XhoI (2)
EcoRI (92)
BssHII (402)
bla coding region
PhnH point mutation
SacII (1021)
ori
BssHII (1385)
PhnI
PhnI point mutation
pMN1
9017 bp
NcoI (2207)
NcoI (6416)
BsaBI (2569)
HindIII (5743)
PhnM point mutation 2 (silent)
PhnJ
SexAI (5657)
BssHII (3207)
BssHII (5405)
BssHII (5255)
PhnK
SexAI (3526)
PhnM
PhnK point mutation
PhnM point Mutation
SexAI (4143)
SacII (4479)
BstEII (4147)
SacII (4405)
BssHII (4160)
PhnL

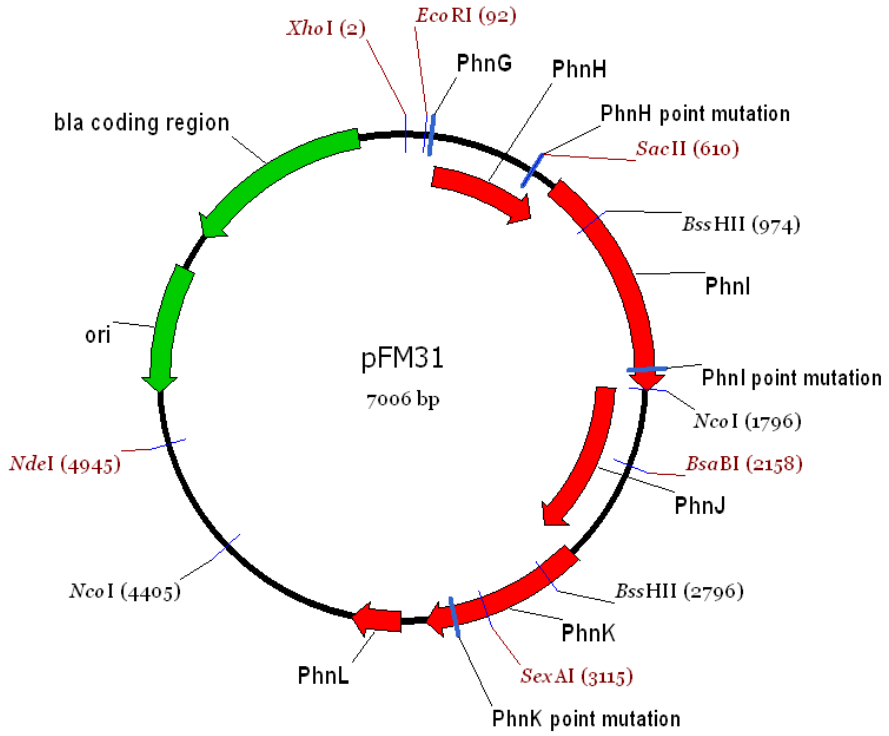
XhoI (2)
EcoRI (92)
PhnG
PhnH
PhnH point mutation
SacII (610)
BssHII (974)
PhnI
PhnI point mutation
NcoI (1796)
BsaBI (2158)
PhnJ
BssHII (2796)
PhnK
SexAI (3115)
PhnK point mutation
PhnL
NcoI (4405)
NdeI (4945)
ori
bla coding region
pFM31
7006 bp

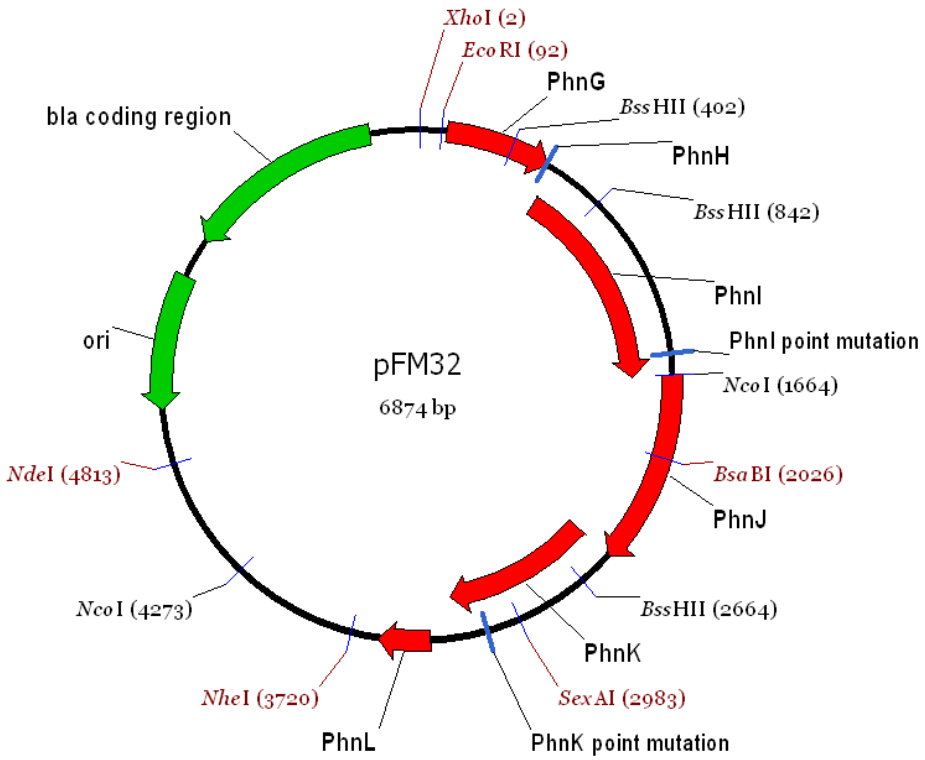
XhoI (2)
EcoRI (92)
PhnG
BssHII (402)
PhnH
BssHII (842)
PhnI
PhnI point mutation
NcoI (1664)
BsaBI (2026)
PhnJ
BssHII (2664)
PhnK
SexAI (2983)
PhnK point mutation
PhnL
NheI (3720)
NcoI (4273)
NdeI (4813)
ori
bla coding region
pFM32
6874 bp

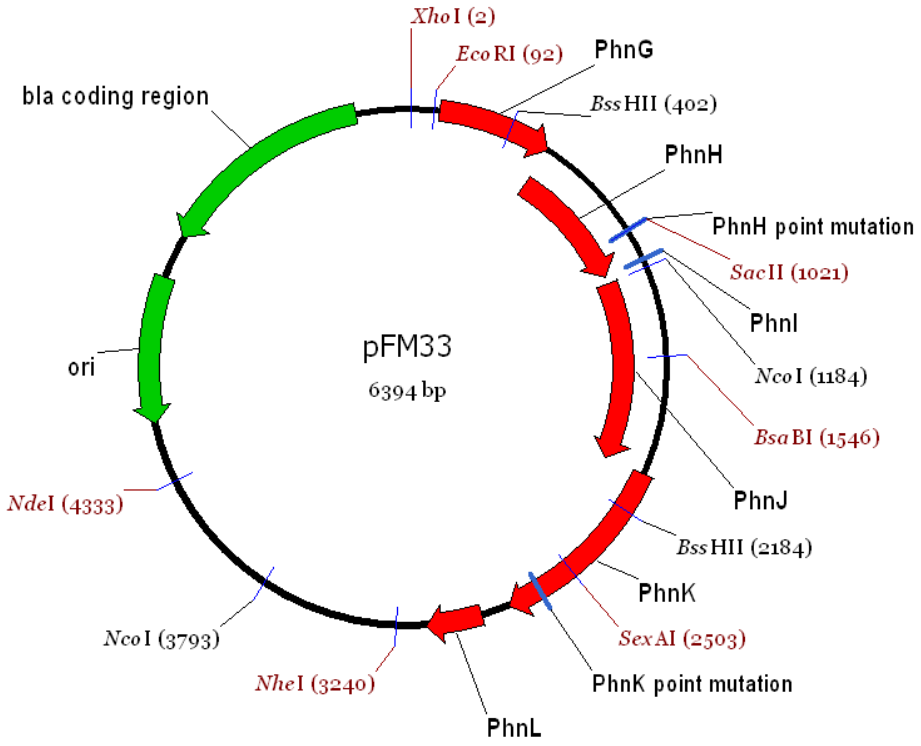
XhoI (2)
EcoRI (92)
PhnG
BssHII (402)
PhnH
PhnH point mutation
SacII (1021)
PhnI
NcoI (1184)
BsaBI (1546)
PhnJ
BssHII (2184)
PhnK
SexAI (2503)
PhnK point mutation
PhnL
NheI (3240)
NcoI (3793)
NdeI (4333)
ori
bla coding region
pFM33
6394 bp

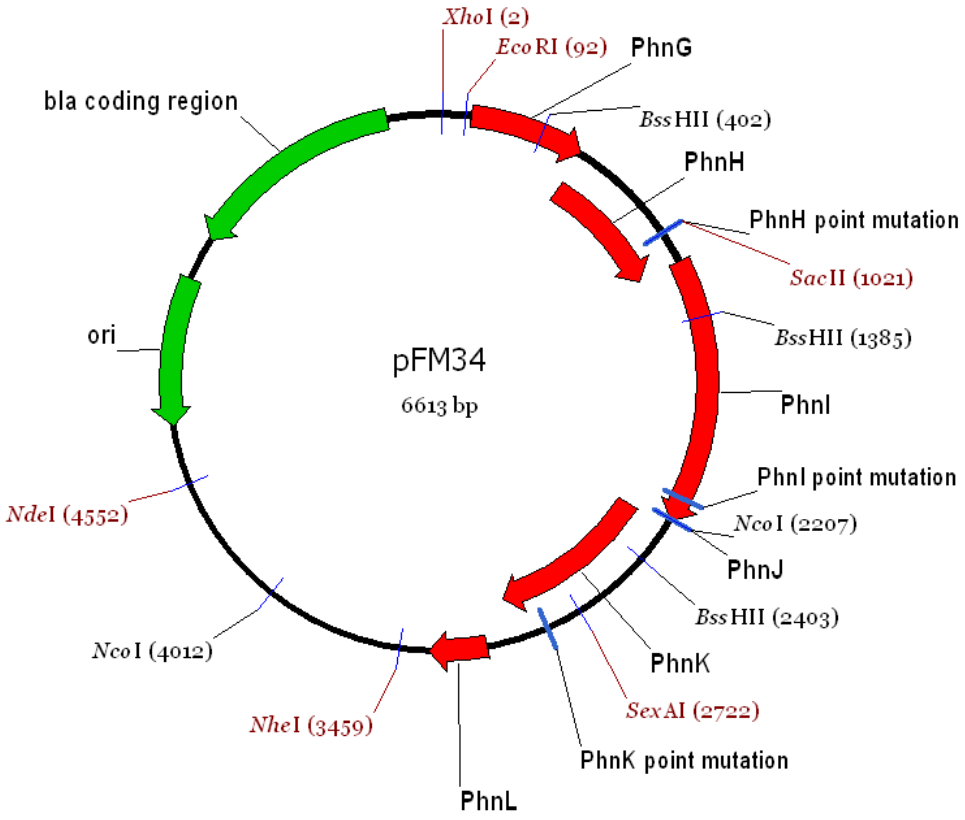
XhoI (2)
EcoRI (92)
PhnG
BssHII (402)
PhnH
PhnH point mutation
SacII (1021)
BssHII (1385)
PhnI
PhnI point mutation
NcoI (2207)
PhnJ
BssHII (2403)
PhnK
SexAI (2722)
PhnK point mutation
PhnL
NheI (3459)
NcoI (4012)
NdeI (4552)
ori
bla coding region
pFM34
6613 bp

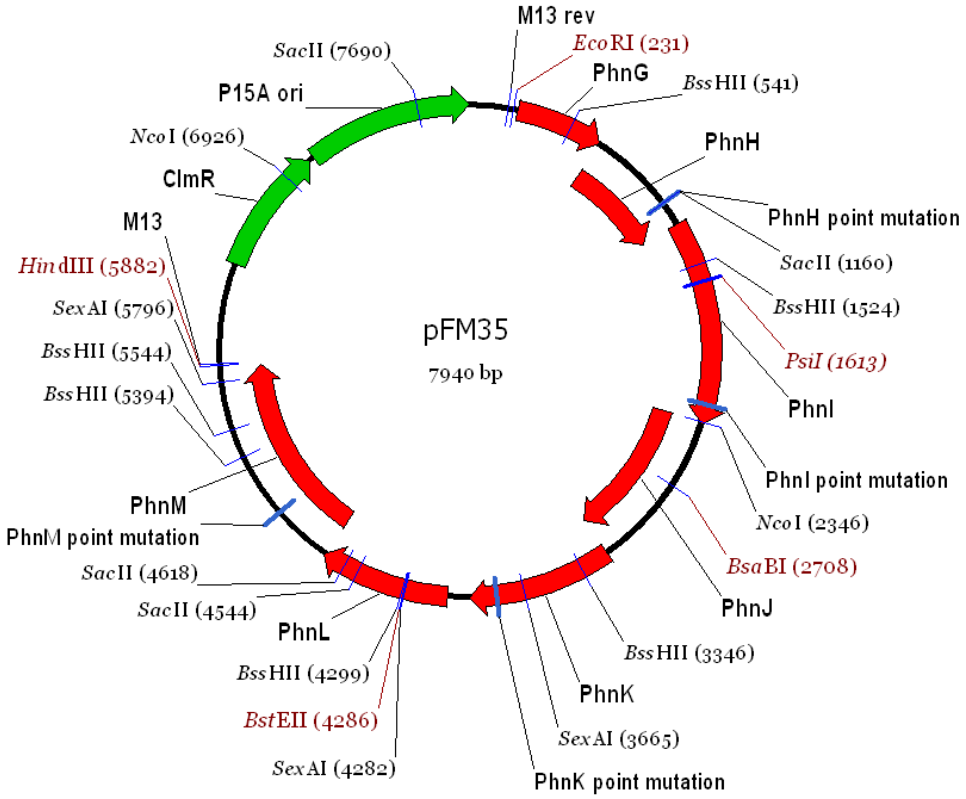
M13 rev
EcoRI (231)
PhnG
BssHII (541)
PhnH
PhnH point mutation
SacII (1160)
BssHII (1524)
PsiI (1613)
PhnI
PhnI point mutation
NcoI (2346)
BsaBI (2708)
PhnJ
BssHII (3346)
PhnK
SexAI (3665)
PhnK point mutation
SexAI (4282)
BstEII (4286)
BssHII (4299)
PhnL
SacII (4544)
SacII (4618)
PhnM point mutation
PhnM
BssHII (5394)
BssHII (5544)
SexAI (5796)
HindIII (5882)
M13
ClmR
NcoI (6926)
P15A ori
SacII (7690)
pFM35
7940 bp

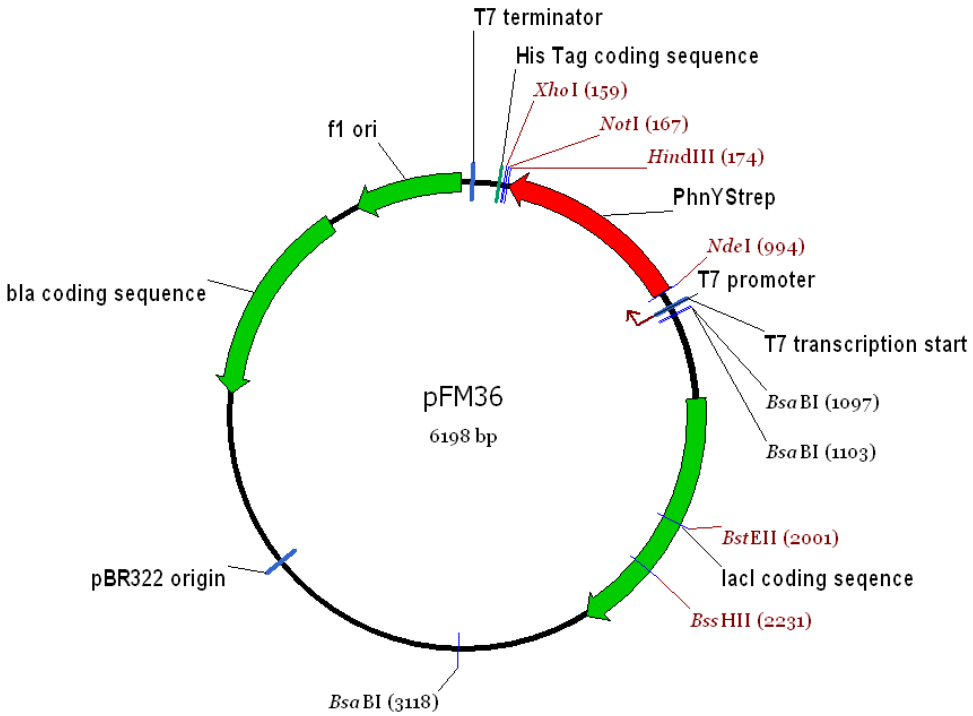
T7 terminator
His Tag coding sequence
XhoI (159)
NotI (167)
HindIII (174)
PhnYStrep
NdeI (994)
T7 promoter
T7 transcription start
BsaBI (1097)
BsaBI (1103)
BstEII (2001)
lacI coding seqence
BssHII (2231)
BsaBI (3118)
pBR322 origin
bla coding sequence
f1 ori
pFM36
6198 bp

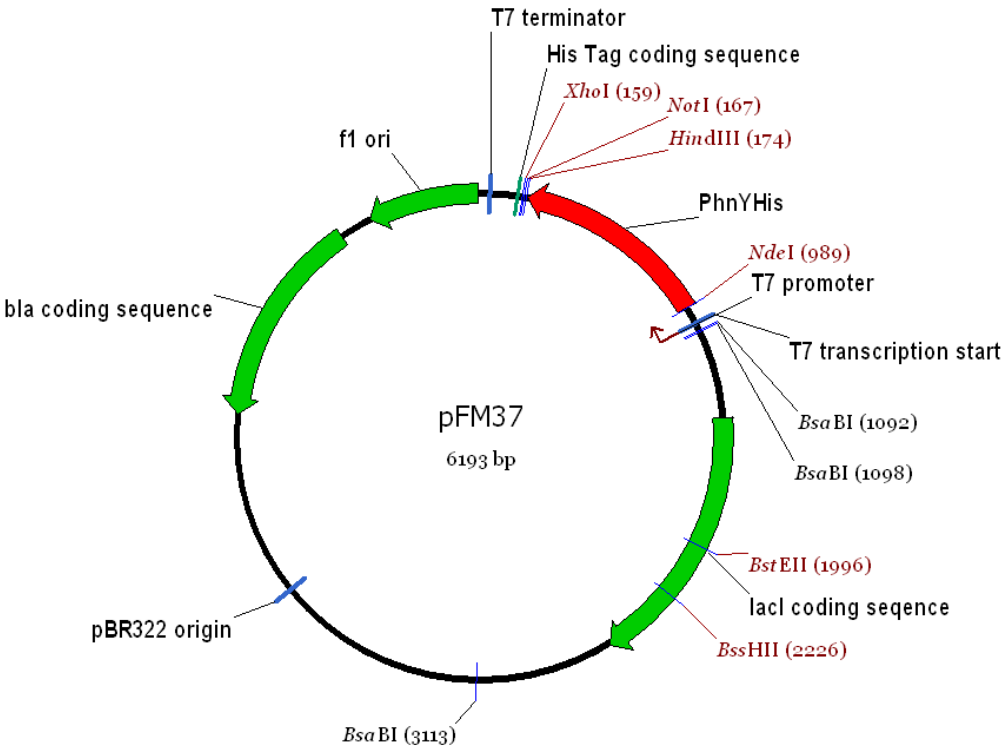
T7 terminator
His Tag coding sequence
XhoI (159)
NotI (167)
HindIII (174)
f1 ori
PhnYHis
NdeI (989)
T7 promoter
bla coding sequence
T7 transcription start
pFM37
6193 bp
BsaBI (1092)
BsaBI (1098)
BstEII (1996)
lacI coding seqence
pBR322 origin
BssHII (2226)
BsaBI (3113)

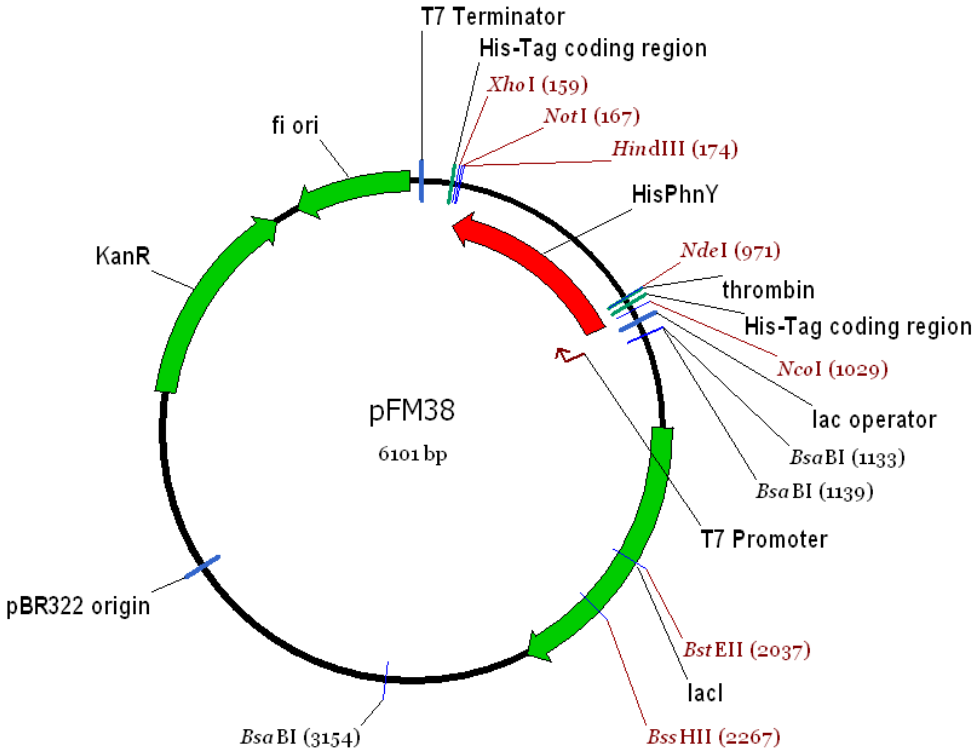
T7 Terminator
His-Tag coding region
XhoI (159)
NotI (167)
HindIII (174)
fi ori
HisPhnY
KanR
NdeI (971)
thrombin
His-Tag coding region
NcoI (1029)
pFM38
6101 bp
lac operator
BsaBI (1133)
BsaBI (1139)
T7 Promoter
pBR322 origin
BstEII (2037)
lacI
BsaBI (3154)
BssHII (2267)

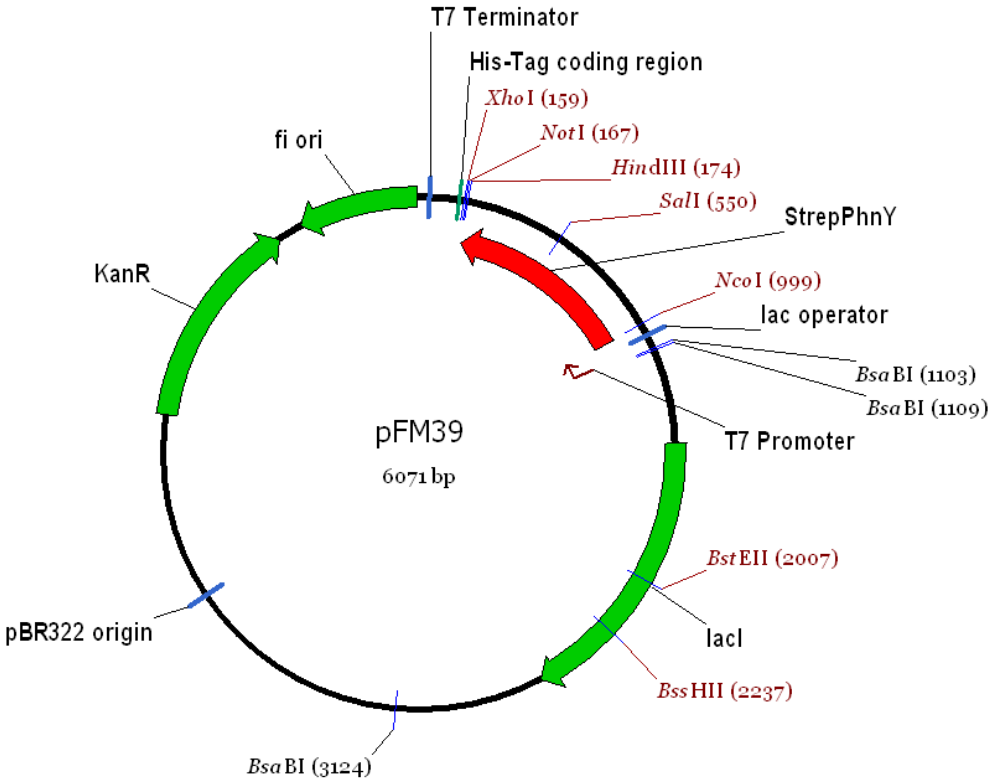
T7 Terminator
His-Tag coding region
XhoI (159)
NotI (167)
HindIII (174)
SalI (550)
StrepPhnY
fi ori
KanR
NcoI (999)
lac operator
BsaBI (1103)
BsaBI (1109)
T7 Promoter
pFM39
6071 bp
BstEII (2007)
lacI
pBR322 origin
BssHII (2237)
BsaBI (3124)

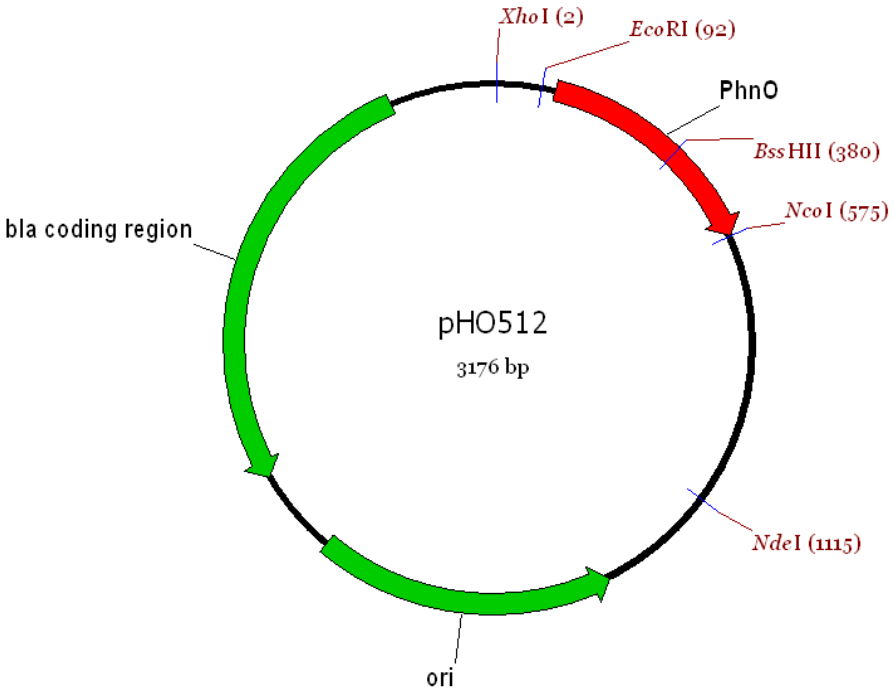
XhoI (2)
EcoRI (92)
PhnO
BssHII (380)
NcoI (575)
bla coding region
pHO512
3176 bp
NdeI (1115)
ori

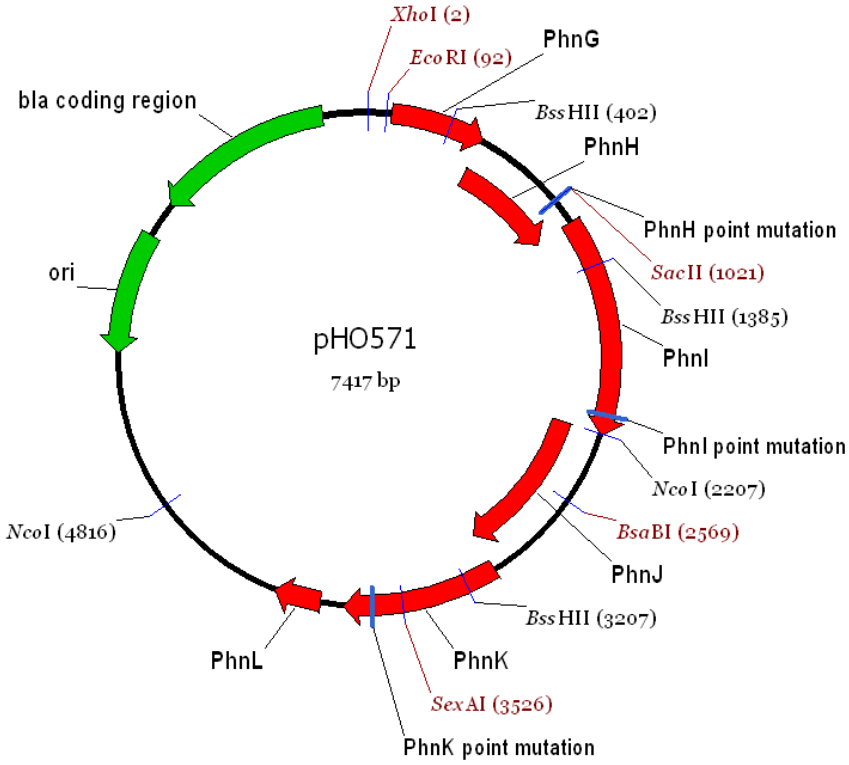
XhoI (2)
EcoRI (92)
PhnG
BssHII (402)
PhnH
PhnH point mutation
SacII (1021)
BssHII (1385)
PhnI
PhnI point mutation
NcoI (2207)
BsaBI (2569)
PhnJ
BssHII (3207)
PhnK
SexAI (3526)
PhnK point mutation
PhnL
NcoI (4816)
ori
bla coding region
pHO571
7417 bp

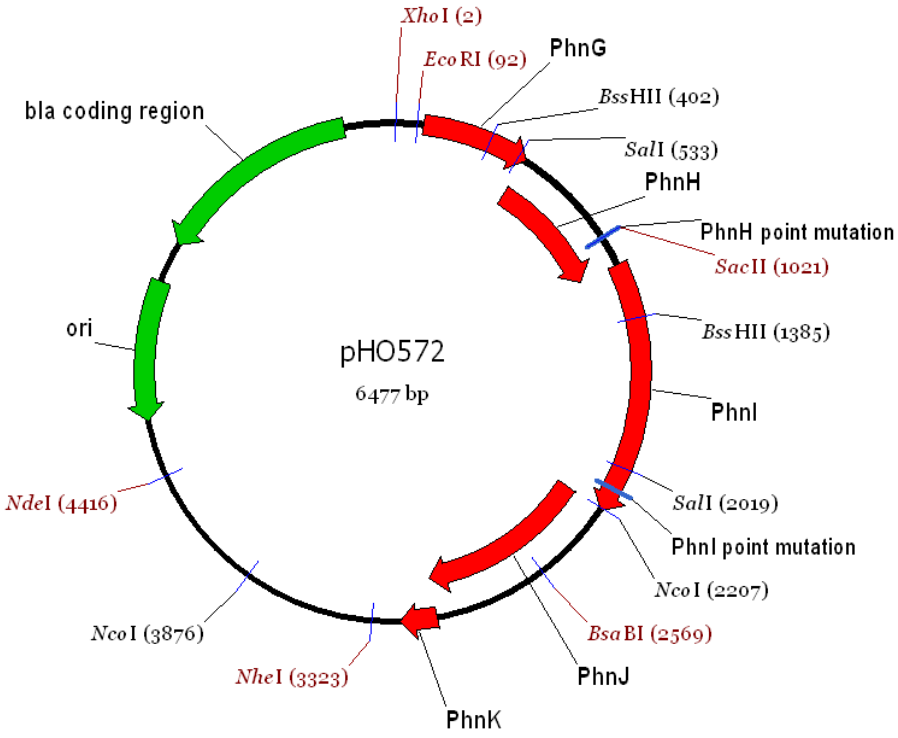
XhoI (2)
EcoRI (92)
PhnG
BssHII (402)
SalI (533)
PhnH
PhnH point mutation
SacII (1021)
BssHII (1385)
PhnI
SalI (2019)
PhnI point mutation
NcoI (2207)
BsaBI (2569)
PhnJ
PhnK
NheI (3323)
NcoI (3876)
NdeI (4416)
ori
bla coding region
pHO572
6477 bp

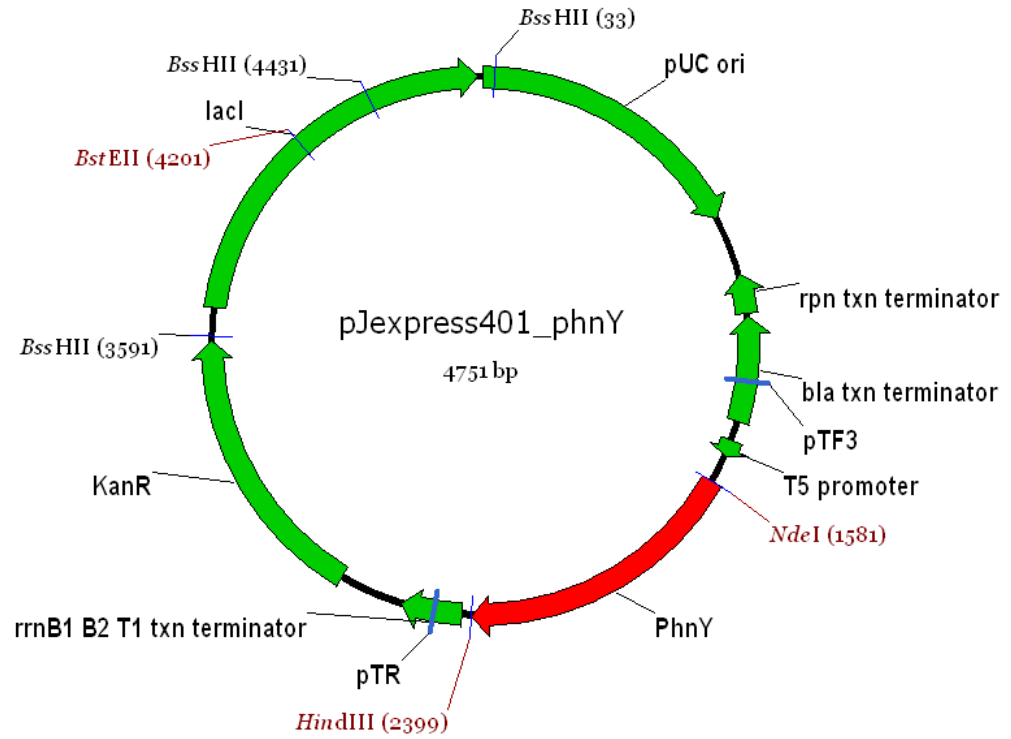
BssHII (33)
pUC ori
BssHII (4431)
lacI
BstEII (4201)
rpn txn terminator
pJexpress401_phnY
4751 bp
BssHII (3591)
bla txn terminator
pTF3
KanR
T5 promoter
NdeI (1581)
rrnB1 B2 T1 txn terminator
PhnY
pTR
HindIII (2399)

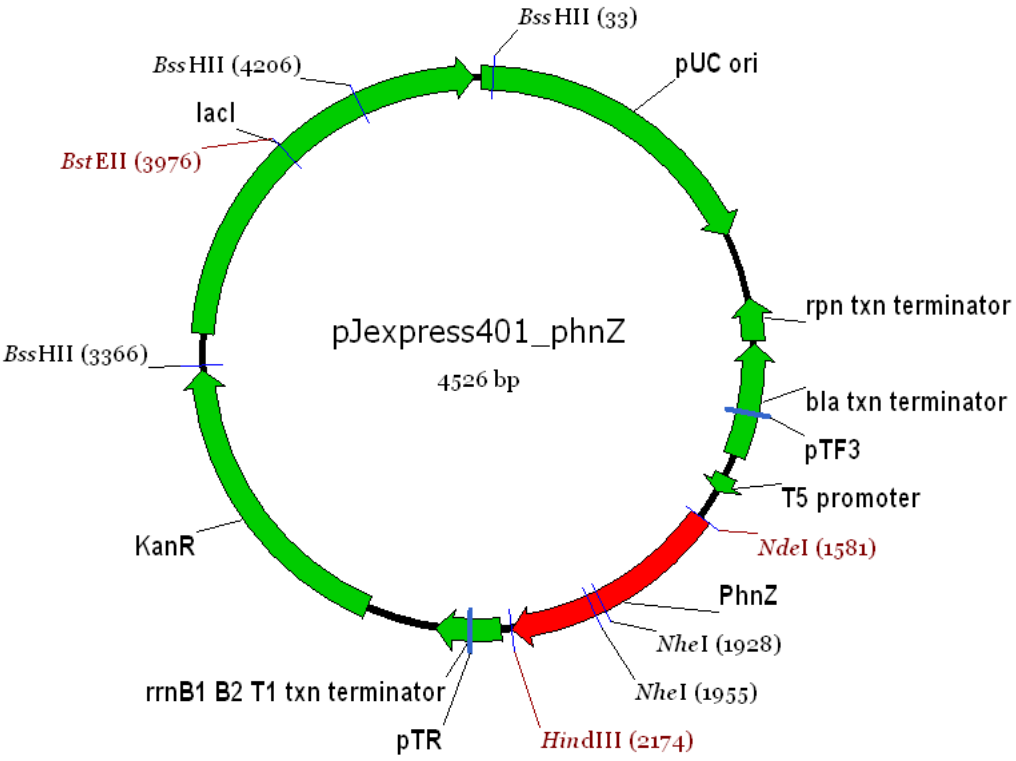
BssHII (33)
pUC ori
BssHII (4206)
lacI
BstEII (3976)
rpn txn terminator
pJexpress401_phnZ
4526 bp
BssHII (3366)
bla txn terminator
pTF3
T5 promoter
KanR
NdeI (1581)
PhnZ
NheI (1928)
NheI (1955)
rrnB1 B2 T1 txn terminator
pTR
HindIII (2174)

Appendix D

Michaelis-Menten curves of PhnZ variants

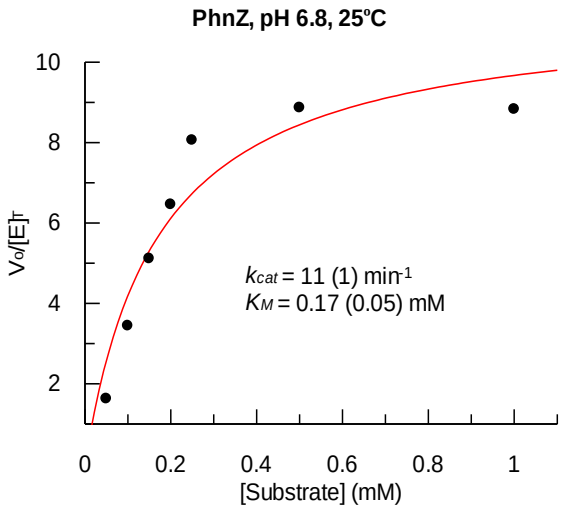

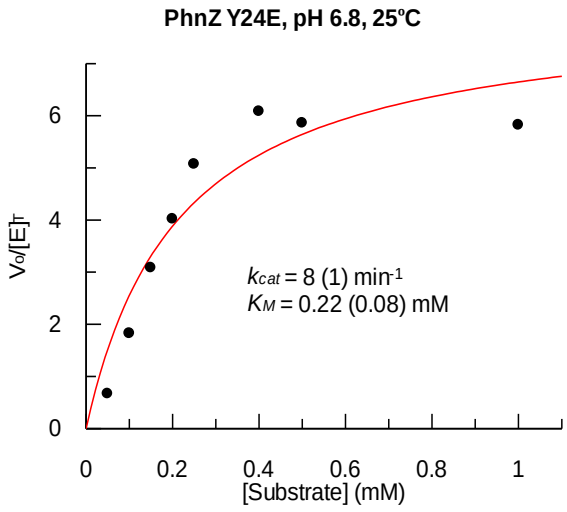

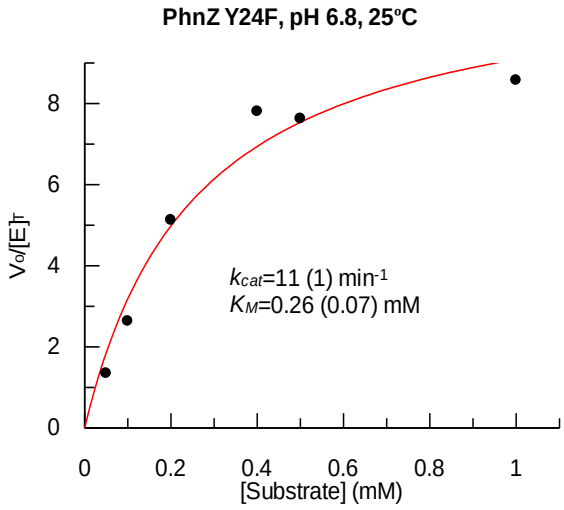

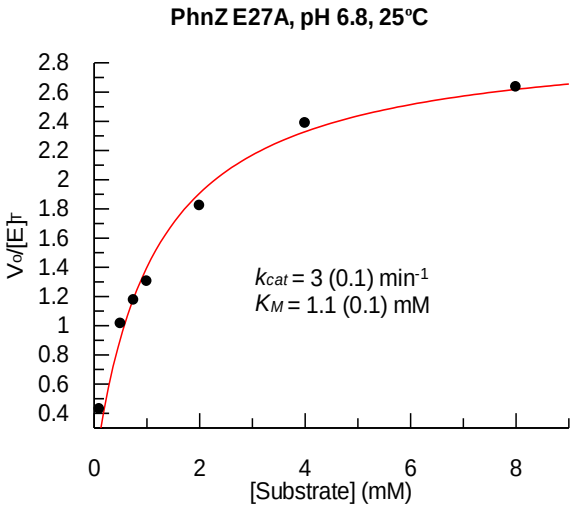

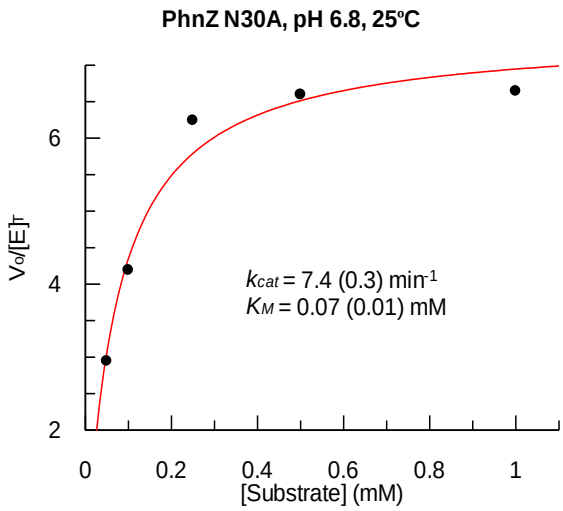
PhnZ N30A, pH 6.8, 25ºC
k_{cat} = 7.4 (0.3) min^{-1}
K_M = 0.07 (0.01) mM
$V_o/[E]_T$
[Substrate] (mM)

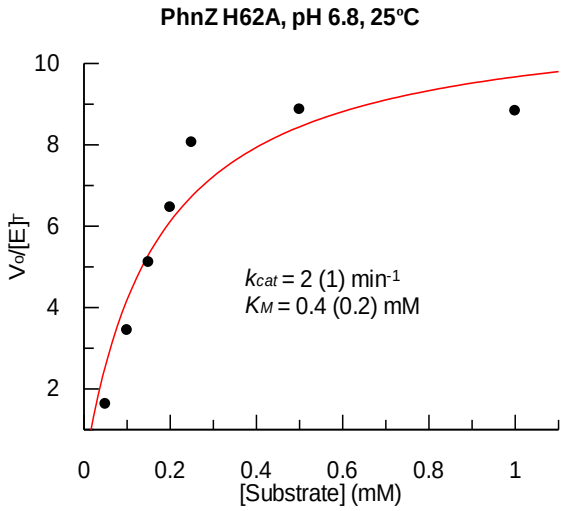
PhnZ H62A, pH 6.8, 25ºC
k_{cat} = 2 (1) min^{-1}
K_M = 0.4 (0.2) mM
$V_o/[E]_T$
[Substrate] (mM)

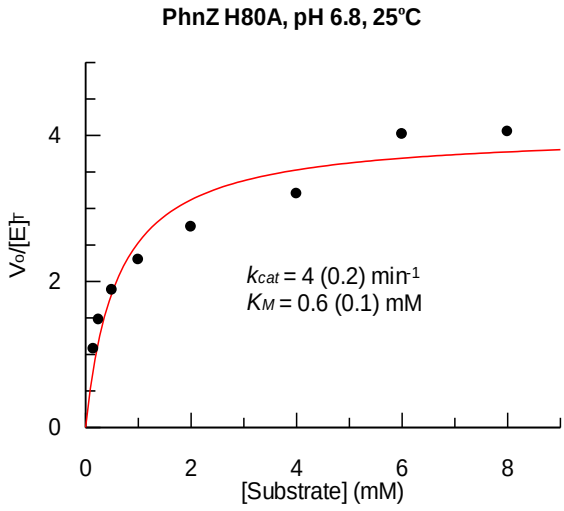
PhnZ H80A, pH 6.8, 25ºC
k_{cat} = 4 (0.2) min^{-1}
K_M = 0.6 (0.1) mM
$V_o/[E]_T$
[Substrate] (mM)

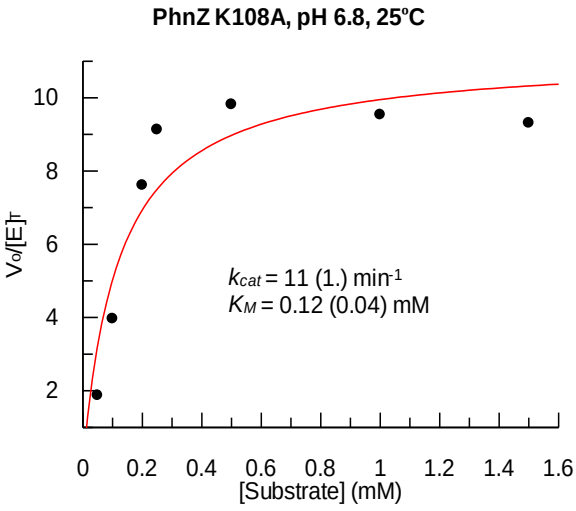
PhnZ K108A, pH 6.8, 25ºC
k_{cat} = 11 (1.) min^{-1}
K_M = 0.12 (0.04) mM
$V_o/[E]_T$
[Substrate] (mM)